

Uniwersytet im. Adama Mickiewicza w Poznaniu
Wydział Chemii

Waloryzacja glicerolu z zastosowaniem katalizatorów węglowych

Valorization of glycerol in the presence of carbon catalysts

mgr Karolina Kinga Ptaszyńska

Rozprawa doktorska przygotowana w formie spójnego tematycznie cyklu artykułów opublikowanych w czasopismach naukowych

Promotor: prof. dr hab. Mieczysław Kozłowski

Promotor pomocniczy: dr Anna Malaika



Zakład Technologii Chemicznej
Poznań (2024)

PODZIĘKOWANIA

Pragnę serdecznie podziękować Panu **prof. dr. hab. Mieczysławowi Kozłowskiemu** za przyjęcie mnie do swojej grupy badawczej, za wieloletnią współpracę, nieocenioną pomoc merytoryczną, wyrozumiałość, okazaną życzliwość oraz cenne rady, które pomogły mi w realizacji niniejszej rozprawy doktorskiej.

Pani **dr Annie Malaice** dziękuję za wieloletnią współpracę, poświęcony mi czas i przekazaną wiedzę, za motywację do działania, cenne wskazówki, miłą atmosferę podczas pracy oraz pomoc w prowadzonych przeze mnie badaniach.

Dziękuję pracownikom Zakładu LSRE-LCM Uniwersytetu w Porto, szczególnie **prof. José Luísowi Figueiredo**, **prof. M. Fernando R. Pereirze** oraz **dr Katarzynie Morawie Eblagon** za współpracę w realizacji wielu ciekawych projektów badawczych, niezwykle ciepłe przyjęcie mnie w swojej grupie badawczej oraz za możliwość zdobycia doświadczenia.

Serdecznie dziękuję swoim **Bliskim** za cierpliwość, wsparcie w trudnych momentach oraz za mobilizację do pracy.

SPIS TREŚCI

ŻYCIORYS NAUKOWY	7
WYKAZ STOSOWANYCH SKRÓTÓW	15
STRESZCZENIE	19
ABSTRACT	23
WYKAZ PUBLIKACJI BĘDĄCYCH PODSTAWĄ ROZPRAWY DOKTORSKIEJ.....	27
CZĘŚĆ LITERATUROWA	29
1. Wprowadzenie	31
1.1. Wpływ stosowania paliw kopalnych na gospodarkę i środowisko	31
1.2. Rozwój przemysłu biodiesla – odnawialnego źródła energii	31
1.3. Sposoby waloryzacji glicerolu – związku otrzymywanego ubocznie w procesie produkcji biodiesla	32
1.3.1. Estryfikacja glicerolu do octanów glicerolu.....	33
1.3.1.1. Katalizatory stosowane w procesie estryfikacji glicerolu	34
1.3.2. Eteryfikacja glicerolu do eterów tert-butyłowych glicerolu.....	35
1.3.2.1. Katalizatory stosowane w procesie eteryfikacji glicerolu	37
1.3.3. Gliceroliza mocznika.....	37
1.3.3.1. Katalizatory stosowane w procesie glicerolizy mocznika.....	39
1.4. Stałe katalizatory na bazie węgla w procesach waloryzacji glicerolu	39
1.4.1. Estryfikacja glicerolu do octanów w obecności katalizatorów na bazie węgla	40
1.4.2. Eteryfikacja glicerolu do eterów tert-butyłowych w obecności katalizatorów na bazie węgla	41
1.4.3. Gliceroliza mocznika w obecności katalizatorów na bazie węgla	42
CEL BADAŃ.....	43
CZĘŚĆ EKSPERYMENTALNA.....	47
2. Materiały węglowe testowane w wybranych procesach konwersji glicerolu.....	49
2.1. Termicznie zredukowany tlenek grafenu o właściwościach kwasowych.....	49
2.2. Sulfonowane włókna węglowe otrzymane z izobutanu lub etylenu w procesie CCVD ...	49
2.3. Funkcjonalizowane komercyjne nanorurki węglowe	49
2.4. Włókna węglowe otrzymane z gazu LPG w roli nośnika tlenków wybranych metali	50
3. Charakterystyka przygotowanych katalizatorów	50
4. Testy katalityczne.....	50
WYNIKI I ICH OMÓWIENIE.....	53

5. Właściwości fizykochemiczne otrzymanych materiałów węglowych.....	55
5.1. Próbki wyjściowe	55
5.1.1. Termicznie zredukowany tlenek grafenu	55
5.1.2. Włókna węglowe otrzymane z izobutanu lub etylenu	55
5.1.3. Komercyjne nanorurki węglowe	56
5.1.4. Włóknisty materiał węglowy otrzymany z gazu LPG	57
5.2. Próbki modyfikowane	57
5.2.1. Funkcjonalizowane materiały węglowe.....	57
5.2.1.1. Modyfikacje węgla za pomocą kwasu siarkowego(VI).....	57
5.2.1.2. Modyfikacje próbek kwasem fosforowym oraz solą diazoniową.....	62
5.2.2. Włókna węglowe w roli nośnika tlenków metali.....	64
6. Wpływ chemii powierzchni przygotowanych materiałów węglowych na aktywność katalityczną w wybranych procesach waloryzacji glicerolu	65
6.1. Estryfikacja glicerolu za pomocą kwasu octowego w obecności katalizatorów na bazie TRGO.....	65
6.2. Eteryfikacja glicerolu za pomocą alkoholu tert-butyłowego w obecności funkcjonalizowanych włóknistych materiałów węglowych	68
6.2.1. Wpływ chemii powierzchni testowanych materiałów na przebieg reakcji eteryfikacji glicerolu	73
6.3. Gliceroliza mocznika w obecności wybranych tlenków metali osadzonych na CF	74
PODSUMOWANIE	79
BIBLIOGRAFIA.....	85

ŻYCIORYS NAUKOWY

1) Dane personalne:

- Imię i nazwisko: Karolina Ptaszyńska
- Tytuł naukowy: magister
- Data i miejsce urodzenia: 02.04.1995, Poznań

2) Wykształcenie:

2019–2024 Szkoła Doktorska, Uniwersytet im. Adama Mickiewicza w Poznaniu, Wydział Chemii

Dyscyplina: nauki chemiczne

Rozprawa doktorska pt. „*Waloryzacja glicerolu z zastosowaniem katalizatorów węglowych*” realizowana w Zakładzie Technologii Chemicznej pod opieką prof. dr. hab. Mieczysława Kozłowskiego oraz dr Anny Malaiki

2017–2019 Studia II stopnia (magisterskie)

Uniwersytet im. Adama Mickiewicza w Poznaniu, Wydział Chemii

Kierunek: chemia ogólna

Praca magisterska pt. „*Estryfikacja i transestryfikacja glicerolu do octanów glicerolu w obecności katalizatorów węglowych – synteza komponentów paliwowych*” realizowana w Zakładzie Technologii Chemicznej pod opieką prof. dr. hab. Mieczysława Kozłowskiego

2014–2017 Studia I stopnia (licencjackie)

Uniwersytet im. Adama Mickiewicza w Poznaniu, Wydział Chemii

Kierunek: chemia ogólna

Praca licencjacka pt. „*Polimery jako środki farmakologiczne wprowadzające leki do organizmu*” realizowana w Zakładzie Technologii Chemicznej pod opieką dr Anny Malaiki

3) Wykaz publikacji:

a) wchodzących w skład rozprawy doktorskiej:

- A. Malaika, K. Ptaszyńska, J. Gaidukevič, M. Kozłowski, *The impact of surface groups of functionalized graphene on glycerol acetylation*, Fuel, 2022, 313(73), 122987.
- K. Ptaszyńska, A. Malaika, M. Kapska, M. Kozłowski, *SO₃H-functionalized carbon fibers for the catalytic transformation of glycerol to glycerol tert-butyl ethers*, Scientific Reports, 2023, 13(1), 565.

- K. Ptaszyńska, A. Malaika, K. Kozigrodzka, M. Kozłowski, *A green approach to obtaining glycerol carbonate by urea glycerolysis using carbon-supported metal oxide catalysts*, *Molecules*, 2023, 28(18), 6534.
- K. Ptaszyńska, A. Malaika, K. Morawa Eblagon, J. L. Figueiredo, M. Kozłowski, *Promoting effect of ball milling on the functionalization and catalytic performance of carbon nanotubes in glycerol etherification*, *Molecules*, 2024, 29(7), 1623.
- K. Ptaszyńska, K. Morawa Eblagon, A. Malaika, J. L. Figueiredo, M. Kozłowski, *The role of mechanochemical treatment of carbon nanotubes in promoting glycerol etherification*, *Catalysis Science & Technology*, 2024, 14(11), 3184–3200.

b) niewchodzących w skład rozprawy doktorskiej:

- B. Krzyżyńska, A. Malaika, K. Ptaszyńska, A. Tolińska, P. Kirszensztein, M. Kozłowski, *Modified activated carbons for esterification of acetic acid with ethanol*, *Diamond and Related Materials*, 2020, 101, 107608.
- K. Morawa Eblagon, A. Malaika, K. Ptaszyńska, M. F. R. Pereira, J. L. Figueiredo, *Impact of thermal treatment of Nb₂O₅ on its performance in glucose dehydration to 5-hydroxymethylfurfural in water*, *Nanomaterials*, 2020, 10(9), 1685.
- A. Malaika, K. Ptaszyńska, M. Kozłowski, *Conversion of renewable feedstock to bio-carbons dedicated for the production of green fuel additives from glycerol*, *Fuel*, 2021, 288(4), 119609.
- A. Malaika, K. Ptaszyńska, K. Morawa Eblagon, M. F. R. Pereira, J. L. Figueiredo, M. Kozłowski, *Solid acid carbon catalysts for sustainable production of biofuel enhancers via transesterification of glycerol with ethyl acetate*, *Fuel*, 2021, 304(3), 121381.
- A. Malaika, K. Ptaszyńska, M. Kozłowski, *Production of valuable chemicals from glycerol using carbon fiber catalysts derived from ethylene*, *Scientific Reports*, 2021, 11(1), 20251.
- K. Morawa Eblagon, A. Malaika, K. Ptaszyńska, M. F. R. Pereira, M. Kozłowski, J. L. Figueiredo, *Niobium oxide-phosphorylated carbon xerogel composites as solid acid catalysts for cascade conversion of glucose to 5-hydroxymethylfurfural (HMF) in pure water*, *Catalysis Today*, 2023, 418, 114070.
- A. Malaika, J. Kowalska-Kuś, K. Końska, K. Ptaszyńska, A. Jankowska, A. Held, K. Wróblewski, M. Kozłowski, *Upgrading pyrolytic residue from end-of-life tires to efficient heterogeneous catalysts for the conversion of glycerol to acetins*. *Molecules*, 2023, 28(24), 8137.
- A. Malaika, K. Ptaszyńska, M. Kapska, M. Kozłowski, *The role of surface chemistry of carbons in the catalytic production of fuel additives by glycerol etherification*, *Fuel*, 2024, 358(2), 130147.

4) **Udział w konferencjach naukowych:**

a) krajowych (autor prezentujący):

- K. Ptaszyńska, A. Malaika, M. Kozłowski, *Estryfikacja i transestryfikacja glicerolu do octanów glicerolu w obecności katalizatorów węglowych – synteza komponentów paliwowych*, 62. Zjazd Naukowy Polskiego Towarzystwa Chemicznego, Warszawa, 2–6 września 2019, S09, Poster P09, str. S09-35.
- K. Ptaszyńska, M. Kapska, A. Malaika, M. Kozłowski, *Zastosowanie modyfikowanych materiałów węglowych w procesie waloryzacji glicerolu – otrzymywanie eterów tert-butyłowych glicerolu*, 62. Zjazd Naukowy Polskiego Towarzystwa Chemicznego, Warszawa, 2–6 września 2019, S09, Poster P11, str. S09-37.
- K. Ptaszyńska, A. Malaika, J. Gaidukevič, M. Kozłowski, *Funkcjonalizowane materiały węglowe na bazie grafenu w syntezie dodatków paliwowych*, 63. Zjazd Naukowy Polskiego Towarzystwa Chemicznego, Łódź, 13–17 września 2021, S08, Poster P002, str. S08-570.
- K. Ptaszyńska, A. Malaika, D. Mesjasz, M. Kozłowski, *Optymalizacja warunków otrzymywania di- i trioctanów glicerolu metodą estryfikacji glicerolu kwasem octowym prowadzonej w obecności katalizatorów węglowych*, 63. Zjazd Naukowy Polskiego Towarzystwa Chemicznego, Łódź, 13–17 września 2021, S08, Poster P003, str. S08-571.
- K. Ptaszyńska, A. Malaika, M. Kozłowski, *Otrzymywanie eterów tert-butyłowych glicerolu w obecności sulfonowalnych nanorurek węglowych jako katalizatorów*, 64. Zjazd Naukowy Polskiego Towarzystwa Chemicznego, 11–16 września 2022, Lublin, Polska, S10, Poster P20, str. 587.
- K. Kozigrodzka, K. Ptaszyńska, A. Malaika, M. Kozłowski, *Zastosowanie tlenków metali osadzonych na nośniku węglowym w roli katalizatorów procesu glicerolizy mocznika*, 64. Zjazd Naukowy Polskiego Towarzystwa Chemicznego, 11–16 września 2022, Lublin, Polska, S10, Poster P21, str. 588.

b) międzynarodowych (autor prezentujący):

- K. Ptaszyńska, A. Malaika, M. Kozłowski, *Esterification and transesterification of glycerol to glycerol acetates in the presence of carbon catalysts – synthesis of fuel additives*, XXV Encontro Galego-Portugués de Quimica, Santiago de Compostela, Hiszpania, 20–22 listopada 2019, Poster CAT09, str. 267.
- K. Ptaszyńska, A. Malaika, K. Morawa Eblagon, M. F. R. Pereira, J. L. Figueiredo, M. Kozłowski, *Production of valuable fuel additives from glycerol and tert-butyl alcohol over carbon nanotubes as catalysts*, NanoTech Poland 2022, 1–3 czerwca 2022, Poznań, Polska, Section A, Poster A41, str. 115.

- K. Kozigrodzka, K. Ptaszyńska, A. Malaika, M. Kozłowski, *Production of glycerol carbonate by urea glycerolysis under ambient pressure using carbon-supported metal oxide catalysts*, NanoTech Poland 2022, 1–3 czerwca 2022, Poznań, Polska, Section A, Poster A29, str. 103.
- M. Kozłowski, K. Ptaszyńska, A. Malaika, *Plastic waste-derived solid acid catalysts for the production of fuel enhancers by glycerol esterification*, 9th International Symposium on Carbon for Catalysis, 28–30 czerwca 2022, Zaragoza, Hiszpania, Fine Chemistry, Poster P44.
- K. Morawa Eblagon, K. Ptaszyńska, A. Malaika, M. F. R. Pereira, J. L. Figueiredo, *Influence of the type of acidic sites in bifunctional Nb₂O₅/carbon catalysts on cascade conversion of glucose to 5-(hydroxymethyl)furfural*, 9th International Symposium on Carbon for Catalysis, 28–30 czerwca 2022, Zaragoza, Hiszpania, Session 4: Biomass conversion, Prezentacja ustna OC13.
- K. Ptaszyńska, A. Malaika, K. Morawa Eblagon, M. Kozłowski, *Modified carbon nanotubes as solid acids for catalytic obtaining of fuel enhancers via glycerol etherification*, NanoTech Poland 2023, 14–16 czerwca 2023, Poznań, Polska, Section A, Poster A27, str. 93.
- K. Ptaszyńska, A. Malaika, M. Kapska, M. Kozłowski, *Diazonium salt-modified carbons as highly active and recyclable heterogeneous catalysts for glycerol valorization*, NanoTech Poland 2023, 14–16 czerwca 2023, Poznań, Polska, Section A, Poster A26, str. 92.
- K. Ptaszyńska, A. Malaika, M. Kozłowski, *The influence of the morphology of spherical-fibrous carbon composites on their functionalization and catalytic activity in glycerol etherification*, NanoTech Poland 2024, 5–7 czerwca 2024, Poznań, Polska, Section A, Poster A27, str. 69.

5) Granty:

- Inicjatywa Doskonałości – Uczelnia Badawcza: Minigranty dla doktorantów szkół doktorskich: konkurs nr 017 (zadanie 02) z dnia 22.03.2021 (numer wniosku: 017/02/SNŚ/0013)

Funkcja: kierownik projektu

Okres realizacji: 10.2021–11.2022

Tytuł projektu: Katalityczna synteza eterów tert-butyłowych glicerolu – efektywnych, "zielonych" dodatków paliwowych, otrzymanych z udziałem funkcjonalizowanych nanorurek węglowych (CNT). Wpływ warunków modyfikacji CNT na ich właściwości katalityczne.

- „Grants for young scientists” na udział w konferencji NanoTech Poland 2022.

- Inicjatywa Doskonałości – Uczelnia Badawcza: Wsparcie publikowania w prestiżowych czasopismach naukowych: konkurs nr 085 (zadanie 08) z dnia 3.01.2023 (numer wniosku 085/08/POB3/0002).

6) Szkolenia (prowadzone przez firmę Merck):

- 25.11.2021: „Filtracja membranowa – rozwiązania EZ-Fit Family dedykowane do badania wody i napojów”
- 02.12.2021: „Pipety automatyczne w laboratorium. Wymagania dotyczące zapewnienia jakości i potwierdzenie metrologiczne”
- 06.12.2021: „Chromatografia gazowa – omówienie techniki, dobór kolumny chromatograficznej, wskazówki praktyczne”
- 09.12.2021: „Mikrobiologiczna kontrola czystości powierzchni produkcyjnych z uwzględnieniem metod alternatywnych: MVP Icon i MC Media Pads”
- 16.12.2021: „Monitorowanie przyrządów pomiarowych w laboratorium. Harmonogram kalibracji i regulacji. Źródła niepewności występujące podczas kalibracji pipet tłokowych”
- 13.12.2021: „Kalibracja i walidacja metod pomiarowych dla zapewnienia wiarygodności w laboratorium”
- 20.12.2021: „Dobra praktyka przy stosowaniu wody do analiz chemicznych, biochemicznych i mikrobiologicznych”
- 10.01.2022: „Przyczyny błędów podczas codziennej pracy z automatycznymi urządzeniami do pomiarów objętości (pipety, dozowniki, biurety)”
- 13.01.2022: „Walidacja metod testowych Spectroquant – arkusz walidacyjny jako jedno z dedykowanych narzędzi”
- 14.01.2022: „Ekstrakcja i oczyszczanie białka z materiału biologicznego”
- 17.01.2022: „Sposób na szybkie i dokładne miareczkowanie”
- 20.01.2022: „Nadzór nad wyposażeniem pomiarowym w laboratorium. Szklane naczynia pomiarowe klasy A”
- 24.01.2022: „Jakość wody w laboratoriach akredytowanych – zgodność z normami ISO 17025 i ISO 11133”
- 24.01.2022: „Wykorzystanie chromatografii cienkowarstwowej do szybkiej analizy jakościowej”
- 27.01.2022: „Mycie, suszenie, praca ze szkłem pomiarowym w laboratorium”
- 31.01.2022: „Analiza kannabinoidów w próbkach żywnościowych”
- 04.02.2022: „Western blotting – wskazówki i porady dotyczące optymalizacji procesu”
- 07.02.2022: „ZooMAb innowacyjne rekombinowane przeciwciała monoklonalne”

- 25.02.2022: „Oczyszczanie DNA”

7) Staże naukowe:

- Associate Laboratory LSRE-LCM, Faculty of Engineering, University of Porto
Rua Dr. Roberto Frias, s/n 4200-465 Porto, Portugal
Staż naukowy sfinansowany ze środków projektu „UNIWERSYTET JUTRA II – zintegrowany program rozwoju Uniwersytetu im. Adama Mickiewicza w Poznaniu”
Okres realizacji: 26.06.2023–28.09.2023
Temat projektu: Catalytic conversion of industrial grade sugarcane molasses to HMF.
Zakres obowiązków: preparatyka katalizatorów, charakterystyka fizykochemiczna przygotowanych materiałów, testy katalityczne (reakcja otrzymywania HMF), analiza produktów reakcji metodą HPLC, opracowanie i graficzna prezentacja wyników.
Opiekunowie stażu: prof. M. Fernando R. Pereira oraz dr Katarzyna Morawa Eblagon
- Associate Laboratory LSRE-LCM, Faculty of Engineering, University of Porto
Rua Dr. Roberto Frias, s/n 4200-465 Porto, Portugal
Staż naukowy sfinansowany ze środków programu Erasmus+
Okres realizacji: 09.09.2019–01.12.2019
Temat projektu: Development of bifunctional catalysts for valorization of carbohydrates.
Zakres obowiązków: preparatyka katalizatorów węglowych, charakterystyka fizykochemiczna przygotowanych materiałów, testy katalityczne (konwersja glukozy do HMF), analiza produktów reakcji metodą HPLC, opracowanie i graficzna prezentacja wyników.
Opiekun stażu: dr Katarzyna Morawa Eblagon

8) Współpraca naukowa:

- Associate Laboratory LSRE-LCM, Faculty of Engineering, University of Porto, Portugal
- Institute of Chemistry, Faculty of Chemistry and Geosciences, Vilnius University, Lithuania

9) Nagrody i inne osiągnięcia naukowe:

- Członkostwo w Polskim Towarzystwie Chemicznym od 24.06.2021.
- Aktywny udział w organizacji Nocy Naukowców na Wydziale Chemii UAM (24.09.2021).

- Stypendium naukowe Rektora przyznawane w 2022 roku za wybitne osiągnięcia publikacyjne w 2021 roku.
- Aktywny udział w organizacji Festiwalu Nauki na Wydziale Chemii UAM (19.05.2023).
- Nagroda „Best Poster Award” za prezentację na międzynarodowej konferencji NanoTech Poland 2023 (komunikat pt. „*Modified carbon nanotubes as solid acids for catalytic obtaining of fuel enhancers via glycerol etherification*”).
- Przygotowanie dwóch recenzji artykułu naukowego (dla czasopisma Renewable Energy; IF(2023): 9.0, 5-Year IF: 8.1).

WYKAZ STOSOWANYCH SKRÓTÓW

- **CCVD** – wspomagany katalitycznie proces chemicznego osadzania z fazy gazowej
- **CF** – włókna węglowe
- **CNT** – nanorurki węglowe
- **BDS** – sól diazoniowa kwasu 4-benzenosulfonowego
- **TRGO** – termicznie redukowany tlenek grafenu
- **TRGO_H₂SO₄** – TRGO funkcjonalizowany za pomocą stężonego kwasu siarkowego(VI) w 140 °C przez 20 h (TRGO_SA w publikacji P1)
- **TRGO_H₃PO₄** – TRGO impregnowany 7 % roztworem H₃PO₄ i poddany obróbce termicznej w 800 °C przez 30 minut w atmosferze gazu obojętnego (TRGO_PA w publikacji P1)
- **TRGO_BDS** – TRGO modyfikowany za pomocą BDS w temperaturze otoczenia przez 20 h
- **CF_{i-bu}** – próbka CF otrzymana w procesie CCVD z izobutanu
- **CF_{i-bu}-H₂SO₄** – próbka CF_{i-bu} funkcjonalizowana za pomocą stężonego kwasu siarkowego(VI) w 140 °C przez 20 h
- **CF_{i-bu}-BDS** – próbka CF_{i-bu} funkcjonalizowana za pomocą BDS w 20 °C przez 20 h
- **CF_{et}** – próbka CF otrzymana w procesie CCVD z etylenu
- **CF_{et}-H₂SO₄** – próbka CF_{et} funkcjonalizowana za pomocą stężonego kwasu siarkowego(VI) w 140 °C przez 20 h
- **CF_{et}-BDS** – próbka CF_{et} funkcjonalizowana za pomocą BDS w 20 °C przez 20 h
- **CNT_{NC3100}** – komercyjne nanorurki węglowe (Nanocyl NC3100) o czystości >95 % (NC3100 w publikacji P4)
- **CNT_{NC7000}** – komercyjne nanorurki węglowe (Nanocyl NC7000) o czystości ~90 % (NC7000 w publikacji P4)
- **CNT_{NC7000}-BM** – próbka CNT_{NC7000} poddana obróbce mechanicznej przy użyciu młyna kulowego (NC7000-BM w publikacji P4)
- **CNT_{NC3100}-H₂SO₄(conc.)-180-20h** – próbka CNT_{NC3100} funkcjonalizowana za pomocą stężonego kwasu siarkowego(VI) w 180 °C przez 20 h
- **CNT_{NC7000}-H₂SO₄(conc.)-180-20h** – próbka CNT_{NC7000} funkcjonalizowana za pomocą stężonego kwasu siarkowego(VI) w 180 °C przez 20 h
- **CNT_{NC7000}-BM-H₂SO₄(conc.)-180-20h** – próbka CNT_{NC7000}-BM funkcjonalizowana za pomocą stężonego kwasu siarkowego(VI) w 180 °C przez 20 h
- **CNT_{NC7000}-BM-H₂SO₄(fum.)-100-8h** – próbka CNT_{NC7000}-BM funkcjonalizowana za pomocą dymiącego kwasu siarkowego w 100 °C przez 8 h

- **CNT_{NC7000-BM-Glu/H₂SO₄(fum.)-180-12h}** – próbka CNT_{NC7000-BM} funkcjonalizowana za pomocą dymiącego kwasu siarkowego i w obecności glukozy w 180 °C przez 12 h
- **CNT_{NC7000-BM-Glu/H₂SO₄(5 M)-150-4h}** – próbka CNT_{NC7000-BM} funkcjonalizowana za pomocą 5 M kwasu siarkowego(VI) i w obecności glukozy w 150 °C przez 4 h
- **CNT_{NC3100-BDS-50}** – próbka CNT_{NC3100} funkcjonalizowana za pomocą BDS w 50 °C przez 20 h (NC3100-BDS-50 w publikacji P4)
- **CNT_{NC7000-BDS-50}** – próbka CNT_{NC7000} funkcjonalizowana za pomocą BDS w 50 °C przez 20 h (NC7000-BDS-50 w publikacji P4)
- **CNT_{NC7000-BDS-20}** – próbka CNT_{NC7000} funkcjonalizowana za pomocą BDS w 20 °C przez 20 h (NC7000-BDS-20 w publikacji P4)
- **CNT_{NC7000-BM-BDS-50}** – próbka CNT_{NC7000-BM} funkcjonalizowana za pomocą BDS w 50 °C przez 20 h (NC7000-BM-BDS-50 w publikacji P4)
- **CF_{ini}ox** – włókna węglowe otrzymane w procesie CCVD z gazu LPG i utlenione w strumieniu powietrza w 300 °C
- **MgO/CF** – MgO osadzony na CF otrzymanych w procesie CCVD z gazu LPG (MgO/CF_{ox} w publikacji P3)
- **Cr₂O₃/CF** – Cr₂O₃ osadzony na CF otrzymanych w procesie CCVD z gazu LPG (Cr₂O₃/CF_{ox} w publikacji P3)
- **BaO/CF** – BaO osadzony na CF otrzymanych w procesie CCVD z gazu LPG (BaO/CF_{ox} w publikacji P3)
- **ZnO/CF** – ZnO osadzony na CF otrzymanych w procesie CCVD z gazu LPG (ZnO/CF_{ox} w publikacji P3)
- **EA** – analiza elementarna
- **TG** – analiza termograwimetryczna
- **XRD** – rentgenowska dyfraktometria proszkowa
- **XPS** – rentgenowska spektroskopia fotoelektronów
- **SEM** – skaningowa mikroskopia elektronowa
- **TEM** – transmisyjna mikroskopia elektronowa
- **TEM-HR** – wysokorozdzielcza transmisyjna mikroskopia elektronowa
- **A_{tot}** – kwasowość całkowita (typu Brønsteda) wyrażona w mmol H⁺/g
- **G** – glicerol
- **AA** – kwas octowy
- **IB** – izobuten
- **TBA** – alkohol tert-butyłowy
- **U** – mocznik

- **Glu** – glukoza
- **MAG** – monoolejany glicerolu
- **DAG** – dioleofany glicerolu
- **TAG** – triooleofan glicerolu
- **TBGE** – eterf tert-butylowe glicerolu
- **MTBGE** – eterf mono-tert-butylowe glicerolu
- **DTBGE** – eterf di-tert-butylowe glicerolu
- **TTBGE** – eterf tri-tert-butylowy glicerolu
- **GC** – węglan glicerolu
- **GU** – produkt przejściowy w procesie glicerolizy mocznika
- **By-P** – produkty uboczne w procesie glicerolizy mocznika
- **X_G** – konwersja glicerolu
- **S_x** – selektywność do produktu x
- **Y_x** – wydajność produktu x

STRESZCZENIE

Celem realizowanej pracy doktorskiej były szczegółowe badania dotyczące opracowania nowych heterogenicznych katalizatorów na bazie węgla, użytecznych w wybranych procesach waloryzacji glicerolu, tj. estryfikacji glicerolu za pomocą kwasu octowego, eteryfikacji glicerolu alkoholem tert-butylovym i glicerolizie mocznika, prowadzących do wartościowych związków chemicznych. Podjęta tematyka jest szczególnie ważna ze względu na konieczność zagospodarowania glicerolu, który otrzymywany jest ubocznie w procesie produkcji biodiesla i występuje obecnie na rynku w znacznym nadmiarze (co zagraża rentowności przemysłu biodiesla). Zasadniczym etapem prowadzonych prac było określenie zależności pomiędzy właściwościami fizykochemicznymi otrzymanych materiałów a ich aktywnością katalityczną w danym procesie waloryzacji glicerolu. Najważniejsze rezultaty przeprowadzonych prac podsumowano w niniejszej rozprawie doktorskiej, która obejmuje cykl 5 spójnych tematycznie artykułów naukowych (P1–P5) oraz komentarz do tych prac.

W pierwszej publikacji (P1) przedstawiono wyniki badań otrzymane dla procesu estryfikacji glicerolu za pomocą kwasu octowego. Reakcję realizowano w obecności katalizatora, którym był termicznie zredukowany tlenek grafenu (TRGO), funkcjonalizowany różnymi czynnikami (tj. kwasem siarkowym(VI), generowaną in situ solą diazoniową (BDS) lub kwasem fosforowym(V)). Przeprowadzone badania udowodniły, że zastosowane metody modyfikacji były efektywne i skutkowały wygenerowaniem dość znacznej kwasowości całkowitej próbek, wynikającej z wprowadzenia ugrupowań zawierających S, O i/lub P na powierzchnię TRGO. Wykazano, że kluczowy wpływ na przebieg procesu estryfikacji glicerolu za pomocą kwasu octowego ma rodzaj wprowadzonych ugrupowań powierzchniowych, tj. proces estryfikacji, najefektywniej zachodził w obecności materiałów z silnie kwasowymi grupami ($-SO_3H$). Potwierdzono, że próbka TRGO modyfikowana BDS pracowała najefektywniej we wspomnianym procesie (w związku wysoką zawartością grup sulfonowych) i nie traciła aktywności katalitycznej przynajmniej przez 4 cykle reakcyjne.

Proces eteryfikacji glicerolu za pomocą alkoholu tert-butylovogo został omówiony w artykułach naukowych P2, P4 i P5. W pierwszym z nich (P2), w roli katalizatorów zastosowano włókna węglowe, otrzymane laboratoryjnie w procesie CCVD z etylenu lub izobutanu, które następnie poddano sulfonowaniu różnymi czynnikami (H_2SO_4 lub BDS). Udowodniono, że modyfikacja za pomocą BDS jest bardziej skuteczną metodą wprowadzania ugrupowań zawierających siarkę do struktury CF niż modyfikacja kwasem siarkowym(VI).

Co więcej, ujawniono, że zastosowanie etylenu skutkowało uzyskaniem próbki węglowej o większej podatności na funkcjonalizację niż w przypadku użycia izobutanu. Materiały modyfikowane BDS (o najwyższym stopniu funkcjonalizacji) pracowały najefektywniej w badanym procesie. Niemniej jednak, w związku z niejednorodną strukturą próbek (obecność włókien o różnych średnicach oraz obecność niewielkiej ilości nanorurek węglowych), nie było możliwe jednoznaczne określenie wpływu wyjściowego węgla na funkcjonalizację i aktywność w badanej reakcji.

W związku z powyższym w kolejnych etapach pracy do preparatyki katalizatorów użytecznych w procesie eteryfikacji glicerolu za pomocą alkoholu tert-butyłowego wykorzystano komercyjne nanorurki węglowe (CNT). Próbki te charakteryzowały się jednorodną strukturą, co ułatwiło ocenę uzyskanych wyników. Materiał wyjściowy funkcjonalizowano za pomocą H_2SO_4 lub generowanej in situ soli diazoniowej (BDS), a otrzymane wyniki przedstawiono w publikacjach P4 i P5. Podjęto również próbę zwiększenia podatności CNT na funkcjonalizację stosując wstępną obróbkę mechaniczną materiału (za pomocą młyna kulowego). Zastosowany zabieg pozytywnie wpłynął na efektywność wprowadzania siarki do struktury węgla, przy czym miało to związek z rozdrobnieniem wiązek CNT i łamaniem pojedynczych włókien, skutkującym wygenerowaniem nowych krawędzi zdolnych do funkcjonalizacji. Co więcej, włączenie glukozy do modyfikacji CNT za pomocą H_2SO_4 dodatkowo uskuteczniło funkcjonalizację, co wynikało z osadzenia węgla otrzymanego z glukozy na CNT, który działał jak „klej” dla grup funkcyjnych. Najbardziej efektywną metodą modyfikacji CNT okazało się zastosowanie BDS, skutkujące wprowadzeniem znacznej ilości siarki do struktury węgla w formie grup $-SO_3H$. W obecności najbardziej aktywnych próbek (wybranych CNT modyfikowanych BDS) uzyskano wyniki konwersji glicerolu oraz wydajności do pożądaných eterów tert-butyłowych przewyższające te uzyskane przy użyciu komercyjnego katalizatora (Amberlyst-15). Co istotne, próbki te nie traciły swojej aktywności przynajmniej przez kilka cykli reakcyjnych. Udowodniono, że grupy sulfonowe są kluczowe w procesie eteryfikacji glicerolu za pomocą alkoholu tert-butyłowego. Niemniej jednak obecność tlenowych ugrupowań również miała pozytywny wpływ na przebieg reakcji, najprawdopodobniej wskutek zwiększenia hydrofilowości materiałów, ułatwiającej adsorpcję reagentów na powierzchni katalizatora.

Publikacja P3 dotyczyła preparatyki nowych katalizatorów na bazie węgla dedykowanych do zastosowania w procesie glicerolizy mocznika do węglanu glicerolu (GC). Opracowano układy składające się z tlenków wybranych metali (Ba, Cr, Mg i Zn) osadzonych

na włóknach węglowych (CF) otrzymanych z gazu LPG w procesie CCVD. Wszystkie otrzymane katalizatory były aktywne w omawianym procesie konwersji glicerolu, jednak uzyskane wyniki katalityczne nieco różniły się pomiędzy próbkami. Wynikało to najprawdopodobniej z różnic w dystrybucji ugrupowań kwasowo-zasadowych w tych materiałach. Udowodniono również, że zastosowanie w reakcji utlenionego nośnika węglowego CF (samodzielnie) miało pozytywny wpływ na przebieg procesu, gdyż skutkowało znacznym zwiększeniem selektywności do GC w porównaniu z reakcją przeprowadzoną bez użycia katalizatora. Dla najefektywniej pracującej próbki ZnO/CF przeprowadzono optymalizację warunków reakcji. Zaprezentowano również dwa sposoby odprowadzania amoniaku (produkt uboczny) ze środowiska reakcyjnego, uwzględniając przepuszczanie gazu obojętnego (Ar) przez reaktor lub przez mieszaninę reakcyjną. Udowodniono, że zastosowanie tej drugiej metody znacząco ogranicza reakcje uboczne.

ABSTRACT

The submitted doctoral dissertation aimed at detailed research on the development of novel heterogeneous carbon-based catalysts for selected glycerol valorization processes, including the esterification of glycerol with acetic acid, the etherification of glycerol with tert-butyl alcohol, and the glycerolysis of urea, all leading to valuable chemical compounds. This topic is of particular importance due to the need for efficient management of glycerol, a by-product in the biodiesel production process, which is currently on the market in significant excess, potentially threatening the profitability of the biodiesel industry. The main purpose of the work was to establish the relationship between the physicochemical properties of the obtained samples and their catalytic activity in the selected glycerol valorization processes. The most significant findings are summarized in the doctoral dissertation, which includes a series of five thematically related scientific articles (P1–P5) along with appropriate commentary.

Article P1 presents the results of the glycerol esterification process with acetic acid. The reaction was carried out in the presence of thermally reduced graphene oxide (TRGO) functionalized with various agents, such as sulfuric acid, in situ generated diazonium salt (BDS), or phosphoric acid, serving as catalysts. Physicochemical analyses of the samples confirmed that the applied modifications were effective, leading to a significant increase in the total acidity of the TRGO due to the introduction of S-, O-, and/or P-containing functional groups onto its surface. It was demonstrated that the type of surface groups had a key impact on glycerol esterification with acetic acid. Specifically, the esterification process was most efficient in the presence of catalysts containing strongly acidic groups, i.e., $-\text{SO}_3\text{H}$ functionalities. The BDS-modified TRGO exhibited the best catalytic performance in the process, attributed to the high content of sulfonic groups, and maintained its catalytic activity for at least four reaction cycles.

Etherification of glycerol with tert-butyl alcohol over fibrous carbon catalysts is discussed in scientific articles P2, P4, and P5.

The P2 article shows the results of using carbon fibers (CF) obtained through the CCVD process from ethylene or isobutane and modified with H_2SO_4 or BDS. It was found that sulfonation with BDS was a more effective method for introducing sulfur-containing moieties into the CF structure compared to modification with sulfuric acid. Furthermore, it was demonstrated that the carbon fibers produced from ethylene were more susceptible to functionalization than those from isobutane. The BDS-modified materials, which presented

the highest functionalization degree with $\text{-SO}_3\text{H}$ groups, worked most effectively in the tested process. However, due to the variable structure of the samples (i.e., the presence of fibers with different diameters and a small number of carbon nanotubes), it was not possible to clearly determine the impact of the initial carbon type on the functionalization of CF and their activity in the tested reaction.

In the subsequent stages of work, commercial carbon nanotubes (CNT) were used to prepare functionalized catalysts for the etherification of glycerol with tert-butyl alcohol. These samples had a uniform structure, which facilitated a more accurate assessment of the results, and the outcomes are presented in articles P4 and P5. Additionally, an attempt was made to increase the CNTs' susceptibility to functionalization through their mechanical pretreatment (using a ball mill). This method positively impacted the efficiency of sulfur incorporation into the carbon structure by fragmenting CNT bundles and breaking individual fibers, thereby generating new edges susceptible to functionalization. Furthermore, adding glucose to carbon nanotubes during their modification with H_2SO_4 improved CNTs' functionalization, as a carbonaceous matter derived from glucose and deposited onto the CNT acted as a "glue" for the introduced groups. The most effective method of modification of CNT was the use of BDS, which introduced a significant amount of sulfur in the form of $\text{-SO}_3\text{H}$ groups into the carbon structure. In the presence of the most active samples (selected CNT modified with BDS), glycerol conversion and yields of the desired tert-butyl ethers exceed those obtained with a commercial catalyst Amberlyst-15. Importantly, these CNT samples retained their activity over several reaction cycles. It was demonstrated that sulfonic groups are crucial for the etherification of glycerol with tert-butyl alcohol. However, the presence of oxygen-containing species also had a positive effect on the reaction, most likely due to the increased hydrophilicity of the materials, which facilitated the adsorption of reagents on the catalyst surface and enabled their contact with active sites.

Article P3 presents the development of novel carbon-based catalysts for the glycerolysis of urea to glycerol carbonate (GC). Systems consisting of oxides of selected metals (Ba, Cr, Mg, and Zn) deposited on carbon fibers (CF) obtained from LPG gas via the CCVD process were prepared in this study. All the catalysts were active in the urea glycerolysis, however, the catalytic results varied slightly between the samples. These differences were most likely due to variations in the distribution of acid-base groups within the materials. It was also shown that the use of oxidized carbon support (CF) in the reaction positively impacted the process, significantly increasing the selectivity to GC compared to the reaction without a catalyst. The reaction conditions were optimized for the best-working sample, i.e., ZnO/CF.

Two methods of removing ammonia (by-product) from the reaction medium were also presented: passing inert gas (Ar) through the reactor or through the reaction mixture. It was demonstrated that the latter method significantly reduces side reactions.

WYKAZ PUBLIKACJI BĘDĄCYCH PODSTAWĄ ROZPRAWY DOKTORSKIEJ

- P1) A. Malaika, K. Ptaszyńska, J. Gaidukevič, M. Kozłowski, *The impact of surface groups of functionalized graphene on glycerol acetylation*, *Fuel*, 2022, 313(73), 122987.
DOI: <https://doi.org/10.1016/j.fuel.2021.122987>
Punkty MNiSW: 140
IF(2022): 7.4
5-Year IF: 6.5
- P2) K. Ptaszyńska, A. Malaika, M. Kapska, M. Kozłowski, *SO₃H-functionalized carbon fibers for the catalytic transformation of glycerol to glycerol tert-butyl ethers*, *Scientific Reports*, 2023, 13(1), 565.
DOI: <https://doi.org/10.1038/s41598-023-27432-7>
Punkty MNiSW: 140
IF(2023): 3.8
5-Year IF: 4.3
- P3) K. Ptaszyńska, A. Malaika, K. Kozigrodzka, M. Kozłowski, *A green approach to obtaining glycerol carbonate by urea glycerolysis using carbon-supported metal oxide catalysts*, *Molecules*, 2023, 28(18), 6534.
DOI: <https://doi.org/10.3390/molecules28186534>
Punkty MNiSW: 140
IF(2023): 4.2
5-Year IF: 4.6
- P4) K. Ptaszyńska, A. Malaika, K. Morawa Eblagon, J. L. Figueiredo, M. Kozłowski, *Promoting effect of ball milling on the functionalization and catalytic performance of carbon nanotubes in glycerol etherification*, *Molecules*, 2024, 29(7), 1623.
DOI: <https://doi.org/10.3390/molecules29071623>
Punkty MNiSW: 140
IF(2023): 4.2
5-Year IF: 4.6
- P5) K. Ptaszyńska, K. Morawa Eblagon, A. Malaika, J. L. Figueiredo, M. Kozłowski, *The role of mechanochemical treatment of carbon nanotubes in promoting glycerol etherification*, *Catalysis Science & Technology*, 2024, 14(11), 3184–3200.
DOI: <https://doi.org/10.1039/D4CY00203B>
Punkty MNiSW: 140
IF(2023): 4.4
5-Year IF: 5.5

CZEŚĆ LITERATUROWA

1. Wprowadzenie

1.1. Wpływ stosowania paliw kopalnych na gospodarkę i środowisko

Paliwa kopalne stosowane tradycyjnie w roli źródeł energii obecnie tracą na znaczeniu, na co wpływ ma kilka czynników. Po pierwsze, zasoby ropy naftowej, węgla kamiennego i gazu ziemnego ulegają stopniowemu wyczerpywaniu. Ponadto są terytorialnie skoncentrowane oraz politycznie zależne, co stanowi poważny problem dla stabilności gospodarki. Po drugie, spalanie paliw kopalnych jest współodpowiedzialne za obserwowane w ostatnich latach gwałtowne zmiany klimatyczne, a także złą jakość powietrza, wpływającą na zwiększenie zachorowalności oraz umieralności [1,2,3]. Zapewnienie ciągłości dostaw energii oraz zabezpieczenie środowiska naturalnego stanowią duże wyzwanie dla rządów państw i sektora energetycznego.

Wykorzystanie odnawialnych źródeł energii (OZE), takich jak energia wiatru, słońca, wody czy geotermalna, proponowane jest jako bezpieczna, zrównoważona i łatwo dostępna alternatywa dla paliw kopalnych. Należy jednak zaznaczyć, że funkcjonalność OZE jest pogodowo zależna, a odpowiednie nasłonecznienie czy siła wiatru nie zawsze mogą być spełnione [1,3]. Rozwiązaniem zyskującym na znaczeniu od kilkunastu lat jest również wykorzystanie biomasy jako źródła energii. Biomasa stosowana jest m.in. do otrzymywania paliw płynnych, takich jak np. biodiesel [3,4].

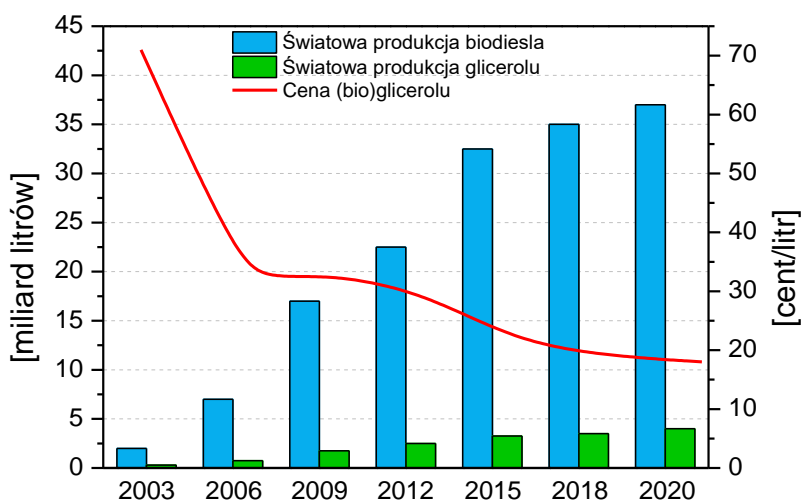
1.2. Rozwój przemysłu biodiesla – odnawialnego źródła energii

Zwyczajowo biodiesel otrzymywany jest z tłuszczów zwierzęcych lub olejów roślinnych w procesie ich transestryfikacji z prostymi alkoholami i w obecności odpowiednich katalizatorów [5]. Co istotne, jako surowiec w ww. procesie można stosować również odpadowe oleje posmażalnicze, dlatego branża biodiesla ma olbrzymi potencjał, by nie konkurować bezpośrednio z przemysłem spożywczym, kosmetycznym czy farmaceutycznym, wykorzystującymi czyste surowce tłuszczowe [4,6,7,8]. Podkreślić trzeba, że w reakcji transestryfikacji olejów i tłuszczów poza biodieslem otrzymywany jest również produkt uboczny w postaci (bio)glicerolu (propano-1,2,3-triol). Stanowi on około 10% mieszaniny poreakcyjnej [9,10].

Przedstawione na Rys. 1 dane wskazują, że produkcja biodiesla w pierwszych dwóch dekadach XXI wieku gwałtownie wzrastała na przestrzeni lat, osiągając wartość ~37 miliardów litrów w 2020 roku [10]. Według danych udostępnionych przez Międzynarodową Agencję Energetyczną (IEA), również w najbliższych latach, mimo coraz

większej popularności innych rozwiązań, globalna produkcja tego biopaliwa będzie wysoka (szacuje się, że w 2025 r., na świecie wyprodukowane zostanie około 46 miliardów litrów biodiesla) [11].

Jak zaznaczono na Rys. 1, sukcesywnemu wzrostowi podaży rynkowej biodiesla w ostatnich kilkunastu latach, towarzyszył wzrost podaży (bio)glicerolu. Glicerol znajduje wprawdzie zastosowanie w wielu branżach przemysłu, m.in. spożywczej, kosmetycznej czy farmaceutycznej, ale obecne zapotrzebowanie na ten surowiec jest dużo mniejsze niż jego rezerwy. Problemem jest także czystość otrzymywanego (bio)glicerolu i koszty jego oczyszczania dla ww. zastosowań. Sytuacja ta wymusza rozwinięcie nowych kierunków zagospodarowania glicerolu pochodzącego z produkcji biodiesla [8,12,13]. Pozwoli to uniknąć problemów związanych m.in. ze składowaniem i wykorzystaniem (bio)glicerolu, a także zwiększy rentowność przemysłu produkcji biodiesla. Argumentem stojącym za sensownością nowych metod wykorzystania (bio)glicerolu jest także coraz niższy koszt tego surowca (Rys. 1) [10,14].



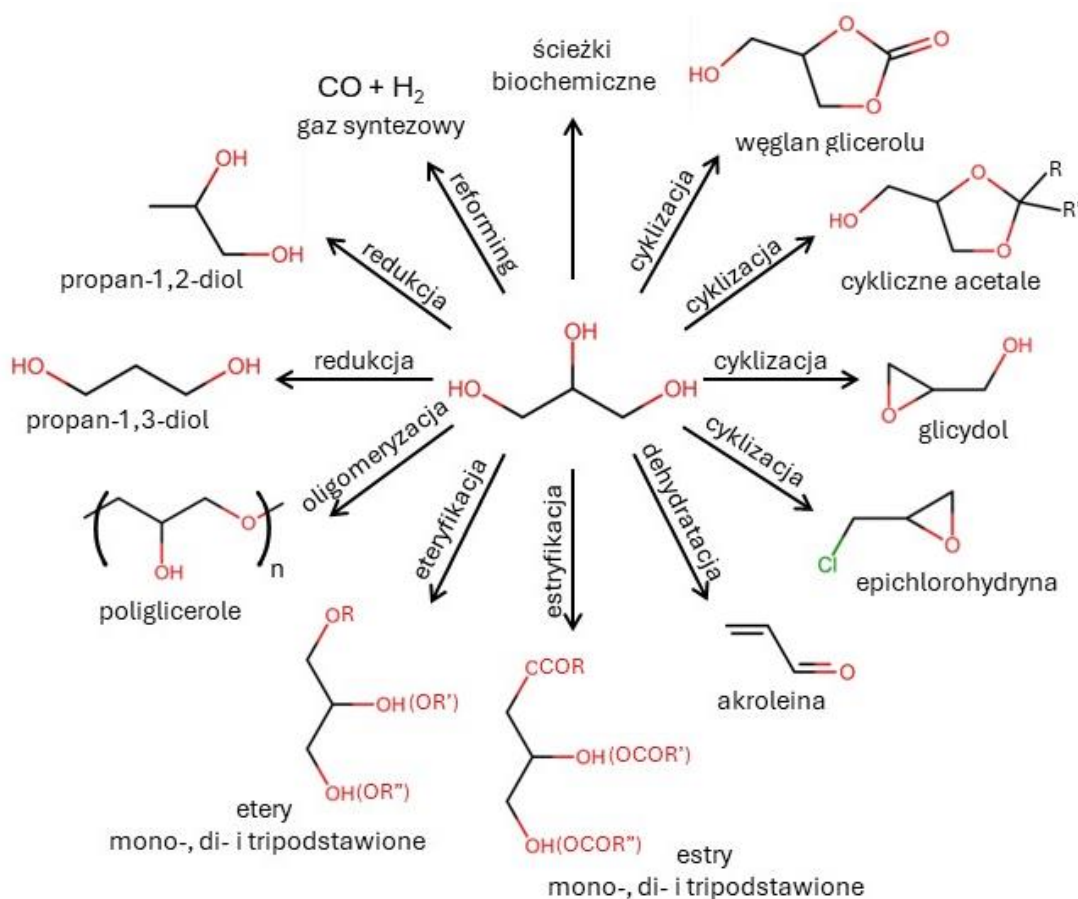
Rys. 1. Światowa produkcja biodiesla [10]

1.3. Sposoby waloryzacji glicerolu – związku otrzymywanego ubocznie w procesie produkcji biodiesla

Prowadzone w ostatnich latach badania nad reaktywnością glicerolu wykazały, że związek ten może być z powodzeniem przekształcany w wiele wartościowych chemikaliów, co podsumowane zostało na Rys. 2 [12,13].

Jednymi z ważniejszych procesów transformacji glicerolu są: i) estryfikacja glicerolu do odpowiednich octanów, ii) eteryfikacja glicerolu do eterów tert-butyłowych glicerolu oraz iii) gliceroliza mocznika do węglanu glicerolu. Otrzymywane pochodne glicerolowe mają szereg zastosowań przemysłowych, niemniej jednak wciąż brakuje dobrze

opracowanych rozwiązań, które pozwoliłyby na efektywne otrzymywanie tych związków na większą skalę. Wobec powyższego niniejsza rozprawa doktorska skoncentrowana była na badaniach procesów waloryzacji glicerolu na drodze estryfikacji, eteryfikacji oraz glicerolizy mocznika w obecności katalizatorów. Ogólna charakterystyka tych procesów i uzyskane wyniki badań katalitycznych zostały szczegółowo omówione w kolejnych rozdziałach tej pracy oraz w załączonych artykułach naukowych (P1–P5).

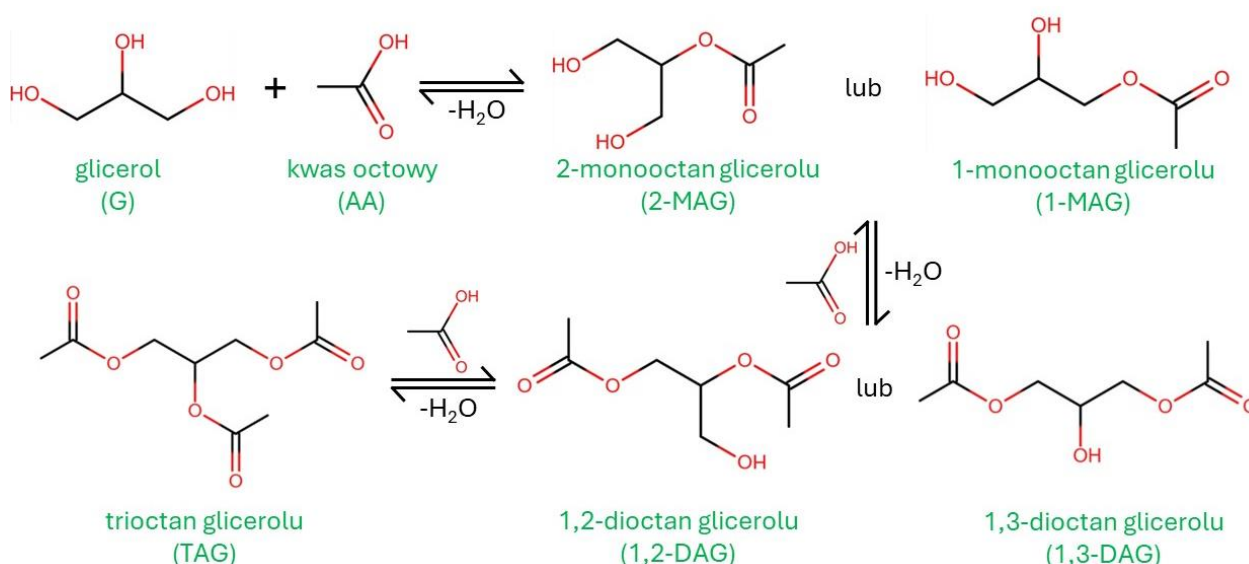


Rys.2. Nowe metody przekształcania glicerolu [12,13]

1.3.1. Estryfikacja glicerolu do octanów glicerolu

Reakcja estryfikacji glicerolu do octanów może być realizowana z zastosowaniem kwasu octowego lub bardziej reaktywnego bezwodnika octowego [15]. Użycie bezwodnika jest jednak mniej preferowane, gdyż surowiec ten jest stosowany do produkcji związków chemicznych o działaniu narkotycznym, stąd jego dostępność w niektórych państwach może być ograniczona. Dodatkowo reakcja glicerolu z bezwodnikiem octowym jest silnie egzotermiczna i trudna do kontrolowania [16,17]. W związku z powyższym czynnikiem estryfikującym najczęściej jest kwas octowy.

Proces estryfikacji glicerolu (G) za pomocą kwasu octowego (AA) wykazuje efekt autokatalityczny i z tego względu pewną konwersję glicerolu można zaobserwować nawet bez użycia katalizatora [18]. Niemniej jednak, aby uzyskać satysfakcjonujące wyniki, reakcję zwyczajowo prowadzi się w obecności katalizatora kwasowego, przy czym jego moc jest kluczowa dla zapewnienia wysokiej wydajności procesu [17,19]. Produktami omawianej reakcji są monoactany, dioctany oraz trioctan glicerolu (odpowiednio: MAG, DAG oraz TAG), które otrzymywane są na drodze reakcji następczych (Rys. 3) [20]. Wszystkie te związki znajdują szerokie zastosowanie w przemyśle, m.in. w sektorze spożywczym, kosmetycznym czy farmaceutycznym. Szczególnie pożądanymi pochodnymi są jednak wyżej podstawione produkty (DAG i TAG), które stosuje się jako cenne dodatki paliwowe. DAG i TAG m.in. poprawiają parametry paliw (takie jak np. lepkość i właściwości przeciwstukowe) oraz redukują emisję szkodliwych substancji podczas spalania paliw [17,19,21,22].



Rys. 3. Schemat reakcji estryfikacji glicerolu za pomocą kwasu octowego [20]

1.3.1.1. Katalizatory stosowane w procesie estryfikacji glicerolu

Zgodnie z dostępnymi danymi literaturowymi najwyższe wydajności octanów glicerolu w reakcji estryfikacji glicerolu uzyskiwano w obecności kwasu siarkowego lub kwasu p-toluenosulfonowego (TsOH) [15,23]. Na przykład: Sun i współpracownicy [23] uzyskali 92,5 % wydajność TAG w obecności TsOH po 8 h reakcji w 120 °C, stosując stosunek molowy reagentów G:AA = 1:6. Niemniej jednak zastosowanie ciekłych kwasów wiąże się z wieloma trudnościami wynikającymi z ogólnych ograniczeń katalizatorów homogenicznych (np. problemy z oddzieleniem katalizatora od mieszaniny poreakcyjnej czy brak możliwości powtórnego użycia). Kłopotliwa może okazać się również natura tych związków

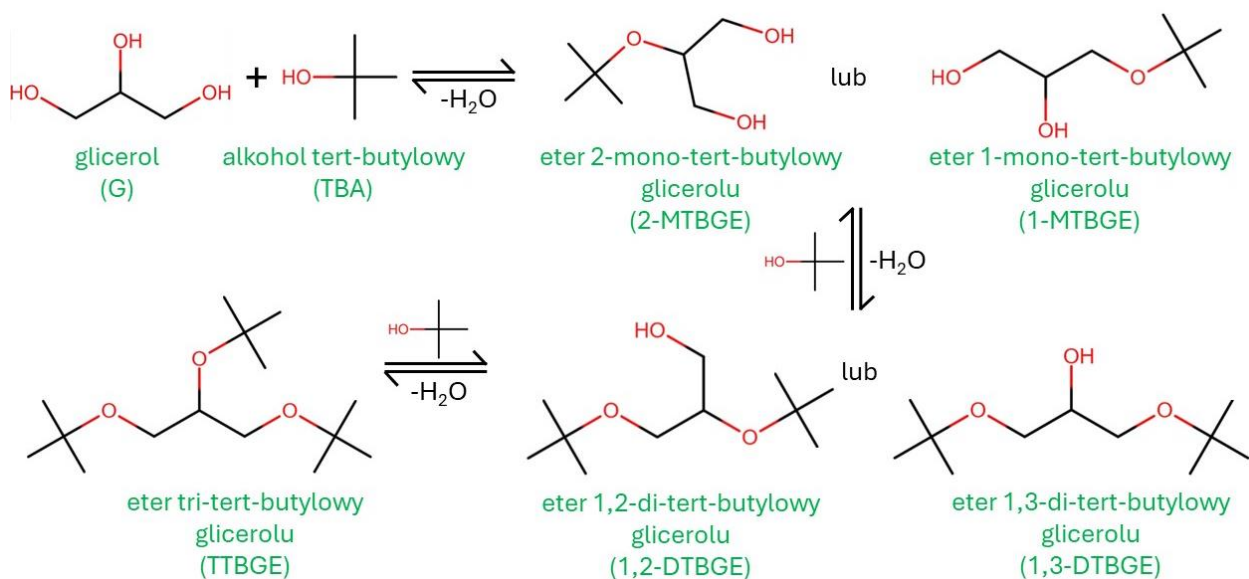
(np. właściwości korozyjne, konieczność neutralizacji generująca ogromne ilości odpadów) [22,24]. Sposobem na radzenie sobie z wyżej wymienionymi ograniczeniami jest opracowanie odpowiednich systemów heterogenicznych.

Wśród najefektywniejszych stałych katalizatorów kwasowych testowanych w procesie estryfikacji glicerolu za pomocą kwasu octowego znajdują się takie materiały jak: zeolity, polimery kwasowe, żywice jonowymienne czy sulfonowane krzemionki [25,26,27,28]. Na przykład: Mou i współpracownicy [25] przygotowali stały kwas na bazie polidwinylobenzenu i uzyskali 88 % wydajność DAG+TAG w zoptymalizowanych warunkach reakcji, tj. po 3 h reakcji w 110 °C, stosując 5 % wag. katalizatora (względem masy glicerolu) oraz stosunek molowy reagentów G:AA = 1:6. Z kolei Bedogni i współpracownicy [26] testowali komercyjny katalizator Amberlyst-36 i osiągnęli 98,8 % konwersję glicerolu z 93 % wydajnością do produktów DAG+TAG po 4 h reakcji w 120 °C (G:AA = 1:6). Niestety, w tym przypadku autorzy zaobserwowali nieodwracalne zmiany w składzie testowanej próbki po jej odzyskaniu, świadczące o stopniowym wymywaniu sulfonowych grup funkcyjnych, odpowiedzialnych za aktywność próbki w procesie. W związku z powyższym w kolejnych cyklach reakcyjnych odnotowano znacząco gorsze wyniki katalityczne. Gautam i współpracownicy [27] osiągnęli 98,3 % konwersję glicerolu po 5 h reakcji w 120 °C, używając w roli katalizatora procesu zeolit ZSM-5 modyfikowany cerem. Niemniej jednak osiągnięcie tych imponujących wyników wymagało zastosowania dość dużej ilości katalizatora (8 % wag. względem masy glicerolu) oraz znacznego nadmiaru środka estryfikującego (9-krotnego). Popova i współpracownicy [28] uzyskali całkowitą konwersję glicerolu oraz ~80 % selektywność do DAG+TAG w obecności sulfonowanej mezoporowatej krzemionki SBA-15 po 3 h procesu. Warto jednak zauważyć, że osiągnięcie tych satysfakcjonujących wyników wymagało zastosowania wysokiej temperatury (130 °C), a jej obniżenie skutkowało drastycznym spadkiem wydajności reakcji.

1.3.2. Eteryfikacja glicerolu do eterów tert-butyłowych glicerolu

Ważnym procesem waloryzacji glicerolu jest także jego eteryfikacja, prowadząca do eterów tert-butyłowych glicerolu. Proces ten może być realizowany za pomocą izobutenu (IB) lub alkoholu tert-butyłowego (TBA) jako środków eteryfikujących [29,30]. Niemniej jednak, ze względów ekonomicznych i ekologicznych, preferowany jest wybór tego drugiego. Co więcej, stosowanie TBA jest bardziej praktyczne, gdyż użycie IB (występującego w fazie gazowej) wymaga specjalnego podejścia umożliwiającego mieszanie tego związku z glicerolem [30,31]. Omawiana reakcja, niezależnie od stosowanego środka eteryfikującego,

najefektywniej zachodzi w obecności silnie kwasowych katalizatorów Brønsteda w podwyższonej temperaturze, a produktami reakcji są odpowiednie etery tert-butyłowe glicerolu (mono-, di-, lub tripodstawione; odpowiednio MTBGE, DTBGE lub TTBGE). Związki te (podobnie jak octany glicerolu) stanowią przyjazne dla środowiska komponenty paliwowe [29,32,33]. Tak jak w przypadku reakcji estryfikacji glicerolu, di- i tri-podstawione pochodne otrzymywane są w wyniku reakcji następczych, jak przedstawiono na Rys. 4. Ze względu na dobrą mieszalność z paliwami (benzyną, dieslem lub biodieslem), związki wyżej podstawione (tj. DTBGE oraz TTBGE) są szczególnie pożądanymi produktami reakcji [29,33,34]. Niemniej jednak etery mono-tert-butyłowe glicerolu, stosowane w odpowiedniej mieszance z eterami di-tert-butyłowymi i tri-tert-butyłowymi glicerolu lub przekształcone w odpowiednie pochodne, również z powodzeniem mogą być wykorzystywane w sektorze paliwowym [33,35]. Warto także zauważyć, że etery tert-butyłowe glicerolu są uważane za bardziej ekologiczne substytuty eteru metylo-tert-butyłowego (MTBE), ważnego komercyjnego dodatku paliwowego, którego neutralność środowiskowa w niektórych państwach jest kwestionowana [29,34,35].



Rys. 4. Schemat reakcji eteryfikacji glicerolu za pomocą alkoholu tert-butyłowego

Jednym z ważniejszych czynników wpływających na efektywną produkcję eterów tert-butyłowych glicerolu (TBGE) jest typ zastosowanego katalizatora (reakcja bez użycia katalizatora praktycznie nie zachodzi) [36]. Ze względu na wspomniane już wcześniej trudności związane ze stosowaniem katalizatorów homogenicznych, w pracach poświęconych eteryfikacji glicerolu szczególną uwagę koncentrowano na opracowaniu odpowiednich katalizatorów heterogenicznych.

1.3.2.1. Katalizatory stosowane w procesie eteryfikacji glicerolu

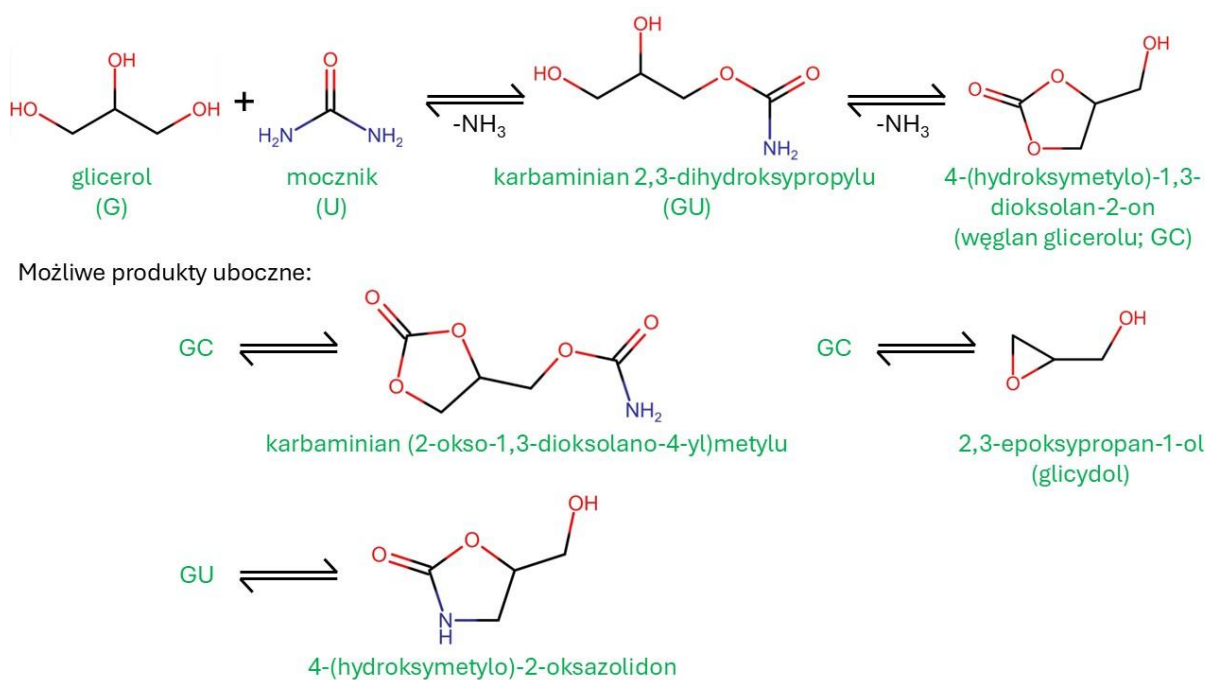
Jednym z chętniej stosowanych w eteryfikacji glicerolu stałych katalizatorów kwasowych jest komercyjny katalizator Amberlyst-15 wykazujący wysoką kwasowość (4,7 mmol/g), wynikającą z obecności sulfonowych grup funkcyjnych (-SO₃H) [37,38]. Gonçaves i współpracownicy [32] wykazali, że wykorzystując ten materiał, po 4 h procesu prowadzonego w temperaturze 120 °C, przy stosunku molowym reagentów TBA:G równym 4:1 i przy użyciu 5 % wag. katalizatora (w przeliczeniu na masę gliceryny), można uzyskać wydajność DTBGE+TTBGE wynoszącą około 12 %. Z kolei Estevez i współpracownicy [30] testowali sulfonowane krzemionki hybrydowe i w przypadku najaktywniejszej próbki osiągnęli 98 % konwersję glicerolu i około 28 % wydajność DTBGE+TTBGE (stosując 5 % wag. katalizatora i temperaturę procesu wynoszącą 75 °C). Niemniej jednak w celu osiągnięcia tych wyróżniających się wyników, autorzy musieli wydłużyć czas reakcji aż do 24 h. Co istotne, w pracy zwrócono uwagę na kluczowy wpływ kwasowości testowanych materiałów oraz ich hydrofilowości na postęp reakcji. Z kolei Liu i współpracownicy [39] zastosowali w reakcji komercyjny katalizator NKC-9 (w ilości jedynie 0,5 % wag. względem masy glicerolu), co skutkowało prawie 60 % konwersją glicerolu i około 7 % wydajnością do najbardziej pożądaných eterów po 24 h reakcji prowadzonej w temperaturze 80 °C. Co ważne, autorzy udowodnili, że użycie w reakcji TBA zamiast IB utrudnia przebieg reakcji niepożądanych.

1.3.3. Gliceroliza mocznika

Reakcja glicerolu z mocznikiem cieszy się w ostatnim czasie coraz większym zainteresowaniem badaczy, co spowodowane jest kilkoma czynnikami. Po pierwsze, proces ten wykorzystuje łatwo dostępne i tanie substancje odpadowe (poza glicerolem także dwutlenek węgla i amoniak, które wykorzystuje się do produkcji mocznika) [40]. Po drugie, reakcja umożliwia przyjazną dla środowiska produkcję węglanu glicerolu (4-(hydroksymetylo)-1,3-dioksolan-2-on; GC), czyli związku, który ma szerokie zastosowanie w przemyśle, np. jako wysokowrzący rozpuszczalnik polarny, półprodukt w syntezie organicznej, a także w produkcji poliwęglanów, poliuretanów, środków powierzchniowo czynnych i kosmetyków [40,41,42]. W rezultacie gliceroliza mocznika zastępuje inną metodę otrzymywania węglanu glicerolu, wykorzystującą toksyczny fosgen [42].

Reakcja otrzymywania węglanu glicerolu z glicerolu i mocznika zachodzi poprzez wytworzenie produktu przejściowego (karbaminian 2,3-dihydroksypropylu; GU), a etap ten,

według doniesień literaturowych, zachodzi samorzutnie z dużą szybkością. Efektywne przekształcenie GU do węglanu glicerolu wymaga już jednak użycia katalizatora [42,43]. Dla przykładu: Hammond i współpracownicy [42] osiągnęli w reakcji glicerolu z mocznikiem prowadzonej w temperaturze 150 °C bez użycia katalizatora dość znaczną konwersję glicerolu wynoszącą ok. 60 % i jedynie 36 % selektywność do GC po 4 h. Należy również wspomnieć, że w procesie glicerolizy mocznika możliwe jest także zachodzenie reakcji ubocznych [44,45]. Schemat reakcji otrzymywania GC z uwzględnieniem wszystkich możliwych reakcji ubocznych przedstawiono na Rys. 5.



Rys. 5. Schemat reakcji glicerolu z mocznikiem oraz możliwe produkty uboczne [44,45]

Jednym ze sposobów radzenia sobie z ww. trudnościami (i w konsekwencji zwiększenia wydajności węglanu glicerolu) jest opracowanie selektywnego katalizatora reakcji oraz dobór odpowiednich warunków procesu. Według doniesień literaturowych możliwych jest kilka mechanizmów reakcji glicerolu z mocznikiem (w zależności od użytego katalizatora), tj. proces może zachodzić w obecności: i) katalizatorów z kwasowymi miejscami aktywnymi Lewisa, ii) katalizatorów z zasadowymi miejscami aktywnymi Lewisa lub iii) z udziałem katalizatora dwufunkcyjnego [40,46,47,48]. Istotnym parametrem determinującym wydajność procesu jest także temperatura. Według doniesień literaturowych zbyt niska utrudnia aktywację reagentów do reakcji, a zbyt wysoka potęguje zachodzenie reakcji ubocznych [43,45,47].

1.3.3.1. Katalizatory stosowane w procesie glicerolizy mocznika

W procesie glicerolizy mocznika najlepsze rezultaty uzyskiwano w obecności katalizatora typu LaCl_3 (95,4 % konwersja glicerolu i niemal 100 % selektywność do GC) lub ZnCl_2 (80,2 % wydajność GC z 99,7 % selektywnością do tego produktu). Warto jednak wspomnieć, że według dostępnych raportów, procesy z użyciem wskazanych wyżej katalizatorów zachodzą na drodze homogenicznej [43,49]. Z tego względu obecnie prowadzone badania skupiają się na próbach opracowania nowych aktywnych układów heterogenicznych dla reakcji glicerolu z mocznikiem. Na przykład: Wang i współpracownicy [48] testowali w procesie glicerolizy mocznika stałe tlenki lantanu i udowodnili, że odpowiednia aktywacja próbki w temperaturze 600 °C skutkowałą wygenerowaniem imponującej aktywności katalizatora, umożliwiającą uzyskanie ~90 % wydajności GC po 4 h reakcji prowadzonej w 140 °C. Ponadto autorzy zaprezentowali ciekawy sposób odprowadzania amoniaku ze środowiska reakcyjnego z wykorzystaniem próżni. Zastosowane rozwiązanie skutkowało przesunięciem równowagi reakcji w kierunku tworzenia węglanu glicerolu z jednoczesnym ograniczeniem zachodzenia niepożądanych reakcji ubocznych. Kondawar i współpracownicy [50] testowali właściwości katalityczne serii mezoporowatych krzemionek MCM-41 zawierających metale przejściowe (Cu, Ni i Zn). Najlepiej pracująca próbka (Zn/MCM-41) pozwoliła na osiągnięcie 75 % konwersji glicerolu z 98 % selektywnością do GC. Co ciekawe, autorzy udowodnili, że istotny wpływ na przebieg procesu miała odpowiednia dystrybucja miejsc kwasowych i zasadowych w testowanych układach katalitycznych. Z kolei Charate i współpracownicy [51] przygotowali heterogeniczne układy typu CuO-ZnO i pokazali, że zastosowanie odpowiedniego stosunku Cu do Zn w katalizatorze i odpowiednich warunków kalcynacji pozwala uzyskać znakomitą konwersję glicerolu (86 %) i 100 % selektywność do GC. Ponadto otrzymany katalizator był w pełni zdolny do ponownego użycia w kolejnych cyklach reakcyjnych mimo pewnych doniesień o homogenicznym przebiegu glicerolizy mocznika w obecności katalizatorów zawierających cynk [52].

1.4. Stałe katalizatory na bazie węgla w procesach waloryzacji glicerolu

Jak wspomniano w poprzednich rozdziałach, w omawianych procesach waloryzacji glicerolu przetestowano wiele katalizatorów heterogenicznych, wśród których znalazły się m.in. zeolity, polimery kwasowe, żywice jonowymiennie, sulfonowane krzemionki, heteropolikwasy czy układy zawierające metale lub ich tlenki. Należy jednak podkreślić, że niektóre z proponowanych katalizatorów, ze względu na wysokie koszty lub złożoną

procedurę otrzymywania, składającą się z wielu czasochłonnych etapów, nie są szczególnie atrakcyjne. W niektórych przypadkach odnotowano także niską stabilność miejsc aktywnych, ograniczającą możliwość powtórnego użycia.

Godną uwagi alternatywą dla ww. katalizatorów transformacji glicerolu są katalizatory węglowe, które posiadają szereg atrakcyjnych cech. Przede wszystkim, materiały węglowe są zazwyczaj odporne na działanie wysokiej temperatury i potencjalnych zanieczyszczeń [53]. Co więcej, mogą być otrzymywane z szerokiej gamy surowców, również substancji odpadowych, co umożliwia ich preparatykę niskim kosztem. Warto również wspomnieć, że dobór odpowiedniej procedury syntezy pozwala na uzyskanie próbek o określonej morfologii i parametrach teksturalnych. Co istotne, materiały węglowe dają się względnie łatwo modyfikować, co umożliwia wprowadzenie na ich powierzchnię grup funkcyjnych o określonym charakterze chemicznym (kwasowym lub zasadowym) [37,53,54,55]. Niektóre typy węgla (np. węgle aktywne czy nanorurki węglowe) charakteryzują się dużą powierzchnią właściwą, co ma istotne znaczenie w przypadku ich zastosowania w roli nośnika fazy aktywnej, takiej jak np. metale lub ich tlenki [53,54,55]. Wreszcie, materiały węglowe mogą być łatwo oddzielane od mieszaniny reakcyjnej i wykorzystywane w kolejnych cyklach reakcyjnych [37].

1.4.1. Estryfikacja glicerolu do octanów w obecności katalizatorów na bazie węgla

Jedna z naszych poprzednich prac (nie wchodząca w skład niniejszej rozprawy doktorskiej) zawiera wyniki katalityczne uzyskane w reakcji estryfikacji glicerolu przy zastosowaniu materiałów węglowych otrzymanych z cukrów w procesie jednoczesnej karbonizacji i sulfonowania w temperaturze 180 °C, i w obecności stężonego kwasu siarkowego(VI). W przypadku najlepiej pracującego katalizatora (otrzymanego ze skrobi) osiągnięto prawie 100 % konwersję glicerolu i 71 % łączną wydajność di- i trioctanów glicerolu już po 2 h reakcji w 110 °C i przy użyciu stosunku molowego reagentów G:AA = 1:6. Co więcej, próbka była w pełni zdolna do ponownego użycia i stabilna przez przynajmniej 4 cykle reakcyjne [56]. Z kolei Perez i współpracownicy [57] przetestowali w procesie estryfikacji surowego glicerolu kwasem octowym sulfonowany węgiel otrzymany z łupin orzechów ziemnych (aktywowany za pomocą KOH). Autorzy uzyskali 99 % konwersję glicerolu z 70,6 % sumaryczną selektywnością do DAG i TAG po 4 h reakcji w 120 °C, wykorzystując 6-krotny nadmiar czynnika estryfikującego. W literaturze dostępne są również doniesienia o zastosowaniu katalizatorów węglowych na bazie grafenu. Na przykład: Hidayati i współpracownicy [58] testowali tlenek grafenu

i uzyskali wysoką konwersję glicerolu (~89 %) wraz z sumaryczną selektywnością do DAG+TAG wynoszącą ~53 % po 2 h reakcji w 120 °C, wykorzystując 9-krotny nadmiar środka estryfikującego i dodatek 5 % wag. katalizatora względem masy glicerolu. Autorzy zasugerowali jednak, że wymagane są dodatkowe badania, mające na celu zwiększenie stabilności testowanego katalizatora w kolejnych cyklach reakcyjnych. Z kolei Riascos i współpracownicy [59] badali aktywność katalityczną chemicznie zredukowanego tlenku grafenu, funkcjonalizowanego generowaną in situ solą diazoniową. Autorzy uzyskali 92 % konwersję glicerolu po 2 h reakcji w 110 °C, wykorzystując 9-krotny nadmiar środka estryfikującego i 5 % wag. katalizatora (względem masy glicerolu). W tym przypadku testy ponownego użycia potwierdziły, że aktywność próbki po 2 cyklach reakcyjnych znacząco spadła, a w trzecim konwersja glicerolu (~56 %) zbliżona była do wyników uzyskanych w reakcji bez użycia katalizatora.

1.4.2. Eteryfikacja glicerolu do eterów tert-butyłowych w obecności katalizatorów na bazie węgla

Proces eteryfikacji glicerolu za pomocą alkoholu tert-butyłowego i katalizatorów węglowych badany był relatywnie rzadko. Gonçaves i współpracownicy [32] prowadzili badania w obecności sulfonowanego węgla otrzymanego z wytlóków z trzciny cukrowej i osiągnęli ~80 % konwersję glicerolu już po 4 h reakcji w temperaturze 120 °C. W tym przypadku selektywność do DTBGE+TTBGE wyniosła ~21,3 %. Co istotne, autorzy zaobserwowali, że dalszy wzrost temperatury reakcji (powyżej 120 °C) promował proces de-eteryfikacji, a w konsekwencji znaczny spadek konwersji glicerolu. Galhardo i współpracownicy [60] otrzymali sulfonowany węgiel z łusek ryżowych i osiągnęli 53 % konwersję glicerolu z 13,2 % wydajnością DTBGE+TTBGE po 4 h reakcji w 120 °C, używając 5 % wag. katalizatora (względem masy glicerolu). Co więcej, autorzy udowodnili, że ubocznie produkowana w reakcji woda nie powodowała dezaktywacji testowanego katalizatora. Z drugiej strony, Miranda i współpracownicy [61] badali aktywność sulfonowanego komercyjnego węgla aktywnego w omawianym procesie. Przeprowadzone testy potwierdziły umiarkowaną aktywność tej próbki, skutkującą jedynie 35 % konwersją glicerolu i 7 % wydajnością DTBGE+TTBGE po 10 h reakcji. Odnaleziono również wzmiankę o zastosowaniu sulfonowanego tlenku grafenu, który dość efektywnie przekształcał glicerol, dając 50 % konwersję glicerolu i ~11 % sumaryczną wydajność DTBGE i TTBGE po 10 h reakcji w 90 °C. Warto jednak wspomnieć, że w tym przypadku zastosowano dość dużą ilość katalizatora (7,5 % wag. względem masy glicerolu).

1.4.3. Gliceroliza mocznika w obecności katalizatorów na bazie węgla

Generalnie proces glicerolizy mocznika był dotychczas prowadzony głównie w obecności metali bądź ich tlenków lub soli, stosowanych samodzielnie bądź osadzonych na różnego rodzaju nośnikach, głównie nieorganicznych [42–52,62–64]. Przeprowadzony przegląd literatury ujawnił tylko jedną wzmiankę o zastosowaniu materiału węglowego w reakcji glicerolizy mocznika, przy czym próbka ta była używana jako nośnik fazy aktywnej (konkretnie złota) [42]. W tym przypadku uzyskano 66 % konwersję glicerolu oraz 34 % selektywność do węglanu glicerolu. Niemniej jednak brak jest jakichkolwiek informacji na temat zależności między właściwościami fizykochemicznymi użytego układu a jego aktywnością w badanym procesie oraz ewentualnego wpływu zastosowanego nośnika węglowego na przebieg reakcji.

CEL BADAÑ

Tematyka podjęta w ramach realizacji niniejszej rozprawy doktorskiej dotyczyła badań związanych z wybranymi procesami waloryzacji glicerolu, tj. estryfikacji glicerolu kwasem octowym, eteryfikacji glicerolu za pomocą alkoholu tert-butyłowego oraz glicerolizy mocznika.

Jak wynika z przedstawionego przeglądu literaturowego, wspomniane reakcje waloryzacji glicerolu najefektywniej zachodzą w obecności katalizatorów homogenicznych. Niemniej jednak celem wyeliminowania ograniczeń typowych dla tego typu układów, w ostatnich latach naukowcy swoją uwagę skupiają na opracowaniu skutecznych katalizatorów heterogenicznych dla reakcji konwersji glicerolu. Szczególnie interesujące wydaje się zastosowanie materiałów węglowych jako katalizatorów omawianych procesów. Wśród dotychczas przetestowanych w estryfikacji i eteryfikacji glicerolu oraz glicerolizie mocznika katalizatorów węglowych znalazły się przede wszystkim proste układy otrzymywane z biomasy lub substancji odpadowych, głównie o strukturze amorficznej. Natomiast analiza doniesień literaturowych dowiodła, iż niewiele jest publikacji dotyczących badań aktywności katalitycznej zaawansowanych materiałów węglowych, takich jak np. próbki na bazie grafenu, włókna czy rurki węglowe. Tymczasem Guan i współpracownicy [65] odnotowali bardzo wysoką aktywność sulfonowanych nanorurek węglowych w podobnych procesach, np. produkcji biodiesla z trilauryny i etanolu. Uzyskana przez autorów wydajność reakcji była porównywalna do otrzymanej w obecności kwasu siarkowego(VI). Warto również zaznaczyć, że w wielu pracach badawczych wskazywano na pozytywny wpływ mobilności elektronów w materiałach na bazie grafenu na aktywność próbek wskutek ułatwionego transferu elektronów podczas reakcji katalitycznych [66,67].

Mając na uwadze wzmiankowane wcześniej zalety katalizatorów węglowych oraz fakt, iż materiały te były stosunkowo rzadko testowane w roli katalizatorów procesów waloryzacji glicerolu, celem niniejszej pracy było opracowanie układów węglowych o zaawansowanej strukturze (takich jak funkcjonalizowane pochodne grafenu, nanorurki lub włókna węglowe) oraz zbadanie ich właściwości katalitycznych w wybranych reakcjach konwersji glicerolu do wartościowych chemikaliów. Biorąc pod uwagę fakt, że tego typu materiały posiadają dość „sztywną” strukturę oporną na wszelkiego rodzaju funkcjonalizacje powierzchni (w porównaniu z innymi rodzajami materiałów węglowych, np. węglami aktywnymi) [68,69] podjęte działania obejmowały również próby zwiększenia podatności wybranych materiałów na modyfikacje. Realizacja powyższego celu obejmowała następujące zadania badawcze:

- 1) *Otrzymanie serii zaawansowanych katalizatorów węglowych o zróżnicowanej budowie i pożądanym charakterze chemicznym powierzchni.*
- 2) *Szczegółowa charakterystyka fizykochemiczna uzyskanych materiałów.*
- 3) *Testy katalityczne z udziałem otrzymanych próbek w wybranych procesach waloryzacji glicerolu.*
- 4) *Testy ponownego użycia dla wybranych materiałów.*
- 5) *Określenie zależności pomiędzy właściwościami fizykochemicznymi badanych węgla a ich aktywnością katalityczną w wybranych reakcjach waloryzacji glicerolu.*

Realizacja tych zadań pozwoliła na udzielenie odpowiedzi na postawione pytania badawcze:

- 1) *Jakie warunki i czynniki modyfikujące będą skutkowały najefektywniejszą funkcjonalizacją uzyskanych materiałów węglowych?*
- 2) *Jakie warunki prowadzenia proponowanych reakcji waloryzacji glicerolu są optymalne w przypadku użycia otrzymanych próbek węglowych?*
- 3) *Czy istnieje zależność między parametrami fizykochemicznymi uzyskanych katalizatorów węglowych a ich aktywnością w badanych procesach?*
- 4) *Czy otrzymane katalizatory działają bez utraty aktywności w przypadku ponownego ich użycia?*

Uzyskane wyniki zaprezentowano w formie spójnego tematycznie cyklu artykułów opublikowanych w czasopismach naukowych (P1–P5).

CZEŚĆ
EKSPERYMENTALNA

2. Materiały węglowe testowane w wybranych procesach konwersji glicerolu

W niniejszej rozprawie doktorskiej zastosowano różne typy materiałów węglowych w roli katalizatorów wybranych procesów waloryzacji glicerolu, tj. estryfikacji glicerolu kwasem octowym, eteryfikacji glicerolu za pomocą alkoholu tert-butyłowego oraz glicerolizy mocznika. Poniżej przedstawiono ogólny opis preparatyki testowanych próbek.

2.1. Termicznie redukowany tlenek grafenu o właściwościach kwasowych

Badania związane z termicznie redukowanym tlenkiem grafenu (TRGO) zaprezentowano w publikacji P1. Powyższy materiał otrzymano na drodze szoku termicznego tlenku grafenu (otrzymanego metodą Hummersa z grafitu). Zabieg ten miał na celu zarówno zwiększenie stabilności próbki, jak i wygenerowanie nowych defektów w strukturze materiału, podatnych na funkcjonalizację [70]. Próbkę wyjściową następnie funkcjonalizowano za pomocą stężonego kwasu siarkowego(VI), generowanej in situ soli diazonowej (BDS) lub kwasu fosforowego(V), celem nadania materiałowi właściwości kwasowych.

2.2. Sulfonowane włókna węglowe otrzymane z izobutanu lub etylenu w procesie CCVD

Włókna węglowe zostały otrzymane z izobutanu (CF_{i-bu}) lub etylenu (CF_{et}) w procesie CCVD (z ang. catalytic chemical vapor deposition), z wykorzystaniem niklu jako katalizatora wzrostu materiału węglowego. Otrzymany materiał następnie funkcjonalizowano z zastosowaniem różnych środków sulfonujących, tj. stężonego kwasu siarkowego(VI) lub generowanej in situ soli diazoniowej (BDS) [P2].

2.3. Funkcjonalizowane komercyjne nanorurki węglowe

W badaniach zastosowano dwa rodzaje komercyjnych nanorurek węglowych różniących się czystością (w związku z tym również ceną). Uwzględniono czyste CNT_{NC3100} ($\%C < 98 \%$) oraz zawierające metaliczne zanieczyszczenia CNT_{NC7000} ($\%C = \sim 90 \%$). Wybraną próbkę (CNT_{NC7000}) poddano również obróbce mechanicznej z zastosowaniem młyna kulowego w celu wygenerowania nowych krawędzi podatnych na funkcjonalizację. Próbki CNT następnie modyfikowano z zastosowaniem różnych czynników sulfonujących, tj. kwasu siarkowego (stężony, dymiący lub 5 M roztwór; stosowany samodzielnie lub w obecności glukozy) lub generowanej in situ soli diazoniowej [P4 i P5].

2.4. Włókna węglowe otrzymane z gazu LPG w roli nośnika tlenków wybranych metali

Materiał węglowy (CF) otrzymano metodą CCVD z zastosowaniem gazu LPG jako źródła węgla oraz metalicznego niklu jako katalizatora. Otrzymaną próbkę następnie wykorzystano w roli nośnika fazy aktywnej, jaką były tlenki wybranych metali (Ba, Cr, Mg lub Zn), które zostały naniesione techniką impregnacji zwilżeniowej z zastosowaniem azotanów odpowiednich metali w roli prekursora fazy tlenkowej oraz odpowiedniej obróbki termicznej [P3].

3. Charakterystyka przygotowanych katalizatorów

Jednym z istotniejszych etapów prac były szczegółowe analizy fizykochemiczne przygotowanych katalizatorów pozwalające na dokładne określenie właściwości próbek, a także powiązanie parametrów fizykochemicznych użytych katalizatorów węglowych z ich aktywnością katalityczną w badanych reakcjach.

W celu ustalenia składu pierwiastkowego (C, H, N, S, P) badanych próbek przeprowadzono analizę elementarną. Zawartość popiołu określono jako pozostałość po spaleniu materiału w 850 °C w atmosferze powietrza. Analizę miareczkową (w tym przypadku potencjometryczne miareczkowanie odwrotne) wykorzystano w celu oznaczenia kwasowości całkowitej (stężenia miejsc kwasowych Brønsteda) badanych węgli. Metody mikroskopowe, tj. transmisyjna mikroskopia elektronowa (TEM) oraz skaningowa mikroskopia elektronowa (SEM), umożliwiły zbadanie morfologii preparowanych materiałów. Z kolei pomiary adsorpcji/desorpcji N₂ w temperaturze -196 °C umożliwiły analizę właściwości teksturalnych przygotowanych próbek. Stabilność termiczna węgli lub wprowadzonych na ich powierzchnię grup funkcyjnych została zbadana przy pomocy analizy termogravimetrycznej (TG), przeprowadzonej w przepływie powietrza lub azotu, w zakresie temperatur 20–1000 °C. Badania rentgenowskiej spektroskopii fotoelektronów (XPS) wykonano w celu określenia charakteru chemicznego powierzchni testowanych katalizatorów. Szczegółowe informacje na temat struktury chemicznej i krystaliczności uzyskano przy pomocy spektroskopii Ramana oraz pomiarów dyfrakcji rentgenowskiej (XRD).

4. Testy katalityczne

Przygotowane materiały węglowe zastosowano w roli katalizatorów wybranych procesów waloryzacji glicerolu do wartościowych chemikaliów.

Procesy prowadzono stosując odpowiedni reaktor i określone warunki reakcji. Próbki mieszaniny poreakcyjnej pobierano w określonych odstępach czasowych i analizowano przy pomocy chromatografii gazowej we wcześniej zoptymalizowanych warunkach pomiarowych. Takie podejście umożliwiło dokładne śledzenie postępów badanych procesów w czasie. Efektywność przeprowadzonych reakcji oceniono na podstawie następujących parametrów: konwersja glicerolu (X_G), wydajność (Y) produktów lub selektywność (S) do konkretnych produktów reakcji. W celach porównawczych niektóre procesy przeprowadzono również w obecności komercyjnych katalizatorów, takich jak Amberlyst-15 (eteryfikacja glicerolu) i $ZnSO_4$ (gliceroliza mocznika). Dla wybranych próbek (najlepiej pracujących w danym procesie) dokonano optymalizacji warunków reakcji (tj. temperatury, stosunku molowego reagentów i/lub ilości użytego katalizatora) oraz przeprowadzono testy ponownego użycia, na podstawie których oceniono stabilność tych materiałów. Ostatecznie określono zależność pomiędzy właściwościami fizykochemicznymi badanych materiałów a ich aktywnością w wybranych procesach waloryzacji glicerolu.

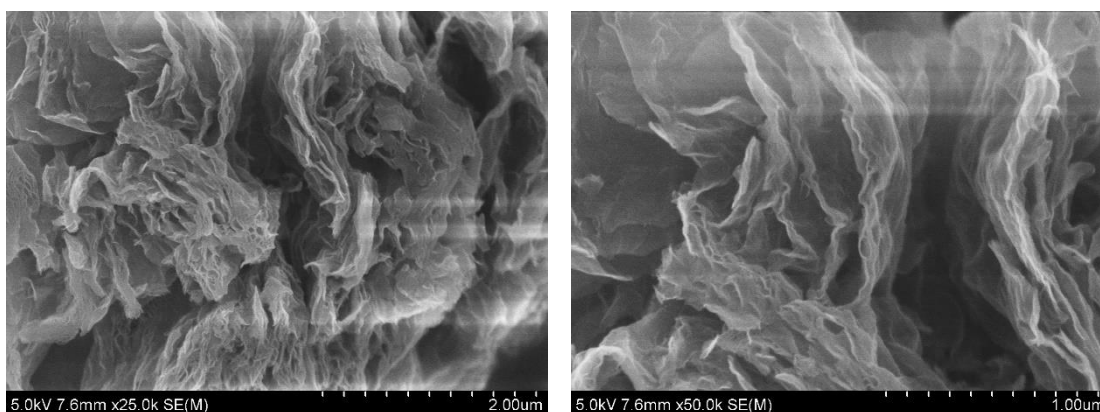
**WYNIKI
I ICH OMÓWIENIE**

5. Właściwości fizykochemiczne otrzymanych materiałów węglowych

5.1. Próbki wyjściowe

5.1.1. Termicznie redukowany tlenek grafenu

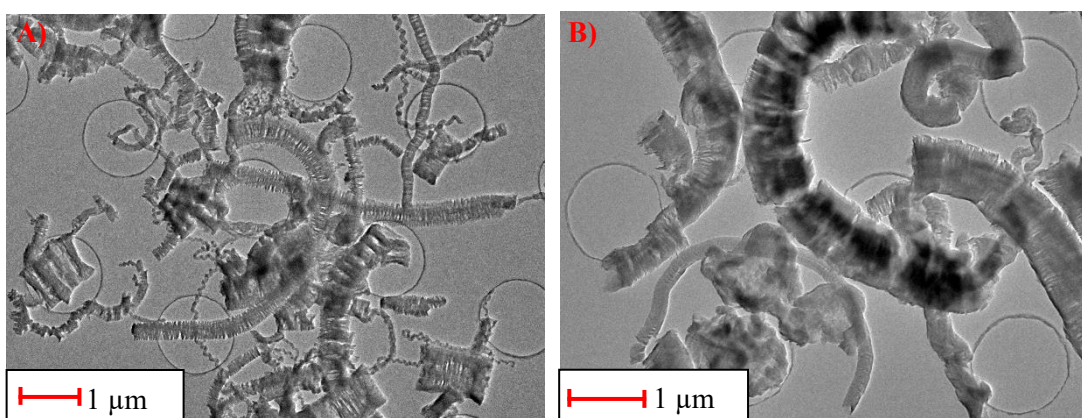
W wyniku przeprowadzonej syntezy otrzymano mezoporowaty materiał o dość wysokiej powierzchni właściwej ($617 \text{ m}^2/\text{g}$) i płatkowej strukturze, typowej dla materiałów na bazie grafenu. Morfologię otrzymanej próbki potwierdziły badania wykonane skaningowym mikroskopem elektronowym, a otrzymany wynik przedstawiono na Rys. 6.



Rys. 6. Zdjęcia SEM termicznie redukowanego tlenku grafenu

5.1.2. Włókna węglowe otrzymane z izobutanu lub etylenu

W obu przypadkach potwierdzono obecność włókien węglowych o różnej średnicy, składających się z warstw węglowych ułożonych równolegle do siebie i prostopadle do osi włókna (układ platelet), jak przedstawiono na Rys. 7. Próbki prezentowały umiarkowaną powierzchnię właściwą (tj. $115 \text{ m}^2/\text{g}$ dla $\text{CF}_{\text{i-bu}}$ oraz $174 \text{ m}^2/\text{g}$ dla CF_{et}) oraz wysoką stabilność termiczną (do $\sim 500 \text{ }^\circ\text{C}$).



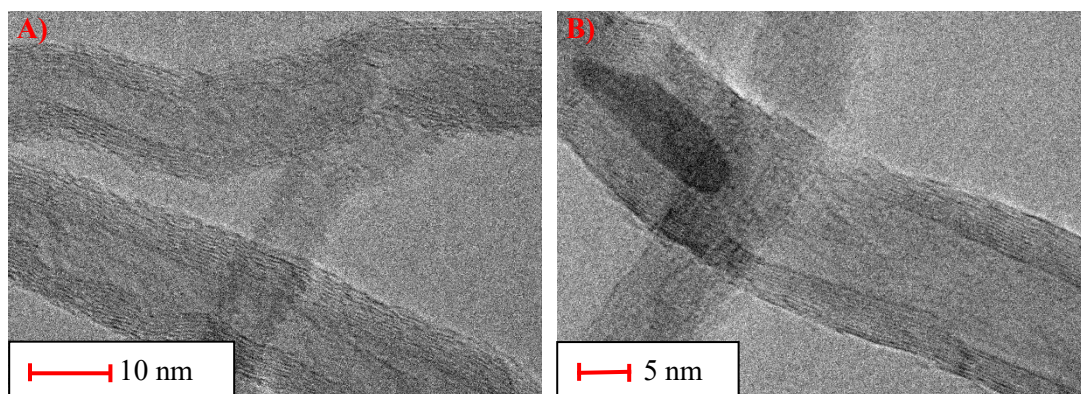
Rys. 7. Zdjęcia TEM materiałów węglowych otrzymanych z etylenu (A) lub izobutanu (B)

Co ważne, struktura próbki otrzymanej z etylenu charakteryzowała się większym stopniem uporządkowania. Zostało to potwierdzone wynikami analiz TEM-HR, XRD

oraz wykonanym widmem Ramana. W otrzymanych obrazach TEM (Rys. 7) zaobserwowano również niewielką ilość nanorurek węglowych obecnych w przypadku obu materiałów.

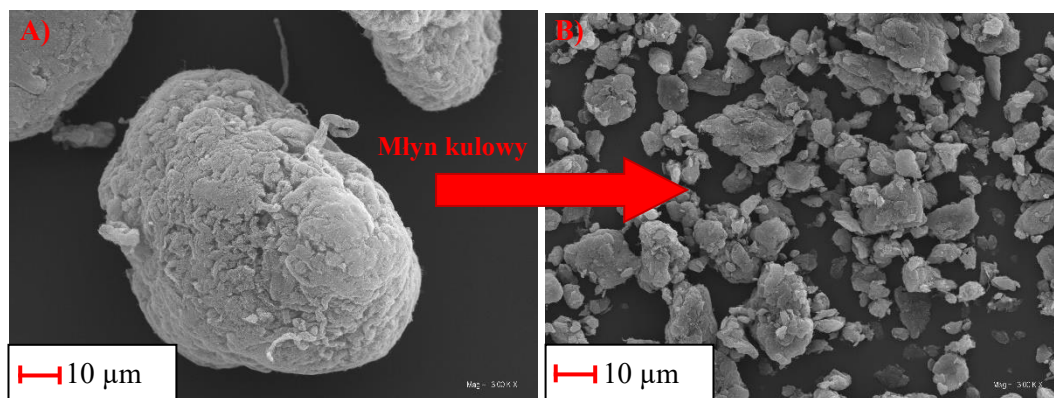
5.1.3. Komercyjne nanorurki węglowe

Przeprowadzone analizy materiału wyjściowego wykonane transmisyjnym mikroskopem elektronowym potwierdziły obecność wielościennych nanorurek węglowych o zbliżonej średnicy (Rys. 8), występujących w postaci splecionych wiązek. Potwierdzono, że CNT_{NC3100} są wolne od zanieczyszczeń. Z kolei CNT_{NC7000} zawierają metaliczne cząstki uwięzione wewnątrz nanorurek, jak zaprezentowano na Rys. 8B. Ustalono, że badane próbki posiadają umiarkowaną powierzchnię właściwą (406 m²/g oraz 243 m²/g, odpowiednio dla CNT_{NC3100} oraz CNT_{NC7000}) oraz wysoką stabilność termiczną (do ~500 °C), co jest charakterystyczne dla materiałów o uporządkowanej strukturze [71].



Rys. 8. Zdjęcia TEM próbek CNT_{NC3100} (A) oraz CNT_{NC7000} (B)

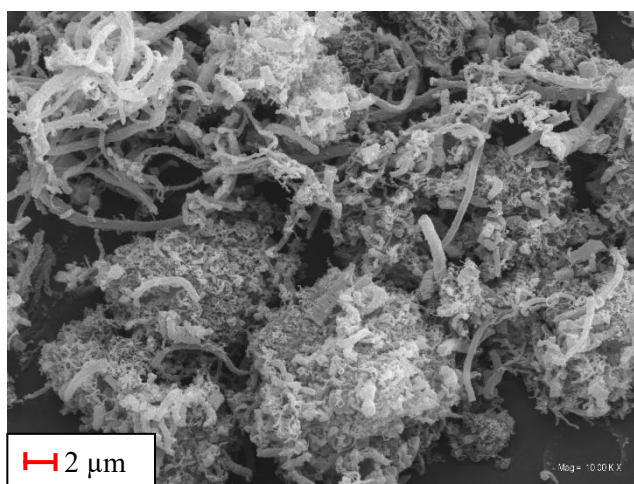
Co więcej, udowodniono, że obróbka mechaniczna CNT_{NC7000} z zastosowaniem młyna kulowego skutkowałą zwiększeniem powierzchni właściwej próbki (z 243 m²/g dla CNT_{NC7000} do 286 m²/g dla CNT_{NC7000-BM}), najprawdopodobniej w wyniku znacznego rozdrobnienia wiązek nanorurek węglowych na mniejsze cząstki i w konsekwencji łamania pojedynczych włókien na mniejsze [72,73]. Wpływ mielenia próbki CNT_{NC7000} na morfologię tego materiału zaprezentowano na Rys. 9. Ważne jest, że przeprowadzona analiza TEM-HR udowodniła, iż obróbka mechaniczna nie spowodowała znacznych zmian w strukturze CNT (zaobserwowano jedynie niewielkie deformacje), co zostało dodatkowo potwierdzone w wykonanych widmach Ramana.



Rys. 9. Zdjęcia SEM CNT_{NC7000} surowych (A) oraz poddanych obróbce mechanicznej (B)

5.1.4. Włóknisty materiał węglowy otrzymany z gazu LPG

W wyniku przeprowadzonego procesu CCVD otrzymano materiał węglowy (CF) składający się z włókien o różnych średnicach, występujących w postaci zbitych wiązek, jak przedstawiono na Rys. 10. Próbkę charakteryzowała się umiarkowaną powierzchnią właściwą ($259 \text{ m}^2/\text{g}$) oraz wysoką stabilnością termiczną (do $\sim 500 \text{ }^\circ\text{C}$).



Rys. 10. Zdjęcie SEM materiału węglowego otrzymanego z gazu LPG

5.2. Próbki modyfikowane

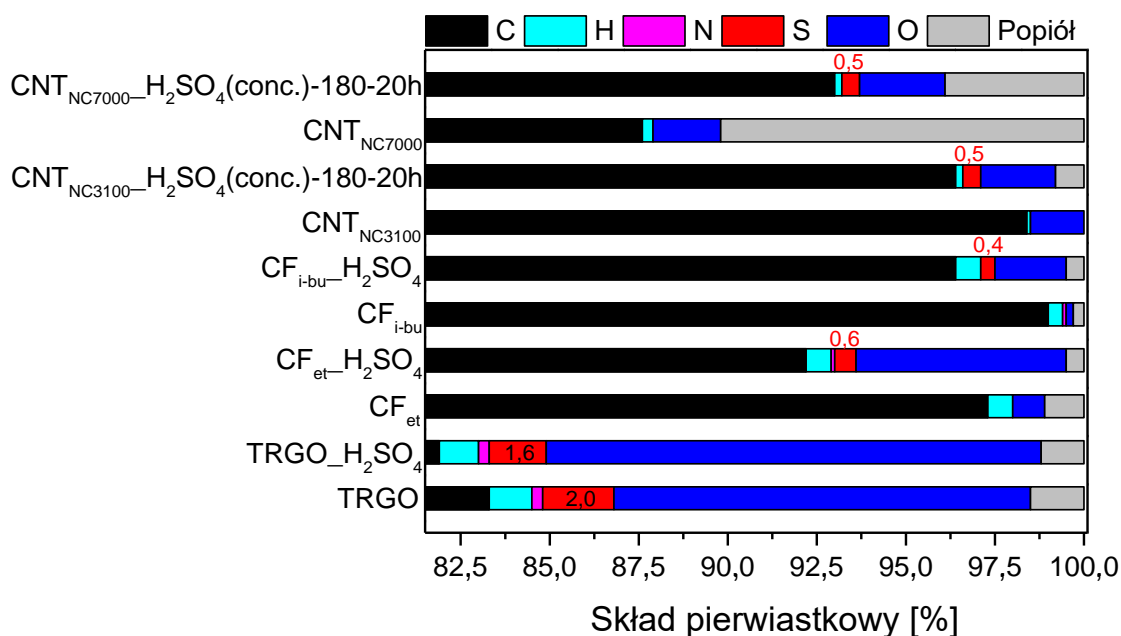
5.2.1. Funkcjonalizowane materiały węglowe

5.2.1.1. Modyfikacje węgla za pomocą kwasu siarkowego(VI)

Preparatyka większości materiałów testowanych w pracy miała na celu wprowadzenie na powierzchnię węgla określonych grup funkcyjnych, nadających próbkom odpowiednie właściwości chemiczne. W związku z tym, że materiały dedykowane dla procesów estryfikacji i eteryfikacji glicerolu wymagają obecności ugrupowań kwasowych, przeprowadzone modyfikacje koncentrowały się na wprowadzaniu na powierzchnię próbek ugrupowań zawierających siarkę i/lub fosfor. Na Rys. 11 zaprezentowano wyniki analizy

elementarnej uzyskane dla surowych oraz funkcjonalizowanych stężonym kwasem siarkowym(VI) próbek, tj. TRGO, CF_{et}, CF_{i-bu}, CNT_{NC3100} oraz CNT_{NC7000}.

Jak pokazano na rysunku, wszystkie otrzymane niemodyfikowane materiały węglowe zawierały głównie węgiel (~83–98 %), którego zawartość była silnie skorelowana z zastosowaną metodą preparatyki. Termicznie redukowany tlenek grafenu charakteryzował się również dość wysoką zawartością tlenu, mimo że metoda otrzymywania tego materiału uwzględniała szok termiczny w temperaturze 800 °C. Wysoka zawartość O mogła wynikać z krótkiego czasu obróbki termicznej lub wysokiej stabilności powierzchniowych grup funkcyjnych TRGO. Z kolei włókna oraz nanorurki węglowe zawierały zdecydowanie niższą zawartość heteroatomów, co wynikało z zastosowania węglowodorów jako źródła węgla w procesie CCVD. Próbka TRGO zawierała również 2 % siarki, której obecność najprawdopodobniej wynikała z pozostałości nieodmytych reagentów w strukturze materiału.

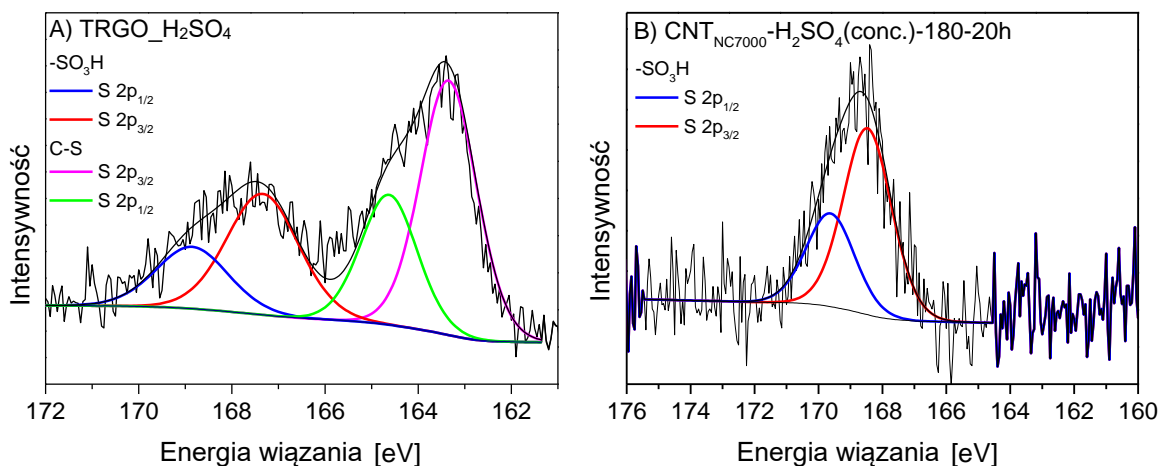


Rys. 11. Zawartość poszczególnych pierwiastków oraz popiołu w próbkach modyfikowanych kwasem siarkowym

Sulfonowany za pomocą kwasu siarkowego(VI) termicznie redukowany tlenek grafenu (TRGO-H₂SO₄) charakteryzował się podwyższoną zawartością tlenu, wynikającą najprawdopodobniej z utleniających właściwości kwasu siarkowego [74,75] (oraz pierwotnych właściwości zastosowanego materiału). Co więcej, w przypadku tej próbki zaobserwowano obniżoną w stosunku do materiału wyjściowego zawartość siarki. Zaproponowano, że w trakcie modyfikacji z H₂SO₄ doszło najprawdopodobniej do wmywania pozostałości nieodmytych wcześniej reagentów z jednoczesnym wprowadzaniem nowych grup funkcyjnych zawierających siarkę. Udowodniono także, że otrzymane z różnych prekursorów włókna węglowe prezentują różną podatność

na funkcjonalizację, tj. modyfikacja CF_{et} zachodziła efektywniej niż w przypadku CF_{i-bu} . W wyniku traktowania próbek H_2SO_4 otrzymano materiały zawierające 0,4 % i 0,6 % S, odpowiednio dla $CF_{i-bu_H_2SO_4}$ i $CF_{et_H_2SO_4}$. Ponadto uzyskane wyniki ujawniły także dość dużą zawartość tlenu w $CF_{et_H_2SO_4}$, sugerując również większą podatność tego materiału na utlenianie. Z kolei w przypadku nanorurek węglowych, przeprowadzone modyfikacje skutkowały wprowadzeniem 0,5 % siarki do struktury materiału (zarówno w przypadku czystych CNT_{NC3100} (próbka $CNT_{NC3100-H_2SO_4}(conc.)-180-20h$), jak i zanieczyszczonych CNT_{NC7000} (próbka $CNT_{NC7000-H_2SO_4}(conc.)-180-20h$)).

Należy zaznaczyć, że wykonanie analizy elementarnej nie daje żadnych informacji na temat rodzaju ugrupowań, w jakich występują wprowadzane heteroatomy. Jedną z metod umożliwiających identyfikację rodzaju grup na powierzchni węgla jest analiza XPS. Na Rys. 12 przedstawiono przykładowe widma XPS S 2p dla wybranych materiałów.



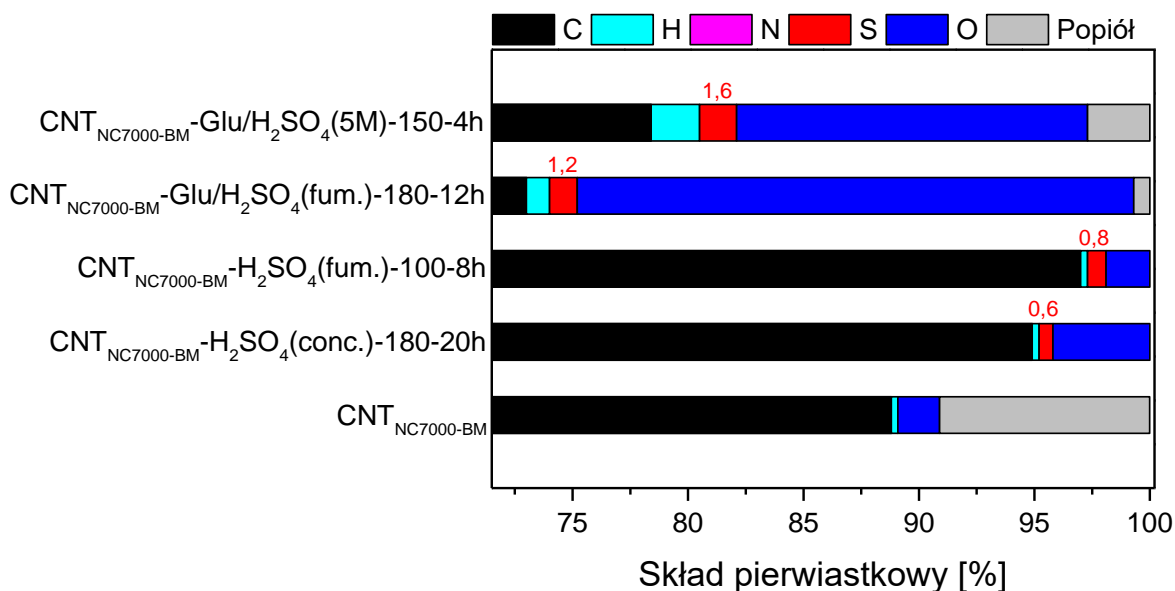
Rys. 12. Wysokorozdzielcze widma XPS S 2p wybranych modyfikowanych próbek węglowych

Przedstawione dane wskazują, że otrzymane materiały posiadają ugrupowania zawierające siarkę w różnej formie. To znaczy, w $TRGO_H_2SO_4$ (Rys. 12A) zaobserwowano dominujący udział ugrupowań C-S (62 %; wynikający z pierwotnego charakteru próbki) oraz niewielki grup $-SO_3H$ (38 %). Inaczej sytuacja wyglądała w przypadku materiału $CNT_{NC7000-H_2SO_4}(conc.)-180-20h$ (Rys. 12B), w przypadku którego siarka występowała jedynie w postaci sulfonowych grup funkcyjnych. Podobnie było w przypadku próbki $CNT_{NC3100-H_2SO_4}(conc.)-180-20h$ (widmo niepokazane).

W związku z tym, że skuteczność funkcjonalizacji badanych węgla kwasem siarkowym była stosunkowo niska, w kolejnym etapie prac skupiono się na próbach zwiększenia efektywności sulfonowania. Do testów wykorzystano komercyjne nanorurki węglowe CNT_{NC7000} , charakteryzujące się jednorodną strukturą, co ułatwiło ocenę uzyskanych

wyników. Ważne jest to, że owe próbki były dużo tańsze niż czyste CNT_{NC3100}, a w konsekwencji bardziej dostępne.

Z przedstawionych na Rys. 13 danych wynika, że zastosowanie wstępnej obróbki mechanicznej CNT_{NC7000} z wykorzystaniem młyna kulowego prowadziło do otrzymania próbki CNT_{NC7000-BM} o praktycznie niezmiennym składzie pierwiastkowym w stosunku do CNT_{NC7000} (Rys. 11).



Rys. 13. Wyniki EA próbek modyfikowanych kwasem siarkowym lub oleum z zastosowaniem dodatkowych modyfikacji (mielenie za pomocą młyna kulowego materiału wyjściowego i/lub zastosowanie glukozy w procesie modyfikacji)

Istotny jest fakt, że zastosowany zabieg skutkowało zwiększeniem podatności nanorurek węglowych na funkcjonalizację za pomocą stężonego H₂SO₄, a ilość wprowadzonej siarki wyniosła 0,6 % w próbce CNT_{NC7000-BM}-H₂SO₄(conc.)-180-20h (czyli o 0,1 % więcej niż w przypadku CNT_{NC7000}-H₂SO₄(conc.)-180-20h). Co więcej, wykorzystanie dymiącego H₂SO₄ dodatkowo zwiększyło skuteczność sulfonowania, w wyniku czego otrzymano materiał CNT_{NC7000-BM}-H₂SO₄(fum.)-100-8h o 0,8 % zawartości siarki. Wyniki te wciąż nie były w pełni zadowalające, na co wpływ mogła mieć sztywna struktura CNT oporna na funkcjonalizację [68,69]. W związku z powyższym do preparatyki modyfikowanych nanorurek włączono użycie cukrowego prekursora węglowego, który naniesiony na powierzchnię CNT mógłby działać jak „klej” dla grup funkcyjnych [76]. W tym celu, CNT_{NC7000-BM} funkcjonalizowano w obecności glukozy oraz dymiącego lub 5 M kwasu siarkowego w autoklawie (próbka odpowiednio CNT_{NC7000-BM}-Glu/H₂SO₄(fum.)-180-12h oraz CNT_{NC7000-BM}-Glu/H₂SO₄(5 M)-150-4h). Takie podejście umożliwiło wprowadzenie 1,2 % oraz 1,6 % siarki, odpowiednio dla CNT_{NC7000-BM}-Glu/H₂SO₄(fum.)-180-12h

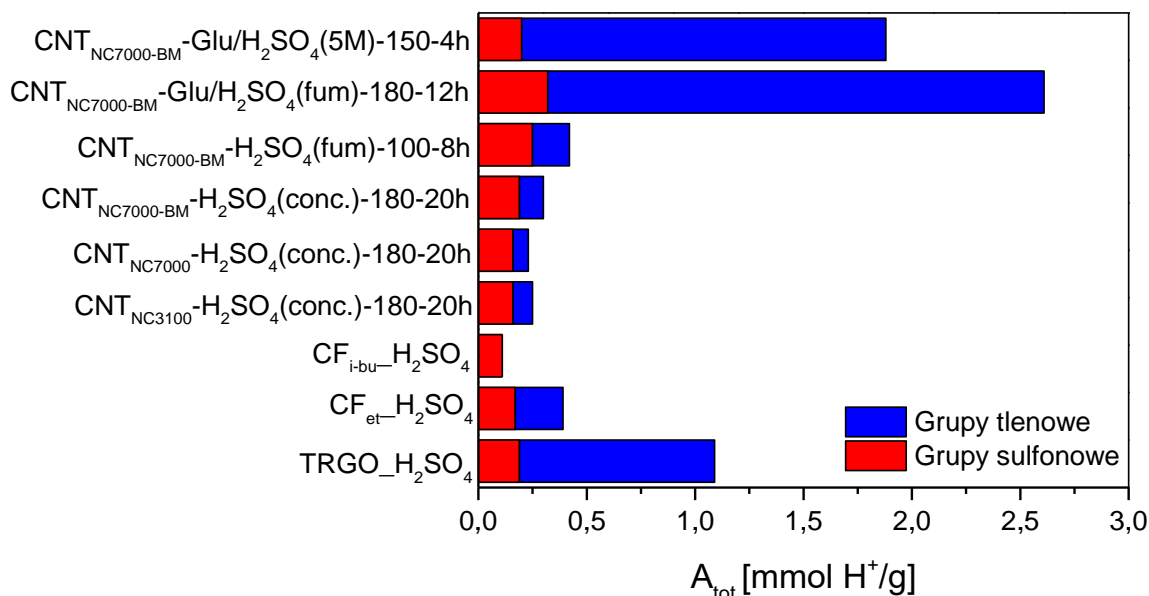
i CNT_{NC7000-BM}-Glu/H₂SO₄(5 M)-150-4h. Ponadto otrzymane próbki wykazywały wysoką zawartość tlenu, najprawdopodobniej pochodzącego z glukozy [56, 77].

W Tabeli 1 zaprezentowano procentowy udział siarki zaangażowanej w tworzenie różnych ugrupowań na powierzchni modyfikowanych nanorurek. Warto zaznaczyć, że próbki wykorzystujące do funkcjonalizacji jedynie kwas siarkowy (stężony lub dymiący) zawierały na powierzchni tylko sulfonowe grupy funkcyjne. Nieco inaczej wyglądało to w przypadku materiałów uwzględniających w syntezie glukozę (Glu), gdyż w tym przypadku wykryto siarkę zarówno w postaci sulfonowych grup funkcyjnych, jak również innych ugrupowań. Warto zaznaczyć, że mimo skutecznej funkcjonalizacji próbki CNT_{NC7000-BM}-Glu/H₂SO₄(5 M)-150-4h (zawierającej dość dużą ilość siarki, tj. 1,6 %), wprowadzona na powierzchnię siarka występowała głównie w niepożądanym zredukowanej formie (~60 %).

Tabela 1. Udział poszczególnych ugrupowań zawierających siarkę na powierzchni CNT (wyrażony w %)

	CNT _{NC7000-BM} -H ₂ SO ₄ (conc.)-180-20h	CNT _{NC7000-BM} -H ₂ SO ₄ (fum.)-100-8h	CNT _{NC7000-BM} -Glu/H ₂ SO ₄ (fum.)-180-12h	CNT _{NC7000-BM} -Glu/H ₂ SO ₄ (5 M)-150-4h
-SO ₃ H	100,0	100,0	85,7	40,4
C-S	0,0	0,0	14,3	59,6

Wprowadzenie nowych ugrupowań na powierzchnię materiałów węglowych skutkowało również generowaniem pewnej kwasowości próbek. Na Rys. 14 graficznie zaprezentowano wkład poszczególnych grup funkcyjnych w generowanie kwasowości całkowitej (A_{tot}) materiałów funkcjonalizowanych za pomocą kwasu siarkowego.



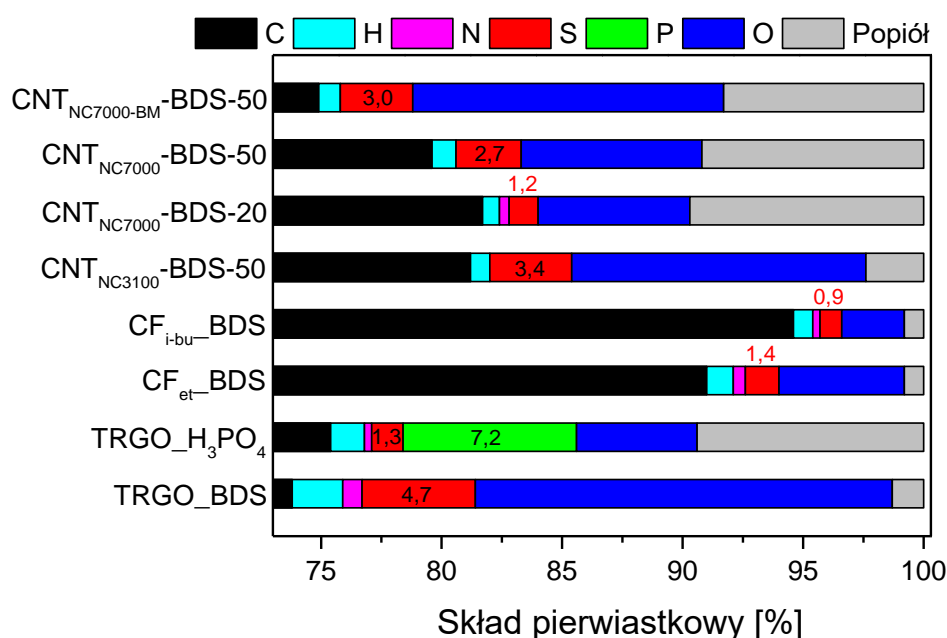
Rys. 14. Kwasowość całkowita próbek funkcjonalizowanych za pomocą kwasu siarkowego

Z przedstawionych danych wynika, że w przypadku wszystkich otrzymanych próbek wpływ na kwasowość całkowitą miały zarówno grupy sulfonowe, jak również ugrupowania zawierające tlen (np. karboksylowe lub hydroksylowe typu fenolowego), co wynikało

z właściwości zastosowanego środka funkcjonalizującego (H_2SO_4 oprócz zdolności do sulfonowania ma również charakter utleniający). Co ważne, w przypadku niektórych materiałów, tj. TRGO_ H_2SO_4 , CNT_{NC7000}-BM-Glu/ H_2SO_4 (fum.)-180-12h oraz CNT_{NC7000}-BM-Glu/ H_2SO_4 (5 M)-150-4h udział tlenowych grup był dominujący. Fakt ten wynikał z charakteru próbki wyjściowej (jak TRGO) lub zastosowanego czynnika współmodyfikującego (Glu), co omówiono wcześniej (Rys. 11 i 13 oraz dyskusja).

5.2.1.2. Modyfikacje próbek kwasem fosforowym oraz solą diazoniową

Dużo bardziej skutecznymi metodami funkcjonalizacji badanych próbek węglowych okazały się modyfikacje powierzchni próbek przy pomocy kwasu fosforowego(V) lub generowanej in situ soli diazoniowej. Uzyskane wyniki analizy elementarnej ilustruje Rys. 15.

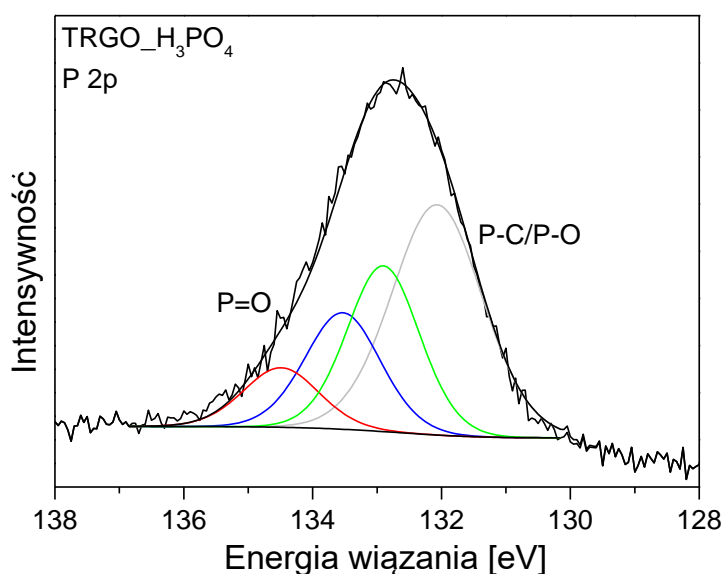


Rys. 15. Analiza elementarna materiałów węglowych funkcjonalizowanych za pomocą BDS

Udowodniono, że w wyniku zastosowania H_3PO_4 wprowadzono znaczną ilość fosforu (7,2 %) do struktury próbki TRGO_ H_3PO_4 . Zastosowanie BDS także prowadziło do skutecznej funkcjonalizacji TRGO, dając próbkę TRGO_BDS o 4,7 % zawartości siarki. Wprowadzanie siarki z wykorzystaniem generowanej in situ soli diazoniowej było również skuteczne w przypadku próbek na bazie CNT, szczególnie w przypadku czystych nanorurek węglowych CNT_{NC3100}, dla których zawartość siarki wyniosła aż 3,4 % (próbka CNT_{NC3100}-BDS-50). Niemniej jednak wykazano, że zastosowanie odpowiednich warunków funkcjonalizacji BDS zanieczyszczonych CNT_{NC7000} skutkowało znacznym zwiększeniem skuteczności wprowadzania S, tzn. podwyższona temperatura reakcji (50 °C) dawała próbkę CNT_{NC7000}-BDS-50 o zwiększonej o 1,5 % zawartości siarki w porównaniu z materiałem modyfikowanym w temperaturze pokojowej (tj. CNT_{NC7000}-BDS-20). Co więcej,

zastosowanie wstępnej obróbki mechanicznej CNT_{NC7000} za pomocą młyna kulowego dodatkowo zwiększyło podatność próbki na funkcjonalizację, umożliwiając wprowadzenie 3,0 % siarki do struktury węgla CNT_{NC7000}-BM-BDS-50. Z kolei modyfikacja za pomocą generowanej in situ soli diazoniowej w przypadku włókien węglowych otrzymanych z izobutanu lub etylenu skutkowało wprowadzeniem odpowiednio 0,9 % i 1,4 % S na powierzchnię próbek. Należy zauważyć, że w tym przypadku próbka CF_{et} również była bardziej podatna na modyfikację niż ta otrzymana z izobutanu (podobnie jak w przypadku funkcjonalizacji za pomocą H₂SO₄).

W pracy wykazano, że próbka TRGO_H₃PO₄ została wzbogacona w fosfor występujący w formie grup fosfonianowych bądź fosforanowych, jak przedstawiono na Rys. 16.



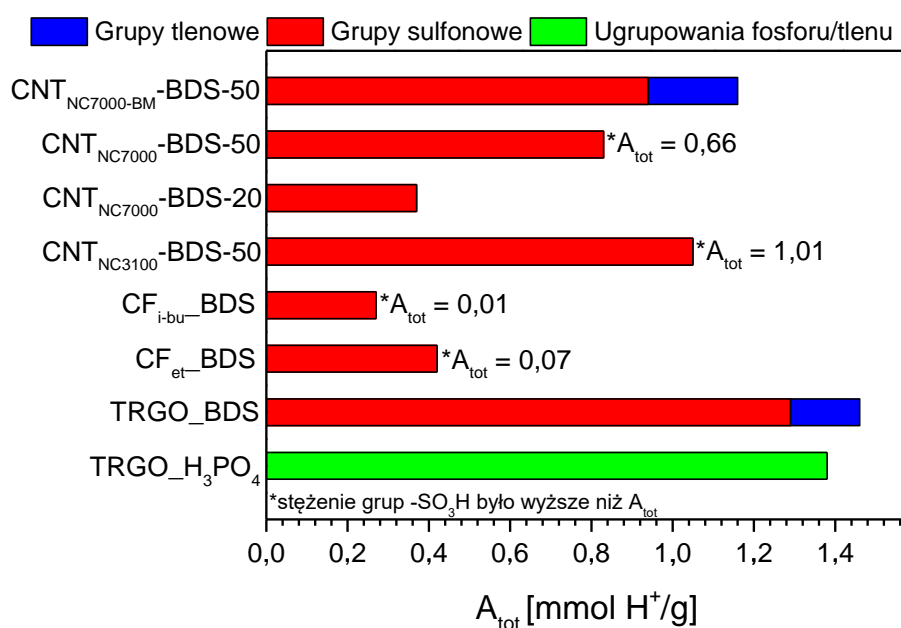
Rys. 16. Wysokorozdzielcze widmo XPS P 2p próbki TRGO_H₃PO₄

Z kolei w przypadku próbek sulfonowanych za pomocą BDS zaobserwowano wyłączny udział sulfonowych grup funkcyjnych. Jedynie dla próbki TRGO_BDS potwierdzono występowanie niewielkiej ilości siarki zaangażowanej w tworzenie innego niż -SO₃H typu ugrupowań, pochodzących najprawdopodobniej z węgla wyjściowego TRGO. Udziały poszczególnych ugrupowań S i P obecnych na powierzchni przygotowanych próbek podsumowano w Tabeli 2.

Tabela 2. Udział poszczególnych rodzajów ugrupowań powierzchniowych zawierających S lub P wyrażony w %

	TRGO_H ₃ PO ₄	TRGO_BDS	CNT _{NC3100} -BDS-50	CNT _{NC7000} -BDS-20	CNT _{NC7000} -BDS-50	CNT _{NC7000} -BM-BDS-50
-SO ₃ H	0,0	88,0	100,0	100,0	100,0	100,0
C-S	0,0	12,0	0,0	0,0	0,0	0,0
P-C/P-O, P=O	100,0	0,0	0,0	0,0	0,0	0,0

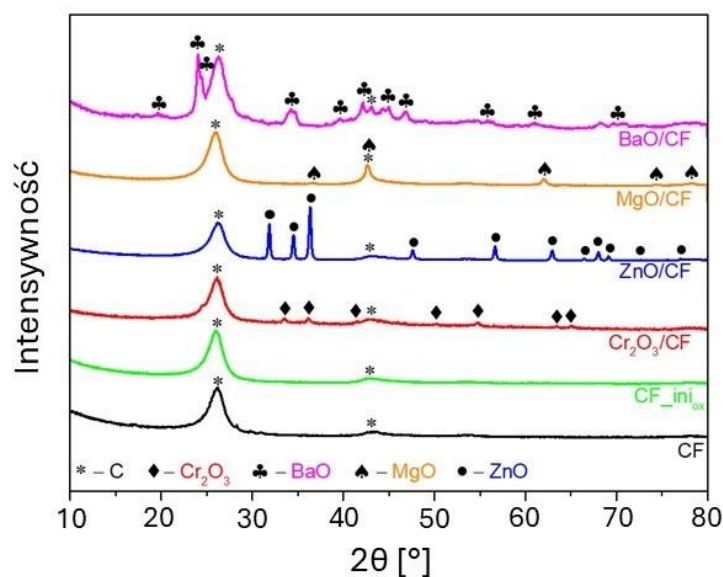
Warto zwrócić uwagę na fakt, że kwasowość całkowita próbek modyfikowanych generowaną in situ solą diazoniową wynikała głównie z obecności sulfonowych grup funkcyjnych, jak zaprezentowano na Rys. 17. Co więcej, w przypadku niektórych materiałów (oznaczonych „*”), zawartość grup $-SO_3H$ była wyższa niż wartość A_{tot} . Zjawisko to jest zazwyczaj obserwowane, gdy następuje neutralizacja miejsc kwasowych na skutek tworzenia się zwitterionów [74]. Innym wyjaśnieniem może być tworzenie się na powierzchni próbki poliwarstwy zbudowanej z grup $-Ph-SO_3H$, z ograniczonym dostępem do miejsc aktywnych [78,79].



Rys. 17. Kwasowość całkowita próbek funkcjonalizowanych za pomocą BDS lub H_3PO_4

5.2.2. Włókna węglowe w roli nośnika tlenków metali

W wyniku przeprowadzonej impregnacji nośnika węglowego (CF z gazu LPG) azotanami odpowiednich metali oraz po obróbce termicznej próbek otrzymano serię układów typu $10\%Me_xO_y/CF$, gdzie Me = Ba, Cr, Mg lub Zn. Badania XRD potwierdziły obecność tlenków metali Me_xO_y w formie krystalicznej w strukturze katalizatorów, co przedstawiono na Rys. 18. Dodatkowo analiza XPS potwierdziła obecność na powierzchni próbki ZnO/CF fazy aktywnej w formie tlenku cynku oraz tlenowych grup funkcyjnych. Warto dodać, że faza aktywna osadzona na materiale CF została również zaobserwowana na zdjęciach SEM [P3].



Rys. 18. Wyniki XRD otrzymane dla próbek CF, CF_{ini_ox} oraz tlenków metali osadzonych na nośniku CF

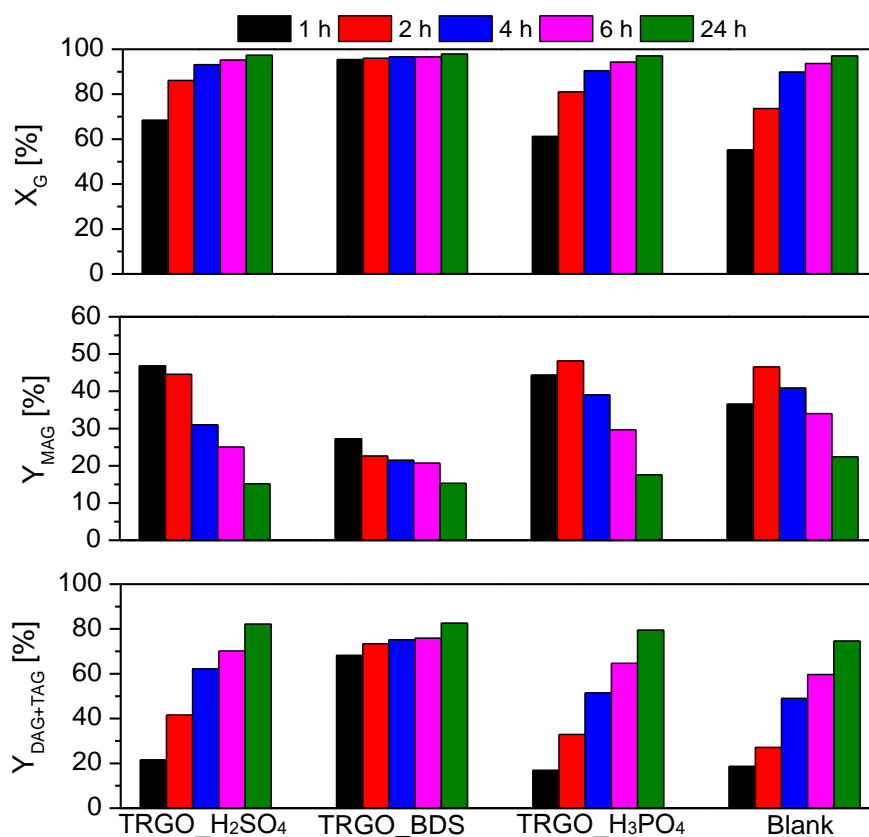
6. Wpływ chemii powierzchni przygotowanych materiałów węglowych na aktywność katalityczną w wybranych procesach waloryzacji glicerolu

Właściwości katalityczne przygotowanych materiałów węglowych przebadano w wybranych reakcjach waloryzacji glicerolu. Najważniejsze wyniki otrzymane podczas prowadzonych badań zostały podsumowane w kolejnych rozdziałach.

6.1. Estryfikacja glicerolu za pomocą kwasu octowego w obecności katalizatorów na bazie TRGO

W procesie estryfikacji glicerolu (G) za pomocą kwasu octowego (AA) testowano funkcjonalizowany różnymi czynnikami (tj. H₂SO₄, BDS lub H₃PO₄) termicznie redukowany tlenek grafenu (TRGO). Aktywność otrzymanych próbek badano uwzględniając następujące warunki reakcji: stosunek molowy reagentów G:AA = 1:6, temperaturę 110 °C, udział katalizatora na poziomie 10 % wag. względem masy glicerolu. Reakcję prowadzono w atmosferze gazu obojętnego przez 24 h, a próbki mieszaniny reakcyjnej analizowano po 1, 2, 4, 6, i 24 h procesu. Rezultaty przeprowadzonych badań zostały szczegółowo opisane w artykule P1, uwzględnionym w wykazie publikacji będących podstawą rozprawy doktorskiej.

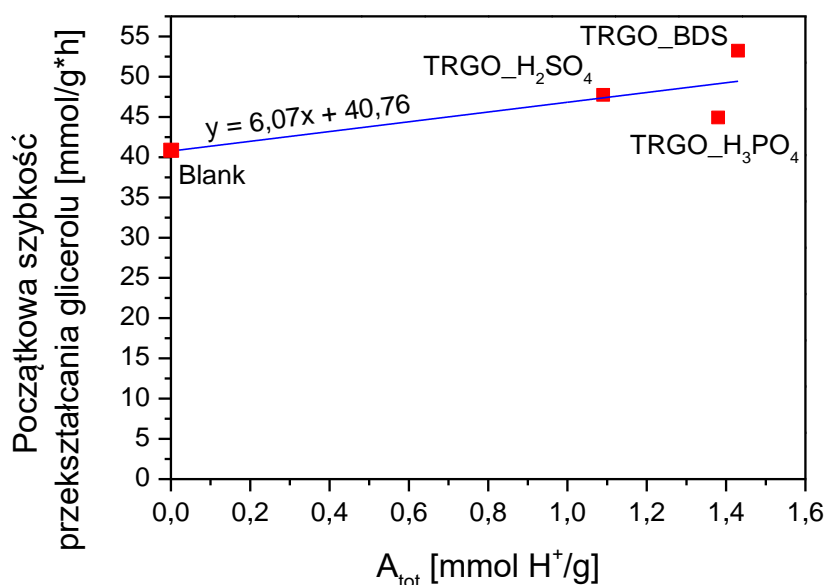
Wyniki konwersji glicerolu (X_G) oraz wydajności (Y) produktów otrzymanych w reakcji prowadzonej bez użycia katalizatora (Blank) oraz w obecności funkcjonalizowanego TRGO przedstawiono na Rys. 19.



Rys. 19. Wyniki reakcji estryfikacji glicerolu za pomocą kwasu octowego otrzymane bez użycia katalizatora (Blank) oraz w obecności funkcjonalizowanego TRGO

Zgodnie z tym co przedstawiono we wstępie, estryfikacja glicerolu za pomocą kwasu octowego jest procesem autokatalitycznym, stąd glicerol jest przekształcany w pewnym stopniu nawet bez użycia zewnętrznego katalizatora (w tym przypadku kwas octowy pełni rolę katalizatora). Należy jednak zaznaczyć, że w powyższej sytuacji satysfakcjonujące wyniki udało się uzyskać dopiero po 24 h. Z drugiej strony, rezultaty testów w obecności modyfikowanego TRGO ujawniły, że zastosowanie przygotowanych katalizatorów skutkowało znacznym zwiększeniem wydajności procesu. Aktywność materiałów różniła się jednak w zależności od zastosowanej metody funkcjonalizacji. Najwyższe wyniki konwersji glicerolu oraz wydajności pożądaných octanów glicerolu (tj. DAG i TAG) uzyskano dla katalizatora TRGO_BDS. W tym przypadku otrzymano ~95 % konwersję glicerolu oraz ~70 % wydajność DAG+TAG już po 1 h procesu, a wydłużenie czasu reakcji dla tej próbki nie wpływało znacząco na uzyskiwane wyniki. W przypadku próbek TRGO_H₂SO₄ i TRGO_H₃PO₄, estryfikacja zachodziła dużo mniej efektywnie (rozpatrując zarówno konwersję glicerolu, jak i skuteczności przekształcania MAG w wyżej podstawione produkty). Niemniej jednak otrzymane rezultaty wciąż przewyższały te otrzymane w reakcji prowadzonej bez użycia katalizatora.

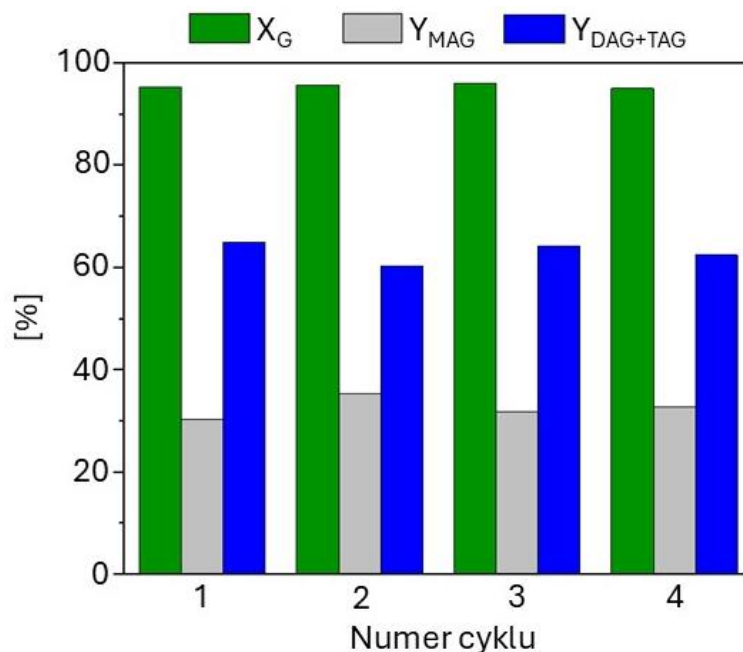
Ustalono, że aktywność katalityczna badanych materiałów jest ściśle związana z chemią ich powierzchni. Na Rys. 20 przedstawiono zależność między kwasowością całkowitą testowanych próbek (A_{tot}) a początkową szybkością przekształcania glicerolu. Z przedstawionych danych wynika, że parametr A_{tot} nie jest kluczowy dla omawianego procesu. Należy jednak zauważyć, że próbki sulfonowane (tj. TRGO_H₂SO₄ i TRGO_BDS) wykazywały większą zdolność do przekształcania glicerolu niż TRGO modyfikowany kwasem fosforowym(V) (tj. TRGO_H₃PO₄). Najaktywniejszym katalizatorem był TRGO_BDS, charakteryzujący się najwyższą kwasowością całkowitą (1,43 mmol H⁺/g), wynikającą głównie z obecności grup -SO₃H (Rys. 17). Próbka TRGO_H₂SO₄ była dużo mniej skuteczna w omawianej reakcji, mimo że charakteryzowała się dość wysokim parametrem A_{tot} (1,09 mmol H⁺/g). Należy jednak zaznaczyć, że wkład grup sulfonowych w wygenerowanie tej kwasowości był niewielki (Rys. 14). Z kolei próbka TRGO_H₃PO₄ charakteryzowała się najmniejszą aktywnością, mimo znacznej kwasowości całkowitej (1,38 mmol H⁺/g). W tym przypadku kwasowość była generowana głównie przez ugrupowania powierzchniowe zawierające fosfor o niskiej mocy kwasowej (pK_{1a} grup fosforanowych = 2,0, z kolei pK_{1a} grup sulfonowych = 0,7) [80]. Ostatecznie ustalono, że kluczowy wpływ na przebieg estryfikacji glicerolu kwasem octowym ma nie tylko kwasowość całkowita próbek, ale również rodzaj wprowadzonych grup funkcyjnych.



Rys. 20. Zależność między kwasowością całkowitą modyfikowanego TRGO a początkową szybkością przekształcania glicerolu w procesie jego estryfikacji kwasem octowym

Dla najaktywniejszej próbki (tj. TRGO_BDS) przeprowadzono testy ponownego użycia. Otrzymane wyniki ilustruje Rys. 21. Przedstawione dane potwierdzają, że katalizator

ten może być z powodzeniem odzyskiwany i wykorzystywany w kolejnych cyklach reakcyjnych bez znacznego spadku aktywności.



Rys. 21. Wyniki testów ponownego użycia przeprowadzonych dla próbki TRGO_BDS

6.2. Eteryfikacja glicerolu za pomocą alkoholu tert-butyłowego w obecności funkcjonalizowanych włóknistych materiałów węglowych

Celem niniejszego zadania była analiza właściwości katalitycznych włóknistych materiałów węglowych funkcjonalizowanych różnymi czynnikami sulfonującymi (H_2SO_4 lub BDS). W badaniach wykorzystano włókna węglowe (CF) otrzymane w warunkach laboratoryjnych z etylenu lub izobutanu (CF_{et} lub CF_{i-bu}) oraz komercyjne nanorurki węglowe (CNT). Aktywność próbek testowano w reakcji glicerolu (G) z alkoholem tert-butyłowym (TBA) prowadzonej w temperaturze $110\text{ }^\circ\text{C}$ oraz z zastosowaniem 4-krotnego nadmiaru środka eteryfikującego (TBA) i 5 % wag. katalizatora (względem masy glicerolu). Próbki mieszaniny reakcyjnej analizowano po 1, 2, 4, 6 i 24 h procesu. Podsumowaniem przeprowadzonych badań są artykuły naukowe nr P2, P4 i P5, uwzględnione w wykazie publikacji będących podstawą rozprawy doktorskiej.

W Tabeli 3 oraz na Rys. 22 przedstawiono dane dotyczące konwersji glicerolu oraz wydajności eterów mono-, di- i tri-tert-butyłowych glicerolu otrzymanych w badanej reakcji (prowadzonej z katalizatorem lub bez – tzw. blank). Ustalono, że proces bez katalizatora praktycznie nie zachodzi (konwersja glicerolu była w tym przypadku znikoma; $\sim 0,13\%$). Zastosowane wyjściowe katalizatory węglowe (niemodyfikowane) również nie wykazywały efektu katalitycznego (Tabela 3).

Tabela 3. Wyniki otrzymane po 24 h reakcji eteryfikacji glicerolu prowadzonej bez użycia katalizatora lub z katalizatorami niemodyfikowanymi

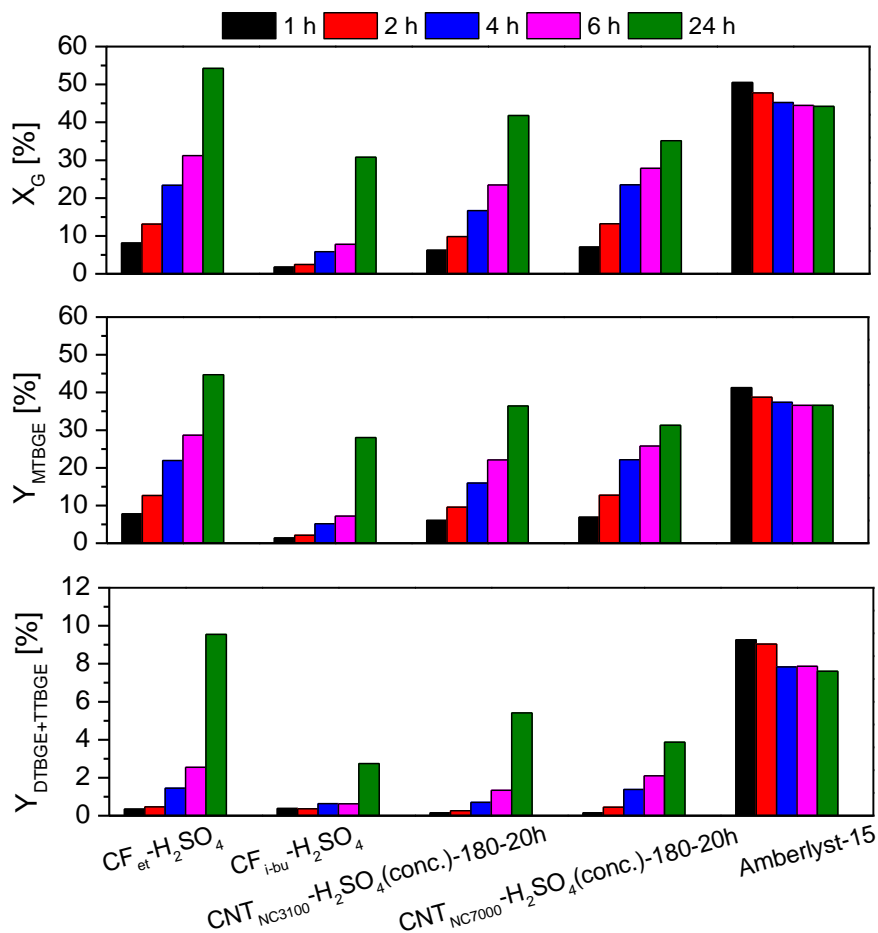
	X _G [%]	Y _{MTBGE} [%]	Y _{DTBGE+TTBGE} [%]
Blank	0,13	0,13	0,00
CF _{et}	0,84	0,69	0,15
CF _{i-bu}	0,00	0,00	0,00
CNT _{NC7000}	0,24	0,24	0,00

Na Rys. 22 przedstawiono wyniki katalityczne otrzymane w reakcji eteryfikacji realizowanej w obecności węgla modyfikowanych za pomocą stężonego kwasu siarkowego(VI). W celach porównawczych zaprezentowano również wyniki otrzymane dla reakcji z komercyjnym katalizatorem Amberlyst-15.

Z przedstawionych danych wynika, że wszystkie otrzymane materiały były aktywne w procesie eteryfikacji glicerolu za pomocą TBA, a uzyskane rezultaty znacznie przekroczyły te otrzymane w reakcji bez użycia katalizatora (Tabela 3). Przeprowadzone modyfikacje węgla były zatem skuteczne. Niemniej jednak zaobserwowano pewne różnice w aktywności próbek, wynikające najprawdopodobniej z różnic w efektywności przeprowadzonych funkcjonalizacji (Rys. 14). Najmniej skutecznie glicerol był przekształcany w obecności CF_{i-bu}_H₂SO₄, czyli próbki o najniższej zawartości ugrupowań zawierających siarkę (0,11 mmol/g) i kwasowości całkowitej (0,09 mmol H⁺/g). W tym przypadku początkowa konwersja glicerolu była niewielka (poniżej 10 % do 6 h reakcji) i wzrosła jedynie do 30 % po 24 h. Co więcej, w reakcji otrzymywano głównie MTBGE, a zawartość wyżej podstawionych produktów była znikoma.

Nieco lepsze działanie katalityczne wykazywały próbki na bazie CNT_{NC3100} oraz CNT_{NC7000}, które przekształcały glicerol skuteczniej niż CF_{i-bu}_H₂SO₄. Próbki CNT_{NC3100}-H₂SO₄(conc.)-180-20h oraz CNT_{NC7000}-H₂SO₄(conc.)-180-20h prezentowały zbliżony stopień funkcjonalizacji (tj. zawartość grup -SO₃H wynosiła 0,16 mmol/g w obu przypadkach), dlatego aktywność tych dwóch próbek była porównywalna. Interesujące wyniki uzyskano dla materiału CF_{et}_H₂SO₄, który wykazywał jedynie niewiele wyższą zawartość sulfonowych grup funkcyjnych niż pozostałe katalizatory (0,17 mmol /g), ale zdecydowanie wyższą kwasowość całkowitą (0,39 mmol H⁺/g) i był najaktywniejszy w badanym procesie (konwersja glicerolu przekroczyła 50 %). Co więcej, w tym przypadku MTBGE były efektywniej przekształcane do wyżej podstawionych produktów (wydajność DTBGE+TTBGE wyniosła prawie 10 %). Niemniej jednak osiągnięcie tych wyników wymagało wydłużenia czasu reakcji do 24 h. Warto zaznaczyć, że próbka CF_{et}_H₂SO₄ była również bogata w tlenowe grupy funkcyjne, których obecność mogła mieć pozytywny wpływ

na przebieg procesu, najprawdopodobniej w wyniku zwiększenia hydrofilowości materiału i ułatwionej adsorpcji reagentów [61,77,81]. Podkreślić jednak trzeba, że otrzymane wyniki były dużo gorsze niż rezultaty uzyskane w obecności komercyjnego katalizatora Amberlyst-15.

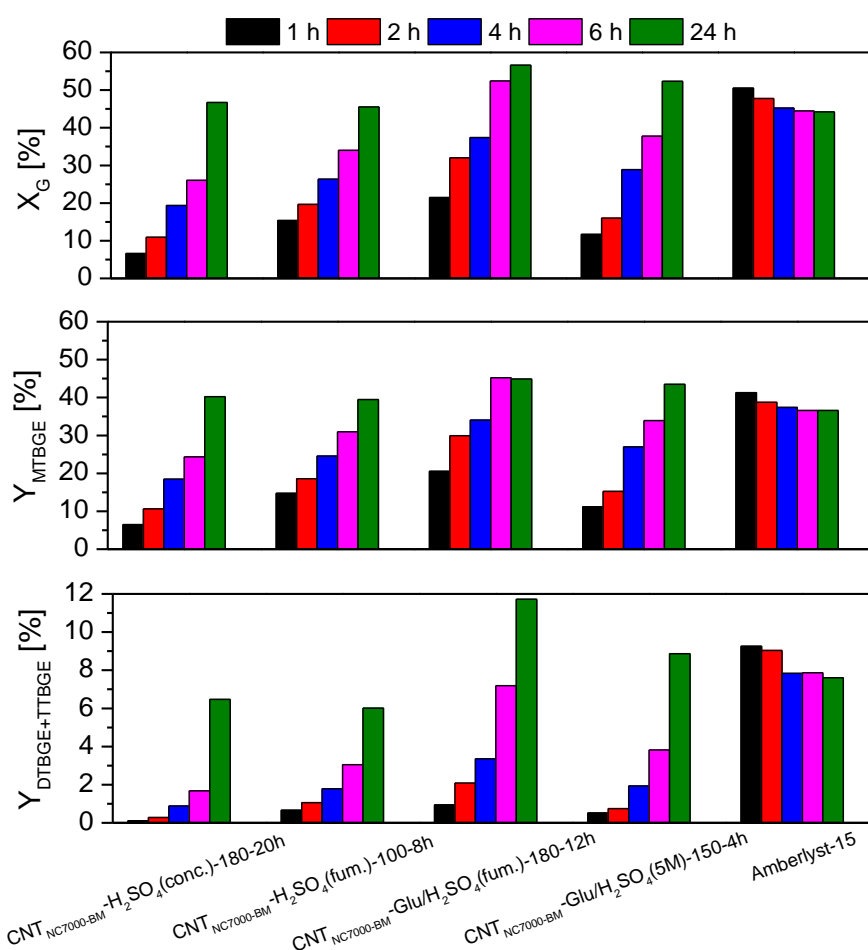


Rys. 22. Wyniki testów katalitycznych przeprowadzonych w obecności CF_{et}, CF_{i-bu}, CNT_{NC3100} oraz CNT_{NC7000} funkcjonalizowanych stężonym kwasem siarkowym(VI) oraz w obecności komercyjnego katalizatora Amberlyst-15

W związku z umiarkowanie satysfakcjonującą aktywnością katalityczną próbek modyfikowanych stężonym kwasem siarkowym(VI), do preparatyki katalizatorów włączono dodatkowe kroki (takie jak mielenie za pomocą młyna kulowego materiału wyjściowego i/lub zastosowanie glukozy w procesie modyfikacji), mające na celu zwiększenie skuteczności przeprowadzonych funkcjonalizacji (Rys. 13) [P5]. Na Rys. 23 przedstawiono wyniki konwersji glicerolu oraz wydajności eterów tert-butyłowych glicerolu otrzymane w reakcji prowadzonej w obecności przygotowanych katalizatorów – modyfikowanego dodatkowymi czynnikami CNT_{NC7000}.

Jak wynika z wykresu, mielenie lub dodatek glukozy skutkowało znacznym zwiększeniem aktywności modyfikowanych CNT_{NC7000} w omawianym procesie w porównaniu z CNT_{NC7000}-H₂SO₄(conc.)-180-20h (Rys. 22 i 23), co najprawdopodobniej

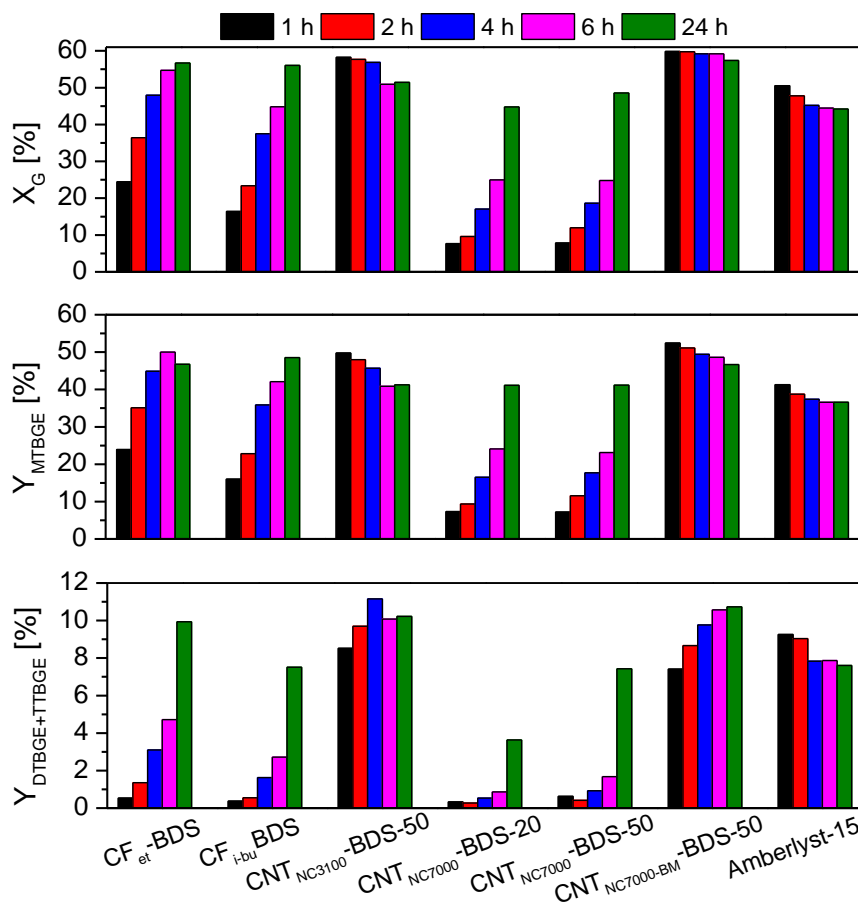
miało związek z większym stopniem funkcjonalizacji tych materiałów (Rys. 14). Dalej, porównując aktywność próbek mielonych i traktowanych kwasem ($\text{CNT}_{\text{NC7000-BM}}-\text{H}_2\text{SO}_4(\text{conc.})-180-20\text{h}$) oraz mielonych i traktowanych kwasem w obecności glukozy ($\text{CNT}_{\text{NC7000-BM-Glu}}/\text{H}_2\text{SO}_4(5\text{ M})-150-4\text{h}$), zawierających zbliżoną ilość grup $-\text{SO}_3\text{H}$, tj. $\sim 0,2\text{ mmol/g}$, można zauważyć, że zastosowanie drugiej z wymienionych próbek skutkowało efektywniejszym przekształcaniem glicerolu do eterów. Jednocześnie efektywniej były produkowane wyżej podstawione produkty. Uznano, że efekt ten jest najprawdopodobniej skutkiem obecności tlenowych grup funkcyjnych obecnych na powierzchni $\text{CNT}_{\text{NC7000-BM-Glu}}/\text{H}_2\text{SO}_4(5\text{ M})-150-4\text{h}$ (Rys. 14).



Rys. 23. Wyniki testów katalitycznych prowadzonych w obecności mielonych $\text{CNT}_{\text{NC7000}}$ funkcjonalizowanych kwasem siarkowym (samodzielnie lub w obecności glukozy) w porównaniu z aktywnością katalizatora Amberlyst-15

Najwyższą aktywność w omawianej grupie materiałów prezentowała próbka $\text{CNT}_{\text{NC7000-BM-Glu}}/\text{H}_2\text{SO}_4(\text{fum.})-180-12\text{h}$, która jednocześnie charakteryzowała się najwyższą zawartością grup sulfonowych oraz kwasowością całkowitą (Rys. 14). W tym przypadku już po 6 h reakcji osiągnięto zadowalające wyniki (tj. $\sim 52\%$ X_G oraz $\sim 7\%$ $Y_{\text{DTBE+TTBE}}$). Należy jednak zauważyć, że rozpatrując początkowe godziny reakcji, aktywność tej próbki wciąż nie dorównywała aktywności katalizatora Amberlyst-15.

Na Rys. 24 przedstawiono wyniki reakcji eteryfikacji glicerolu, otrzymane w obecności próbek węglowych modyfikowanych za pomocą generowanej in situ soli diazoniowej. Zaznaczyć należy, że w przypadku tej grupy materiałów stopień funkcjonalizacji był najwyższy (Rys. 14 i 17), stąd aktywność tych próbek w badanym procesie była znaczna.



Rys. 24. Wyniki testów katalitycznych prowadzonych w obecności próbek funkcjonalizowanych BDS w porównaniu z aktywnością katalizatora Amberlyst-15

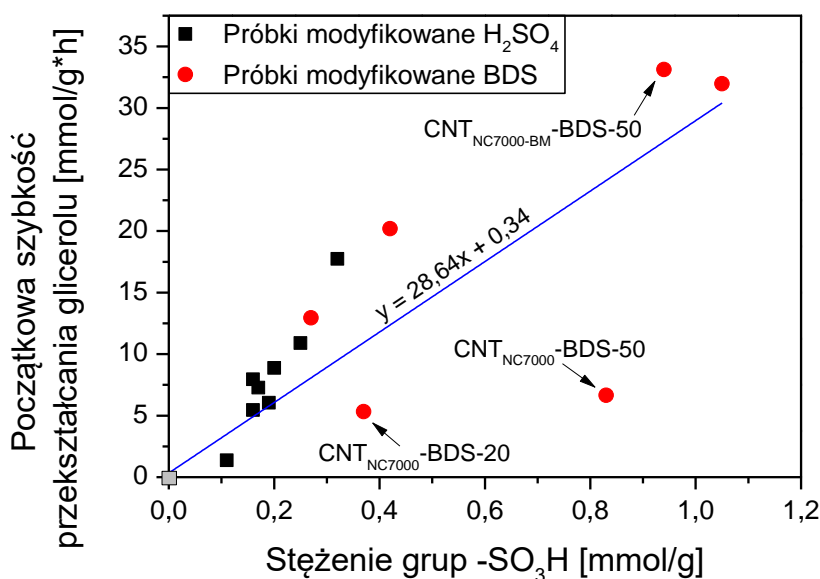
Najbardziej aktywne w procesie były materiały CNT_{NC3100}-BDS-50 oraz CNT_{NC7000}-BM-BDS-50, czyli próbki o wysokiej zawartości grup -SO₃H (odpowiednio 1,05 i 0,94 mmol/g) i jednocześnie prezentujące znaczną kwasowość całkowitą (1,01 i 1,16 mmol H⁺/g, odpowiednio dla CNT_{NC3100}-BDS-50 oraz CNT_{NC7000}-BM-BDS-50). W reakcji z udziałem tych katalizatorów osiągnięto prawie 60 % konwersję glicerolu już po 1 h reakcji, co przewyższyło wynik uzyskany w procesie katalizowanym przez próbkę Amberlyst-15. Wartość konwersji glicerolu praktycznie nie zmieniała się w czasie, co sugeruje osiągnięcie stanu równowagi termodynamicznej [32]. Co ciekawe, w obu wskazanych wyżej przypadkach, wydajność MTBGE osiągnęła maksimum już po 1 h reakcji, a w kolejnych godzinach reakcji produkty te były jedynie przekształcane w wyżej podstawione etery tert-butyłowe glicerolu. Warto zauważyć, że X_G dla próbki CNT_{NC3100}-BDS-50 po 6 h reakcji delikatnie spadała, co było konsekwencją obecności wody w środowisku reakcyjnym, powodującej proces de-eteryfikacji

[32]. W przypadku pozostałych próbek modyfikowanych BDS efekt katalityczny był niższy, a wiązało się to z mniej efektywną funkcjonalizacją tych materiałów (Rys. 17).

6.2.1. Wpływ chemii powierzchni testowanych materiałów na przebieg reakcji eteryfikacji glicerolu

Na Rys. 25 przedstawiono zależność pomiędzy początkową szybkością eteryfikacji glicerolu katalizowanej otrzymanymi próbkami a stężeniem powierzchniowych grup $-SO_3H$.

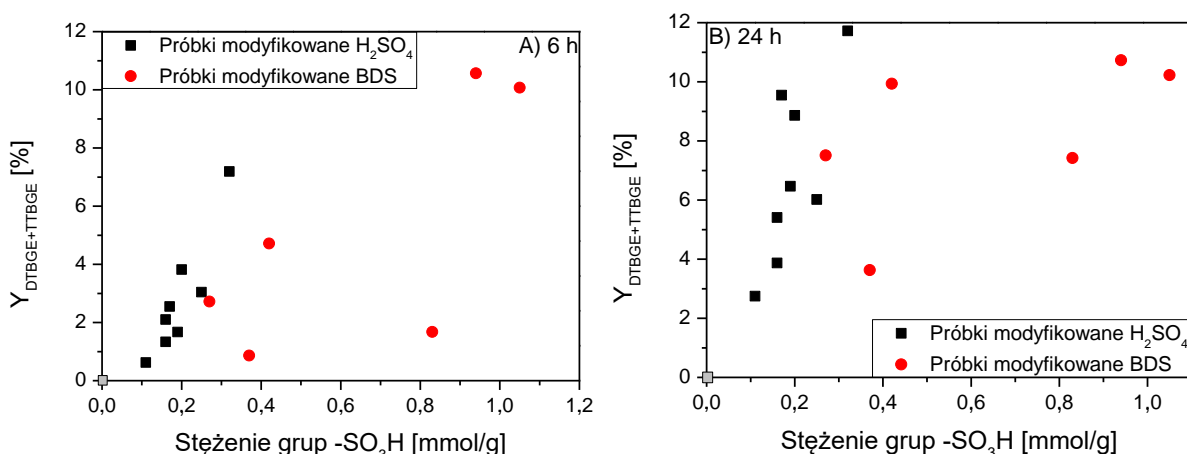
Jak można zaobserwować, istnieje silna zależność pomiędzy wskazanymi parametrami, co wskazuje na kluczową rolę silnie kwasowych grup $-SO_3H$ w przemianie glicerolu w etery tert-butyłowe glicerolu. Zaobserwowano jedynie dwa odstępstwa od tej zależności (próbki $CNT_{NC7000-BDS-20}$ oraz $CNT_{NC7000-BDS-50}$). Można przypuszczać, że istotne znaczenie w aktywności wskazanych próbek mógł mieć również stopień rozdrobnienia materiału (mogący wpływać na dostępność miejsc aktywnych), gdyż początkowa szybkość przekształcania glicerolu dla $CNT_{NC7000-BDS-50}$ i $CNT_{NC7000-BM-BDS-50}$ mocno się różniła mimo zbliżonej ilości sulfonowych grup funkcyjnych na powierzchni tych próbek (tj. 0.83 vs. 0.94 mmol/g, odpowiednio dla $CNT_{NC7000-BDS-50}$ i $CNT_{NC7000-BM-BDS-50}$, Rys. 17).



Rys. 25. Wpływ stężenia grup sulfonowych na początkową szybkość przekształcania glicerolu

Stężenie grup sulfonowych w próbkach miało też istotny wpływ na przekształcanie MTBGE w wyżej podstawione etery tert-butyłowe glicerolu, jak ilustruje Rys. 26. Niemniej jednak zależność ta nie była tak oczywista, co jest widoczne szczególnie w przypadku próbek modyfikowanych H_2SO_4 . Próbki te, jak omówiono już wcześniej, zawierały nie tylko grupy sulfonowe, ale były także bogate w ugrupowania zawierające tlen. Bardzo dobre rezultaty wydajności wyższych eterów ($Y_{DTBGE+TTBGE}$) uzyskane dla tej grupy katalizatorów (wyższe,

mimo niższej zawartości $-\text{SO}_3\text{H}$) przypisano efektowi synergicznemu pomiędzy grupami sulfonowymi i ugrupowaniami zawierającymi tlen [P2 i P5].



Rys. 26. Wpływ stężenia grup sulfonowych na wydajność DTBGE+TTBGE po 6 h reakcji (A) oraz 24 h (B)

Dla najlepiej pracującej próbki (tj. $\text{CNT}_{\text{NC}3100}\text{-BDS-50}$) przeprowadzono optymalizację warunków reakcji. Uwzględniono zastosowanie różnych temperatur reakcji (90, 110 lub 120 °C) oraz wykorzystanie różnej ilości katalizatora (1,0, 2,5, lub 5,0 % wag. względem masy glicerolu). Ustalono, że zastosowanie podwyższonej temperatury (120 °C) oraz zredukowanej ilości katalizatora (2,5 % wag.) umożliwiło osiągnięcie bardzo dobrych wyników już po 1 h reakcji, tj. ~60 % konwersję glicerolu i ~10 % wydajność DTBGE+TTBGE. W tym przypadku wydłużenie czasu reakcji nie miało uzasadnienia, gdyż po 4 h procesu zaobserwowano spadek konwersji glicerolu związany z osiągnięciem równowagi termodynamicznej i następującym procesem de-eteryfikacji.

W kolejnych etapach prac udowodniono również, że próbki $\text{CNT}_{\text{NC}3100}\text{-BDS-50}$ oraz $\text{CNT}_{\text{NC}7000}\text{-BM-BDS-50}$ mogą być z powodzeniem odzyskiwane z mieszaniny poreakcyjnej i wykorzystywane w kolejnych cyklach reakcyjnych bez znacznego spadku aktywności. Możliwość ponownego wykorzystania odnotowano również w przypadku materiałów $\text{CF}_{\text{et}}\text{-BDS}$ oraz $\text{CNT}_{\text{NC}7000}\text{-BM-Glu}/\text{H}_2\text{SO}_4(\text{fum.})\text{-180-12h}$ [P2, P4 i P5].

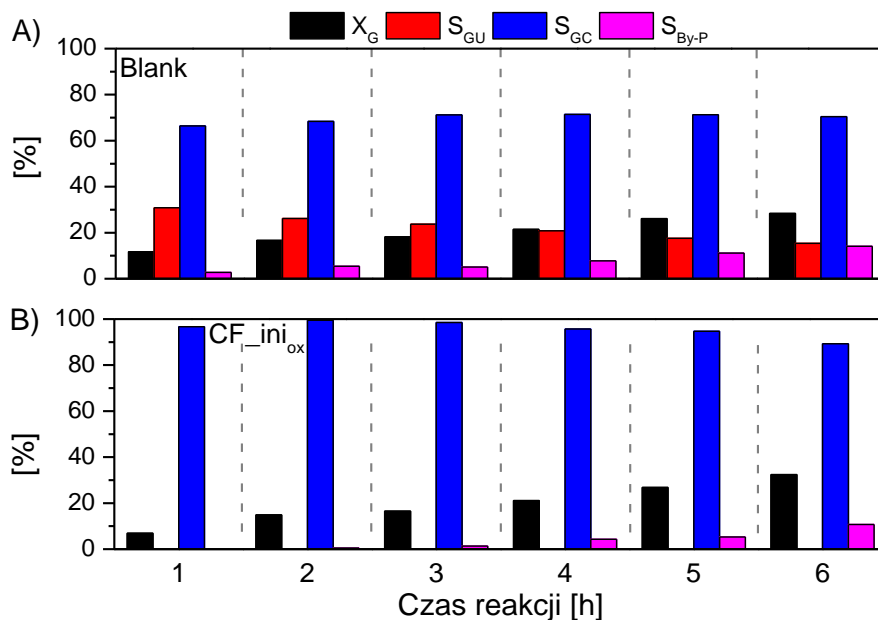
6.3. Gliceroliza mocznika w obecności wybranych tlenków metali osadzonych na CF

Badania nad reakcją glicerolu (G) z mocznikiem (U) realizowano w obecności tlenków wybranych metali ($\text{Me} = \text{Mg}, \text{Ba}, \text{Cr}, \text{lub Zn}$) osadzonych na włóknach węglowych (CF) otrzymanych w warunkach laboratoryjnych w procesie CCVD z gazu LPG (Rozdział 2.4). Efekty tych prac zostały przedstawione w artykule naukowym P3, uwzględnionym w wykazie publikacji będących podstawą rozprawy doktorskiej.

Proces glicerolizy mocznika prowadzono w temperaturze 140 °C pod ciśnieniem atmosferycznym przez 6 h (próbki mieszaniny reakcyjnej analizowano co godzinę),

wykorzystując stosunek molowy reagentów G:U = 1:1 oraz 3 % wag. katalizatora (względem masy glicerolu). Przeprowadzone prace obejmowały zarówno badania aktywności przygotowanych układów $\text{Me}_x\text{O}_y/\text{CF}$, jak i samego nośnika (utleniony CF oznaczony jako $\text{CF}_{\text{ini}_{\text{ox}}}$) – celem określenia jego wpływu na pracę uzyskanych katalizatorów.

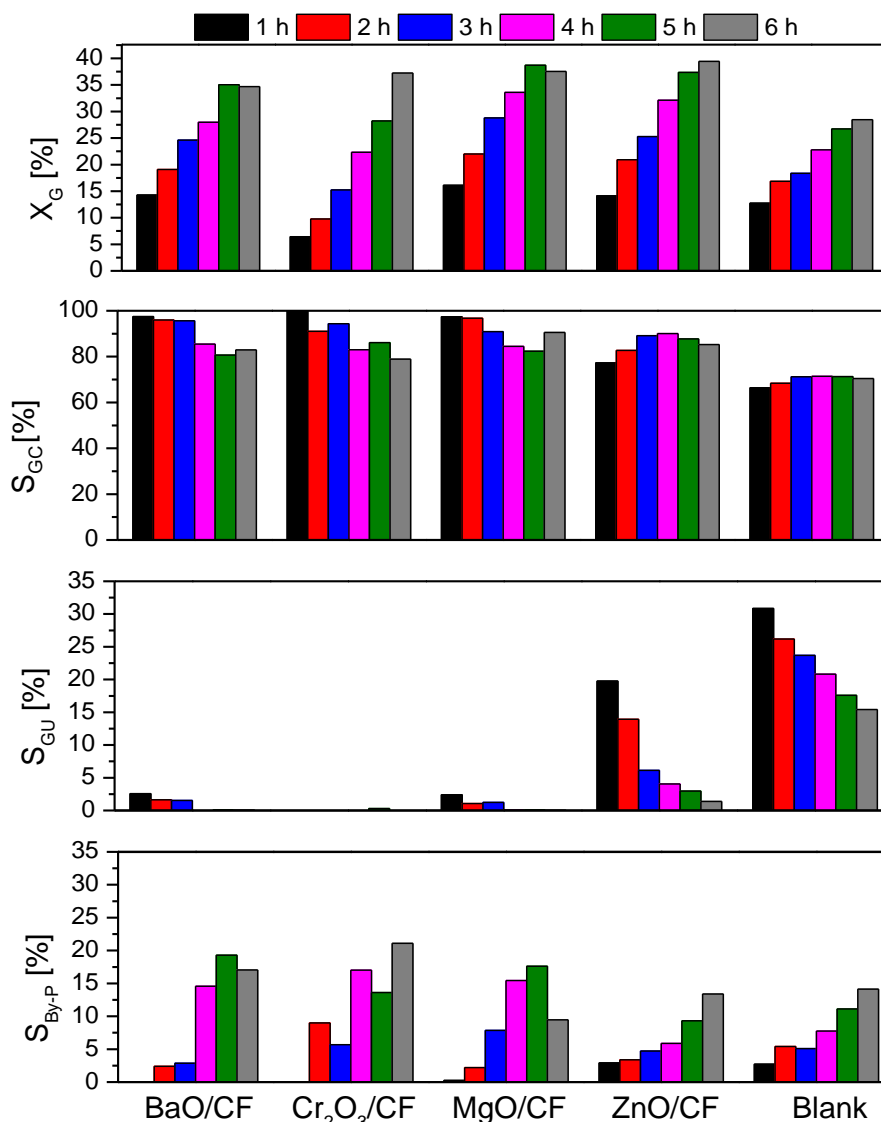
Na Rys. 27 porównano wyniki otrzymane w reakcji glicerolizy mocznika bez użycia katalizatora (A) oraz w procesie realizowanym w obecności samego nośnika węglowego (B). Ustalono, że zastosowanie $\text{CF}_{\text{ini}_{\text{ox}}}$ skutkowało efektywniejszym przekształcaniem produktu przejściowego (karbaminian 2,3-dihydroksypropylu, GU) w węglan glicerolu. Co więcej, również ilość otrzymywanych produktów ubocznych (By-P) została znacznie zredukowana, co w konsekwencji skutkowało zwiększeniem selektywności do węglanu glicerolu (S do GC ~100 %) w stosunku do ślepej próby. Należy zauważyć, że w początkowych godzinach reakcji wyniki konwersji glicerolu otrzymane dla $\text{CF}_{\text{ini}_{\text{ox}}}$ były nieco niższe niż te otrzymane w reakcji bez użycia katalizatora, co najprawdopodobniej było spowodowane bardziej złożonym mechanizmem reakcji (składającym się z wielu etapów) w obecności katalizatora heterogenicznego. Niemniej jednak parametr ten znacznie wzrastał w miarę upływu czasu, przewyższając wielkość konwersji glicerolu uzyskaną w przypadku ślepej próby (tj. 28,5 % vs. 33,1 % po 6 h, odpowiednio dla ślepej próby i $\text{CF}_{\text{ini}_{\text{ox}}}$).



Rys. 27. Wyniki uzyskane w reakcji glicerolizy mocznika prowadzonej bez użycia katalizatora (A) oraz w obecności nośnika węglowego $\text{CF}_{\text{ini}_{\text{ox}}}$

Obecność fazy tlenkowej na nośniku węglowym skutkowała poprawą właściwości katalitycznych otrzymanych układów (w szczególności w odniesieniu do konwersji glicerolu). Niemniej jednak zaobserwowano pewne różnice w aktywności przygotowanych próbek.

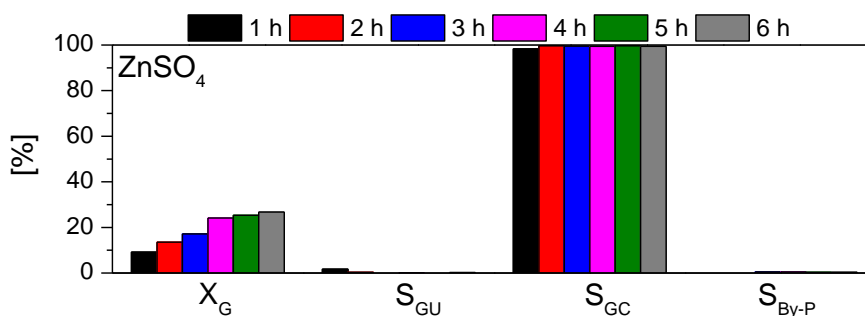
Wynikały one najprawdopodobniej z różnic w dystrybucji ugrupowań kwasowo-zasadowych w badanych materiałach [50]. Otrzymane wyniki przedstawiono na Rys. 28.



Rys. 28. Wyniki uzyskane w reakcji glicerolizy mocznika prowadzonej bez użycia katalizatora (Blank) oraz w obecności układów Me_xO_y/CF (140 °C, G:U = 1:1, Ar przepuszczany przez reaktor)

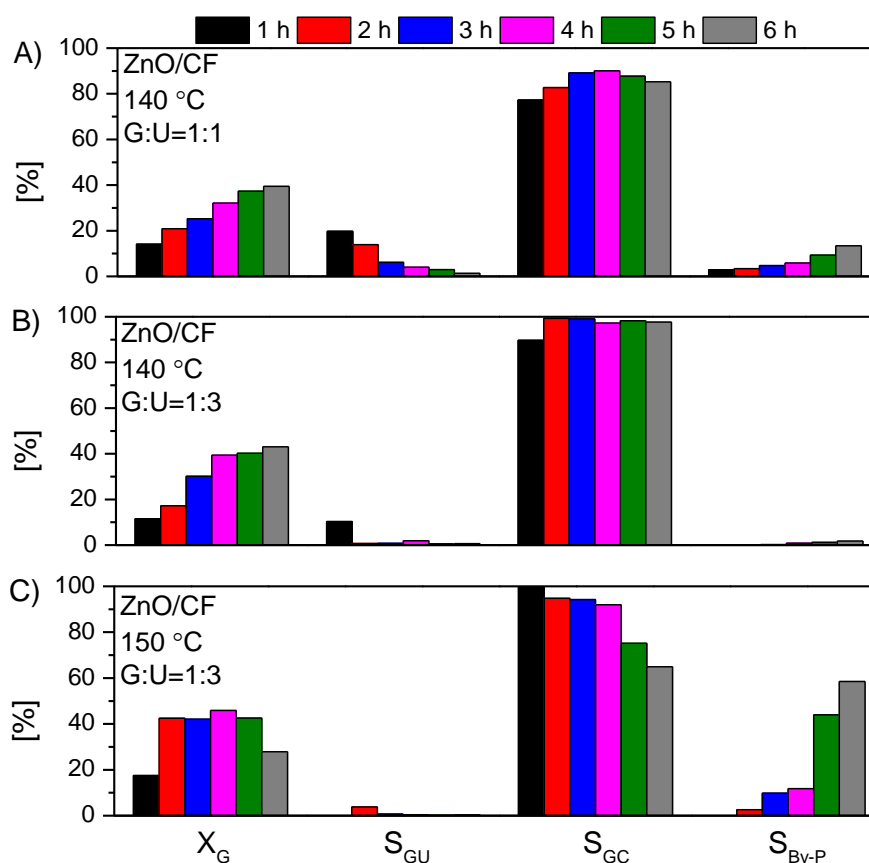
W przypadku materiałów BaO/CF, Cr₂O₃/CF oraz MgO/CF zaobserwowano silne ukierunkowanie procesu na tworzenie produktów ubocznych. Nieco inaczej wyglądało to w przypadku próbki ZnO/CF, gdyż efekt ten był dużo mniej zauważalny. Jednocześnie, w obecności próbki ZnO/CF zaobserwowano nieco mniej skuteczne przekształcanie produktu przejściowego w węglan glicerolu w porównaniu z pozostałymi katalizatorami. Generalnie, najlepsze wyniki w badanym procesie otrzymano w obecności próbek MgO/CF oraz ZnO/CF. W obu przypadkach odnotowano ~40 % konwersję glicerolu oraz ~34 % wydajność GC po 5–6 h reakcji. W związku z mniejszym ukierunkowaniem próbki ZnO/CF na reakcje uboczne (po 5 h), kolejne etapy prac (mające na celu poprawę skuteczności reakcji) przeprowadzono w obecności tego właśnie materiału.

Aktywność wybranej próbki (ZnO/CF) porównano z pracą homogenicznego katalizatora cynkowego ($ZnSO_4$). Przeprowadzone badania ujawniły, że zastosowany siarczan cynku działa bardzo selektywnie ($S_{GC} = \sim 100\%$), jednak glicerol jest przekształcany znacznie mniej efektywnie ($X_G = \sim 27\%$ po 6 h) niż w obecności próbki ZnO/CF, ostatecznie skutkując osiągnięciem niższej wydajności procesu (Rys. 28 i 29).



Rys. 29. Wyniki uzyskane w reakcji glicerolizy mocznika przeprowadzonej w obecności $ZnSO_4$

Dalsze prace miały na celu poprawę efektywności prowadzonej reakcji. Uzyskane wyniki przedstawiono na Rys. 30.

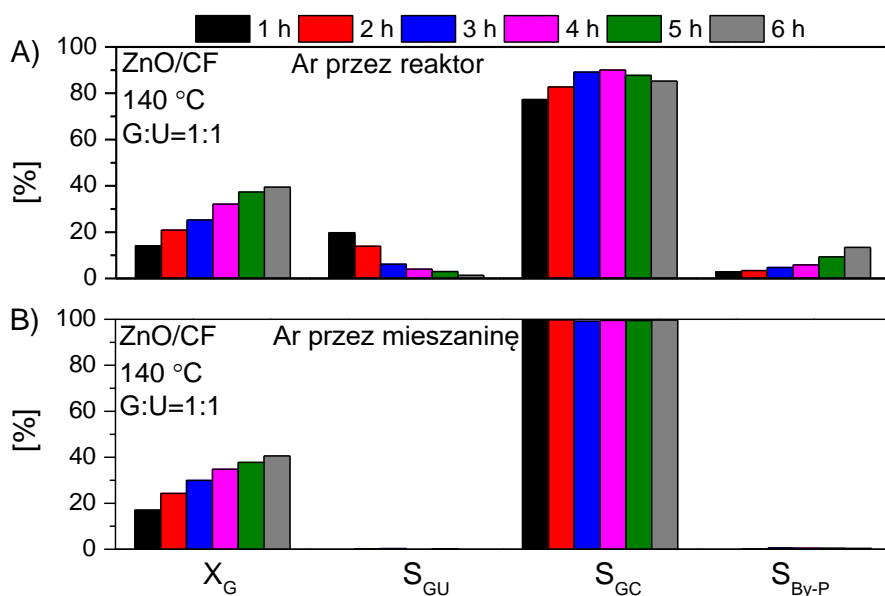


Rys. 30. Wyniki uzyskane w glicerolizy mocznika prowadzonej w obecności ZnO/CF z uwzględnieniem różnych warunków reakcji, tj. 140 °C i G:U = 1:1 (A), 140 °C i G:U = 1:3 (B) oraz 150 °C i G:U = 1:3 (C)

Ustalono, że zwiększenie udziału mocznika w układzie reakcyjnym (stosunek molowy G:U = 1:3; Rys. 30B) ma pozytywny wpływ na przebieg procesu. Prawdopodobnie ma to związek z przesunięciem równowagi reakcji w stronę tworzenia węglanu glicerolu,

poprzez efektywniejsze przekształcanie produktu przejściowego (zgodnie z zasadą przekory). W konsekwencji selektywność do pożądanego produktu znacznie wzrosła, osiągając prawie 100 % po 2 h reakcji, a efekt ten utrzymywał się do 6 h. Określono także, że zastosowanie wyższej temperatury procesu (150 °C) początkowo skutkuje efektywniejszym przekształcaniem glicerolu do GC (40 % konwersja glicerolu z ~100 % selektywnością do GC już po 2 h reakcji). W kolejnych godzinach procesu zaobserwowano jednak dość drastyczny spadek selektywności do węglanu glicerolu, wskutek tworzenia się produktów ubocznych, najprawdopodobniej wynikający z mało efektywnego usuwania amoniaku ze środowiska reakcyjnego i/lub niepożądaną reakcją węglanu glicerolu z mocznikiem (Rys. 5) [47].

W celu większego ukierunkowania reakcji na produkcję węglanu glicerolu, w kolejnym etapie badań uwzględniono inną metodę usuwania amoniaku ze środowiska reakcyjnego. W tym celu, proces glicerolizy mocznika przeprowadzono przepuszczając gaz obojętny (Ar) przez mieszaninę reakcyjną (zamiast przez reaktor), co miało na celu „wymuszenie” usuwania NH₃ [40,48]. Zastosowany zabieg skutkowało zwiększeniem selektywności do GC do 100 %, a wartość tego parametru nie zmieniała się w czasie (Rys. 31). Ostatecznie, w tych warunkach reakcji otrzymano ~40 % wydajność węglanu glicerolu po 6 h stosując ZnO/CF w roli katalizatora.



Rys. 31. Wyniki uzyskane w glicerolizie mocznika przeprowadzonej w obecności ZnO/CF z uwzględnieniem przepuszczenia Ar przez reaktor (A) oraz przez mieszaninę reakcyjną (B)

PODSUMOWANIE

W ramach niniejszej rozprawy doktorskiej przeprowadzono szczegółowe badania dotyczące preparatyki nowych stałych katalizatorów kwasowych opartych na węglach, takich jak termicznie redukowany tlenek grafenu, włókna i nanorurki węglowe. Uwzględniono również preparatykę układów składających się z tlenków wybranych metali osadzonych na włóknach węglowych. Prowadzone badania miały na celu określenie aktywności katalitycznej otrzymanych materiałów w wybranych procesach waloryzacji glicerolu, tj. estryfikacji glicerolu za pomocą kwasu octowego, eteryfikacji glicerolu alkoholem tert-butylovym oraz glicerolizie mocznika. Poniżej przedstawiono najważniejsze obserwacje i wnioski odnotowane podczas prowadzonych badań.

1) Estryfikacja glicerolu za pomocą kwasu octowego w obecności funkcjonalizowanego TRGO:

- Zastosowana metoda syntezy termicznie redukowanego tlenku grafenu skutkowała otrzymaniem mezoporowatego materiału o dość dużej powierzchni właściwej ($617 \text{ m}^2/\text{g}$).
- Przeprowadzone funkcjonalizacje wygenerowały dość wysoką kwasowość przygotowanych próbek tj. 1,09, 1,38 oraz 1,46 mmol H^+/g , odpowiednio dla TRGO_ H_2SO_4 , TRGO_ H_3PO_4 oraz TRGO_BDS, wynikającą z obecności ugrupowań powierzchniowych zawierających siarkę, tlen i/lub fosfor.
- Generowana in situ sól diazoniowa była bardziej efektywnym czynnikiem sulfonującym TRGO niż kwas siarkowy.
- Modyfikacja kwasem fosforowym umożliwiła skuteczne wprowadzenie ugrupowań zawierających fosfor na powierzchnię węgla.
- Najwyższą aktywność katalityczną w procesie estryfikacji glicerolu za pomocą kwasu octowego ($\sim 100\% X_G$ i $\sim 70\% S_{\text{DAG+TAG}}$ już po 1 h reakcji) prezentowała próbka TRGO_BDS, czyli materiał o najwyższej kwasowości całkowitej i wysokiej zawartości grup sulfonowych.
- Wydłużenie czasu reakcji dla TRGO_BDS nie powodowało znaczących zmian wydajności procesu ze względu na osiągnięcie równowagi termodynamicznej.
- Próbką TRGO_BDS nie traciła aktywności katalitycznej przez przynajmniej 4 cykle reakcyjne.
- Zastosowanie materiału TRGO_ H_3PO_4 skutkowało najmniej efektywnym przekształcaniem glicerolu mimo skutecznej funkcjonalizacji i wysokiej kwasowości całkowitej ($1,38 \text{ mmol H}^+/\text{g}$).
- Rodzaj wprowadzonych na powierzchnię TRGO grup funkcyjnych miał kluczowy wpływ na aktywność katalityczną próbek w procesie estryfikacji glicerolu za pomocą kwasu octowego, tj. materiały wzbogacone w grupy sulfonowe efektywniej

(w porównaniu z próbką zawierającą ugrupowania zawierające fosfor) katalizowały proces estryfikacji ze względu na silną moc kwasową.

2) Eteryfikacja glicerolu za pomocą alkoholu tert-butyłowego w obecności włóknistych materiałów węglowych, tj. sulfonowanych włókien węglowych otrzymanych z etylenu lub izobutanu w procesie CCVD oraz funkcjonalizowanych komercyjnych nanorurek węglowych:

- Zastosowanie katalizatora Ni oraz etylenu lub izobutanu jako źródła węgla w procesie CCVD umożliwiło produkcję włóknistych materiałów węglowych o niejednorodnej morfologii (obecność włókien o różnych średnicach oraz niewielkiej ilości nanorurek) i umiarkowanej powierzchni właściwej (tj. $115 \text{ m}^2/\text{g}$ dla $\text{CF}_{\text{i-bu}}$ oraz $174 \text{ m}^2/\text{g}$ dla CF_{et}).
- Włókna węglowe otrzymane z etylenu charakteryzowały się większym stopniem uporządkowania warstw grafenowych niż próbka wyprodukowana z izobutanu.
- Komercyjne nanorurki węglowe składały się z wielościennych CNT o zbliżonych średnicach i różnej czystości ($\text{CNT}_{\text{NC3100}}$: $\%C > 98 \%$ i $\text{CNT}_{\text{NC7000}}$: $\%C = \sim 90 \%$) prezentujących umiarkowaną powierzchnię właściwą ($\text{CNT}_{\text{NC3100}}$: $406 \text{ m}^2/\text{g}$ i $\text{CNT}_{\text{NC7000}}$: $243 \text{ m}^2/\text{g}$).
- Modyfikacja powierzchni węgla za pomocą kwasu siarkowego skutkowała wzbogaceniem materiałów w grupy zawierające siarkę i tlen, jednakże stopień funkcjonalizacji był dość niski (tj. 0,4–0,6 % wprowadzonej siarki).
- Modyfikacja z wykorzystaniem generowanej in situ soli diazoniowej była najefektywniejszą metodą funkcjonalizacji badanych materiałów, skutkującą wprowadzeniem znaczącej ilości siarki (do 3,4 %) występującej wyłącznie w formie silnie kwasowych grup $-\text{SO}_3\text{H}$.
- Zastosowanie wstępnej obróbki mechanicznej CNT (za pomocą młyna kulowego) skutkowało zwiększeniem podatności tych materiałów na funkcjonalizację.
- Włączenie glukozy do modyfikacji CNT za pomocą H_2SO_4 skutkowało wytworzeniem warstwy węgla na powierzchni CNT, która działała jak „klej” dla grup funkcyjnych, co skutkowało wzrostem stopnia funkcjonalizacji (1,2–1,6 %S), jednakże wprowadzona siarka występowała zarówno w formie grup $-\text{SO}_3\text{H}$ jak i innych ugrupowań.
- Wszystkie testowane próbki były aktywne w procesie eteryfikacji glicerolu za pomocą alkoholu tert-butyłowego, jednakże zaobserwowano pewne różnice w skuteczności przekształcania glicerolu do jego pochodnych tert-butyłowych.
- Istnieje silna zależność między zawartością grup $-\text{SO}_3\text{H}$ w próbkach a konwersją glicerolu i wydajnością do wyżej podstawionych eterów tert-butyłowych glicerolu.
- Obecność tlenowych grup funkcyjnych wpływała pozytywnie na przebieg omawianej reakcji, najprawdopodobniej ze względu na zwiększenie hydrofilowości próbek ułatwiającą adsorpcję reagentów na powierzchni katalizatora i ich reakcję.

- Pozytywny wpływ na aktywność CNT miało również rozdrobnienie materiału (wskutek mielenia kulowego), co najprawdopodobniej ułatwiało kontakt katalizatora z reagentami.
- Obecność w próbkach CF_{et} i CF_{i-bu} węgla w różnej formie (włókna i nanorurki) utrudniało ocenę wpływu materiału wyjściowego na skuteczność funkcjonalizacji i aktywności w badanym procesie konwersji glicerolu.
- Optymalizacja warunków reakcji wykonana dla najaktywniejszej próbki (CNT_{NC3100}-BDS-50) wykazała, że osiągnięcie satysfakcjonujących wyników było możliwe już po 1 h reakcji w 120 °C i z użyciem niewielkiej ilości katalizatora (2,5 % wag. względem masy glicerolu).
- Próbki CNT_{NC7000}-BM-Glu/H₂SO₄(fum.)-180-12h, CF_{et}-BDS, CNT_{NC3100}-BDS-50 i CNT_{NC7000}-BM-BDS-50 mogły być z powodzeniem odzyskiwane i wykorzystywane w kolejnych cyklach reakcyjnych.
- Uzyskane w obecności CNT_{NC3100}-BDS-50 oraz CNT_{NC7000}-BM-BDS-50 wyniki katalityczne były lepsze niż te otrzymane w obecności komercyjnego katalizatora Amberlyst-15.

3) Gliceroliza mocznika w obecności tlenków metali osadzonych na włóknach węglowych

- Wykorzystanie gazu LPG i niklu procesie CCVD umożliwiło produkcję włóknistych materiałów węglowych (CF) o różnej średnicy i umiarkowanej powierzchni właściwej (tj. 259 m²/g).
- Obróbka termiczna CF w 300 °C i strumieniu powietrza skutkowała wprowadzeniem tlenowych grup funkcyjnych na powierzchnię węgla.
- Impregnacja CF azotanami wybranych metali (Ba, Cr, Mg, Zn) i następująca po niej obróbka termiczna skutkowała osadzeniem tlenków tych metali na powierzchni CF.
- Zastosowanie utlenionego węgla wyjściowego (CF_{ini_ox}) w reakcji glicerolizy mocznika znacząco poprawiło selektywność do węglanu glicerolu w porównaniu z reakcją prowadzoną bez użycia katalizatora.
- W obecności otrzymanych układów Me_xO_y/CF uzyskano lepsze wyniki konwersji glicerolu do węglanu glicerolu niż w przypadku reakcji przeprowadzonej bez katalizatora, jednak zaobserwowano pewne różnice w aktywności tych próbek wynikające najprawdopodobniej z różnic w dystrybucji ugrupowań kwasowo-zasadowych.
- Najwyższą aktywnością charakteryzowały się próbki MgO/CF oraz ZnO/CF, w obecności których osiągnięto ~40 % konwersję glicerolu i ~34 % wydajność węglanu glicerolu po 6 h.
- próbka ZnO/CF działała efektywniej w badanym procesie niż homogeniczny katalizator ZnSO₄.

- Zastosowanie 3-krotnego nadmiaru mocznika w reakcji (w porównaniu z reakcją przeprowadzoną z wykorzystaniem stosunku molowego reagentów G:U = 1:1) znacząco poprawiło produkcję węglanu glicerolu.
- Wzrost temperatury procesu (ze 140 °C do 150 °C) wpłynął pozytywnie na przebieg reakcji w początkowych godzinach, jednakże po 2 h promował reakcje uboczne.
- Przepuszczanie gazu obojętnego przez mieszaninę reakcyjną (zamiast przez reaktor) ułatwiło usuwanie amoniaku z układu, redukując reakcje uboczne i zwiększając selektywność do węglanu glicerolu do ~100 %.
- W zoptymalizowanych warunkach (tj. wykorzystując stosunek molowy reagentów G:U = 1:3 i temperaturę 150 °C) i z zastosowaniem ZnO/CF w roli katalizatora osiągnięto ~40 % wydajność GC już po 2 h reakcji.

BIBLIOGRAFIA

- [1] G. E. Halkos, E. C. Gkampoura, *Reviewing usage, potentials, and limitations of renewable energy sources*, *Energies*, 2020, 13, 2906.
- [2] J. Kotcher, E. Maibach, W.-T. Cho, *Fossil fuels are harming our brains: identifying key messages about the health effects of air pollution from fossil fuels*, *BMC Public Health*, 2019, 19, 1079.
- [3] E. T. Sayed, A. G. Olabi, A. H. Alami, A. Radwan, A. Mdallal, A. Rezk, M. A. Abdelkareem, *Renewable energy and energy storage systems*, *Energies*, 2023, 16, 1415.
- [4] M. Elkelawy, E. A. El Shenawy, H. A. E. Bastawissi, I. A. El Shennawy, *The effect of using the WCO biodiesel as an alternative fuel in compression ignition diesel engine on performance and emissions characteristics*, *Journal of Physics: Conference Series*, 2022, 2299, 012023.
- [5] V. Gerpen, *Biodiesel processing and production*, *Fuel Processing Technology*, 2005, 86, 1097–1107.
- [6] M. U. H. Suzihaque, Habsah Alwi, Umami Kalthum Ibrahim, Sureena Abdullah, Normah Haron, *Biodiesel production from waste cooking oil: A brief review*, *Materials Today: Proceedings*, 2022, 63(1), S490–S495.
- [7] M. Harabi, S. N. Bouguerra, F. Marrakchi, L. P. Chrysikou, S. Bezergianni, M. Bouaziz, *Biodiesel and crude glycerol from waste frying oil: Production, characterization and evaluation of biodiesel oxidative stability with diesel blends*, *Sustainability*, 2019, 11, 1937.
- [8] N. I. W. Azelee, A. N. M. Ramli, N. H. A. Manas, N. Salamun, R. C. Man, H. El Enshasy, *Glycerol in food, cosmetics and pharmaceutical industries: basics and new applications*, *International Journal of Scientific & Technology Research*, 2019, 8(12), 553–558.
- [9] M. R. Monteiro, C. L. Kugelmeier, R. S. Pinheiro, M. O. Batalha, A. da Silva César, *Glycerol from biodiesel production: Technological paths for sustainability*, *Renewable and Sustainable Energy Reviews*, 2018, 88, 109–122.
- [10] S. Nomanbhay, R. Hussein, M. Y. Ong, *Sustainability of biodiesel production in Malaysia by production of bio-oil from crude glycerol using microwave pyrolysis: a review*, *Green Chemistry Letters and Reviews*, 2018, 11(2), 135–157.
- [11] IEA (2020), *Renewables 2020*, IEA, Paris; <https://www.iea.org/reports/renewables-2020/transport-biofuels>.
- [12] C. Len, R. Luque, *Continuous flow transformations of glycerol to valuable products: an overview*, *Sustainable Chemical Processes*, 2014, 2, 1.
- [13] S. Veluturla, N. Archana, D. Subba Rao, N. Hezil, I. S. Indrajaya, S. Spoorthi, *Catalytic valorization of raw glycerol derived from biodiesel: a review*, *Biofuels*, 2016, 9(3), 305–314.

- [14] R. P. Asopa, R. Bhoi, V. K. Saharan, *Valorization of glycerol into value-added products: A comprehensive review on biochemical route*, Bioresource Technology Reports, 2022, 20, 101290.
- [15] Y. Jiang, X. Lia, H. Zhao, Z. Hou, *Esterification of glycerol with acetic acid over SO₃H-functionalized phenolic resin*, Fuel, 2019, 255, 115842.
- [16] S. Hosztafi, *Heroin. Part II. Preparation, hydrolysis, stability, pharmacokinetics*, Acta Pharmaceutica Hungarica, 2001, 71, 373–83.
- [17] P. U. Okoye, A. Z. Abdullah, B. H. Hameed, *Synthesis of oxygenated fuel additives via glycerol esterification with acetic acid over bio-derived carbon catalyst*, Fuel, 2017, 209, 538–544.
- [18] R. Mou, X. Wang, Z. Wang, D. Zhang, Z. Yin, Y. Lv, Z. Wei, *Synthesis of fuel bioadditive by esterification of glycerol with acetic acid over hydrophobic polymer-based solid acid*, Fuel, 2021, 302, 121175.
- [19] S. A. Rane, S. M. Pudi, P. Biswas, *Esterification of glycerol with acetic acid over highly active and stable alumina-based catalysts: A reaction kinetics study*, Chemical and Biochemical Engineering Quarterly, 2016, 30(1), 33–45.
- [20] G. Mota, J. V. C. do Carmo, C. B. Paz, G. D. Saraiva, A. Campos, G. Duarte, E. C. da Silva Filho, A. C. Oliveira, J. M. Soares, E. Rodríguez-Castellón, E. Rodríguez-Aguado, *Influence of the metal incorporation into hydroxyapatites on the deactivation behavior of the solids in the esterification of glycerol*, Catalysts, 2022, 12(1), 10.
- [21] P. U. Okoye, B. H. Hameed, *Review on recent progress in catalytic carboxylation and acetylation of glycerol as a byproduct of biodiesel production*, Renewable and Sustainable Energy Reviews, 2016, 53, 558–574.
- [22] P. U. Okoye, A. Z. Abdullah, B. H. Hameed, *A review on recent developments and progress in the kinetics and deactivation of catalytic acetylation of glycerol-A byproduct of biodiesel*, Renewable and Sustainable Energy Reviews, 2017, 74, 387–401.
- [23] Y. Sun, J. Hu, S. An, Q. Zhang, Y. Guo, D. Song, Q. Shang, *Selective esterification of glycerol with acetic acid or lauric acid over rod-like carbon-based sulfonic acid functionalized ionic liquids*, Fuel, 2017, 207, 136–145.
- [24] J. Lilja, J. Aumo, T. Salmi, D. Yu. Murzin, P. Mäki-Arvela, M. Sundell, K. Ekman, R. Peltonen, H. Vainio, *Kinetics of esterification of propanoic acid with methanol over a fibrous polymer-supported sulphonic acid catalyst*, Applied Catalysis A: General, 2002, 228, 253–267.
- [25] R. Mou, X. Wang, Z. Wang, D. Zhang, Z. Yin, Y. Lv, Z. Wei, *Synthesis of fuel bioadditive by esterification of glycerol with acetic acid over hydrophobic polymer-based solid acid*, Fuel, 2021, 302, 121175.

- [26] G. A. Bedogni, M. D. Acevedo, F. Aguzín, N. B. Okulik, C. L. Padró, *Synthesis of bioadditives of fuels from biodiesel-derived glycerol by esterification with acetic acid on solid catalysts*, Environmental Technology, 2017, 39(15), 1955–1966.
- [27] P. Gautam, S. Barman, A. Ali, *Catalytic performance of cerium-modified ZSM-5 zeolite as a catalyst for the esterification of glycerol with acetic acid*, International Journal of Chemical Reactor Engineering, 2020, 18(9), 20200081.
- [28] M. Popova, H. Lazarova, A. Szegedi, M. R. Mihályi, M. Rangus, B. Likozar, V. D. B. C. Dasireddy, *Renewable glycerol esterification over sulfonic-modified mesoporous silicas*, Journal of the Serbian Chemical Society, 2018, 83(1), 39–50.
- [29] W. Zhao, B. Yang, C. Yi, Z. Lei, J. Xu, *Etherification of glycerol with isobutylene to produce oxygenate additive using sulfonated peanut shell catalyst*, Industrial & Engineering Chemistry Research, 2010, 49(24), 12399–12404.
- [30] R. Estevez, M. I. López, C. Jiménez-Sanchidrián, D. Luna, F. J. Romero-Salguero, F. M. Bautista, *Etherification of glycerol with tert-butyl alcohol over sulfonated hybrid silicas*, Applied Catalysis A: General, 2016, 526, 155–163.
- [31] N. Viswanadham, S. K. Saxena, *Etherification of glycerol for improved production of oxygenates*, Fuel, 2013, 103, 980–986.
- [32] M. Gonçalves, V. C. Souza, T. S. Galhardo, M. Mantovani, F. C. A. Figueiredo, D. Mandelli, W. A. Carvalho, *Glycerol conversion catalyzed by carbons prepared from agroindustrial wastes*, Industrial & Engineering Chemistry Research, 2013, 52, 2832–2839.
- [33] Ö. D. Bozkurt, F. Yılmaz, N. Bağlar, S. Çelebi, A. Uzun, *Compatibility of di- and tri-tert-butyl glycerol ethers with gasoline*, Fuel, 2019, 255, 115767.
- [34] Ö. D. Bozkurt, F. M. Tunç, N. Bağlar, S. Çelebi, İ. D. Günbaş, A. Uzun, *Alternative fuel additives from glycerol by etherification with isobutene: Structure-performance relationships in solid catalysts*, Fuel Processing Technology, 2015, 138, 780–804.
- [35] P. M. Veiga, C. O. Veloso, A. G. Dias, C. A. Henriques, *Identification of ethyl and t-butyl glyceryl ethers using gas chromatography coupled with mass spectrometry*, Journal of the Brazilian Chemical Society, 2018, 29(6), 1328–1335.
- [36] F. Frusteri, F. Arena, G. Bonura, C. Cannilla, L. Spadaro, O. Di Blasi, *Catalytic etherification of glycerol by tert-butyl alcohol to produce oxygenated additives for diesel fuel*, Applied Catalysis A: General, 2009, 367, 77–83.
- [37] M. Gonçalves, M. Mantovani, W. A. Carvalho, R. Rodrigues, D. Mandelli, J. S. Albero, *Biodiesel wastes: An abundant and promising source for the preparation of acidic catalysts for utilization in etherification reaction*, Chemical Engineering Journal, 2014, 256, 468–474.

- [38] A. Rudra Paul, S. Sarkar, J. Hossain, S. A. Hussain, S. Majumdar, *Design and synthesis of bis-coumarinyl methanes from 4-hydroxy-coumarin and aldehydes catalysed by Amberlyst 15 via dual C-C coupling: introducing coumarin based thin film organic nano-materials for memory devices*, *Research on Chemical Intermediates*, 2022, 48, 4963–4985.
- [39] J. Liu, Y. Jiang, P. Zhang, B. Yang, *Enhance glycerol conversion through co-etherification with isobutene and tert-butanol*, *Fuel Processing Technology*, 2021, 218, 106838.
- [40] H. Zhang, H. Liu, A. Wang, C. Xu, S. Yang, *Progress of catalytic valorization of bio-glycerol with urea into glycerol carbonate as a monomer for polymeric materials*, *Advances in Polymer Technology*, 2020, 2020, 7207068.
- [41] P. de Caro, M. Bandres, M. Urrutigoñy, C. Cecutti, S. Thiebaud-Roux, *Recent Progress in Synthesis of Glycerol Carbonate and Evaluation of Its Plasticizing Properties*, *Frontiers in Chemistry*, 2019, 7, 308.
- [42] C. Hammond, J.A. Lopez-Sanchez, M. Hasbi Ab Rahim, N. Dimitratos, R. L. Jenkins, A. F. Carley, Q. He, C. J. Kiely, D. W. Knighta, G. J. Hutchings, *Synthesis of glycerol carbonate from glycerol and urea with gold-based catalysts*, *Dalton Transactions*, 2011, 40, 3927.
- [43] D. Wang, X. Zhang, C. Liu, T. Cheng, *Synthesis of glycerol carbonate from glycerol and urea over lanthanum compounds*, *Reaction Kinetics, Mechanisms and Catalysis*, 2015, 115, 597–609.
- [44] F. Rubio-Marcos, V. Calvino-Casilda, M. A. Bañares, J. F. Fernandez, *Novel hierarchical Co₃O₄/ZnO mixtures by dry nanodispersion and their catalytic application in the carbonylation of glycerol*, *Journal of Catalysis*, 2010, 275, 288–293.
- [45] M. Bartoli, C. Zhu, M. Chae, D. Bressler, *Value-added products from urea glycerolysis using a heterogeneous biosolids-based catalyst*, *Catalysts*, 2018, 8, 373.
- [46] N. Narkhede, A. Patel, *Facile synthesis of glycerol carbonate via glycerolysis of urea catalysed by silicotungstates impregnated to MCM-41*, *RSC Advances*, 2015, 5, 52801–52808.
- [47] B. Mallesham, A. Rangaswamy, B. G. Rao, T. V. Rao, B. M. Reddy, *Solvent-free production of glycerol carbonate from bioglycerol with urea over nanostructured promoted SnO₂ catalysts*, *Catalysis Letters*, 2020, 150, 3626–3641.
- [48] L. Wang, Y. Ma, Y. Wang, S. Liu, Y. Deng, *Efficient synthesis of glycerol carbonate from glycerol and urea with lanthanum oxide as a solid base catalyst*, *Catalysis Communications*, 2011, 12, 1458–1462.
- [49] J.-H. Park, J. S. Choi, S. K. Woo, S. D. Lee, M. Cheong, H. S. Kim, H. Lee, *Isolation and characterization of intermediate catalytic species in the Zn-catalyzed glycerolysis of urea*, *Applied Catalysis A: General*, 2012, 433–434, 35–40.

- [50] S. E. Kondawar, A. S. Potdar, C. V. Rode, *Solvent-free carbonylation of glycerol with urea using metal loaded MCM-41 catalysts*, RSC Advances, 2015, 5, 16452–16460.
- [51] S. Charate, S. Shinde, S. Kondawar, U. Desai, P. Wadgaonkar, C. Rode, *Role of preparation parameters of Cu-Zn mixed oxide catalyst in solvent free glycerol carbonylation with urea*, Journal of the Indian Chemical Society, 2021, 98, 100090.
- [52] S. Fujita, Y. Yamanishi, M. Arai, *Synthesis of glycerol carbonate from glycerol and urea using zinc-containing solid catalysts: A homogeneous reaction*, Journal of Catalysis, 2013, 297, 137–141.
- [53] N. Muradov, F. Smith, A. T-Raissi, *Catalytic activity of carbons for methane decomposition reaction*, Catalysis Today, 2005, 102–103, 225–233.
- [54] M. Iwanow, T. Gärtner, V. Sieber, B. König, *Activated carbon as catalyst support: precursors, preparation, modification and characterization*, Beilstein Journal of Organic Chemistry, 2020, 16, 1188–1202.
- [55] K. Chizari, I. Janowska, M. Houllé, I. Florea, O. Ersen, T. Romero, P. Bernhardt, M. J. Ledoux, C. Pham-Huu, *Tuning of nitrogen-doped carbon nanotubes as catalyst support for liquid-phase reaction*, Applied Catalysis A: General, 2010, 380, 72–80.
- [56] A. Malaika, K. Ptaszyńska, M. Kozłowski, *Conversion of renewable feedstock to bio-carbons dedicated for the production of green fuel additives from glycerol*, Fuel, 2021, 288, 119609.
- [57] F. M. Perez, M. N. Gatti, C. S. Fermanelli, C. Saux, M. Soledad Renzini, F. Pompeo, *Crude glycerol esterification using biomass-derived carbon acid catalysts*, Next Materials, 2024, 2, 100125.
- [58] N. Hidayati, I. R. Maulida, H. Purnama, M. Musthofa, A. Ur Rahmah, *Optimisation of the glycerol acetylation process using graphene oxide catalyst*, South African Journal of Chemical Engineering, 2024, 48, 254–264.
- [59] L. D. R. Riascos, A. E. R. Sanabria, G. A. T. Rodríguez, A. Sachse, C. D. M. Muñoz, *Sulfonated reduced graphene oxide: an acid catalyst that efficiently promotes the esterification of glycerol*, Topics in Catalysis, 2022, 65, 957–965.
- [60] T. S. Galhardo, N. Simone, M. Gonçalves, F. C. A. Figueiredo, D. Mandelli, W. A. Carvalho, *Preparation of sulfonated carbons from rice husk and their application in catalytic conversion of glycerol*, ACS Sustainable Chemistry & Engineering, 2013, 1(11), 1381–1389.
- [61] C. Miranda, A. Ramírez, A. Sachse, Y. Pouilloux, J. Urresta, L. Pinard, *Sulfonated graphenes: Efficient solid acid catalyst for the glycerol valorization*, Applied Catalysis A: General, 2019, 580, 167–177.
- [62] H. Nguyen-Phu, L. T. Do, E. W. Shin, *Investigation of glycerolysis of urea over various ZnMeO (Me = Co, Cr, and Fe) mixed oxide catalysts*, Catalysis Today, 2020, 352, 80–87.
- [63] G. P. Fernandes, G. D. Yadav, *Selective glycerolysis of urea to glycerol carbonate using combustion synthesized magnesium oxide as catalyst*, Catalysis Today, 2018, 309, 153–160.

- [64] S. E. Kondawar, R. B. Mane, A. Vasishta, S. B. More, S. D. Dhengale, C. V. Rode, *Carbonylation of glycerol with urea to glycerol carbonate over supported Zn catalysts*, Applied Petrochemical Research, 2017, 7, 41–53.
- [65] Q. Guan, Y. Li, Y. Chen, Y. Shi, J. Gu, B. Li, R. Miao, Q. Chen, P. Ning, *Sulfonated multi-walled carbon nanotubes for biodiesel production through triglycerides transesterification*, RSC Advances, 2017, 7, 7250–7258.
- [66] J. Gaidukevič, J. Barkauskas, A. Malaika, P. Rechnia-Gorący, A. Możdżyńska, V. Jasulaitienė, M. Kozłowski, *Modified graphene-based materials as effective catalysts for transesterification of rapeseed oil to biodiesel fuel*, Chinese Journal of Catalysis, 2018, 39, 1633–1645.
- [67] B. F. Machado, P. Serp, *Graphene-based materials for catalysis*, Catalysis Science & Technology, 2012, 2, 54–75.
- [68] P. Nowicki, W. Szymanowski, R. Pietrzak, *Textural, surface, thermal and sorption properties of the functionalized activated carbons and carbon nanotubes*, Polish Journal of Chemical Technology, 2015, 17, 120–127.
- [69] L. J. Konwar, P. Mäki-Arvela, J.-P. Mikkola, *SO₃H-containing functional carbon materials: Synthesis, structure, and acid catalysis*, Chemical Reviews, 2019, 119, 11576–11630.
- [70] J. Gaidukevič, J. Barkauskas, A. Malaika, V. Jasulaitienė, M. Kozłowski, *Preparation and characterization of basic graphene-based catalysts and their application in biodiesel synthesis*, Applied Surface Science, 2021, 554, 149588.
- [71] L. F. Giraldo, W. Brostow, E. Devaux, B. L. López, L. D. Pérez, *Scratch and wear resistance of polyamide 6 reinforced with multiwall carbon nanotubes*, Journal of Nanoscience and Nanotechnology, 2008, 8, 3176–3183.
- [72] O. S. G. P. Soares, A. G. Gonçalves, J. J. Delgado, J. J. M. Órfão, M. F. R. Pereira, *Modification of carbon nanotubes by ball-milling to be used as ozonation catalysts*, Catalysis Today, 2015, 249, 199–203.
- [73] M. Gomes, L. C. Gomes, R. Teixeira-Santos, M. F. R. Pereira, O. S. G. P. Soares, F. J. Mergulhão, *Optimizing CNT loading in antimicrobial composites for urinary tract application*, Applied Sciences, 2021, 11, 4038.
- [74] P. Rechnia, A. Malaika, M. Kozłowski, *Synthesis of tert-amyl methyl ether (TAME) over modified activated carbon catalysts*, Fuel, 154, 2015, 338–345.
- [75] A. Corrêa, R. Bastos, G. Filho, J. Zamian, L. Conceição, *Preparation of sulfonated carbon-based catalysts from murumuru kernel shell and their performance in the esterification reaction*, RSC Advances, 2020, 10, 20245–20256.
- [76] H. Ji, J. Fu, T. Wang, *Pyrolyzing renewable sugar and taurine on the surface of multi-walled carbon nanotubes as heterogeneous catalysts for hydroxymethylfurfural production*, Catalysts, 2018, 8, 517.
- [77] A. Malaika, M. Heinrich, J. Gościańska, M. Kozłowski, *Synergistic effect of functional groups in carbonaceous spheres on the formation of fuel enhancers from glycerol*, Fuel, 2020, 280, 118523.

- [78] S. Betelu, I. Tijunelyte, L. Boubekeur-Lecaque, I. Ignatiadis, J. Ibrahim, S. Gaboreau, C. Berho, T. Toury, E. Guenin, N. Lidgi-Guigui, N. Félidj, E. Rinnert, M. L. de la Chapelle, *Evidence of the grafting mechanisms of diazonium salts on gold nanostructures*, *The Journal of Physical Chemistry C*, 2016, 120, 18158–18166.
- [79] M. Sandomierski, A. Voelkel, *Diazonium modification of inorganic and organic fillers for the design of robust composites: A review*, *Journal of Inorganic and Organometallic Polymers and Materials*, 2021, 31, 1–21.
- [80] P. Rechnia-Gorący, A. Malaika, M. Kozłowski, *Acidic activated carbons as catalysts of biodiesel formation*, *Diamond and Related Materials*, 2018, 87, 124–33.
- [81] J. Yang, H. Zhang, Z. Ao, S. Zhang, *Hydrothermal carbon enriched with sulfonic and carboxyl groups as an efficient solid acid catalyst for butanolysis of furfuryl alcohol*, *Catalysis Communications*, 2019, 123, 109–113.

**KOPIE ARTYKUŁÓW
NAUKOWYCH
BĘDĄCYCH PODSTAWĄ
ROZPRAWY
DOKTORSKIEJ**

P1



Full Length Article

The impact of surface groups of functionalized graphene on glycerol acetylation

Anna Malaika^{a,*}, Karolina Ptaszyńska^a, Justina Gaidukevič^b, Mieczysław Kozłowski^a

^a Faculty of Chemistry, Adam Mickiewicz University in Poznań, Uniwersytetu Poznańskiego 8, 61-614 Poznań, Poland

^b Faculty of Chemistry and Geosciences, Institute of Chemistry, Vilnius University, Naugarduko 24, LT-03225 Vilnius, Lithuania



ARTICLE INFO

Keywords:

Thermally reduced graphene oxide
Glycerol valorization
Acetins
Fuel additives

ABSTRACT

Thermally reduced graphene oxide (TRGO) was functionalized using sulfuric acid, phosphoric acid, and 4-benzenediazonium sulfonate generated *in situ* to obtain solid acid graphene-based catalysts. The prepared samples were characterized using different techniques, i.e., elemental and textural analyses, microscope investigations, thermogravimetric analysis, XPS measurements, and acid-base titration. The obtained results revealed differences in the susceptibility of TRGO to functionalization with various modifying agents and in the chemical properties of the final carbon products. The catalytic performance of the graphene-based samples was further tested in the reaction of glycerol esterification performed with acetic acid at 110 °C using glycerol to acetic acid molar ratio of 1:6. The catalysts were found to be active in the tested process, however, satisfactory results were obtained only in the presence of TRGO modified with 4-benzenediazonium sulfonate (TRGO_BDS). This sample gave almost 100% conversion of glycerol just within 1 h of the reaction, along with a very high combined yield of di- and triacetins, i.e., the products of interest, of about 70%. The excellent activity of TRGO_BDS was ascribed to a high content of surface SO₃H groups which were found to promote a high rate of reaction and the formation of higher acetins. The phosphate groups present on the surface of TRGO modified with phosphoric acid were also able to catalyze the process, however, their catalytic efficiency in the reaction was considerably lower than that of sulfonic groups.

1. Introduction

Global biodiesel production has been growing considerably in recent years. For instance, more than 47 billion liters of biodiesel were produced in 2020. This is about 50% more compared to 2015. In addition, it is estimated that in the nearest future biodiesel production will continue to increase, reaching over 50 billion liters in 2025 [1]. Importantly, the process of biodiesel production is accompanied by the formation of significant amounts of a by-product, which is glycerol (it constitutes at least 10 v/v% of the resulting mixture [2]). The effective usage/valorization of this glycerol could considerably improve the profitability of biodiesel production.

One of the most important ways to valorize glycerol is its esterification with acetic acid. The products of this reaction are mono-, di- and triacetins (MA, DA and TA, respectively). All these glycerol derivatives find interesting applications, e.g., in cosmetic, plastic or food industries [3]. The acetins of the highest importance are, however, DA and TA, which are particularly valuable for the automotive industry. In this

sector, DA and TA are used as fuel enhancers improving the viscosity and anti-knock properties of fuel as well as fuel additives reducing the noxious gas emissions [4].

Glycerol esterification to acetins is often performed in the presence of homogeneous acid catalysts, e.g., sulfuric or p-toluenesulfonic acid [5]. These catalysts allowed obtaining high process efficiency, however, their usage shows a number of disadvantages, including difficulties in separating and purifying the products, reusing the catalyst, or protecting equipment against corrosion [6,7]. All these limitations have caused a significant change in the current trends in catalysis, namely replacing the homogeneous catalysts with heterogeneous ones that are more practical to use, more environmentally friendly, and reusable [8,9].

Among the most interesting heterogeneous catalysts that have gained a special interest in the field of modern catalysis are carbon-based structures. This is due to several reasons, e.g., high thermal stability of carbons, the possibility of their production from wastes, or occurrence of carbons in various morphological forms [10,11]. The most important factor seems to be, however, the high versatility of such

* Corresponding author.

E-mail address: amalaika@amu.edu.pl (A. Malaika).

<https://doi.org/10.1016/j.fuel.2021.122987>

Received 26 September 2021; Received in revised form 12 December 2021; Accepted 15 December 2021

Available online 29 December 2021

0016-2361/© 2021 Elsevier Ltd. All rights reserved.

materials, resulting from the ease of tailoring their properties [12]. For example, our previous studies showed that modified activated carbons obtained from pine sawdust were active in biodiesel formation and in the synthesis of fuel additives [13–15]. Furthermore, carbon xerogels containing various functionalities were found to catalyze the hydrolysis of cellobiose [16], whereas oxygen-modified activated carbons were effective in the coupled reaction of ethylbenzene dehydrogenation/nitrobenzene hydrogenation [17]. In regard to glycerol esterification, carbon xerogels and spheres synthesized in our laboratory were able to effectively convert glycerol and produce acetins at 80 °C [11]. Modified ordered mesoporous carbons obtained from sucrose via a hard template method gave a combined selectivity to DA + TA of about 77% at 110 °C within 6 h [18], whereas bio-carbons synthesized from glycerol or sugars via a facile approach of partial carbonization produced di- and triacetins with a selectivity of about 70% just within 2 h [19].

Graphene is a carbon material that has received special research attention in recent decades. This results from its extraordinary properties, such as chemical, thermal, optical, and electrochemical stability, a large theoretical specific surface area (up to 2630 m²/g), excellent electron mobility, and a number of possible applications, also in catalysis [20]. Graphene oxide (GO) has already been tested in glycerol esterification. Gao et al. [21] obtained a complete glycerol conversion with a 90.2% combined selectivity to DA and TA over unmodified GO at 120 °C within 6 h, using glycerol to acetic acid molar ratio of 1:10 and the catalyst loading of 5 wt.%. In the this work, thermally reduced graphene oxide (TRGO) was synthesized in order to have the carbon sample with a number of structural defects ready for functionalization. TRGO was further treated with different reagents, i.e., 4-benzenediazonium sulfonate (BDS), sulfuric acid (SA,) and phosphoric acid (PA), to introduce various functionalities into its structure. The functionalized graphene samples were then investigated in glycerol esterification for the first time. The obtained results allowed us to elucidate the effect of different acidic groups present on the TRGO surface on the catalyst ability to form higher acetins.

2. Experimental part

2.1. Preparation of graphene-based catalysts

Thermally reduced graphene oxide (TRGO) was obtained from graphite powder (Merck, ≥99.5%), which was at first treated with concentrated H₂SO₄, K₂S₂O₈ and P₂O₅, and then oxidized by the Hummers' method using NaNO₃, H₂SO₄ and KMnO₄ [22,23]. The obtained graphite oxide (GO) was rinsed thoroughly with distilled water, dried and stored in a desiccator. Finally, GO was exposed to a sudden change in temperature (800 °C, argon flow of 100 cm³/min), which led to simultaneous exfoliation and reduction of graphite oxide and the formation of TRGO [24]. Details of the preparation procedure can be found in our previous paper [20].

The TRGO sample was modified with different agents, i.e., sulfuric acid, phosphoric acid, and 4-benzenediazonium sulfonate (BDS), to introduce acidic functional groups on its surface.

For the modification of TRGO with concentrated sulfuric acid, 3 g of TRGO and 140 cm³ of 95% H₂SO₄ were mixed in a three-neck round bottom flask, equipped with a magnetic stirrer, thermocouple and a silicon oil bath, working under reflux conditions. The mixture was heated under Ar flow. After a 20-hour reaction at 140 °C, it was cooled and slowly poured into a beaker with distilled water. Afterwards, the obtained carbon product was filtered and washed thoroughly with hot distilled water until a pH value of ~ 7 was achieved. Finally, the carbon sample was dried at 110 °C overnight and sieved to a uniform particle size of ≤ 0.4 mm. The resulting material was labeled here as TRGO.SA.

The modification of TRGO with BDS was performed as follows: 2 g of TRGO and 100 cm³ of distilled water were mixed in a round-bottom flask. Sulfanilic acid (2.87 g), sodium nitrite (1.15 g), and concentrated hydrochloric acid (35–35%, 20 cm³) were then added to the

mixture. The reaction was carried out at room temperature for 20 h. The resulting carbon product was washed with distilled water, methanol, dimethylformamide (DMF), and acetone. Finally, it was dried at 110 °C overnight and sieved (to a particle size of ≤ 0.4 mm). The as-prepared sample was labeled as TRGO.BDS.

The modification of TRGO with phosphoric acid was started by impregnating the TRGO sample (2.5 g) with a 7.0% H₃PO₄ solution (53.8 g). The impregnation process was performed upon continuous mechanical stirring at ambient temperature for 4 h. The impregnated TRGO sample was then dried at 190 °C overnight and finally, it was thermally treated under argon flow (800 °C, 30 min). The resulting material was washed with distilled water, dried at 110 °C overnight and sieved to a uniform size range of ≤ 0.4 mm. The received modified TRGO was labeled here as TRGO_PA.

A schematic diagram illustrating the expected functional groups introduced into the graphene structure via functionalizations used in this work is presented in Fig. 1 SM (Supplementary Material).

2.2. Characterization of samples

The prepared graphene-based materials were characterized in detail using different techniques. Quantitative CHNS (carbon, hydrogen, nitrogen, and sulfur) elemental analysis was made by means of a Vario EL III Elemental Analyzer by burning the samples at high temperature (~1200 °C) in an oxygen-rich environment. The amount of phosphorus in TRGO_PA was determined using Inductively Coupled Plasma Optical Emission Spectrometry (ICP-OES). The sample subjected to ICP-OES analysis was first mineralized through pressurized digestion in concentrated nitric acid in a MARS 5 microwave oven (CEM) at the temperature of 210 °C for 30 min. The obtained solution was then diluted and analyzed using a Varian ICP-OES VISTA-MPX apparatus. The total acidities of the catalysts were determined by a potentiometric back titration method, using a Cerko Lab microtitration unit. Briefly, carbon samples were dried at 110 °C and then mixed with a sodium hydroxide solution (100 mg of carbon + 50 cm³ of 0.01 M NaOH). Thus obtained mixtures were shaken for 20 h at room temperature. After filtration, the filtrates (20 cm³) were titrated with a solution of HCl (0.05 M). A blank test was also performed. The textural properties of carbons (i.e., apparent surface areas and porosity) were evaluated on the basis of nitrogen adsorption/desorption isotherms measured at –196 °C, using a Quantachrome Autosorb IQ apparatus. Prior the analysis, the samples were outgassed at 150 °C until the pressure stabilization (usually 12 h). BET surface areas (i.e., S_{BET}) were assessed using the Brunauer-Emmett-Teller equation, while micropore volumes (V_{micro}) and external surface areas (S_{ext}) of the carbons were determined using the t-plot method. The total volumes of pores (V_{tot}) were calculated from the amount of N₂ adsorbed at a relative pressure close to 1. The morphological features of the samples were described on the basis of SEM images obtained using a Hitachi SU-70 scanning electron microscope. A PerkinElmer Pyris 1 instrument was used for thermogravimetric (TG) analysis of carbons. The experiments were performed at the temperature of 20–800 °C (heating rate of 10 °C/min) under nitrogen atmosphere. X-ray photoelectron spectroscopy (XPS) studies were done by means of a VG Scientific ESCALAB MKII spectrometer (Thermo Fisher Scientific) equipped with a non-monochromatized Mg K α X-ray source (h ν = 1253.6 eV).

2.3. Catalytic tests

The obtained graphene-based materials were tested as catalysts in glycerol esterification with acetic acid. The reaction was carried out in a three-neck round-bottom flask (50 cm³) equipped with a magnetic stirrer, reflux condenser and a thermocouple. In each run, acetic acid (28.9 cm³) was first mixed with catalyst (0.7 g) and heated under argon flow. Once the reaction temperature (110 °C) was attained, glycerol (7.75 g; glycerol to acetic acid molar ratio of 1:6) was introduced into the flask. To monitor the process, aliquots of the reaction mixture were

taken from the system periodically. After centrifuging the catalyst, the samples were diluted with ethanol and analyzed by means of a SRI 8610C gas chromatograph equipped with a flame ionization detector (FID) and a 30 m InterCap WAX capillary column. The analyses were performed in the column temperature range of 130–210 °C.

The catalytic performances of the tested catalysts were expressed as the conversion of glycerol, selectivities towards acetins, and yields of individual glycerol acetates, in accordance with the formulas presented in literature [25]. The reusability experiments (testing the catalysts in subsequent reaction cycles) were also performed. After each run, the spent catalyst was recovered by filtration, washed with hot distilled water, and acetone. Finally, it was dried at 110° overnight. The amounts of reagents taken for subsequent runs were calculated on the basis of the catalyst weight recovered from each reaction.

3. Results and discussion

The obtained TRGO-based samples were thoroughly analyzed by means of various methods. The most important data on the catalyst characterization, i.e., those necessary for the interpretation of the catalytic results, are shown below. Detailed description of the physico-chemical properties of the carbons obtained can be found in our previous paper [20].

3.1. Elemental composition and surface acidities of the graphene-based samples

The elemental composition of the graphene-based samples as well as their surface acidities are shown in Fig. 1. As can be observed, the initial carbon sample, i.e., TRGO, contained significant amounts of elemental carbon, which were over 82.5%. This result was rather expected, taking into account the type of a precursor used in the TRGO synthesis (graphite) and the thermal history of the sample (see Experimental part). Interestingly, TRGO also showed a relatively high oxygen content (of about 11.7%) despite being prepared at high temperature (i.e., 800 °C). Therefore, it can be supposed that TRGO contained some oxygen functionalities of high thermal stability (stable at least up to 800 °C). These groups can be carbonyl, quinone, or pyrone structures [26–28]. Moreover, it can be expected that the oxygen species present in GO could also have been transformed into edge ethers, which are the most stable form of oxygen in graphene as reported by M. Acik et al. [29]. Another option, however, can also be considered, namely some less thermally stable O-functionalities, such as phenolic ones [28], could have remained in the TRGO structure due to the short time of GO reduction (see

Experimental). The presence of these groups may also explain some acidity shown by TRGO (Fig. 1). Fig. 2SM in Supplementary Material presents the deconvoluted XPS O 1 s spectrum of the TRGO sample, confirming the occurrence of the abovementioned phenolic functionalities on the surface of TRGO (with a the relative concentration of about 57%). The obtained results are also in line with the observations of Ganguly et al. for thermally reduced GO [30]. According to the depicted data, the TRGO sample also contained sulfur (2.0%) in its structure. Most likely, the presence of this element resulted from incomplete removal of the reagents used in the synthesis of thermally reduced graphene oxide (see Experimental).

As can be seen in Fig. 1, modifications of TRGO with concentrated sulfuric acid and BDS altered the composition of the parent sample, resulting in the introduction of certain amounts of sulfur and oxygen to TRGO (in the case of modification with BDS) or only oxygen – when using H₂SO₄. The observed differences in the amounts of oxygen and sulfur introduced were due to the fact that the modification of TRGO with concentrated sulfuric acid was probably ineffective in the formation of sulfonic groups on the TRGO surface (comparable contents of S for TRGO and TRGO_SA). On the other hand, oxidation of the sample occurred – with the formation of oxygen functionalities, e.g., carboxylic ones (the oxidizing properties of sulfuric acid were also signaled in other works [13,14,31]). Much more effective was the reaction of TRGO with BDS, where the observed increase in oxygen and sulfur was probably due to incorporation of SO₃H groups into the TRGO structure (see also XPS results). Consequently, TRGO_BDS contained 4.7% of sulfur and 17.3% of oxygen compared to 1.6% and 13.9% of S and O, respectively, observed for TRGO_SA. Therefore, it can be concluded that modification of graphene-based samples with BDS is a very efficient method of functionalization. This is also in line with our previous studies regarding modifications of activated or ordered mesoporous carbons [13,18]. Importantly, the direct effect of TRGO modification with sulfuric acid or BDS was an increase in the sample acidity. This can confirm the formation of acidic groups in the processes of TRGO functionalization – the sulfonic and carboxylic functionalities mentioned above.

The modification of TRGO with phosphoric acid led to effective incorporation of P-groups into the structure of this sample, as evidenced by an increase in the phosphorus content in TRGO_PA (up to 7.2%) compared to the pristine TRGO. Importantly, the introduction of phosphorous was accompanied by a significant increase in the acidity of the PA-modified graphene sample (i.e., up to 1.38 mmol H⁺/g).

3.2. Thermogravimetric analysis

TG analysis performed in this study was used to evaluate the thermal stability of TRGO-based samples as well as the degree of their functionalization with heteroatoms such as oxygen and sulfur (as the O- and S-containing groups are decomposed at certain temperatures of TG analysis and released as volatiles). The results of TG measurements obtained for all the graphene-based materials are presented in Fig. 2 (as TG and DTG curves) and in Table 1 (as the weight losses of samples at the final temperature of TG analysis).

According to the presented data, TRGO was quite thermally stable. The weight loss reported at the temperature of 800 °C for this sample was about 11.5% (see Fig. 2 and Table 1). Generally, this amount of released volatiles agreed well with the results of EA showing about 13.7% of oxygen + sulfur in the TRGO structure. As can be seen from the DTG curve in Fig. 2, a first slight drop of TRGO weight was noted above 200 °C, whereas the second, more significant, started above 480 °C. Probably, the first observed weight change was due to the decomposition of some S-containing groups (see also XPS results), while the second was mainly related to the decomposition of oxygen groups such as phenolic ones present in TRGO [12,14].

It can be observed from Fig. 2 that the modified graphene-based samples differed from the pristine TRGO. TRGO_SA and TRGO_BDS showed higher weight losses at specific temperatures of TG analysis than

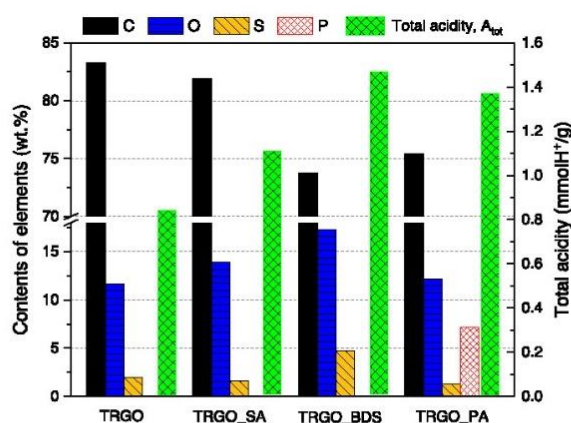


Fig. 1. The contents of carbon, oxygen, sulfur, and phosphorous in the pristine and functionalized graphene samples (in wt.%) as well as the total acidities of these materials.

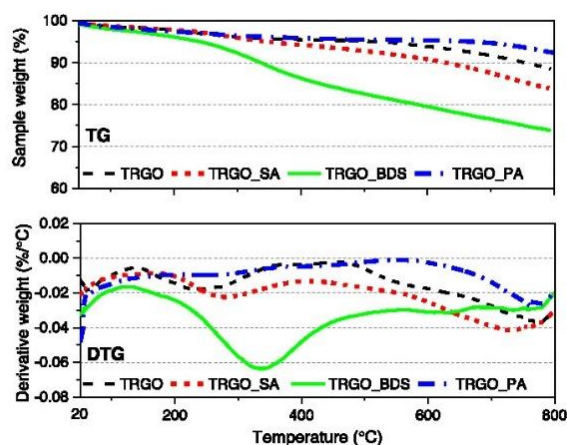


Fig. 2. DTG analysis of the obtained samples under N_2 flow.

Table 1
Results of TG analysis at T_{final} .

Sample	Weight loss at T_{final} (800 °C) [%]
TRGO	11.5
TRGO_SA	16.5
TRGO_BDS	26.2
TRGO_PA	7.6

the initial sample. Finally, the weight drops noted for these materials reached the values of 16.2% and 26.6%, respectively (Fig. 2 and Table 1). The obtained results reflect the degree of TRGO functionalization, namely TRGO_BDS was modified significantly more efficiently than TRGO_SA, which is also consistent with the data from EA. The DTG curve of TRGO_BDS showed only one peak (with a minimum of about 320 °C), which corresponds to the decomposition of $PhSO_3H$ groups introduced into TRGO during its functionalization [32]. The chemistry of TRGO_SA was more complex (quite similar to the pristine carbon), as the sample contained functionalities of different thermal stability (decomposing at about 250 °C and above 500 °C). TRGO_PA was characterized by the lowest weigh changes among all the prepared samples. The higher sample stability was probably due to removal of some oxygen groups from TRGO (compare to the DTG curve of TRGO in Fig. 2) at the temperature of TRGO_PA preparation (which was 800 °C, see Experimental), and the formation of phosphate groups of high temperature resistance [33] (thus the oxygen contents in TRGO and TRGO_PA differ only slightly, Fig. 1).

3.3. Textural analysis

Table 2 shows the results of textural analysis of the prepared graphene-based samples.

As can be seen, TRGO presented quite a significant S_{BET} , which was 617 m^2/g , and quite a large total volume of pores (V_{tot} of 3.83 cm^3/g). The surface area of TRGO resulted from the presence of mesopores (and possibly macropores), as the contribution of S_{ext} to S_{BET} was 100%. The

Table 2
The results of textural analysis of the prepared samples.

Sample	S_{BET} [m^2/g]	S_{ext}/S_{BET} [%]	V_{tot} [cm^3/g]	V_{micro}/V_{tot} [%]
TRGO	617	100.0	3.83	0.0
TRGO_SA	513	99.6	2.29	0.0
TRGO_BDS	422	97.9	2.76	0.0
TRGO_PA	300	68.7	0.99	0.1

additional confirmation of the presence of mesopores in the porous structure of TRGO is the shape of the N_2 adsorption–desorption isotherm obtained for this sample, with a hysteresis loop typical for mesoporous materials [34] (Fig. 3). The sample did not contain a measurable number of micropores (as $V_{micro}/V_{tot} = 0\%$).

The modifications of TRGO caused deterioration of the textural properties of the parent sample. This can result from introducing new functional groups onto the TRGO surface (see EA in Fig. 1), occupying some pore space (the functional groups are most likely located at the entrance of pores, blocking access to them [18]). The above supposition can be confirmed by a decrease in the total volumes of pores (V_{tot}) observed for modifying samples. Importantly, the smallest reduction in the textural parameters was observed for TRGO_SA, whereas significantly higher in the case of TRGO_BDS and TRGO_PA. These results are in line with those of EA (Fig. 1), showing that modifications of TRGO with BDS or phosphoric acid were more effective than the treatment of TRGO with H_2SO_4 . All the functionalized samples contained mainly mesopores in their structures, as indicated by the values of S_{ext}/S_{BET} and V_{micro}/V_{tot} parameters (Table 2) as well as the shapes of N_2 adsorption–desorption isotherms (Fig. 3).

3.4. SEM analysis

Fig. 4 depicts SEM images of selected samples. As can be observed in Fig. 4a, TRGO showed a flake-like structure, typical for graphene-based materials [35], with exfoliated, separated layers (although creased, wrinkled, twisted, and crumbled), and holes, canals, and gaps between these carbon planes. These morphological features are probably responsible for the developed texture of TRGO (see Table 2). Fig. 4b presents the structure of a representative functionalized sample, i.e., TRGO treated with benzenediazonium sulfonate (TRGO_BDS). As can be seen, the modification used did not cause visible changes in the sample morphology. The same was the effect of TRGO treatment with phosphoric and sulfuric acids (images not shown). Consequently, all the modified carbons retained their flake-like structures.

3.5. XPS results

The quantitative data obtained from the XPS measurements (in wt. %) are gathered in Table 3.

In general, the performed analysis confirmed the introduction of heteroatoms such as S and P into the structure of the pristine TRGO (increased S or P contents in the modified samples compared to the initial one), thus indicating the effectiveness of sample functionalizations.

Comparing the XPS results with those obtained from the elemental

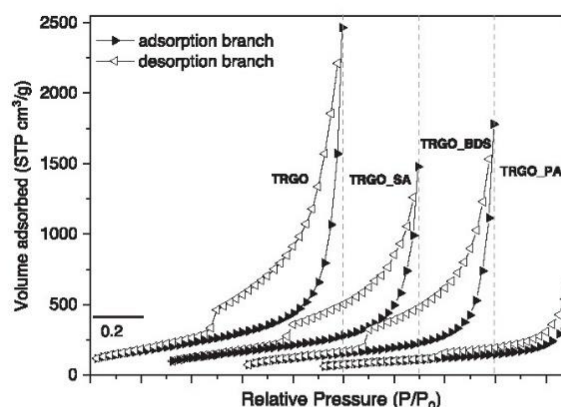


Fig. 3. Nitrogen adsorption/desorption isotherms of the TRGO-based samples.

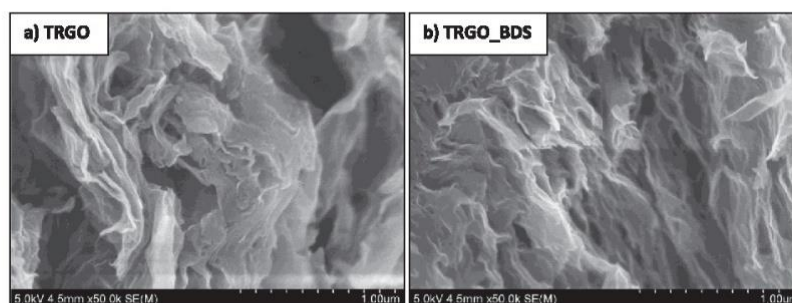


Fig. 4. SEM images of selected graphene-based samples: a) TRGO and b) TRGO_BDS.

Table 3

Amounts of carbon and heteroatoms such as: oxygen, sulfur, and phosphorous on the surface of pristine and functionalized samples according to XPS analysis (in wt.%).

Sample	C	O	S (P)
TRGO	82.6	14.8	2.6 (0.0)
TRGO_SA	83.0	14.1	2.9 (0.0)
TRGO_BDS	73.1	17.9	8.1 (0.0)
TRGO_PA	79.6	12.8	0.0 (7.6)

analysis (EA, Fig. 1), it can be concluded that sulfur present in TRGO, TRGO_SA, and TRGO_BDS was not homogeneously distributed between the surface and the bulk, as EA \neq XPS. This is particularly well seen in the case of SA- and BDS-modified samples presenting significantly higher concentration of S on the surface than in the bulk (XPS > EA; about 1.7–1.8 times higher in both cases). When considering the composition of TRGO_PA, it is clear that phosphorus is homogeneously distributed within the sample, as the contents of P from EA and XPS are almost the same (7.2 wt% of P from EA vs. 7.6 wt% of P from XPS). The same applies to oxygen (also in other samples). Importantly, XPS did not detect sulfur on the surface of TRGO_PA. Thus, all sulfur present in this material was observed in the bulk (as S from EA > S XPS, see Fig. 1 and Table 3).

Fig. 5 summarizes the results of deconvolution of the high-resolution S 2p and P 2p XPS spectra of the prepared graphene-based catalysts, showing the type and concentration of various S and P species on the surface of these samples (full XPS profiles are not shown here as they are given in our previous work [20]).

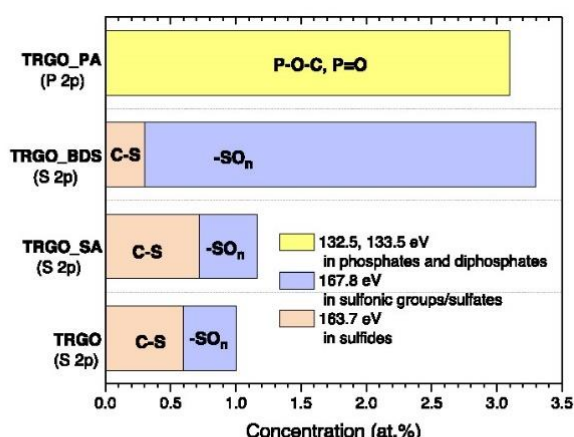


Fig. 5. Quantitative results of the deconvolution of the S 2p and P 2p spectra of TRGO-based samples.

As presented in Fig. 1 and Table 3, the parent TRGO sample contained some sulfur, possibly due to the incomplete removal of reagents after the oxidation step (see Experimental). It was found from the XPS spectra analysis that the dominant state of S in TRGO was C-S in sulfides (signal at the B.E. of about 163.5–164.5 eV); however, the sample showed also some sulfonic or sulfate groups (as the deconvoluted peak at 168–169 eV was observed) [16,36]. Presumably, the C-S structures were formed as a result of the high temperature reduction of H₂SO₄ and K₂S₂O₈-treated graphite (the GO employed to prepare TRGO could contain residual intercalated H₂SO₄ and/or sulfates, which were not completely washed out after the oxidation step; see also Experimental). The modification of TRGO with concentrated sulfuric acid did not affect significantly the content of S and the distribution of the surface S functionalities. Thus, the TRGO_SA contained mainly C-S (relative abundance above 62%), whereas S in -SO_n functionalities was about 38%. As can be seen in Fig. 5, the functionalization of TRGO with BDS increased considerably the content of S groups. The surface density of -SO_n moieties was increased from 0.4 at.% in TRGO to 3.0 at.% in TRGO_BDS. The relative abundance of C-S was only about 11.8%. Importantly, these species were not introduced to the structure of the sample during the modification, but were originally present in TRGO. This outcome is also in line with our previous studies suggesting that the treatment with BDS leads to introduction of only SO₃H groups [13,18]. The presence of SO₃H moieties in the BDS-modified sample was also confirmed by the results of FTIR analysis presented in our previous paper (the peaks at 1120, 1043, 804, and 612 cm⁻¹) [20]. Overall, the presented results indicate that quantitative and qualitative functionalization of TRGO with sulfur strongly depended on the modifying agent used. The modification with BDS was found to be significantly more effective in introducing a high number of sulfonic species into the TRGO than the TRGO treatment with sulfuric acid.

The high-resolution P 2p XPS spectrum of TRGO_PA showed generally only one peak (see also our previous work [20]). To simplify the interpretation of the XPS P 2p results, this region was deconvoluted into two main signals (without taking into account the split orbit splitting into P 2p_{1/2} and P 2p_{3/2}) at the binding energies of about 132.5 and 133.5 eV, related to the presence of P bonded to carbon through oxygen and P double bonded to O, respectively, in phosphate and diphosphate groups (Fig. 5) [13,36]. These surface functionalities endow the TRGO sample with acidic properties (see also total acidity of TRGO_PA in Fig. 1).

3.6. Catalytic results

The obtained graphene-based materials were tested in synthesis of glycerol acetates.

The catalytic performances of samples were assessed based on the results of glycerol conversion, selectivities towards different acetins (MA, DA, and TA), and yields of individual products.

The obtained results (including blank test) are shown in Figs. 6–8.

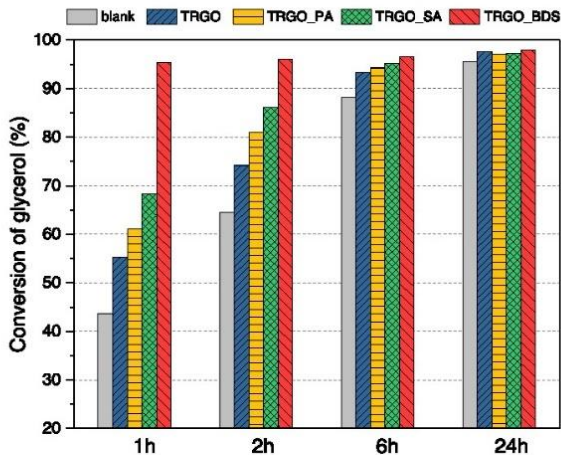


Fig. 6. Conversion of glycerol obtained in the process with modified graphene-based samples.

Fig. 6 presents the results of glycerol conversion versus time. As can be seen, the graphene samples differed significantly in their catalytic performances. The observed differences were the highest at the

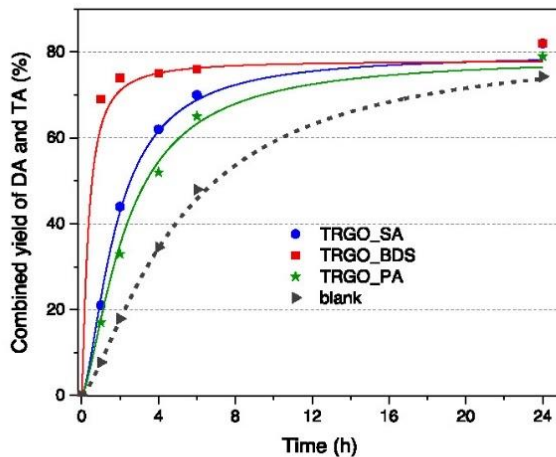


Fig. 8. The combined yield of DA and TA obtained in glycerol acetylation using the prepared graphene-based samples versus time.

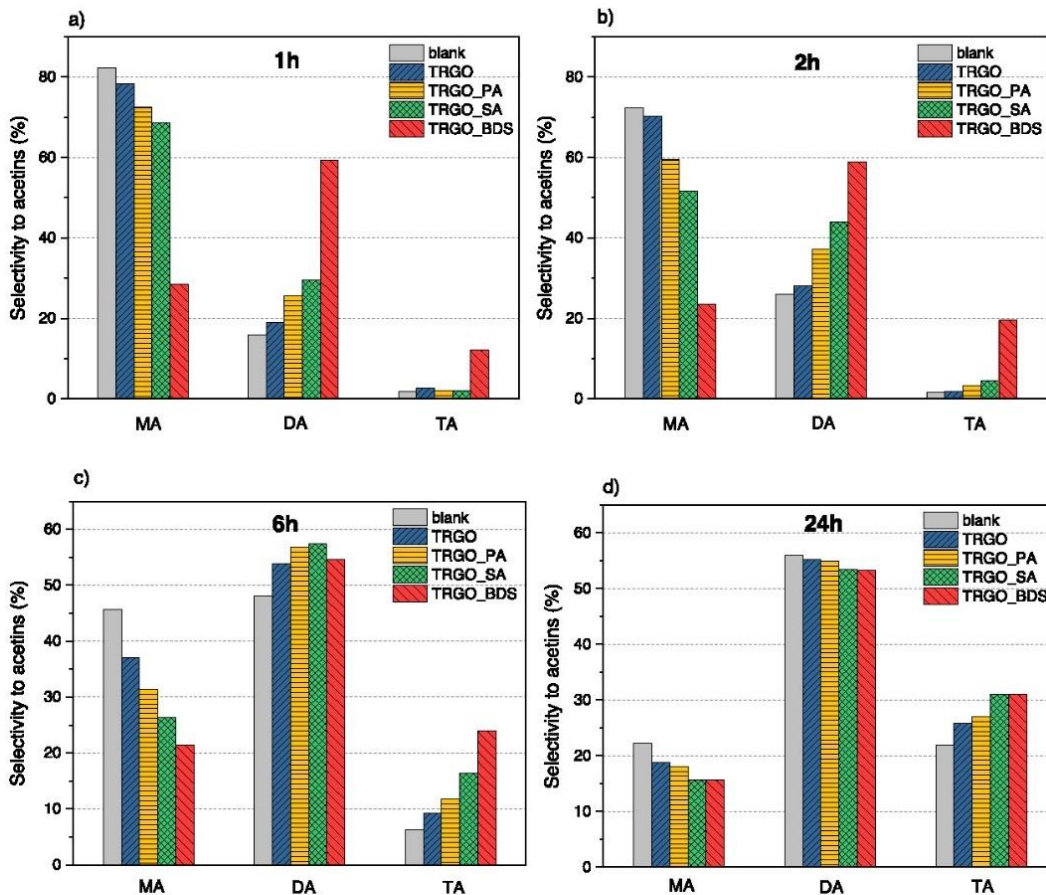


Fig. 7. Catalytic performance of the modified graphene-based samples versus time.

beginning of the process, e.g., after 1 h, and TRGO_BDS converted by about 30% more glycerol than TRGO_PA. The conversion increased with time in almost all cases, however, the longer the reaction time, the smaller differences in the sample activities were reported. Thus, after 24 h, all the prepared catalysts (also the blank) showed almost comparable conversion results, which were about 95%. The observed phenomenon is due to approaching/reaching the reaction equilibrium.

In general, the worst catalytic results among the modified materials were recorded for TRGO_PA. In this case, the conversion of glycerol after 1 h of the reaction was about 60% and was not so much higher than that obtained in the blank experiment. Better catalytic performance was shown by the TRGO_SA sample, which transformed about 70% of glycerol present in the system after 1 h of the process. The best catalytic results were attained for TRGO_BDS. Importantly, this catalyst allowed us to obtain a very high glycerol conversion (about 95%) just within 1 h of the reaction.

Fig. 7 depicts the distribution of various products formed in the glycerol esterification for selected reaction times.

Under the conditions used, the prepared catalysts produced only mono-, di- and triacetins. Initially, the contribution of MA to the mixture of acetins was quite high in most cases, i.e., TRGO_PA gave about 72.5% selectivity to MA, and TRGO_SA showed about 68.5% selectivity to monoacetins after 1 h. Other situation was observed in the case of TRGO_BDS, which transformed glycerol mainly to DA (selectivity to DA after 1 h was about 60%) (Fig. 7a). Importantly, this catalyst was also able to produce high amounts of TA within a short period of time (selectivity to TA about 20%, see Fig. 7b, and glycerol conversion of about 96%, see Fig. 6, after 2 h). Furthermore, the results presented in Fig. 7 reflect the transformations of individual products taking place during the process. As can be seen, the selectivities to MA decreased over time in all cases. At the same time, the selectivities to higher acetins (i.e., DA and TA, which are the products of special interest) were increased. The observed changes in selectivities to individual acetins allow us to conclude that glycerol esterification over graphene catalysts occurs in three consecutive steps. First, MA is formed in the process. In the second step, MA is converted to DA. Finally, DA is transformed to TA. This mechanism is in full accordance with previously published studies [37,38]. In view of the above, the most active catalyst should be a sample that allows a rapid transformation of MA to higher esters (i.e., DA and TA). In our case, this is TRGO_BDS, which was found to work effectively, converting high amounts of glycerol to di- and triacetins within a short period of time.

As mentioned above, the most desirable products of glycerol esterification are di- and triacetins, which are used as valuable fuel additives. Fig. 8 presents the combined yield of DA and TA (Y_{DA+TA}) obtained with the use of prepared graphene-based catalysts over time. For the sake of comparison, also the results of the blank test are depicted. As can be seen, the initial Y_{DA+TA} (assumed here as measured after 1 h) obtained over TRGO modified with sulfuric acid or phosphoric acid (TRGO_SA and TRGO_PA, respectively) was rather low, as this combined yield was only about 18–20% in both cases. This parameter increased significantly over time and for the more active sample (i.e., TRGO_SA), Y_{DA+TA} was about 62% after 4 h. The best catalyst among tested here was TRGO modified with BDS, for which a combined yield of DA and TA after 1 h reached a very high value of about 70%, i.e., over three times higher than that observed for the other modified samples and the blank. The yield of di- and triacetins produced with the TRGO_BDS sample increased over time, however, not so significantly as with the other catalysts, and finally, Y_{DA+TA} was over 80% after 24 h.

It was concluded before that the yield of higher acetins formed in glycerol esterification over carbon materials such as bio-carbons from sugars or glycerol [19,39,40] corresponds well with the number of SO_3H groups. Apparently, the extremely high activity presented by TRGO_BDS also results from its chemical features, namely the presence of sulfonic groups, the abundance of which was confirmed in the sample (see Fig. 5). Importantly, the results obtained in this work using TRGO_BDS

were comparable or even better than those achieved with other types of carbon catalysts tested by us, e.g., ordered mesoporous carbons – OMCs [18], despite using 2 times less catalyst in the process performed with modified graphene. Therefore, it can be assumed that the role of graphene as catalysts results from its unique accessible structure on both surfaces of graphene sheets in which catalytically active sites of different types can be freely exposed, and thus available. Because of that the time required for reactants to diffuse to an active site can be significantly reduced, also the internal diffusion is limited. Finally, the mass transfer limitations are considerably lower, hence increasing the rate of heterogeneous catalytic processes [41]. The catalytic performance of H_2SO_4 -modified TRGO is also due to the presence of SO_3H groups despite the fact that this sample also contains high amounts of C-S functionalities. These structures, however, cannot catalyze the esterification process. In the case of TRGO_SA, the number of SO_3H functionalities is significantly lower than that present on the surface of TRGO_BDS, thus TRGO_SA presents considerably lower catalytic performance. As can be seen in Fig. 8, TRGO modified with phosphoric acid (i.e., TRGO_PA) shows a catalytic effect in the glycerol esterification even though there are no SO_3H groups on its surface (as presented in Table 3). Thus, also other functionalities than sulfonic ones, namely phosphate structures (these were detected on the TRGO_PA surface, see Fig. 5) can catalyze the glycerol esterification. Importantly, the activity of TRGO_PA was significantly lower than that of SO_3H -containing catalysts although the H_3PO_4 -modified sample exhibited a high content of P (7.2%) and a significant total acidity (about $1.4 \text{ mmol H}^+/\text{g}$), which was comparable to that of TRGO_BDS (about $1.5 \text{ mmol H}^+/\text{g}$, Fig. 1). Apparently, low catalytic effect shown by TRGO_PA is due to much weaker acidic character of phosphate groups than sulfonic ones (pK_{1a} of phosphate groups = 2, pK_{1a} of sulfonic groups = 0.7) [14]. Thus, it can be stated that the type of acidic functional groups is more significant for the performed process than the total acidity shown by the catalysts. This conclusion agrees well with our previous findings concerning the activity of hydrothermal carbons in the glycerol esterification reaction [42].

Fig. 9 depicts the results of reusability tests performed for the best working sample, i.e., TRGO_BDS, in four reaction cycles.

As can be seen, the catalyst retained its catalytic performance in subsequent experiments, giving a very high conversion of glycerol (about 95%) in each run just within 1 h of the process. The yields of the desired products (i.e., DA and TA) did not change significantly in subsequent processes, and were almost as high as in the first reaction (about 60–63%). This can indicate that leaching of active sites was negligible.

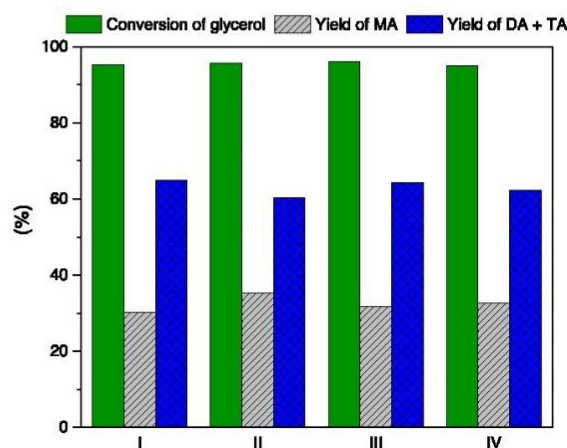


Fig. 9. Reusability tests performed for a selected catalyst (TRGO_BDS); reaction time 1 h.

4. Conclusions

S- or P-functionalized graphene-based samples were prepared from graphite via its thermal exfoliation and modification with sulfuric acid, diazonium salt, and phosphoric acid. The last two functionalization methods were very effective in introducing heteroatoms into the graphene structure. These modifications enabled the incorporation of a high number of SO₃H or phosphate groups and a significant increase in the total acidity of the parent material (to a quite similar level in both cases). Further, the catalytic data obtained in the reaction of glycerol with acetic acid allowed us to conclude that the presence of strong acidic sites is of great importance to the process. The best catalytic performance was presented by the sample modified with diazonium salt and showing the highest content of SO₃H groups (i.e., TRGO_BDS), which gave a very high conversion of glycerol and a high yield of di- and triacetins (the products of interest) just within 1 h. Furthermore, this catalyst presented high catalytic stability in subsequent reaction cycles. The highly P-functionalized sample (i.e., TRGO_PA) showed significantly lower activity in the process than TRGO_BDS. This is a consequence of much lower acid strength of phosphate groups comparing to sulfonic ones.

CRedit authorship contribution statement

Anna Malaika: Conceptualization, Methodology, Validation, Visualization, Writing – original draft, Writing – review & editing. **Karolina Ptaszyńska:** Investigation, Formal analysis. **Justina Gaidukevič:** Investigation, Validation, Formal analysis, Writing – review & editing. **Mieczysław Kozłowski:** Funding acquisition, Supervision, Writing – review & editing.

Declaration of Competing Interest

The authors declare that they have no known competing financial interests or personal relationships that could have appeared to influence the work reported in this paper.

Acknowledgments

J.G. thanks The Education Exchanges Support Foundation for the national scholarship of the LR Ministry of Education and Science. Agreement No. AM-PL-2014-LT-1225.

Appendix A. Supplementary data

Supplementary data to this article can be found online at <https://doi.org/10.1016/j.fuel.2021.122987>.

References

- [1] OECD/FAO. OECD-FAO Rodrigues Agricultural Outlook 2021–2030 2021 OECD Publishing Paris 10.1787/19428846-en.
- [2] Rodrigues A, Bordado JC, dos Santos RG. Upgrading the glycerol from biodiesel production as a source of energy carriers and chemicals— A technological review for three chemical pathways. *Energies* 2017;10:1617–53. <https://doi.org/10.3390/EN10111617>.
- [3] Kong PS, Aroua MK, Daud WMAW, Lee HV, Cognet P, Pèrès Y. Catalytic role of solid acid catalysts in glycerol acetylation for the production of bio-additives: a review. *RSC Adv* 2016;6(73):68885–905. <https://doi.org/10.1039/C6RA10686B>.
- [4] Okoye PU, Abdullah AZ, Hameed BH. Synthesis of oxygenated fuel additives via glycerol esterification with acetic acid over bio-derived carbon catalyst. *Fuel* 2017; 209:538–44. <https://doi.org/10.1016/j.fuel.2017.08.024>.
- [5] Nda-Umar UI, Ramli IB, Muhamad EM, Azri N, Amadi UF, Taufiq-Yap YH. Influence of heterogeneous catalysts and reaction parameters on the acetylation of glycerol to acetin: a review. *Appl Sci* 2020;10:7155. <https://doi.org/10.3390/app10207155>.
- [6] Cahyono RB, Muftodi Z, Hidayat A, Budiman A. Acetylation of glycerol for triacetin production using Zr-natural zeolite catalyst. *J Eng Appl Sci* 2016;11:5194–7.
- [7] Fadhil AZ, Poll et P, Liotta CL, Eckert CA. Combining the benefits of homogeneous and heterogeneous catalysis with tunable solvents and nearcritical water. *Molecules* 2010;15:8400–24. <https://doi.org/10.3390/molecules15118400>.
- [8] Sudarsanam P, Zhong R, Van den Bosch S, Coman SM, Parvulescu VI, Sels BF. Functionalised heterogeneous catalysts for sustainable biomass valorization. *Chem Soc Rev* 2018;47:8349–402. <https://doi.org/10.1039/C8CS00410B>.
- [9] Liao X, Zhu Y, Wang S-G, Li Y. Producing triacetyl glycerol with glycerol by two steps: esterification and acetylation. *Fuel Process Technol* 2009;90(7-8):988–93. <https://doi.org/10.1016/j.fuproc.2009.03.015>.
- [10] Kazmierczak-Razna J, Pietrzak R, Nowicki P. Synthesis of new carbon-nitrogen composites based on waste sweet drinks. *Physicochem Probl Miner Process* 2019; 55:1366–74. <https://doi.org/10.5277/ppmp19052>.
- [11] Malaika A, Kozłowski M. Glycerol conversion towards valuable fuel blending compounds with the assistance of SO₃H-functionalized carbon xerogels and spheres. *Fuel Process Technol* 2019;184:19–26. <https://doi.org/10.1016/j.fuproc.2018.11.006>.
- [12] Figueiredo JL. Functionalization of porous carbons for catalytic applications. *J Mater Chem A* 2013;1:9351–64. <https://doi.org/10.1039/C3TA10876G>.
- [13] Rechnia P, Malaika A, Kozłowski M. Synthesis of tert-amyl methyl ether (TAME) over modified activated carbon catalysts. *Fuel* 2015;154:338–45. <https://doi.org/10.1016/j.fuel.2015.03.086>.
- [14] Rechnia-Goraćy P, Malaika A, Kozłowski M. Acidic activated carbons as catalysts of biodiesel formation. *Diam Relat Matter* 2018;87:124–33. <https://doi.org/10.1016/j.diamond.2018.05.015>.
- [15] Malaika A, Rechnia-Goraćy P, Kot M, Kozłowski M. Selective and efficient dimerization of isobutene over H₃PO₄/activated carbon catalysts. *Catal Today* 2018;301:266–73. <https://doi.org/10.1016/j.cattod.2017.02.038>.
- [16] Morawa Eblagon K, Malaika A, Pereira MFR, Figueiredo JL. Cutting the green waste. Structure-performance relationship in functionalised carbon xerogels for hydrolysis of cellobiose. *ChemCatChem* 2018;10:4934–46. <https://doi.org/10.1002/cssc.201800649>.
- [17] Malaika A, Rechnia P, Krzyżyńska B, Tolińska A, Kawaiko A, Kozłowski M. Simultaneous synthesis of styrene and aniline over activated carbon catalysts. Influence of the surface chemistry. *Appl Catal A* 2013;452:39–47. <https://doi.org/10.1016/j.apcata.2012.11.032>.
- [18] Goscińska J, Malaika A. A facile post-synthetic modification of ordered mesoporous carbon to get efficient catalysts for the formation of acetins. *Catal Today* 2020;357:84–93. <https://doi.org/10.1016/j.cattod.2019.02.049>.
- [19] Malaika A, Ptaszyńska K, Kozłowski M. Conversion of renewable feedstock to bio-carbons dedicated for the production of green fuel additives from glycerol. *Fuel* 2021;288:119609. <https://doi.org/10.1016/j.fuel.2020.119609>.
- [20] Gaidukevič J, Barkauskas J, Malaika A, Rechnia-Goraćy P, Mozdzyńska A, Jasulaitienė V, et al. Modified graphene-based materials as effective catalysts for transesterification of rapeseed oil to biodiesel fuel. *Chin J Catal* 2018;39(10): 1633–45. [https://doi.org/10.1016/S1872-2067\(18\)63087-6](https://doi.org/10.1016/S1872-2067(18)63087-6).
- [21] Gao X, Zhu S, Li Y. Graphene oxide as a facile solid acid catalyst for the production of bioadditives from glycerol esterification. *Catal Commun* 2015;62:48–51. <https://doi.org/10.1016/j.catcom.2015.01.007>.
- [22] Yan X, Chen J, Yang J, Xue Q, Miele P. Fabrication of free-standing, electrochemically active, and biocompatible graphene oxide-polyaniline and graphene-polyaniline hybrid papers. *ACS Appl Mater Interfaces* 2010;2(9):2521–9. <https://doi.org/10.1021/am100293r>.
- [23] Hummers WS, Offeman RE. Preparation of graphitic oxide. *J Am Chem Soc* 1958; 80(6):1339. <https://doi.org/10.1021/ja01539a017>.
- [24] Šakinytė I, Barkauskas J, Gaidukevič J, Razumiene J. Thermally reduced graphene oxide: The study and use for reagentless amperometric D-fructose biosensors. *Talanta* 2015;144:1096–103. <https://doi.org/10.1016/j.talanta.2015.07.072>.
- [25] Dalla Costa BO, Decolatti HP, Legnoverde MS, Querini CA. Influence of acidic properties of different solid acid catalysts for glycerol acetylation. *Catal Today* 2017;289:222–30. <https://doi.org/10.1016/j.cattod.2016.09.015>.
- [26] Figueiredo JL, Pereira MFR, Freitas MMA, Orfao JJM. Modification of the surface chemistry of activated carbons. *Carbon* 1999;37(9):1379–89. [https://doi.org/10.1016/S0008-6223\(98\)00333-9](https://doi.org/10.1016/S0008-6223(98)00333-9).
- [27] Szymanski GS, Karpinski Z, Biniak S, Swiatkowski A. The effect of the gradual thermal decomposition of surface oxygen species on the chemical and catalytic properties of oxidized activated carbon. *Carbon* 2002;40:2627–39. [https://doi.org/10.1016/S0008-6223\(02\)00188-4](https://doi.org/10.1016/S0008-6223(02)00188-4).
- [28] Machado BF, Serp P. Graphene-based materials for catalysis. *Catal Sci Technol* 2012;2:54–75. <https://doi.org/10.1039/C1CY00361E>.
- [29] Acik M, Lee G, Mattevi C, Chhowalla M, Cho K, Chabal YJ. Unusual infrared-absorption mechanism in thermally reduced graphene oxide. *Nat Mater* 2010;9(10):840–5. <https://doi.org/10.1038/nmat2858>.
- [30] Ganguly A, Sharma S, Papakonstantinou P, Hamilton J. Probing the thermal deoxygenation of graphene oxide using high-resolution in situ x-ray-based spectroscopies. *J Phys Chem* 2011;115(34):17009–19. <https://doi.org/10.1021/jp203741y>.
- [31] Mo X, Lopez D, Suwannakarn K, Liu Y, Lotero E, Goodwin J, et al. Activation and deactivation characteristics of sulfonated carbon catalysts. *J Catal* 2008;254(2): 332–8. <https://doi.org/10.1016/j.jcat.2008.01.011>.
- [32] Guo Y, Shi Z, Chen M, Wang C. Hierarchical porous carbon derived from sulfonated pitch for electrical double layer capacitors. *J Power Sour* 2014;252:235–43. <https://doi.org/10.1016/j.jpowsour.2013.11.114>.
- [33] Kazmierczak-Razna J, Nowicki P, Wiśniewska M, Nosal-Wiercińska A, Pietrzak R. Thermal and physicochemical properties of phosphorus-containing activated carbons obtained from biomass. *J Taiwan Inst Chem Eng* 2017;000:1–8. <https://doi.org/10.1016/j.jtice.2017.09.015>.
- [34] Thommes M, Kaneko K, Neimark AV, Olivier JP, Rodriguez Reinoso F, Rouquerol J, Sing KSW. Physisorption of gases, with special reference to the evaluation of

- surface area and pore size distribution (IUPAC Technical Report). *Pure Appl Chem* 2015;87:1051-1069. <https://doi.org/10.1515/pac-2014-1117>.
- [35] Gurzęda B, Buchwald T, Nocuń M, Bąkiewicz A, Krawczyk P. Graphene material preparation through thermal treatment of graphite oxide electrochemically synthesized in aqueous sulfuric acid. *RSC Adv* 2017;7(32):19904-11. <https://doi.org/10.1039/C7RA01678F>.
- [36] Seredyeh M, Wu CT, Brender P, Ania CO, Vix-Guterl C, Bandosz TJ. Role of phosphorus in carbon matrix in desulfurization of diesel fuel using adsorption process. *Fuel* 2012;92(1):318-26. <https://doi.org/10.1016/j.fuel.2011.08.007>.
- [37] Muftođi Z, Rochmadi R, Sutijan S, Budiman A. Synthesis acetylation of glycerol using batch reactor and continuous reactive distillation column. *Eng J* 2014;18(2): 29-40. <https://doi.org/10.4186/ej.2014.18.2.29>.
- [38] Appaturi JN, Ramalingam RJ, Selvaraj M, Chia S, Tan SH, Khoerunnisa F, et al. Selective synthesis of triacetyl glyceride biofuel additive via acetylation of glycerol over NiO-supported TiO₂ catalyst enhanced by non-microwave instant heating. *Appl Surf Sci* 2021;545:149017. <https://doi.org/10.1016/j.apsusc.2021.149017>.
- [39] de la Calle C, Fraile Jos  m, Garc  a-Bordej   E, Pires E, Rold  n L. Biobased catalyst in biorefinery processes: sulfonated hydrothermal carbon for glycerol esterification. *Catal Sci Technol* 2015;5(5):2897-903. <https://doi.org/10.1039/C5CY00059A>.
- [40] S  nchez Juli  nA, Hern  ndez DL, Moreno JA, Mondrag  n E, Fern  ndez JJ. Alternative carbon based acid catalyst for selective esterification of glycerol to acetylglycerols. *Appl Catal A* 2011;405(1-2):55-60. <https://doi.org/10.1016/j.apcata.2011.07.027>.
- [41] Yan Y, Shin WI, Chen H, Lee S-M, Manickam S, Hanson S, et al. A recent trend: application of graphene in catalysis. *Carbon Lett* 2021;31(2):177-99. <https://doi.org/10.1007/s42823-020-00200-7>.
- [42] Malaika A, Heinrich M, Goscianska J, Kozłowski M. Synergistic effect of functional groups in carbonaceous spheres on the formation of fuel enhancers from glycerol. *Fuel* 2020;280:118523. <https://doi.org/10.1016/j.fuel.2020.118523>.

SUPPLEMENTARY MATERIALS

The impact of surface groups of functionalized graphene on glycerol acetylation

Anna Malaika^{a*}, Karolina Ptaszyńska^a, Justina Gaidukevič^b, Mieczysław Kozłowski^a

^a Faculty of Chemistry, Adam Mickiewicz University in Poznań
Uniwersytetu Poznańskiego 8, 61-614 Poznań, Poland

^b Faculty of Chemistry and Geosciences, Institute of Chemistry, Vilnius University,
Naugarduko 24, LT-03225 Vilnius, Lithuania

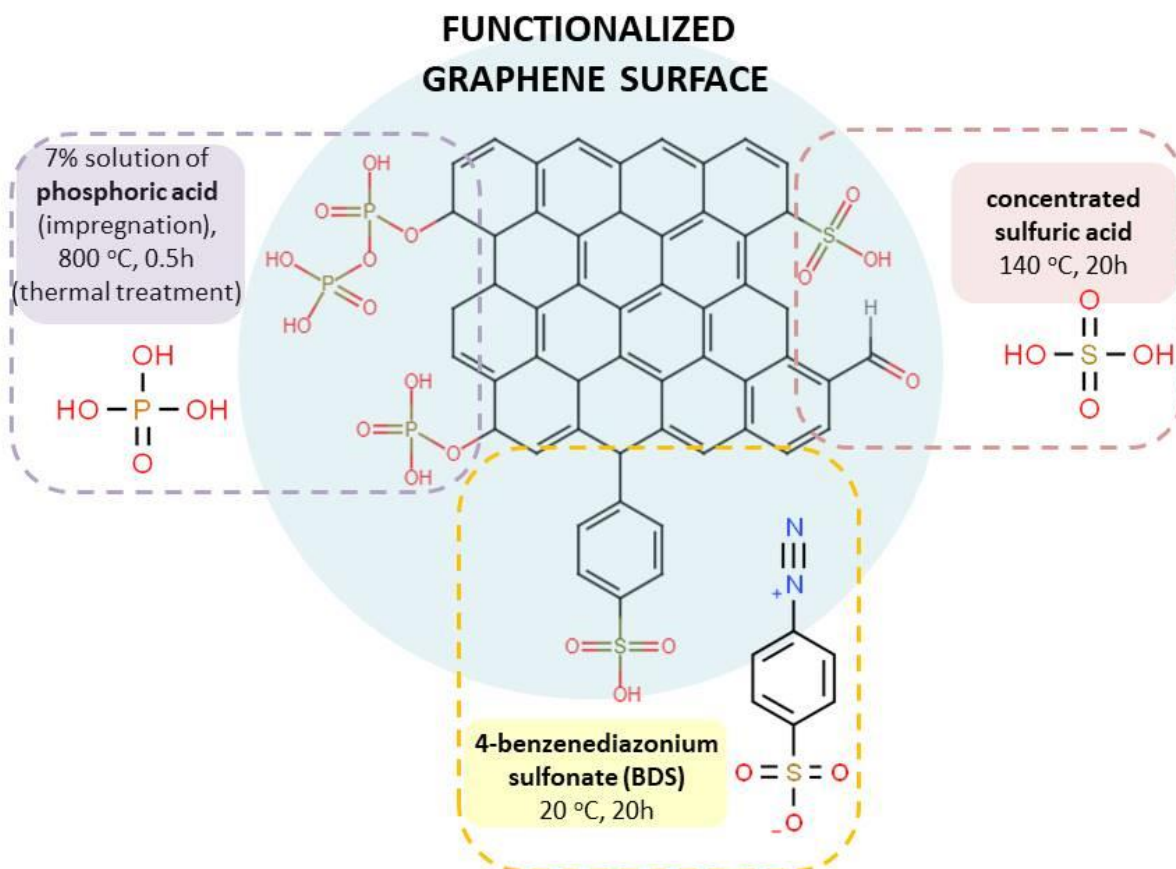


Fig. 1 SM. A schematic diagram illustrating the expected functional groups introduced into the carbon matrix via the functionalization processes used [1,2]

The XPS O 1s analysis was performed to evaluate the type of functional groups presents in the TRGO sample. The quantitative data obtained showed that TRGO contained 11.7 wt% of oxygen. On the other hand, the deconvolution of XPS core-level spectrum of O 1s obtained for TRGO gave complementary qualitative information about the nature of the TRGO surface. The O 1s signal obtained for TRGO (Fig. 1) was deconvoluted into three peaks at the B.E. of about 530.0 eV, 531.6 eV and 533.2 eV. These regions can be assigned to: oxygen double bonded to aromatic carbon atoms in quinone groups, carbonyl oxygen atoms in esters, hydroxyls or ethers (oxygen single bonded to aliphatic carbon), and phenolic groups (oxygen single bonded to aromatic carbon), respectively [3-5]. The relative concentrations of these species were 16.8%, 25.8% and 57.4%, suggesting a very high content of phenolic groups. These groups are probably responsible for some acidic properties shown by TRGO (i.e., 0.83 mmolH⁺/g; Fig. 1). The obtained results are also in line with the observations of Ganguly et al. for thermally reduced GO [4].

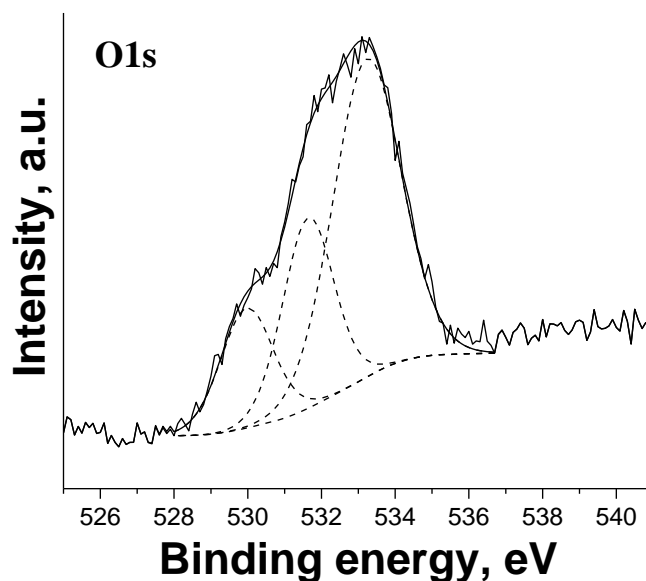


Fig. 2 SM. XPS O 1s spectrum of TRGO

References:

- [1] Rechnia P, Malaika A, Kozłowski M. Synthesis of tert-amyl methyl ether (TAME) over modified activated carbon catalysts. *Fuel* 2015;154:338-345.
- [2] Rechnia-Gorący P, Malaika A, Kozłowski M. Acidic activated carbons as catalysts of biodiesel formation, *Diam Relat Matter* 2018;87:124-133.

- [3] Viana MM, Lima MCFS, Forsythe JC, Gangoli VS, Cho M, Cheng Y, Silva GG, Wong MS, Caliman V. Facile Graphene Oxide Preparation by Microwave-Assisted Acid Method. *J Braz Chem Soc* 2015;26:978-984.
- [4] Ganguly A, Sharma S, Papakonstantinou P, Hamilton J. Probing the Thermal Deoxygenation of Graphene Oxide Using High-Resolution In Situ X-ray-Based Spectroscopies. *J Phys Chem* 2011;115:17009-17019.
- [5] Díez N, Śliwak A, Gryglewicz S, Grzyb B, Gryglewicz G. Enhanced reduction of graphene oxide by highpressure hydrothermal treatment. *RSC Adv* 2015;5:81831.

P2



OPEN SO_3H -functionalized carbon fibers for the catalytic transformation of glycerol to glycerol tert-butyl ethers

Karolina Ptaszyńska, Anna Malaika[✉], Magdalena Kapska & Mieczysław Kozłowski

Carbon fibers (CFs) of high quality were produced from hydrocarbons such as isobutane or ethylene using the catalytic chemical vapor deposition method (CCVD) and Ni catalyst. The as-prepared samples were functionalized with acidic groups using concentrated sulfuric acid or 4-benzenediazonium sulfonate (BDS) generated in situ from sulfanilic acid and sodium nitrite. The morphological features of the materials were confirmed by transmission electron microscopy, whereas their physicochemical properties were characterized by means of elemental and textural analyses, thermogravimetric (TG) method, Raman spectroscopy, potentiometric back titration, and X-ray diffraction analysis. The obtained CFs were used as catalysts in glycerol etherification with tert-butyl alcohol at 110 °C under autogenous pressure. The BDS-modified CFs were particularly effective in the reaction, showing high glycerol conversions (of about 45–55% after 6 h) and substantial yields of mono- and di-glycerol ethers. It was found that the chemistry of the sample surface was crucial for the process. The high concentration of $-\text{SO}_3\text{H}$ groups decorating CFs boosted the formation of di- and tri-tert-butyl glycerol ethers. Surface oxygen functionalities also had a positive effect on the reaction, however, their impact on the catalytic performances of CFs was significantly weaker compared to that shown by $-\text{SO}_3\text{H}$ groups and it was probably due to the adsorption of reagents on the catalyst surface.

Dangerous global climate changes resulting from greenhouse gas emissions have been troubling the world for years. Among the main anthropogenic sources of air pollutants are emissions from the fossil fuel-based industry and the transportation sector^{1,2}. Combustion of coal, oil, and gas provides about 84% of global primary energy³. However, these non-renewable energy sources are significant providers of hazardous CO_2 , NO_x , SO_x , or particulate matter (PM) released into the atmosphere^{2,4,5}. Therefore, the development of clean and renewable energy resources is highly justified^{1,6}.

The use of wind, solar, and geothermal energy, or hydropower can significantly limit climate changes^{1,7}. Unfortunately, the main limitations of renewable-energy power plants are special weather conditions needed for operation, such as wind force or sunlight, the maintenance of which is not always possible¹. Biomass is another sustainable energy source of large versatility, e.g., it can be easily converted into liquid fuels such as biodiesel. According to the data provided by the International Energy Agency (IEA), global biodiesel production was about 43 billion L in 2021. This value is expected to be maintained in the nearest future⁸.

The process of biodiesel production is accompanied by the release of large quantities of a by-product in the form of (bio)glycerol. It is estimated that for every 1 tonne of biodiesel, 100 kg of glycerol is co-formed⁹. Thus, to make biodiesel fuel more profitable and more competitive with traditional petroleum-based fuels, there is an urgent need to valorize the co-produced glycerol, preferably by converting it into industrially valuable chemicals^{9,10}.

Tert-butyl glycerol ethers, TBGE, especially di- and tri-substituted products (DTBGE and TTBGE, respectively), are one of the most attractive compounds obtained from glycerol. These high-substituted glycerol derivatives (h-glycerol ethers) can be widely used in the fuel sector, where they can serve as valuable fuel oxygenates reducing the emissions of harmful gases into the atmosphere during fuel combustion (diesel, biodiesel, or gasoline). Glycerol ethers also improve viscosity, cloud points, or pour points of biodiesel, showing a positive effect on the performance properties of this fuel. Importantly, DTBGE and TTBGE are excellent alternatives to another

Faculty of Chemistry, Adam Mickiewicz University, Uniwersytetu Poznańskiego 8, 61-614 Poznań, Poland. ✉email: amalaika@amu.edu.pl

popular fuel additive, i.e., methyl tert-butyl ether (MTBE), which is considered an environmentally troublesome chemical substance with limited usage in some countries^{11–14}.

Typically, tert-butyl glycerol ethers are obtained by the catalytic etherification of glycerol with tert-butyl alcohol (TBA) or isobutene (IB). Despite the lower efficiency of the process with TBA, the use of alcohol is more practical, as IB is more expensive, non-renewable, and requires special reaction conditions to keep the gas in the liquid phase^{15,16}.

Conversion of glycerol to TBGE is an acid-catalyzed reaction in which heterogeneous catalysts are preferred over homogeneous ones. Solids have several advantages, e.g., they can be easily separated from the reaction mixture, are not corrosive, and are more environmentally friendly than homogeneous catalysts^{11,12,17}. The scheme of reaction between glycerol and TBA (prepared according to a commonly accepted mechanism) is shown in Fig. 1. As can be seen, five different glycerol tert-butyl ethers can be formed. Importantly, due to the steric effects (a tert-butyl group is of voluminous size), the formation of primary ethers (i.e., 1-substituted and 1,3-substituted) is favored¹⁸.

Ion exchange resins, modified zeolites, and silicas are solid catalysts most frequently tested in glycerol etherification, which is due to their high activities^{12,19–22}. For instance, Melero et al.²¹ demonstrated that sulfonic acid-functionalized mesostructured silicas showed excellent catalytic behavior in the etherification of glycerol with IB, giving glycerol conversions up to 100% and combined selectivities toward DTBGE and TTBGE over 92% within 4 h. Frusteri et al.²³ tested spherical silica-supported Hyflon[®] catalysts (SSHC) in the process between glycerol and IB and found that the best catalytic system led to complete conversion of glycerol and high combined selectivity to the desired ethers (i.e., DTBGE and TTBGE), of about 97%, just within 6 h. The catalyst also showed high resistance to deactivation. Xiao et al.²⁰ investigated glycerol etherification with IB over HY zeolites modified with citric acid and achieved glycerol conversion and a combined selectivity to di- and tri-tert-butyl glycerol ethers of 91% and 64%, respectively, within 7 h of the reaction. On the other hand, Klepáčová et al.¹⁸ performed glycerol etherification with tert-butyl alcohol using Amberlyst-15 and large-porous zeolites such as H-BEA. The conversions of glycerol were comparable for both samples (> 80 and 90% after 6 h); however, H-BEA formed nearly twice as much di-ethers as Amberlyst-15 (45% vs. 25%).

Carbon materials have been relatively rarely used in glycerol etherification. Meanwhile, these catalysts offer several advantages over typical catalytic systems, e.g., high thermal stability, ease of tuning their physicochemical properties, and various morphological forms^{17,24}. For instance, Zhao et al.¹¹ obtained very good catalytic results in glycerol etherification performed over a sulfonated carbon catalyst synthesized from peanut shells, i.e., complete conversion of glycerol and a 92.1% combined selectivity to DTBGE and TTBGE just within 2 h; however, the process used isobutylene which presents several disadvantages compared to TBA. Gonçalves et al.²⁵ tested

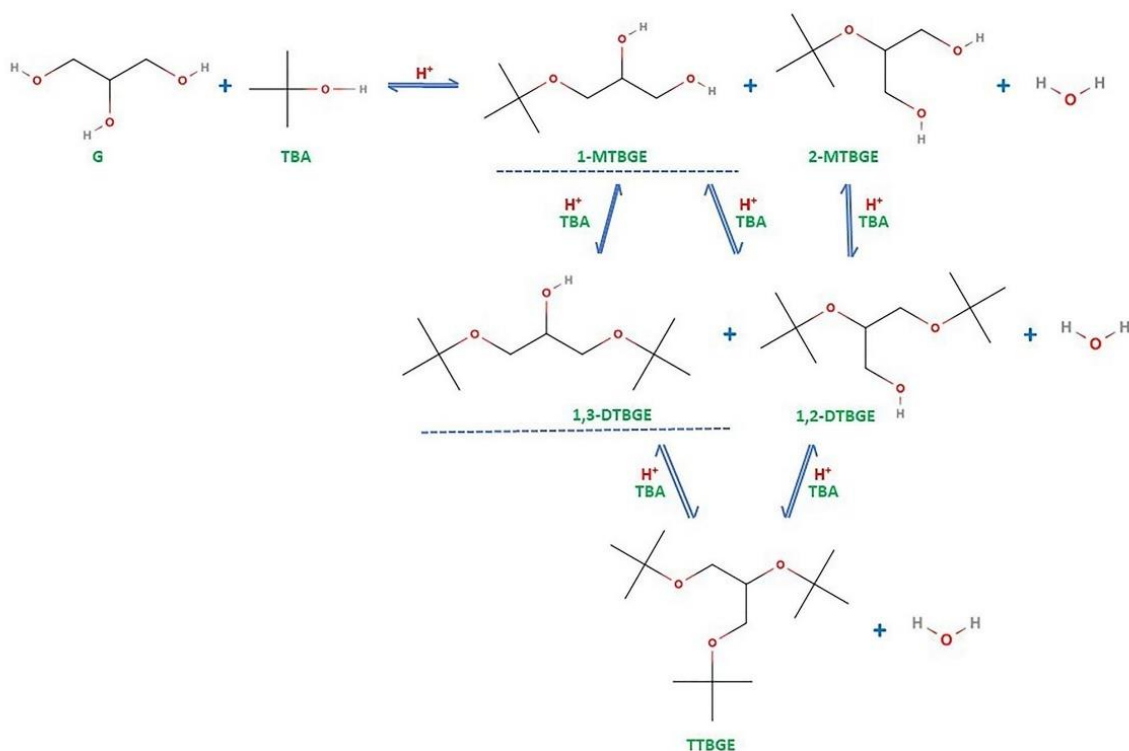


Figure 1. The scheme of reaction between glycerol and tert-butyl alcohol under acidic conditions.

sulfonated carbon-based catalysts in the etherification of glycerol with TBA. Over 80% glycerol conversion and about 21% selectivity to DTBGE and TTBGE were achieved after 4 h of the reaction at 120 °C. The catalytic activity of the prepared carbon samples was ascribed mainly to the presence of strongly acidic surface sulfonic groups; however, no detailed studies on the influence of the carbon catalyst properties on the material activity have been performed. In turn, Estevez et al.²⁶ demonstrated that sulfonated carbon obtained from olive stones gave a 21% yield of higher glycerol ethers just within 15 min. Additionally, the prepared catalyst exhibited high stability, maintaining its activity after being used in several consecutive reactions. However, the process required a microwave to achieve these promising results.

The current work presents the results on the catalytic performances of the SO₃H-functionalized carbon fibers produced from isobutane or ethylene in glycerol etherification carried out with sustainable and easy-to-handle TBA. Importantly, the collected data enabled us to determine the relationship between the chemical structure and the carbon fibers' performance in the formation of di- and tri-glycerol ethers (DTBGE and TTBGE, respectively), i.e., the products of interest. We believe that these findings can set the direction of future research aimed at maximizing the production of h-glycerol ethers and at developing new effective acid carbon catalysts for the glycerol valorization processes. Furthermore, to the best of our knowledge, modified ethylene- and isobutane-derived CF catalysts have never been tested in TBA-assisted etherification of glycerol.

Experimental section

Preparation of the carbon samples. Carbon fibers (CFs) were prepared by catalytic chemical vapor deposition (CCVD) using gaseous hydrocarbons such as isobutane or ethylene as carbon feedstocks, and nickel as a catalyst. The process was conducted under the optimized conditions established earlier^{27,28}. Briefly, NiO (100 mg in the case of isobutane and 30 mg in the case of ethylene) was placed in a quartz boat in a horizontal tube furnace and heated under Ar flow to 550 °C. At this temperature, the reduction of Ni oxide was performed using a 20% H₂/80% Ar mixture (total flow of gases of 100 cm³/min) for 2 h. Afterward, the CCVD process of hydrocarbons was initiated by switching the H₂/Ar gases to a mixture of 75% H₂/25% ethylene or 50% H₂/50% isobutane. The first reaction was performed at 550 °C, whereas the second at 600 °C, both for 4 h. In both cases, the obtained carbon product was treated with a 21% HCl solution and heated for 2 h under reflux to remove the Ni catalyst from the sample. Afterward, the material was washed with hot distilled water, dried at 110 °C overnight, and finally, sieved to a particle size ≤ 0.4 mm. The resultant samples were denoted as CF_{i-bu} and CF_{et} depending on the carbon precursor used in the CCVD process (i.e., carbon fibers from isobutane or ethylene, respectively).

The prepared CF samples were functionalized with acidic sites using sulfuric acid or 4-benzenediazonium sulfonate (BDS) generated *in situ*. Details of the modifications are given below.

The modification of CFs with sulfuric acid was carried out by mixing 3.5 g of the sample with 90 cm³ of concentrated H₂SO₄. The mixture was heated at 140 °C for 20 h under argon flow. After the functionalization, the carbon was filtered out, thoroughly washed with hot distilled water until a neutral pH, and dried overnight at 110 °C. Finally, it was sieved to a particle size of ≤ 0.4 mm. The resultant CF samples were labeled as CF_{i-bu}-H₂SO₄ and CF_{et}-H₂SO₄.

The reaction of CFs with BDS was carried out according to a modified procedure proposed originally by Toupin and Bélanger²⁹. The process was performed using 3.5 g of the carbon that was mixed with distilled water (175 cm³), sulfanilic acid (5 g), and sodium nitrite (2 g). In the next step, concentrated hydrochloric acid (35 cm³) was added dropwise to the mixture. The modification was performed at 20 °C for 20 h. Afterward, the sample was washed with distilled water, then with methanol, dimethylformamide (DMF), and acetone. Finally, it was dried overnight at 110 °C and sieved to a particle size of ≤ 0.4 mm. The resultant samples were denoted as CF_{i-bu}-BDS and CF_{et}-BDS.

Characterization of the samples. The obtained carbon samples were characterized using various techniques, i.e., elemental and textural analyses, electron microscopy, potentiometric back titration method, Raman spectroscopy, thermogravimetric analysis, and XRD technique.

The elemental CHNS composition of the samples was determined using an elemental analyzer Vario EL III. Textural parameters of the carbons were examined by means of a Quantachrome Autosorb IQ apparatus based on N₂ adsorption/desorption measurements performed at -196 °C. The samples were outgassed under vacuum conditions at 150 °C before the analysis. Apparent surface areas of the samples (S_{BET}) were calculated using the Brunauer–Emmett–Teller (BET) model, while the micropore volumes (V_{micro}) and external surface areas (of meso- and macropores; S_{ext}) were determined using the t-plot method. In turn, the total volumes of pores (V_{tot}) were calculated from the amount of nitrogen adsorbed at a relative pressure close to 1. A potentiometric back titration method was used to measure the total acidity of the prepared carbons. For this purpose, a Cerko Lab microtitration unit was applied. The measurement procedure included mixing a sample (100 mg) with a 0.01 M NaOH solution (50 cm³) and shaking the obtained suspension at room temperature for 20 h. Afterward, the mixture was filtered and a clear solution was titrated with 0.05 M HCl. The morphological features of the prepared materials were examined using a TEM JEOL 2000 transmission electron microscope operating at 80 kV. In turn, high-resolution TEM (HR-TEM) images were obtained by means of an FEI Tecnai G2 20 X-TWIN apparatus. A Bruker AXS D8 Advance diffractometer was applied to perform X-ray diffraction (XRD) measurements. Raman spectra were acquired using a Renishaw InVia Reflex confocal Raman spectrometer equipped with an argon laser as an excitation source (λ = 514 nm, P = 1 mW). In turn, thermogravimetric analysis (TG) was performed using a Setaram Setsys 1200 thermal analyzer in nitrogen or air flow in the temperature range of 20–950 °C and with a heating rate of 10 °C/min.

Catalytic measurements. Etherification of glycerol was carried out in a hand-made high-pressure stainless steel laboratory autoclave. This model consisted of a reactor body, a thermocouple inserted into the reaction mixture to precisely control the process temperature, an inlet gas valve for purging the reactor, a pressure gauge to monitor the current reaction pressure, a heating jacket, a magnetic stirrer, and a sampling capillary with an outlet valve enabling in-situ collecting the samples. The reactor was charged with 10.2 g of glycerol (G) and 42 cm³ of tert-butyl alcohol (TBA; TBA:G molar ratio of 4:1). Afterward, the catalyst was added to the mixture (5 wt.% based on the glycerol weight). To remove air from the reactor, the autoclave was flushed with argon several times. The etherification process was performed at 110 °C for 24 h under autogenous pressure. To monitor the progress of reaction, samples of the reaction mixtures were taken after 1, 2, 4, 6, and 24 h. The used sampling procedure did not change notably the pressure inside the reactor.

The analysis of the liquid samples was performed with the use of a gas chromatograph (SRI 8610C) equipped with a RESTEK MXT⁺—WAX capillary column (30 m × 0.25 mm × 0.25 μm) and a flame ionization detector (FID) working at the temperature of 210 °C and powered by hydrogen and air with flows of about 25 cm³/min and 270 cm³/min, respectively. Helium was used as the carrier gas (1 cm³/min) and a split injector (temperature of 230 °C and a split ratio of about 30) was applied for the analyses. Measurements were carried out according to the following temperature program: 40 °C (7 min) and 210 °C (17 min; increase rate of 30 °C/min). The identification of the reaction components was confirmed by a GC–MS (Gas Chromatography–Mass Spectrometry) technique.

The activity of catalysts was expressed as conversions of glycerol (X_G) and yields of the corresponding glycerol ethers (i.e., Y_{MTBGE} —yield of MTBGE, Y_{DTBGE} —yield of DTBGE, and Y_{TTBGE} —yield of TTBGE), or selectivity to individual reaction products (i.e., S_{MTBGE} —selectivity to MTBGE, S_{DTBGE} —selectivity to DTBGE, and S_{TTBGE} —selectivity to TTBGE).

Results and discussion

The calculated yields of the carbon fibers obtained from ethylene and isobutane (both used in a mixture with hydrogen; see Experimental) were about 143 and 52 gCFs/gNi, respectively. These values were quite comparable or even significantly higher than those achieved by other authors. For example, Toebes et al.³⁰ obtained a yield of CFs of about 20 g/gMe using a C₂H₄/H₂ mixture and Ni as a catalyst. Moreover, the use of ethylene as a carbon source was found to be more advantageous than the use of other hydrocarbons. For instance, according to our previous study²⁷, the use of methane in CCVD resulted in a very low yield of carbon nanofibers, i.e., about 4 gCFs/gNi. Similarly, studies by Miniach et al.³¹ showed that the activity of Ni/hydroxyapatite in the CFs formation via CCVD of methane was only about 10 gCFs/gCat. Filamentous carbon was also produced from acetylene—31.6 g of coiled CFs per 1 g of a Fe-based catalyst was obtained in this case³². In view of the above, the results of yields obtained in this study seem to be quite promising, even those achieved for CF_{i-bu} produced with lower efficiency.

A thorough characterization of the obtained samples as well as the results of their catalytic performances are presented below.

Characterization of the samples. The elemental composition of the prepared materials is presented in Table 1. As can be observed, the initial CFs showed a very high content of carbon, which was about 97% in the case of CF_{i-bu} and 99% for CF_{et}. Only traces of heteroatoms were detected (the O contents between 0.2 and 0.9%). These results are not surprising as the preparation of CFs involved the use of hydrocarbons as carbon feedstocks, thus the compounds with no oxygen atoms in their structures (traces of O in CFs probably come from the oxidation processes taking place during the sample storage). In the case of functionalized materials, a reduction in the content of elemental carbon was observed, although the C contents in the modified samples were still very high—over 90%. At the same time, an increase in the contents of heteroatoms such as sulfur and oxygen was noticed. This indicates that the methods used here for the modifications of CFs were successful. It should be stressed, however, that the degree of sample functionalization was not very high (the S contents between 0.4 and 1.4% were attained), which is not surprising taking into account a rigid and ordered structure of typical carbon fibers^{28,33}. For comparison, our previous studies showed that modifications of carbon xerogels can produce samples with a 1.4–2.3% S content, while functionalization of carbon polymeric spheres can give materials with a sulfur content of 4.3%³⁴. In turn, the sulfonated bio-carbons obtained in the process of simultaneous partial carbonization and sulfonation contained 0.7–5.0% of sulfur in their structures³⁵.

The functionalization degree of the CF samples varied depending on the modifying approach used. In the case of CFs modified with sulfuric acid, the amount of S was 0.4% and 0.6% (for CF_{i-bu}-H₂SO₄ and CF_{et}-BDS,

Sample	Ash	C	H	N	S	O*	-SO ₃ H [†]	A _{tot}
CF _{i-bu}	0.3	99.0	0.4	0.1	0.0	0.2	0.00	0.00
CF _{i-bu} -H ₂ SO ₄	0.5	96.4	0.7	0.0	0.4	2.0	0.11	0.09
CF _{i-bu} -BDS	0.8	94.6	0.8	0.3	0.9	2.6	0.27	0.01
CF _{et}	1.1	97.3	0.7	0.0	0.0	0.9	0.00	0.03
CF _{et} -H ₂ SO ₄	0.5	92.2	0.7	0.1	0.6	5.9	0.17	0.39
CF _{et} -BDS	0.8	91.0	1.1	0.5	1.4	5.2	0.42	0.07

Table 1. Results of the elemental analysis (wt.%), total acidity measurements (A_{tot}, mmol H⁺/g), sulfonic groups (-SO₃H, mmol/g) and ash content determinations for the obtained samples. *Calculated by difference; †calculated from the elemental analysis.

respectively), while the reaction of CFs with diazonium salt introduced about twice as much sulfur into the CF structure (see Table 1). Importantly, sulfur in the BDS-modified carbons was probably anchored to the sample surface in the form of $-\text{PhSO}_3\text{H}$ groups, which was also suggested by literature data^{36,37}. For the BDS-modified carbons, there was a noticeable increase in the content of nitrogen. This may indicate the presence of azo bonds in the prepared materials, which were formed in coupling reactions between diazonium cations and the surface of carbons³⁹.

Generally, the modifications of CFs with H_2SO_4 turned out to be less effective than those with BDS. This is also in line with literature data indicating lower susceptibility of graphite-like materials to sulfonation with concentrated sulfuric acid compared to that of amorphous ones³⁸. As depicted in Table 1, the unmodified carbons practically did not show acidic properties as A_{tot} measured for $\text{CF}_{1-\text{bu}}$ and CF_{et} was very low. Generally, the used modifications increased A_{tot} ; however, the changes between the functionalized and parent CFs were not so significant, especially in the case of $\text{CF}_{1-\text{bu}}-\text{H}_2\text{SO}_4$ and for BDS-modified samples. Interestingly, the total acidities measured for BDS-modified CFs were lower than those resulting from the number of surface sulfonic groups (calculated based on the sulfur content). This may be related to the neutralization of some $-\text{SO}_3\text{H}$ structures, e.g., by the formation of zwitterions and finally, the creation of SO_3^- moieties on the carbon surface^{36,39–41}. The opposite effect was observed for $\text{CF}_{\text{et}}-\text{H}_2\text{SO}_4$, i.e., the total acidity measured for this sample was higher than that resulted from the presence of $-\text{SO}_3\text{H}$ groups. This can indicate the formation of surface oxygen groups of acidic properties during the CF_{et} reaction with H_2SO_4 apart from the sulfonic functionalities (see also the oxygen contents in $\text{CF}_{\text{et}}-\text{H}_2\text{SO}_4$ and CF_{et} in Table 1). This is in accordance with previous literature reports suggesting oxidizing properties of concentrated sulfuric acid^{41–43}. The surface of $\text{CF}_{1-\text{bu}}$ seemed to be more resistant to oxidation (as $-\text{SO}_3\text{H} \approx A_{\text{tot}}$) as well as the functionalization in general ($\text{CF}_{1-\text{bu}}$ was functionalized less effectively compared to CF_{et}).

Table 2 presents the textural properties of the obtained samples. The unmodified CFs showed moderate apparent surface areas (S_{BET}) which differed slightly depending on the carbon precursor used during the CCVD process. Both types of the initial samples showed a significant contribution of the external surface area to the apparent surface area ($S_{\text{ext}}/S_{\text{BET}}$), and only a small number of micropores was detected in both cases (as evidenced by a low contribution of the micropore volume to the total volume of pores; $V_{\text{micro}}/V_{\text{tot}}$). The modifications of CFs with sulfuric acid caused only slight decreases in S_{BET} , while the reactions with BDS resulted in more significant S_{BET} changes. This was probably due to introducing high volume $-\text{PhSO}_3\text{H}$ groups into the structure of CFs during the reaction with BDS, blocking the smallest pores in the samples (as $V_{\text{micro}}/V_{\text{tot}}$ for both BDS-treated samples decreased to 0%). A similar phenomenon was also observed elsewhere^{35,44}. Interestingly, the observed decrease in S_{BET} was higher in the case of $\text{CF}_{\text{et}}-\text{BDS}$, suggesting more effective functionalization of this sample compared to $\text{CF}_{1-\text{bu}}-\text{BDS}$. This conclusion is also in line with the results of elemental analysis (see also the contents of S in Table 1).

The morphology of selected carbon samples prepared via the CCVD method is presented in Fig. 2. As can be observed from Fig. 2A, the process with the use of isobutane and Ni as catalyst led to a mixture of different carbon structures, differing in their sizes and shapes. Among them, mostly carbon fibers were identified—rather short, with a fairly large diameter (marked as CF in the TEM image). Probably, also carbon nanotubes with small diameters were formed in the process, as long fine hollow structures are visible in Fig. 2A (marked as CNT).

Figure 2B shows a TEM image of the sample produced from ethylene. Similarly to $\text{CF}_{1-\text{bu}}$, CF_{et} consisted of carbon fibers with rather large diameters (however, slightly smaller than in the case of $\text{CF}_{1-\text{bu}}$). Individual filaments showed irregular shapes and surfaces—from smooth to presenting sharp edges. Trace amounts of CNT are also visible.

The high-resolution TEM images of different magnifications obtained for CFs produced from isobutane and ethylene are shown in Fig. 1SM.

The presented pictures revealed the partial graphitic structure of $\text{CF}_{1-\text{bu}}$ and CF_{et} , as the ordered orientation of the graphene sheets was visible for most of the produced fibers. In the case of CFs obtained from ethylene, the graphene sheets were arranged parallel to each other and perpendicular to the fiber axis, forming platelet carbon fibers (Fig. 1SM E). CFs produced from isobutane also resembled platelet-like structures, however, a slightly lower degree of order than that observed for CF_{et} was noticed, as randomly oriented graphene sheets were also found in the HR-TEM images of $\text{CF}_{1-\text{bu}}$ (Fig. 1SM B).

The XRD patterns of the unmodified carbon fibers (i.e., CF_{et} and $\text{CF}_{1-\text{bu}}$) are shown in Fig. 3. In both cases, two signals characteristic of carbon materials and attributed to graphite-like structures are visible—a sharp diffraction peak at 2-theta of 26° and a less intense one at 2-theta of 43° , which corresponds to diffraction on the (002) and (100) planes, respectively. A weak signal at 2-theta of 55° is also noticeable, probably representing the (004) graphite-type reflection^{45–49}. The XRD patterns also show a diffraction line at 2-theta of 78° , possibly

Sample	S_{BET} (m ² /g)	$S_{\text{ext}}/S_{\text{BET}} \times 100$ (%)	$V_{\text{micro}}/V_{\text{tot}} \times 100$ (%)
$\text{CF}_{1-\text{bu}}$	115	59	8.93
$\text{CF}_{1-\text{bu}}-\text{H}_2\text{SO}_4$	102	58	9.62
$\text{CF}_{1-\text{bu}}-\text{BDS}$	42	100	0.00
CF_{et}	174	62	8.63
$\text{CF}_{\text{et}}-\text{H}_2\text{SO}_4$	171	67	8.76
$\text{CF}_{\text{et}}-\text{BDS}$	58	100	0.00

Table 2. Textural analysis of the samples.

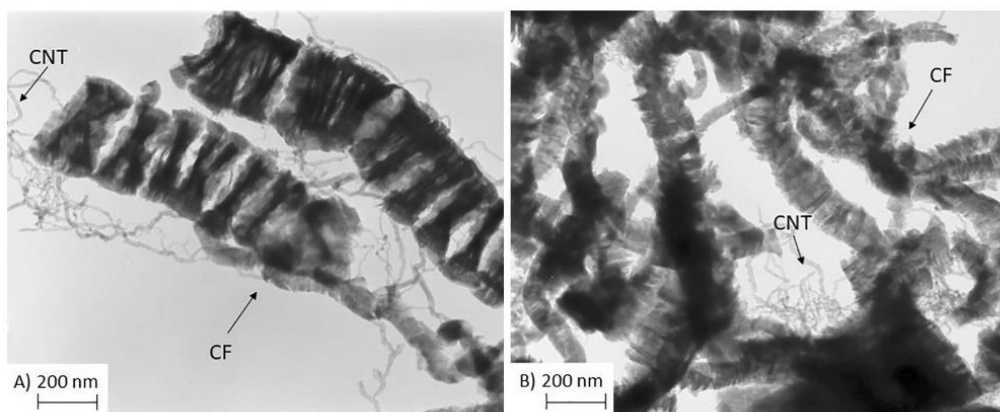


Figure 2. TEM micrographs of (A) CF_{i-bu} and (B) CF_{et} .

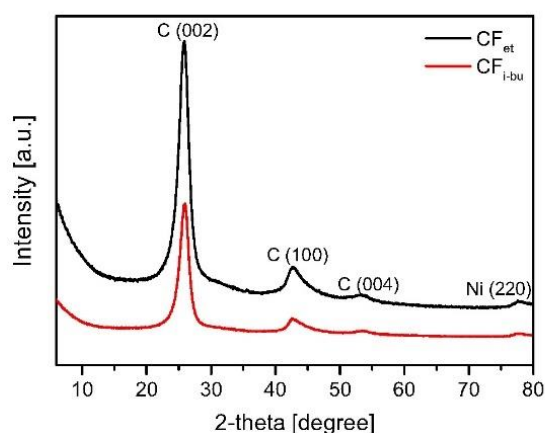


Figure 3. The XRD patterns of the prepared initial CF samples.

belonging to the (110) plane of graphitic materials⁵⁰ or metallic nickel^{27,51}. The presence of this peak can suggest that some traces of catalyst remained in the carbon product despite the sample boiling with a solution of HCl (see Experimental).

Figure 4 presents the Raman spectra obtained for the CFs produced from different precursors as well as the data achieved for a series of modified carbons. As can be observed, all the samples showed peaks typical for carbon materials, i.e., at about 1350 and 1580 cm^{-1} . The first signal (D band) is typically attributed to defects and disorders in the lattice structure of carbons, while the latter (G band) is related to the graphitized carbon motifs where the C-atoms are sp^2 hybridized. Importantly, the relative intensity ratio of the D to G band (I_D/I_G) can serve as an indicator of carbon sample graphitization and simultaneously as an indicator of structural defects of carbons⁵².

As shown in Fig. 4, the I_D/I_G value calculated for CFs produced from ethylene was significantly lower than that of CFs synthesized from isobutane (~ 1.11 vs. ~ 1.76), implying a higher degree of CF_{et} graphitization and its less defective nature. This conclusion is also in line with the results achieved in the HR-TEM analysis (see Fig. 1SM). The modified carbon fibers showed slightly higher values of I_D/I_G ratios as compared to the parent sample, which indicates that some defects at the sidewalls of the fibers appeared after the functionalizations. It might be supposed that these defects were due to the carbon sp^2 to sp^3 hybridization, being a result of the binding of new functional groups to the carbon surface (see also the results of EA in Table 1)⁵³ As sulfuric acid is a more aggressive reagent than BDS and additionally shows oxidizing properties (as discussed earlier), $CF_{et}-H_2SO_4$ was found to be slightly more defective than $CF_{et}-BDS$, which was suggested by a slightly higher value of I_D/I_G obtained for $CF_{et}-H_2SO_4$ compared to that achieved for $CF_{et}-BDS$.

Figure 5 shows the results of thermogravimetric (TG) analysis of CF_{et} and CF_{i-bu} samples performed in an air atmosphere. As can be seen from the TG pattern (Fig. 5A), both samples were thermally stable up to about 500 °C. Over this temperature, a sharp weight loss was detected in both cases. The complete combustion of the materials was noted at 700 °C and 780 °C. The residue after combustion was 0.3% and 1.1% for CF_{i-bu} and CF_{et} , respectively, and its presence was probably related to Ni remaining in the samples after the CCVD process. Under

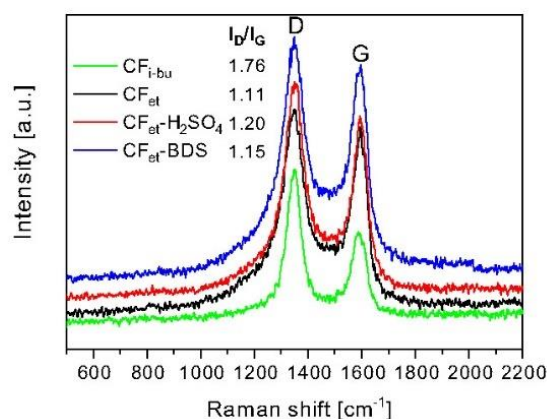


Figure 4. Raman spectra of selected samples.

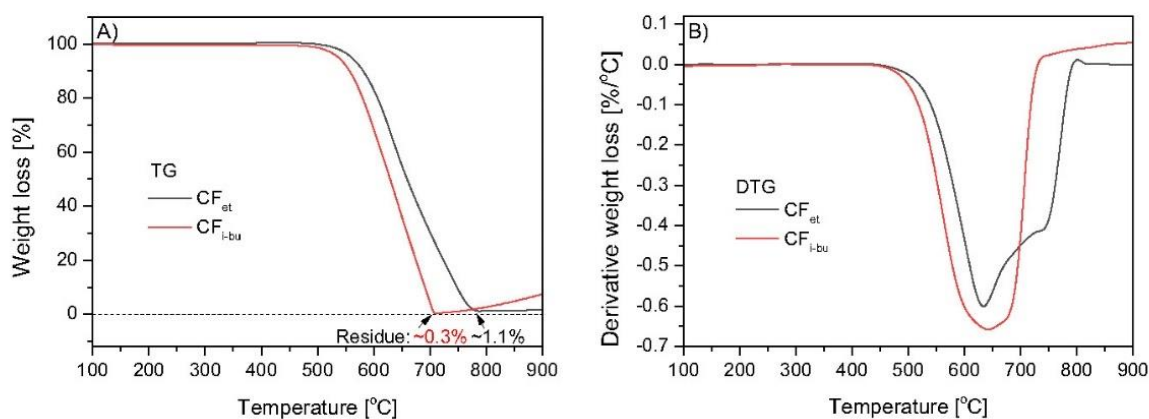


Figure 5. TG (A) and DTG (B) curves of the CF_{et} and CF_{i-bu} samples (air flow).

the measurement conditions, a slight weight gain was also observed at high temperatures as a result of the metal oxidation⁵⁴. As shown earlier, traces of Ni in the CF samples were also confirmed by the XRD analysis (see also Fig. 3). In general, the DTG patterns of the samples (Fig. 5B) show intense peaks with the minima at a temperature of about 640 °C. These signals can be attributed to the combustion of well-ordered filamentous carbon^{27,54–56}. Furthermore, in the DTG curve of CF_{et} , an additional poorly separated signal can be distinguished (at about 750 °C). The above observations can suggest the presence of phases with a different number of defects in CF_{et} , i.e., a slightly more defective phase (with a minimum at 640 °C), and the one more stable and well-organized (with a minimum at 750 °C)^{28,57}. The absence of lower-temperature peaks excludes contamination of the samples with less thermally stable types of carbon, e.g., amorphous carbon (combustion temp. below 400 °C)^{27,54,55}.

Figure 6 shows the results of the TG analysis performed for the pristine and modified CF_{et} and CF_{i-bu} in nitrogen flow. In the case of unmodified materials (Fig. 6A), only a slight decrease in the sample weight with increasing temperature was observed, which proves the high thermal resistance of the samples tested. At the final temperature of TG measurement, the weight loss was ~6% for CF_{et} and ~3% for CF_{i-bu} . The DTG profiles of the parent carbons show two small peaks with minima at about 200 °C and 280 °C, suggesting the presence of oxygen surface groups (such as carboxylic ones) in CFs. These groups could spontaneously form on the carbon surface during the sample contact with air⁵⁸. The existence of oxygen-type functionalities was also confirmed by elemental analysis (see also Table 1).

Significantly higher weight losses were observed for the modified CF samples (Fig. 6B), reflecting the degree of functionalization of these materials. Only a slight decrease in the sample weight was observed for $CF_{i-bu}-H_2SO_4$ (~6%), indicating a low number of groups released as volatiles. This is also in line with the results of elemental analysis (see Table 1). On the other hand, the most significant changes in the sample mass were observed for $CF_{et}-BDS$ (~11%) which was considered the most functionalized material among the prepared modified CFs (see also Table 1). Importantly, the DTG patterns of H_2SO_4 -modified samples indicate the presence of signals with minima at 280 °C, which can be attributed to the decomposition of surface sulfonic groups^{39,42,59}. Moreover, the DTG profile of $CF_{et}-H_2SO_4$ depicts a broad peak starting from about 500 °C, which probably is due to the presence

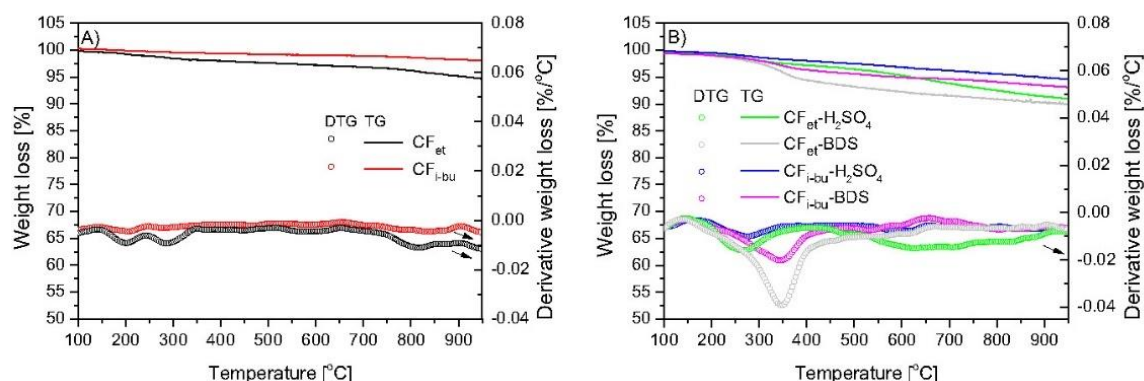


Figure 6. TG and DTG curves of the parent samples (A) and the modified CFs (B) for the analyses performed in nitrogen flow.

of more stable oxygen groups, e.g., phenolic ones, formed during the sample modification with concentrated H_2SO_4 ^{39,42,58,59}. A much lower intensity of this peak in the profile of $\text{CF}_{i\text{-bu}}\text{-H}_2\text{SO}_4$ indicates higher resistance of $\text{CF}_{i\text{-bu}}$ to oxidation, which was also concluded based on the elemental analysis (Table 1). Different DTG curves were observed for the samples modified with BDS as they both show an intense peak with a minimum at 350 °C. This signal can be ascribed to the decomposition of $-\text{PhSO}_3\text{H}$ groups^{39,60}. No signals were observed at higher temperatures, which proves that the applied functionalization method did not oxidize the sample.

Catalytic results. The obtained functionalized CFs were tested as catalysts in the process of glycerol etherification with tert-butyl alcohol. For the sake of comparison, also a blank test and a reaction with a commercial catalyst, Amberlyst-15, were performed.

The results obtained in the reaction over unmodified CFs showed that the catalytic effect of the parent samples was negligible as glycerol conversion achieved after 24 h was below 2% in both cases. Much better results were attained for the modified CFs. The catalytic performances of the functionalized materials are gathered in Figs. 7 and 8.

As can be observed, the catalytic properties of H_2SO_4 - and BDS-modified $\text{CF}_{i\text{-bu}}$ differed significantly. In the case of $\text{CF}_{i\text{-bu}}\text{-H}_2\text{SO}_4$ (Fig. 7A), only small amounts of glycerol were reacted at the beginning of the process, i.e., X_G after 1 h was only about 2%. As the reaction progressed, this parameter increased to approximately 30% (after 24 h). The yields of individual ethers varied considerably. The dominant products at every stage of the process were mono-substituted ethers (i.e., MTBGE). After 1 h of the reaction, their yield was about 2%. Y_{MTBGE} increased linearly with time—to about 28% after 24 h of the process. The yield of DTBGE was significantly lower and after 24 h, it was less than 3%. A tri-substituted product (i.e., TTBGE) was formed only in traces. Comparing the catalytic activity of $\text{CF}_{i\text{-bu}}\text{-H}_2\text{SO}_4$ to that of the unmodified sample, it was obvious that the observed catalytic effect was a result of the acidic treatment of $\text{CF}_{i\text{-bu}}$ and a consequent slight increase in the $-\text{SO}_3\text{H}$ content and

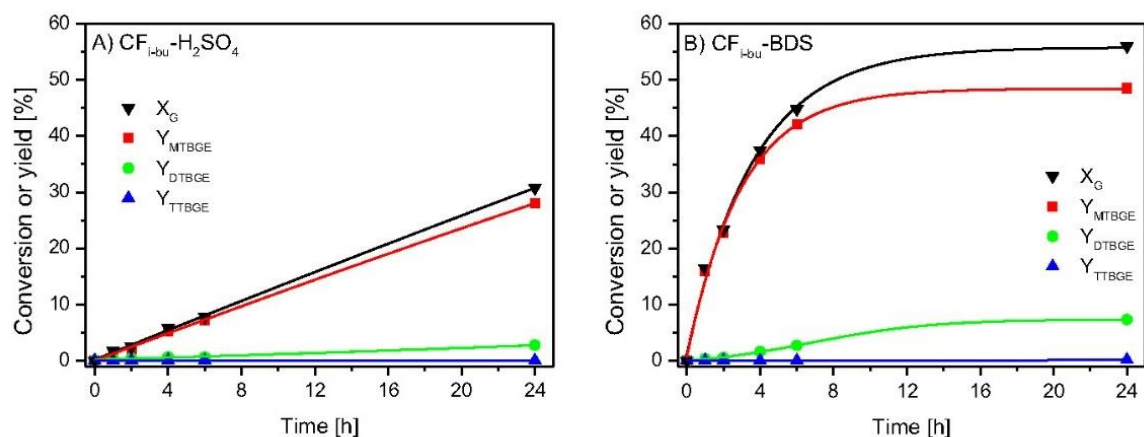


Figure 7. Conversions of glycerol (X_G) and yields (Y) of individual products obtained in the glycerol etherification performed with tert-butyl alcohol over (A) $\text{CF}_{i\text{-bu}}\text{-H}_2\text{SO}_4$, (B) $\text{CF}_{i\text{-bu}}\text{-BDS}$.

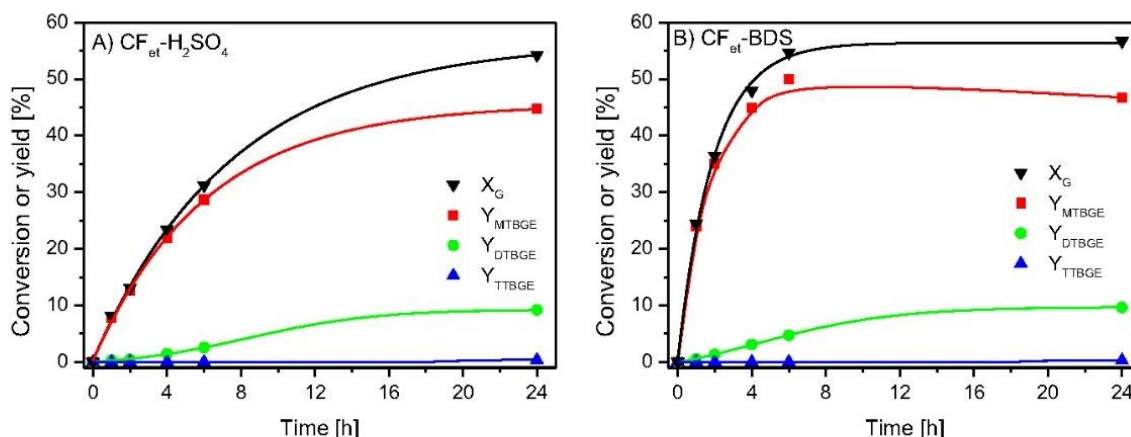


Figure 8. Conversions of glycerol (X_G) and yields (Y) of individual products obtained in the glycerol etherification performed with tert-butyl alcohol over (A) $CF_{et}-H_2SO_4$ and (B) $CF_{et}-BDS$.

the sample acidity (see Table 1). However, as the functionalization was not very effective, the obtained catalytic data were not so impressive.

It can be seen in Fig. 7B that $CF_{i-bu}-BDS$ catalyzed the reaction quite effectively, as significant amounts of glycerol were transformed into glycerol ethers in the first hours of the process. Over 16% of glycerol was converted within 1 h of the reaction and after 6 h, X_G was about 45%. As before, the glycerol conversion increased over time, and finally, it reached about 56%. The yields of individual ethers differed significantly. Mono-substituted products were formed preferentially and the yield of MTBGE after 24 h was about 45%. The DTBGE yield was much lower and it reached just over 7% after 24 h of the process. TTBGE was formed in the smallest amounts (Y_{TTBGE} after 24 h was less than 0.2%).

CFs obtained from various carbon precursors (i.e., isobutane and ethylene) worked differently (compare Figs. 7 and 8). The modified CFs produced from ethylene were generally more active in glycerol etherification than their counterparts produced from isobutane. This was due to the susceptibility of the obtained fibers to functionalization, especially with sulfuric acid, and the chemistry of their surfaces (see Table 1 and discussion in 3.1). As can be observed in Fig. 8A, $CF_{et}-H_2SO_4$ transformed glycerol quite effectively. After 1 h, X_G was slightly above 8%, and finally, it reached the value of 54%. The MTBGE products were mostly formed and their yield after 1 h of the reaction was about 8%. After 24 h, Y_{MTBGE} increased up to 45%. Di-substituted ethers were formed to a much lesser extent; however, their yield was higher than in the reaction performed in the presence of $CF_{i-bu}-H_2SO_4$. TTBGE was again created only in traces. Quite good catalytic results obtained for $CF_{et}-H_2SO_4$ can be attributed to the relatively high acidity of this sample (0.39 mmol H^+ /g, see Table 1). On the other hand, it should be stressed that in this case the concentration of $-SO_3H$ groups was not very high (i.e., 0.17 mmol/g, Table 1) and, as mentioned before, the sample acidity was partially generated also by the presence of oxygen acidic groups (such as phenolic or carboxylic ones^{34,41–43}). Thus, it can be supposed that the role of such functionalities in the etherification reaction might also be significant (which will be discussed later).

The $CF_{et}-BDS$ sample was more active in the process than its H_2SO_4 -modified counterpart (especially at the beginning of the reaction), which was probably related to a high concentration of $-SO_3H$ groups on the carbon surface (0.42 mmol/g, Table 1). As can be seen in Fig. 8B, a 25% glycerol conversion was obtained after 1 h of the reaction. X_G after 24 h increased to 57%. Mono-substituted compounds were formed in the highest amounts (Y_{MTBGE} about 25% vs. $Y_{DTBGE} \sim 0.5\%$ after 1 h). Interestingly, the MTBGE yield began to drop after 6 h of the process, and finally, it reached about 47%. At the same time, quite a significant increase in Y_{DTBGE} was observed. Probably, this phenomenon was due to the reaction mechanism and transformation of mono-substituted glycerol ethers to di-substituted ones. The yield of TTBGE after 24 h was less than 0.3%.

Figure 9 presents a comparison of the catalytic performances of all modified CFs to that of a commercial catalyst, Amberlyst-15 (expressed as glycerol conversions and selectivities to individual glycerol ethers after 6 and 24 h).

As can be seen, there was a group of catalysts that worked very effectively in the process, giving a high glycerol conversion and selectivity to di-substituted ethers just within 6 h of the reaction. These samples were both CFs modified with BDS and a commercial catalyst, Amberlyst 15. For these catalysts, an extension of the reaction time to 24 h did not affect significantly the conversion of glycerol as X_G changed rather slightly with time. Interestingly, X_G obtained after 24 h in the reaction over Amberlyst-15 was even lower than the results achieved with the prepared CFs (apart from $CF_{i-bu}-H_2SO_4$). Considering the selectivities to different ethers, MTBGE was the main product in each of the performed processes. However, CFs and Amberlyst-15 worked a little bit differently, i.e., in the case of modified CFs, S_{MTBGE} after 6 h was over 90%, while Amberlyst-15 presented S_{MTBGE} of $\sim 80\%$. On the other hand, S_{DTBGE} obtained in the reaction with the modified CFs did not exceed 10% after 6 h, while in the process with Amberlyst-15, it was almost 19%. This can indicate a faster transformation of mono-substituted ethers to di-substituted products in the case of Amberlyst-15, probably due to the high acidity

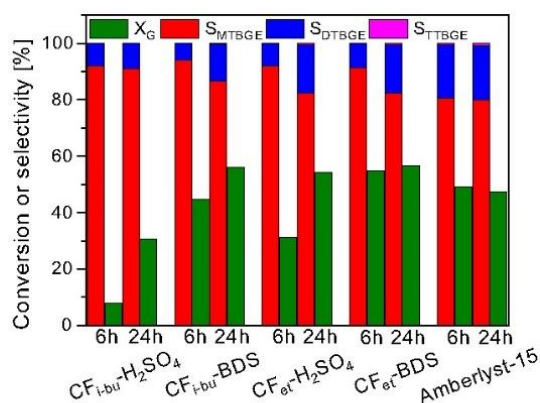


Figure 9. Glycerol conversions and selectivities to individual products after 6 and 24 h of the reaction using the prepared CFs and a commercial catalyst, Amberlyst-15.

shown by this catalyst (4.7 mmol/g)¹⁷. In most cases, the selectivities to MTBGE decreased with time in favor of DTBGE production, which can confirm that the mechanism of glycerol etherification performed with TBA over carbon catalysts includes a series of consecutive reactions (Fig. 1). The selectivity to TTBGE was close to zero in all the discussed processes and did not change significantly with time. Overall, the highest selectivities to the target ethers (i.e., DTBGE and TTBGE) were obtained after 24 h for Amberlyst-15 (~20%) and CF_{et}-BDS (~18%). On the other hand, the process catalyzed by CF_{i-bu}-H₂SO₄ was the least effective towards the formation of the high-substituted glycerol ethers (as S_{DTBGE+TTBGE} was ~9% after 24 h).

A comparison of the presented catalytic data (Figs. 7, 8, 9) with the physicochemical properties of CFs clearly indicates that the catalytic performances of the samples depended mainly on the acidic features of the prepared carbon fibers. Figure 10 depicts the relationship between the conversion of glycerol and the content of -SO₃H groups for the obtained modified CFs.

As can be seen, there is a clear relationship between glycerol conversions obtained using modified CFs and the content of their surface -SO₃H groups. Namely, the samples with a higher number of sulfonic groups worked significantly better in the process. This was especially well seen for the shorter reaction time (i.e., 6 h). After 24 h of the process, the differences were not so important, probably due to reaching the reaction equilibrium. It is worth noting that for the glycerol etherification lasting 6 h, CFs showing the lowest concentration of sulfonic groups (i.e., 0.11 mmol/g, see Table 1) gave X_G of only about 7.5%, while for CFs with the highest density of -SO₃H sites (i.e., 0.42 mmol/g), X_G was several times higher (over 50%).

The most desirable products of glycerol etherification are di- and tri-tert-butyl glycerol ethers (i.e., DTBGE and TTBGE). Figure 11 presents the relationship between the yield of DTBGE + TTBGE obtained in the reaction using the modified CFs and the content of surface -SO₃H sites.

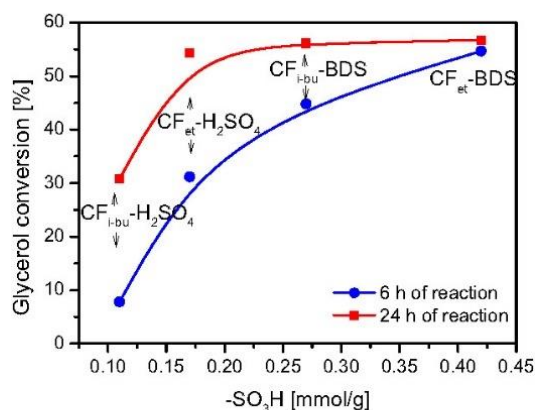


Figure 10. Glycerol conversions versus the concentration of sulfonic groups on CFs for the glycerol etherification with TBA.

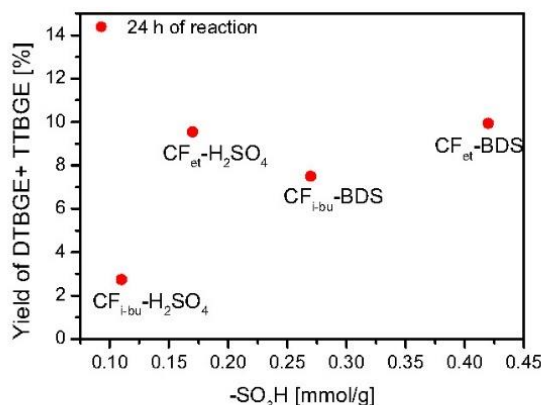


Figure 11. The influence of the content of sulfonic groups on the yield of DTBGE + TTBGE obtained in the etherification of glycerol with TBA.

Generally, the higher the number of sulfonic groups, the higher the combined yield of di- and tri-substituted ethers was obtained. However, the relationship was not as obvious as in the case of X_C vs $-\text{SO}_3\text{H}$ content (Fig. 10). An interesting sample was $\text{CF}_{\text{et}}-\text{H}_2\text{SO}_4$. Despite a rather moderate amount of $-\text{SO}_3\text{H}$ (i.e., 0.17 mmol/g; see Table 1), $\text{CF}_{\text{et}}-\text{H}_2\text{SO}_4$ effectively converted MTBGE ethers to DTBGE and TTBGE (see also Fig. 8A). The observed phenomenon was probably related to the relatively high A_{tot} of $\text{CF}_{\text{et}}-\text{H}_2\text{SO}_4$ (0.39 mmol H^+ /g, Table 1), compared to the other samples, resulting not only from the existence of sulfonic groups but also from the presence of acidic oxygen moieties. Thus, it can be supposed that oxygen functionalities may also have a positive effect on glycerol etherification. Similar conclusions were also drawn for glycerol acetylation performed over functionalized carbonaceous spheres⁶¹. Generally, it was found there that $-\text{SO}_3\text{H}$ groups are active sites of the process; however, oxygen functionalities, even though they do not catalyze the reaction themselves, can improve the reaction by adsorbing the substrates on the catalyst surface, and thus facilitate the contact between reagents and the active sites. The results presented above suggest that such an explanation may also be correct in the case of glycerol etherification over carbon materials. On the other hand, the catalyst porous architecture was probably a parameter of rather secondary importance. For example, the samples modified with BDS showed better catalytic properties than those modified with H_2SO_4 , even though the BDS-treated CFs presented smaller surface areas (please compare Table 2 and Figs. 7 and 8). This can suggest that S_{BET} is not the critical parameter for obtaining carbon catalysts highly active in glycerol etherification.

Conclusions

Glycerol etherification leads to valuable glycerol derivatives which may find important applications in many branches of industry. The current research showed that modified carbon fibers obtained from various hydrocarbons by a CCVD process can work as effective catalysts for the reaction between glycerol and tert-butyl alcohol. There were, however, some differences in the susceptibility of CFs to functionalization with sulfonating agents (i.e., concentrated H_2SO_4 or benzenediazonium salt generated in situ; BDS) and thus, the sample catalytic activity. The CFs obtained from ethylene were functionalized with $-\text{SO}_3\text{H}$ groups more effectively than those prepared from isobutane. Furthermore, a more efficient functionalization method was found to be the modification of CFs with BDS—this approach resulted in introducing significantly higher numbers of $-\text{SO}_3\text{H}$ functionalities onto the carbon surface than the reaction of CFs with sulfuric acid. The best catalytic performance in glycerol etherification was observed for $\text{CF}_{\text{et}}-\text{BDS}$ which presented nearly 57% glycerol conversion and about 18% combined selectivity to DTBGE and TTBGE within 24 h of the process. These results were generally better than those obtained using Amberlyst-15 under similar conditions. Furthermore, it was found that glycerol conversion is strongly dependent on the contents of $-\text{SO}_3\text{H}$ groups. The content of sulfonic functionalities also influenced the observed distribution of products. The presence of oxygen-containing groups also played an important role in the process, acting probably as adsorption sites for the reagents and improving the obtained catalytic results.

Data availability

The dataset generated and/or analyzed during the current study is too large to be retained or publicly archived with available resources, thus is not publicly available. Documentation and methods used to support this study are available from the corresponding author upon reasonable request.

Received: 23 October 2022; Accepted: 2 January 2023

Published online: 11 January 2023

References

1. Halkos, G. E. & Gkampoura, E. C. Reviewing usage, potentials, and limitations of renewable energy sources. *Energies* **13**, 2906 (2020).

2. Eurostat. Energy, transport and environment statistics. <https://ec.europa.eu/eurostat/> (2019).
3. Ritchie, H., Roser, M. & Rosado, P. Energy. <https://ourworldindata.org/energy> (2020).
4. Andres, R. J. *et al.* A synthesis of carbon dioxide emissions from fossil-fuel combustion. *Biogeosciences* **9**, 1845–1871 (2012).
5. Luque, R. *et al.* Biofuels: a technological perspective. *Energy Environ. Sci.* **1**, 542–564 (2008).
6. Meng, X. Biodiesel production from oleaginous microorganisms. *Renew. Energy* **34**, 1–5 (2009).
7. Nagy, K. & Körmendi, K. Use of renewable energy sources in light of the “New Energy Strategy for Europe 2011–2020”. *Appl. Energ.* **96**, 393–399 (2012).
8. IEA (2020). Renewables 2020, IEA, Paris; <https://www.iea.org/reports/renewables-2020/transport-biofuels>
9. Monteiro, M. R., Kugelmeier, C. L., Pinheiro, R. S., Batalha, M. O. & da Silva César, A. Glycerol from biodiesel production: Technological paths for sustainability. *Renew. Sust. Energ. Rev.* **88**, 109–122 (2018).
10. Luo, X., Ge, X., Cui, S. & Li, Y. Value-added processing of crude glycerol into chemicals and polymers. *Bioresour. Technol.* **215**, 144–154 (2016).
11. Zhao, W., Yang, B., Yi, Ch., Lei, Z. & Xu, J. Etherification of glycerol with isobutylene to produce oxygenate additive using sulfonated peanut shell. *Ind. Eng. Chem. Res.* **49**, 12399–12404 (2010).
12. Bozkurt, Ö. D. *et al.* Alternative fuel additives from glycerol by etherification with isobutene: Structure—performance relationships in solid catalysts. *Fuel Process. Technol.* **138**, 780–804 (2015).
13. Klepáčová, K., Mravec, D. & Bajus, M. Tert-butylolation of glycerol catalysed by ion-exchange resins. *Appl. Catal. A Gen.* **294**, 141–147 (2005).
14. Bozkurt, Ö. D., Yılmaz, F., Bağlar, N., Çelebi, S. & Uzun, A. Compatibility of di- and tri-tert-butyl glycerol ethers with gasoline. *Fuel* **255**, 115767 (2019).
15. Estevez, R. *et al.* Etherification of glycerol with tert-butyl alcohol over sulfonated hybrid silicas. *Appl. Catal. A Gen.* **526**, 155–163 (2016).
16. Viswanadham, N. & Saxena, S. K. Etherification of glycerol for improved production of oxygenates. *Fuel* **103**, 980–986 (2013).
17. Gonçalves, M. *et al.* Biodiesel wastes: An abundant and promising source for the preparation of acidic catalysts for utilization in etherification reaction. *Chem. Eng. J.* **256**, 468–474 (2014).
18. Klepáčová, K., Mravec, D., Hájeková, E. & Bajus, M. Etherification of glycerol. *Pet. Coal* **45**, 54–57 (2003).
19. Galhardo, T. S. *et al.* Preparation of sulfonated carbons from rice husk and their application in catalytic conversion of glycerol. *ACS Sustain. Chem. Eng.* **1**, 1381–1389 (2013).
20. Xiao, L., Mao, J., Zhou, J., Guo, X. & Zhang, S. Enhanced performance of HY zeolites by acid wash for glycerol etherification with isobutene. *Appl. Catal. A: Gen.* **393**, 88–95 (2011).
21. Melero, J. A. *et al.* Acid-catalyzed etherification of bio-glycerol and isobutylene over sulfonic mesostructured silicas. *Appl. Catal. A Gen.* **346**, 44–51 (2008).
22. Frusteri, F. *et al.* Catalytic etherification of glycerol by tert-butyl alcohol to produce oxygenated additives for diesel fuel. *Appl. Catal. A Gen.* **367**, 77–83 (2009).
23. Frusteri, F., Frusteri, L., Cannilla, C. & Bonura, G. Catalytic etherification of glycerol to produce biofuels over novel spherical silica supported Hyflon® catalysts. *Bioresour. Technol.* **118**, 350–358 (2012).
24. Muradov, N., Smith, F. & T-Raissi, A. Catalytic activity of carbons for methane decomposition reaction. *Catal. Today* **102–103**, 225–233 (2005).
25. Gonçalves, M. *et al.* Glycerol conversion catalyzed by carbons prepared from agroindustrial wastes. *Ind. Eng. Chem. Res.* **52**, 2832–2839 (2013).
26. Estevez, R., Aguado-Deblas, L., Montes, V., Caballero, A. & Bautista, E. M. Sulfonated carbons from olive stones as catalysts in the microwave-assisted etherification of glycerol with tert-butyl alcohol. *Mol. Catal.* **488**, 110921 (2020).
27. Malaika, A., Mozdzyńska, A., Piwecki, D. & Kozłowski, M. Comparative studies of the CCVD-based synthesis of carbon nanofibers – the quantitative aspect. *Diam. Relat. Mater.* **80**, 125–132 (2017).
28. Malaika, A., Ptasińska, K. & Kozłowski, M. Production of valuable chemicals from glycerol using carbon fiber catalysts derived from ethylene. *Sci. Rep.* **11**, 20251 (2021).
29. Toupin, M. & Bélanger, D. Spontaneous functionalization of carbon black by reaction with 4-nitrophenyldiazonium cations. *Langmuir* **24**, 1910–1917 (2008).
30. Toebes, M. L., Bitter, J. H., Jos van Dillen, A. & de Jong, K. P. Impact of the structure and reactivity of nickel particles on the catalytic growth of carbon nanofibers. *Catal. Today* **76**, 33–42 (2002).
31. Miniach, E., Sliwak, A., Moysseowicz, A. & Gryglewicz, G. Growth of carbon nanofibers from methane on a hydroxyapatite-supported nickel catalyst. *J. Mater. Sci.* **51**, 5367–5376 (2016).
32. Tang, N., Zhong, W., Gedanken, A. & Du, Y. High magnetization helical carbon nanofibers produced by nanoparticle catalysis. *J. Phys. Chem. B* **110**, 11772–11774 (2006).
33. Bhatt, P. & Goe, A. Carbon fibres: production, properties and potential use. *Mat. Sci. Res. India* **14**, 52–57 (2017).
34. Malaika, A. & Kozłowski, M. Glycerol conversion towards valuable fuel blending compounds with the assistance of SO₃H-functionalized carbon xerogels and spheres. *Fuel Process. Technol.* **184**, 19–26 (2019).
35. Malaika, A., Ptasińska, K. & Kozłowski, M. Conversion of renewable feedstock to bio-carbons dedicated for the production of green fuel additives from glycerol. *Fuel* **288**, 119609 (2021).
36. Lebègue, E. *et al.* Modification of activated carbons based on diazonium ions in situ produced from aminobenzeneorganic acid without addition of other acid. *J. Mater. Chem.* **21**, 12221–12223 (2011).
37. Hetemi, D., Noël, V. & Pinson, J. Grafting of diazonium salts on surfaces: application to biosensors. *Biosensors* <https://doi.org/10.3390/bios10010004> (2020).
38. Konwar, L. J., Maki-Arvela, P. & Mikkola, J.-P. SO₃H-containing functional carbon materials: synthesis, structure, and acid catalysis. *Chem. Rev.* **119**, 11576–11630 (2019).
39. Gościńska, J. & Malaika, A. A facile post-synthetic modification of ordered mesoporous carbon to get efficient catalysts for the formation of acetins. *Catal. Today* **357**, 84–93 (2020).
40. Hopkins, H. P., Wu, C.-H. & Hepler, L. G. Thermochemistry of aqueous aminosulfonic acids. Sulfamic and sulfanilic acids and taurine. *J. Phys. Chem.* **69**, 2244–2248 (1965).
41. Rechnia, P., Malaika, A. & Kozłowski, M. Synthesis of tert-amyl methyl ether (TAME) over modified activated carbon catalysts. *Fuel* **154**, 338–345 (2015).
42. Corrêa, A., Bastos, R., Filho, G., Zamian, J. & Conceição, L. Preparation of sulfonated carbon-based catalysts from murumuru kernel shell and their performance in the esterification reaction. *RSC Adv.* **10**, 20245–20256 (2020).
43. Mo, X. *et al.* Activation and deactivation characteristics of sulfonated carbon catalysts. *J. Catal.* **254**, 332–338 (2008).
44. Gaidukevič, J. *et al.* Modified graphene-based materials as effective catalysts for transesterification of rapeseed oil to biodiesel fuel. *Chin. J. Catal.* **39**, 1633–1645 (2018).
45. Gaidukevič, J., Barkauskas, J., Malaika, A., Jasulaitien, V. & Kozłowski, M. Preparation and characterization of basic graphene-based catalysts and their application in biodiesel synthesis. *Appl. Surf. Sci.* **554**, 149588 (2021).
46. Kamali, A. R., Schwandt, C. & Fray, D. J. Effect of the graphite electrode material on the characteristics of molten salt electrolytically produced carbon nanomaterials. *Mater. Charact.* **62**, 987–994 (2011).

47. Todica, M., Stefan, T., Simon, S., Balasz, I. & Daraban, L. UV-Vis and XRD investigation of graphite-doped poly(acrylic) acid membranes. *Turk. J. Phys.* **38**, 261–267 (2014).
48. Ain, Q. T., Haq, S. H., Alshammari, A., Al-Mutlaq, M. A. & Anjum, M. N. The systemic effect of PEG-nGO-induced oxidative stress in vivo in a rodent model. *Beilstein J. Nanotechnol.* **10**, 901–911 (2019).
49. Li, J. *et al.* Preparation of micron sized graphite using a spark plasma technique. *RSC Adv.* **6**, 50776–50779 (2016).
50. Popova, A. N. Crystallographic analysis of graphite by X-ray diffraction. *Coke Chem.* **60**, 361–365 (2017).
51. Yung, T.-Y. *et al.* Synthesis and characterizations of Ni-NiO nanoparticles on PDDA-modified graphene for oxygen reduction reaction. *Nanoscale Res. Lett.* **9**, 444 (2014).
52. Youssry, M., Kamand, F. Z., Magzoub, M. I. & Nasser, M. S. Aqueous dispersions of carbon black and its hybrid with carbon nanofibers. *RSC Adv.* **8**, 32119–32131 (2018).
53. Nazib, A. *et al.* Study on dispersion and characterization of functionalized MWCNTs prepared by wet oxidation. *Appl. Mech. Mater.* **661**, 8–13 (2014).
54. Li, J. & Zhang, Y. A simple purification for single-walled carbon nanotubes. *Phys. E.* **28**, 309–312 (2005).
55. Hu, H., Zhao, B., Itkis, M. E. & Haddon, R. C. Nitric acid purification of single-walled carbon nanotubes. *J. Phys. Chem. B.* **107**, 13838–13842 (2003).
56. Ghaemi, F. *et al.* Comparative study of the electrochemical, biomedical, and thermal properties of natural and synthetic nanomaterials. *Nanoscale Res. Lett.* **13**, 112 (2018).
57. Yaya, A. *et al.* Purification of single-walled carbon nanotubes. *EPJ Appl. Phys.* **54**, 10401–10408 (2011).
58. Li, L. *et al.* Thermal stability of oxygen-containing functional groups on activated carbon surfaces in a thermal oxidative environment. *J. Chem. Eng. Jpn.* **47**, 21–27 (2014).
59. Rechnia-Goraćy, P., Malaika, A. & Kozłowski, M. Acidic activated carbons as catalysts of biodiesel formation. *Diam. Relat. Mater.* **87**, 124–133 (2018).
60. Guo, Y., Shi, Z., Chen, M. & Wang, C. Hierarchical porous carbon derived from sulfonated pitch for electrical double layer capacitors. *J. Power Sources* **252**, 235–243 (2014).
61. Malaika, A., Heinrich, M., Gościńska, J. & Kozłowski, M. Synergistic effect of functional groups in carbonaceous spheres on the formation of fuel enhancers from glycerol. *Fuel* **280**, 118523 (2020).

Acknowledgements

This work was financially supported by Grant No 017/02/SNŚ/0013 from AMU (ID-UB Project: Excellence Initiative—Research University).

Author contributions

K.P.—Investigation; Validation; Formal analysis; Writing; A.M.—Methodology; Investigation; Validation, Writing; M.Ka. Investigation; Formal analysis; M.K.—Supervision. All authors have read and agreed to the published version of the manuscript.

Competing interests

The authors declare no competing interests.

Additional information

Supplementary Information The online version contains supplementary material available at <https://doi.org/10.1038/s41598-023-27432-7>.

Correspondence and requests for materials should be addressed to A.M.

Reprints and permissions information is available at www.nature.com/reprints.

Publisher's note Springer Nature remains neutral with regard to jurisdictional claims in published maps and institutional affiliations.



Open Access This article is licensed under a Creative Commons Attribution 4.0 International License, which permits use, sharing, adaptation, distribution and reproduction in any medium or format, as long as you give appropriate credit to the original author(s) and the source, provide a link to the Creative Commons licence, and indicate if changes were made. The images or other third party material in this article are included in the article's Creative Commons licence, unless indicated otherwise in a credit line to the material. If material is not included in the article's Creative Commons licence and your intended use is not permitted by statutory regulation or exceeds the permitted use, you will need to obtain permission directly from the copyright holder. To view a copy of this licence, visit <http://creativecommons.org/licenses/by/4.0/>.

© The Author(s) 2023

SUPPLEMENTARY MATERIALS

SO₃H-functionalized carbon fibers for the catalytic transformation of glycerol to glycerol tert-butyl ethers

Karolina Ptaszyńska, Anna Malaika*, Magdalena Kapska, Mieczysław Kozłowski

Faculty of Chemistry, Adam Mickiewicz University

Uniwersytetu Poznańskiego 8, 61-614 Poznań, Poland

Fig. 1SM shows the high-resolution TEM images of different magnifications obtained for CFs produced from isobutane and ethylene.

The presented pictures revealed the partial graphitic structure of CF_{i-bu} and CF_{et}, as the ordered orientation of the graphene sheets was visible for part of the produced fibers. In the case of CFs obtained from ethylene, the graphene sheets were arranged parallel to each other and perpendicular to the fiber axis, forming platelet carbon fibers (Fig. 2 E). CFs produced from isobutane also resembled platelet-like structures, however, a slightly lower degree of order than that observed for CF_{et} was noticed, as randomly oriented graphene sheets were also found in the HR-TEM images of CF_{i-bu} (Fig. 1SM B).

*Corresponding author; e-mail: amalaika@amu.edu.pl; phone: +48 61 829 1800; fax: +48 61 829 1555

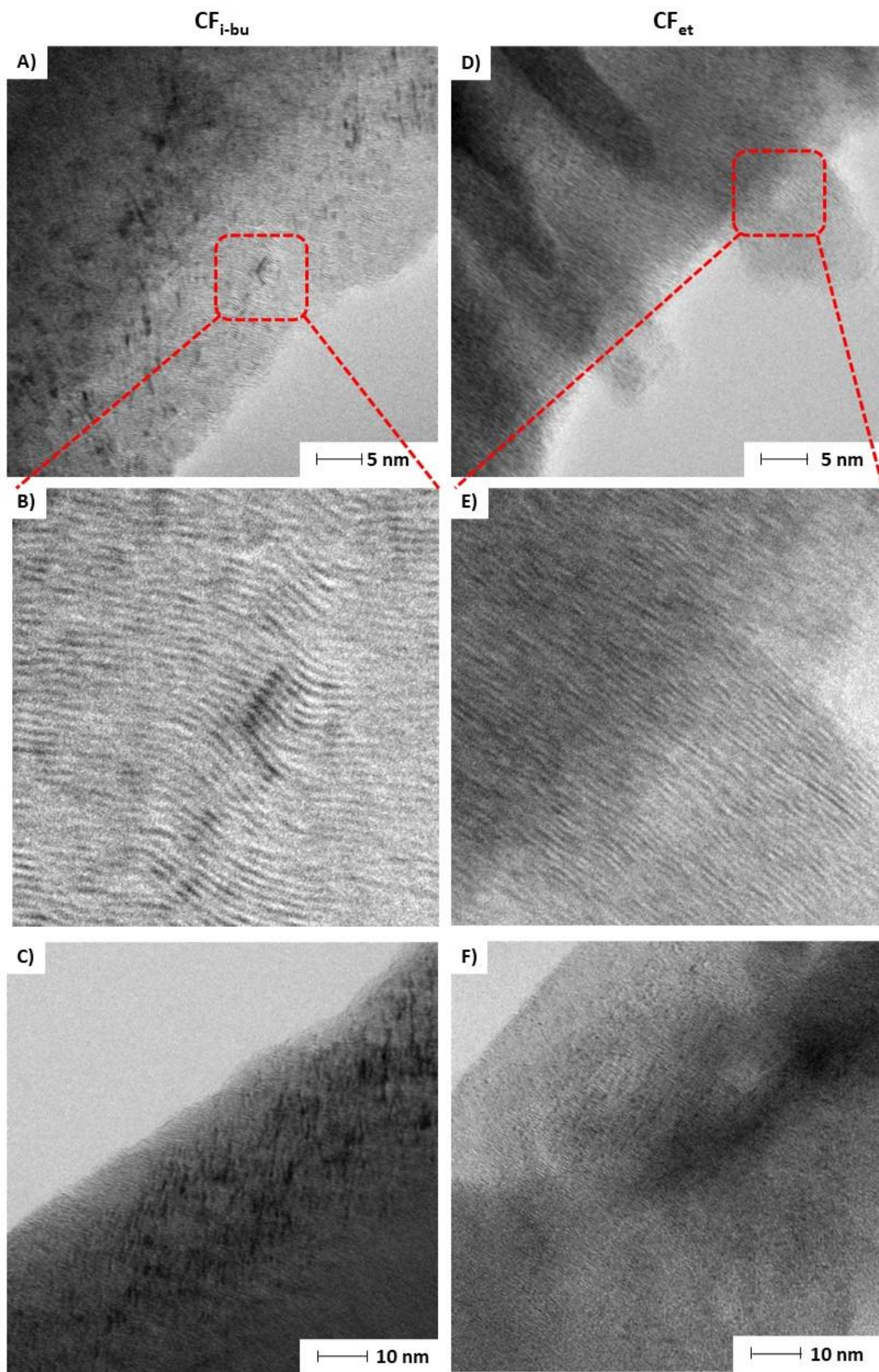


Fig. 1. HR-TEM images of the carbon fibers produced from isobutane (A-C) and ethylene (D-F)

P3

Article

A Green Approach to Obtaining Glycerol Carbonate by Urea Glycerolysis Using Carbon-Supported Metal Oxide Catalysts

Karolina Ptaszyńska *, Anna Malaika, Klaudia Kozigrodzka and Mieczysław Kozłowski *

Faculty of Chemistry, Adam Mickiewicz University in Poznań, Uniwersytetu Poznańskiego 8, 61-614 Poznań, Poland; amalaika@amu.edu.pl (A.M.); klakoz3@st.amu.edu.pl (K.K.)

* Correspondence: karolina.ptaszynska@amu.edu.pl (K.P.); mkozlow@amu.edu.pl (M.K.)

Abstract: The results of sustainable and selective synthesis of glycerol carbonate (GC) from urea and glycerol under ambient pressure using carbon-fiber-supported metal oxide catalysts are reported. Carbon fibers (CF) were prepared via a catalytic chemical vapor deposition method (CCVD) using Ni as a catalyst and liquefied petroleum gas (LPG) as a cheap carbon source. Supported metal oxide catalysts were obtained by an incipient wetness impregnation technique using Zn, Ba, Cr, and Mg nitrates. Finally, the samples were pyrolyzed and oxidized in an air flow. The obtained catalysts (10%Me_xO_y/CF_{ox}) were tested in the reaction of urea glycerolysis at 140 °C for 6 h under atmospheric pressure, using an equimolar ratio of reagents and an inert gas flow for NH₃ removal. Under the applied conditions, all of the prepared catalysts increased the glycerol conversion and glycerol carbonate yield compared to the blank test, and the best catalytic performance was shown by the CF_{ox}-supported ZnO and MgO systems. Screening of the reaction conditions was carried out by applying ZnO/CF_{ox} as a catalyst and considering the effect of reaction temperature, molar ratio of reagents, and the mode of the inert gas flow through the reactor on the catalytic process. Finally, a maximum yield of GC of about 40%, together with a selectivity to glycerol carbonate of ~100%, was obtained within 6 h of reaction at 140 °C using a glycerol-to-urea molar ratio of 1:1 while flowing Ar through the reaction mixture. Furthermore, a positive heterogeneous catalytic effect of the CF_{ox} support on the process was noticed.

Keywords: glycerol valorization; carbon support; carbon fibers; glycerolysis; glycerol carbonate



Citation: Ptaszyńska, K.; Malaika, A.; Kozigrodzka, K.; Kozłowski, M. A Green Approach to Obtaining Glycerol Carbonate by Urea Glycerolysis Using Carbon-Supported Metal Oxide Catalysts. *Molecules* **2023**, *28*, 6534. <https://doi.org/10.3390/molecules28186534>

Academic Editors: Małgorzata Wiśniewska and Piotr Nowicki

Received: 31 July 2023

Revised: 4 September 2023

Accepted: 6 September 2023

Published: 9 September 2023



Copyright: © 2023 by the authors. Licensee MDPI, Basel, Switzerland. This article is an open access article distributed under the terms and conditions of the Creative Commons Attribution (CC BY) license (<https://creativecommons.org/licenses/by/4.0/>).

1. Introduction

In recent years, using biomass feedstocks instead of non-renewable petrochemical resources to sustainably produce commodities and chemicals has been gaining significant importance. Glycerol (Gly), obtained in vast amounts as a by-product in biomass-based biodiesel technology, can be used as a green, renewable, readily available, and versatile feedstock for obtaining higher-value-added chemical products such as glycerol carbonate (GC), among others [1]. Glycerol carbonate (4-hydroxymethyl-1,3-dioxolan-2-one) has a wide range of industrial applications, including the production of high-performance hyperbranched polymers, coatings, adhesives, and lubricants. It is also used as a solvent, detergent, and curing agent for cement and concrete, in the lithium-ion battery industry, or in gas separation units [1–3]. Among possible GC synthesis routes, urea glycerolysis (Figure 1) is considered an economically attractive and environmentally benign approach [4], and can be an alternative to the conventional method of GC production using toxic phosgene [5]. According to literature reports, several reaction pathways of urea glycerolysis are possible, and the process requires acidic or basic Lewis active sites, or the presence of a bifunctional catalyst [4–7].

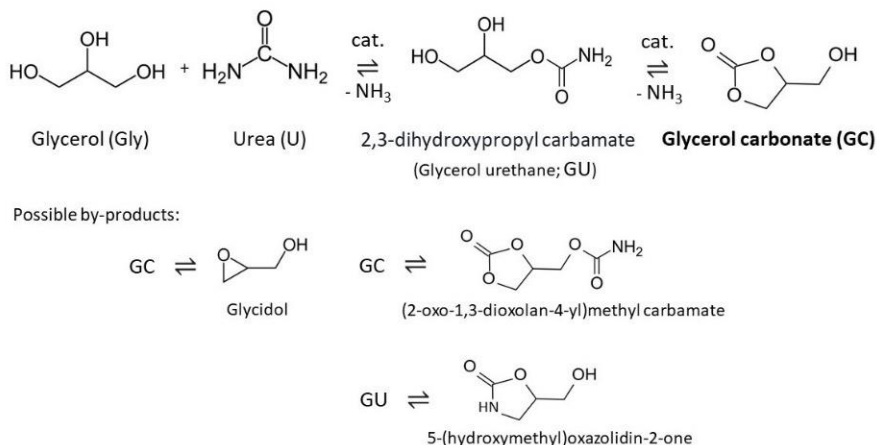


Figure 1. Synthesis of glycerol carbonate (GC) from glycerol and urea (based on [8,9]).

Urea glycerolysis can be effectively homogeneously catalyzed by various metal-based compounds. For example, Wang et al. [10] found that LaCl_3 could give a 95.4% conversion of Gly with almost 100% selectivity to glycerol carbonate under optimized reaction conditions, i.e., 3 h, 150 °C, and 5 kPa. Park et al. [11] reported that homogeneous ZnCl_2 yielded 80.2% of GC with 99.7% selectivity to this product when the reaction was conducted at 150 °C for 2 h under reduced pressure. In turn, Turney et al. [12] showed that polymeric monoglycerolate complexes of zinc and cobalt could give such a high glycerol conversion as 98% and a GC yield of 83% at 140 °C within 7 h.

Despite the promising results typically obtained in urea glycerolysis with homogeneous catalysts, these processes usually show serious drawbacks such as separation difficulties and catalyst unrecoverability [13]. Thus, a more practical and economical option for producing GC via urea glycerolysis is to use heterogeneous metal-based catalysts in this reaction. For example, Wang et al. [7] tested different forms of lanthanum oxide as solid catalysts for glycerolysis of urea performed at 140 °C, obtaining a very high GC yield and selectivity to glycerol carbonate of ~90 and 97%, respectively, for the best-working sample (La_2O_3 -600). The enhanced catalytic performance of the La_2O_3 -600 was attributed to the increased strength of Lewis basic sites, and the catalyst was reused without significant loss in its activity during recycling tests. Aresta et al. [13] obtained 80% glycerol conversion and 100% selectivity towards glycerol carbonate using γ -Zr phosphate. Furthermore, the authors found this catalyst to be easily recoverable and reusable in subsequent reaction cycles. An efficient reusable catalyst for urea glycerolysis was also $\text{Sn}(\text{OH})_2$, which showed 87% conversion of glycerol and 85% selectivity to GC in the reaction that lasted 4 h [14]. Interesting results were also presented by Fernandes et al. [15] who tested MgO as a catalyst for GC production under atmospheric pressure. The authors found that the sample exhibited excellent catalytic behavior, giving glycerol conversions of up to 70% with a 100% selectivity to GC within 6 h. Solid zinc-based catalysts have also been widely investigated [16,17]. For example, Zn-based mixed oxides (ZnMeO ; Me = Co, Cr, and Fe) were used in urea glycerolysis performed at 140 °C under vacuum pressure. The Zn-rich mixed oxides showed better performance in the process than the Zn-poor ones, presenting 74–76% conversion of Gly and about 70–74% selectivity to GC within 3 h. However, the process occurred mainly homogeneously, which is a common problem of Zn-type catalysts [18]. On the other hand, information about the full recoverability of ZnO in properly prepared systems, e.g., with the addition of CuO, has also been reported [17].

In recent years, carbon materials such as carbon nanotubes and fibers (CNT and CNF, respectively), graphene, carbon dots (CD), hydrothermal carbons (HTC), and activated carbons (AC) have gained increasing attention in the field of catalysis. It has been found

that adequately tailored carbons can be used as efficient heterogeneous catalysts for various catalytic processes, including the sustainable transformation of biomass or (bio)glycerol to value-added chemicals [19–21]. Carbons can also be applied as attractive supports for enzymes, metals, or metal oxide catalysts [22–24]. This is due to their key advantages, which include high surface area, resistance to acidic or basic media, tunable physicochemical structure, and different options for active phase immobilization [25]. Importantly, the role of carbons as supports in heterogeneous reactions is not only limited to the deposition and dispersion of the active phase on a solid sample. Carbon supports can also increase the catalyst efficiency by means of active phase–support interactions, reagent adsorption, or the presence of defects [26,27].

Various supports for the active phase have been tested in urea glycerolysis. Kondawar et al. [28] deposited Zn oxide on MCM-41, SBA-15, ZrO₂, SiO₂, Al₂O₃, and sulfated ZrO₂ (s-ZrO₂) using a wet impregnation method. It was found that the nature of support influenced the surface area, crystallinity, and acid/base properties of the respective catalysts. The samples varied significantly in their catalytic performances. 5%Zn/SiO₂ was the least active, giving only a 20% conversion of glycerol. Using s-ZrO₂ as support instead of ZrO₂ led to a significant improvement in selectivity to GC while maintaining the conversion of Gly (~50%). Finally, the best catalytic results (X_{Gly} = 78%, S_{GC} = 98%) were shown by 5%Zn/MCM-41 presenting weak acidity; however, offering maximum dispersion of ZnO due to the high MCM-41 apparent surface area. Furthermore, the possible role of the -OH groups of the MCM-41 support was also stressed. In turn, Hammond et al. [29] evaluated the activity of gold supported on TiO₂, commercial carbon, Nb₂O₅, ZnO, and MgO in urea glycerolysis. A significantly increased conversion of Gly and selectivity to GC (80% and ~70%, respectively, after 4 h) compared to the blank were obtained using MgO as support. The other supported Au catalysts exhibited moderate activity in the reaction and a rather low selectivity to GC.

Although several studies on urea glycerolysis have been performed to date, most of the reported catalysts were used under reduced pressure. In the current work, carbon fibers prepared by a facile CCVD method using a cheap carbon precursor, i.e., liquefied petroleum gas (LPG), were applied as support for different metal oxides (ZnO, BaO, Cr₂O₃, and MgO). These samples were tested in a solvent-free reaction of urea with glycerol under ambient pressure for the first time. Effects of the reaction parameters such as temperature, glycerol to urea molar ratio, and Ar flowing mode were also investigated.

2. Discussion of the Results

2.1. Characterization of the Samples

Figure 2 shows SEM micrographs of the initial CF, CF_{ini_ox}, and a selected CF_{ox}-supported metal oxide catalyst. As can be seen in Figure 2A, the applied CCVD method of carbon production gave a sample formed by entangled fibers organized into agglomerates of various shapes and sizes; however, single filaments could also be observed. Details of the morphology of CF are shown in Figure 2B. According to the presented image, the fibers formed agglomerates differing in their morphological features. A part of the produced structures presented low-diameter fibers that were curled and twisted, and resembled sheep's wool. The other structures showed diameters that were several times higher and rather smooth surfaces. The visible cross-sections of the fibers suggested that they were solid inside. All the formed structures were densely packed, and no significant numbers of holes or channels could be observed between the individual filaments. The morphological features of CF_{ini_ox} were quite similar to those of CF, as can be observed by comparing Figure 2A,B with Figure 2C,D.

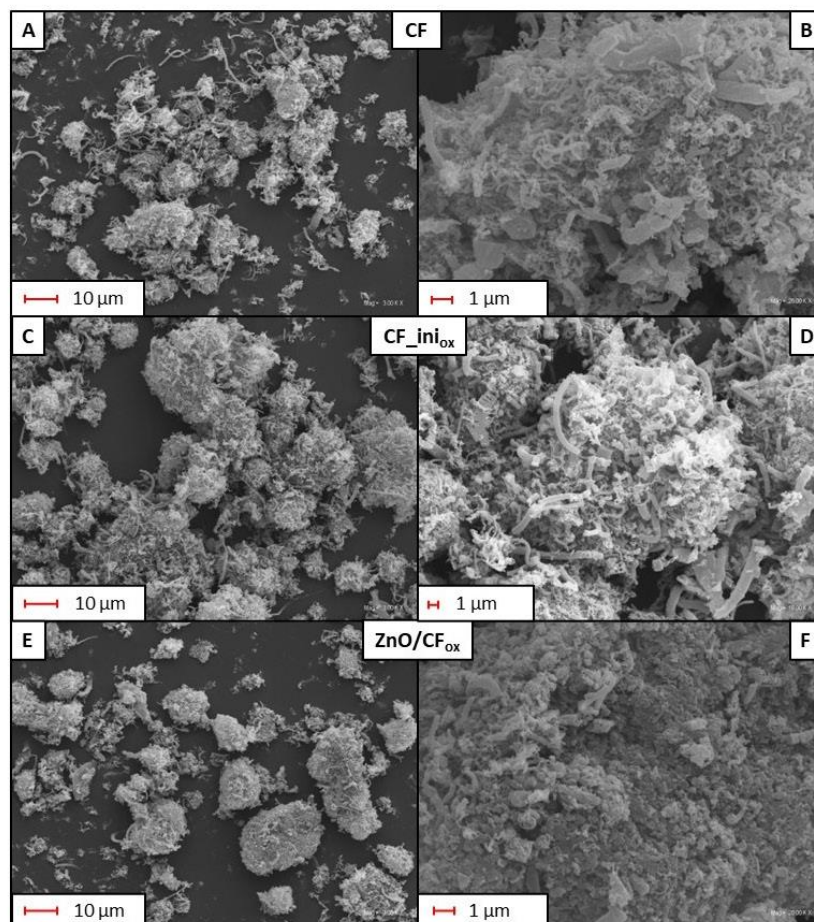


Figure 2. SEM micrographs obtained for the CF (A,B), CF_{ini_ox} (C,D), and a selected CF_{ox}-supported catalyst (E,F) at different magnifications.

The morphology of the CF_{ox}-supported metal oxide catalysts was significantly different from that of the CF-type samples discussed above. As presented for an exemplary material (ZnO/CF_{ox}) in Figure 2E, the original carbon agglomerates were smoother, and the carbon fibers were barely visible, as the crust (most likely formed by deposited zinc oxide) covering the fibers was produced (see Figure 2F). Similar observations were also made by Arsalani et al. [30], who deposited ZnO on the surface of carbon nanotubes.

Table 1 presents the results of the textural analysis of the obtained products, i.e., CF-type samples and CF_{ox}-supported metal oxides. It can be seen that the produced CF possessed a quite significant apparent surface area of 259 m²/g. This resulted mainly from the presence of the external surface area, i.e., the area of meso- and macropores, which was almost 187 m²/g. Interestingly, the total volume of pores (V_{tot}) was also significant and was mostly related to the presence of spaces of meso- and macropore sizes between the agglomerates (see also Figure 2A,C), as V_{micro} was negligible. This is also in agreement with the observations from the SEM analysis (see the discussion on Figure 2), suggesting the tightly packed structure of the agglomerates. The textural parameters of CF_{ini_ox} were only slightly different from those of CF. The only exception was the V_{tot} value of CF_{ini_ox}, which was reduced compared to that of CF, suggesting the efficient introduction of oxygen groups

into the CF matrix during the oxidation process (see Section 3: Materials and Methods) and their location at the entrances of the existing pores [31].

Table 1. Textural parameters of the prepared CF, CF_{ini_ox}, and CF_{ox}-supported samples.

Sample	S _{BET} [m ² /g]	S _{ext} [m ² /g]	V _{tot} [cm ³ /g]	V _{micro} [cm ³ /g]
CF	259	187	1.22	0.04
CF _{ini_ox}	267	193	0.97	0.04
Cr ₂ O ₃ /CF _{ox}	236	159	0.70	0.04
BaO/CF _{ox}	214	214	1.02	0.00
MgO/CF _{ox}	213	163	0.86	0.03
ZnO/CF _{ox}	238	170	0.79	0.04

In general, the Me_xO_y/CF_{ox} systems showed slightly decreased textural parameters, i.e., S_{BET}, S_{ext}, and V_{tot}, compared to CF_{ini_ox}, which confirmed the efficient loading of the respective metal oxides into the support matrix—either on its surface or in their pores [32]. This is also in accordance with the results of the SEM measurements. The mesoporous structure of the pristine CF_{ini_ox} was maintained after the deposition of metal oxides, which was suggested by a high contribution of S_{ext} to S_{BET} being achieved for the Me_xO_y/CF_{ox} systems, and also by the shape of the N₂ adsorption–desorption isotherms obtained for the CF_{ini_ox} and an exemplary CF_{ox}-supported sample presented in Figure 3 (IVa type acc. IUPAC classification [33]), which is typical for materials containing mesopores.

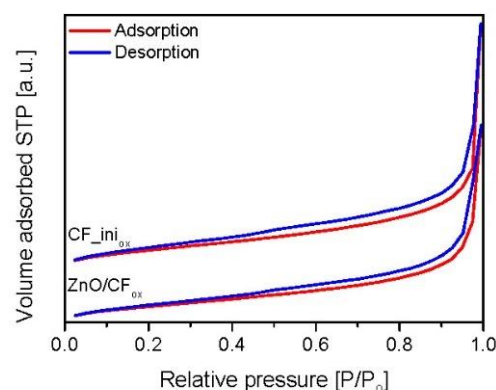


Figure 3. N₂ adsorption–desorption isotherms obtained for the CF_{ini_ox} and ZnO/CF_{ox} samples.

The XRD diffraction patterns of the prepared samples are presented in Figure 4. The diffractograms obtained for CF and CF_{ini_ox} showed an intense peak at 2-theta of 26° and a small one at 44°. These signals are typical for graphite-like carbons and can be assigned to the C(002) and C(100) reflections of the hexagonal structure of graphite and the atomic structure of the graphene sheets, respectively [34–36]. No other peaks were observed in the CF and CF_{ini_ox} diffraction patterns, suggesting thorough purification of the samples from the catalyst after the CCVD process (see Section 3: Materials and Methods). The XRD diffractograms of Me_xO_y/CF_{ox} samples showed additional signals besides those at 26° and 44° obtained for CF-type materials, indicating the efficient loading of the respective oxides [37–40] to the carbon matrix and suggesting their crystalline forms.

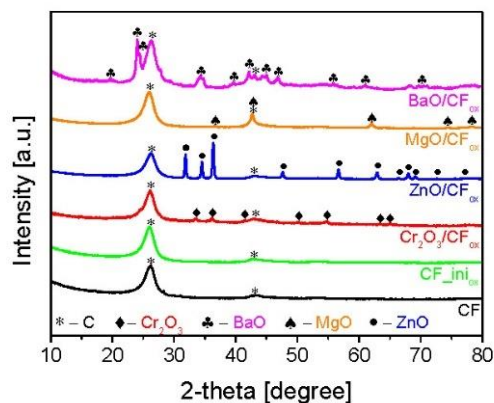


Figure 4. XRD patterns of CF, CF_{ini,ox}, and CF_{ox}-supported metal oxide samples.

Figure 5 presents the results of the TG analysis obtained for selected samples. As can be seen in Figure 5A, no significant changes in the mass of the initial CF support were observed up to about 500 °C. Rapid weight loss started at 530 °C, and the sample was completely oxidized at ~740 °C. The residue after combustion was 0%, indicating high sample purity (i.e., efficient removal of Ni catalyst after the preparation process, see Section 3: Materials and Methods) and is also in line with the results of XRD analysis (Figure 4). The DTG pattern of the initial CF (Figure 5B) resembles profiles obtained for fibrous carbons produced using the CCVD method [41]. The presence of two poorly separated peaks with minima at ~620 °C and ~740 °C indicates the existence of phases with various thermal stability, resulting from differences in the sample crystallinity, number of defects, or fiber diameters [41,42], as also suggested by the SEM results (Figure 2).

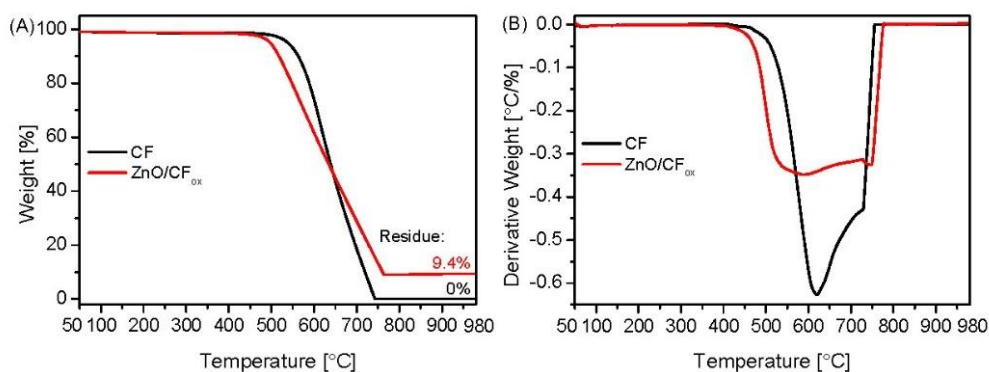


Figure 5. The results of (A) TG and (B) DTG analysis performed for selected samples (air flow).

The TG profile of an exemplary metal-oxide-type sample, i.e., ZnO/CF_{ox}, depicted in Figure 5A, suggested a slightly lower stability of the supported catalyst compared to the initial CF, as the weight loss of the ZnO/CF_{ox} started at ~480 °C. This shift in the onset temperature was probably related to the release of some oxygen groups present on the surface of the CF_{ox} support [43], introduced during the sample oxidation step (see Section 3: Materials and Methods). Interestingly, at a temperature of 760 °C, the carbon material was totally oxidized, and the residue after combustion was 9.4%. This residue was due to the presence of zinc oxide in the sample, and the obtained value was close to the assumed one (10 wt.%, see Section 3: Materials and Methods). The DTG pattern of ZnO/CF_{ox} in Figure 5B resembles that of CF, and the changes in the profile shape could be attributed to

the formation of ZnO coating the support [44]. This also agrees well with the results of the SEM analysis presented in Figure 2F.

The X-ray photoelectron spectroscopy (XPS) technique was used to study the surface chemistry of the ZnO/CF_{ox} sample. The achieved results are collected in Table 2 and Figure 6. The obtained data confirmed the presence of C, O, and Zn in the material. The content of elemental carbon (Table 2) was dominant, which was not surprising considering the assumed role and the amount of carbon fibers in the system. The presence of oxygen and zinc confirmed the successful loading of ZnO to the carbon matrix. The presence of oxygen could also result from the oxidation of the support during the preparation stage (see Section 3: Materials and Methods). Interestingly, the estimated zinc oxide content was 9.3%, which is also in line with the value determined by the TG analysis (see Figure 5A).

Table 2. The contents of elements measured for the ZnO/CF_{ox} sample by the XPS technique.

Sample	C [wt.%]	O [wt.%]	Zn [wt.%]	ZnO in ZnO/CF _{ox} * [wt.%]
ZnO/CF _{ox}	87.1	5.4	7.5	9.3

* ZnO content calculated based on the amount of zinc from XPS.

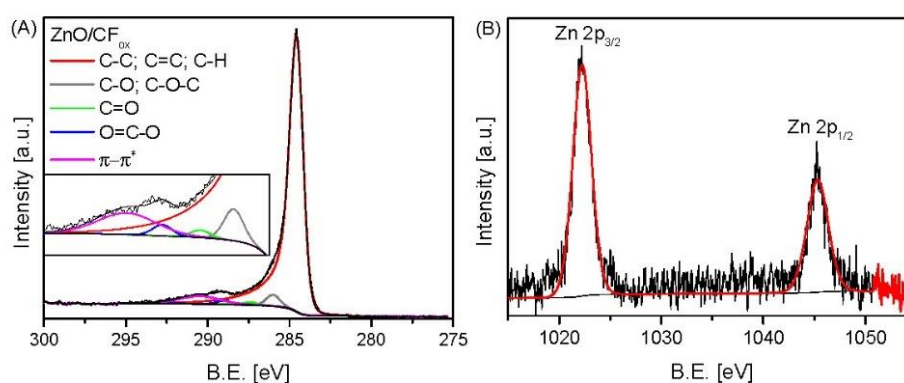


Figure 6. The high-resolution XPS C 1s (A) and Zn 2p (B) spectra of the ZnO/CF_{ox} sample.

Figure 6A shows the high-resolution C 1s and Zn 2p XPS spectra obtained for the ZnO/CF_{ox} sample. As can be observed, five different carbon species were found in the C 1s spectrum—at a B.E. of ~284.5 eV (assigned to sp³/sp² carbon), 286.0 eV (assigned to C-O/C-O-C groups), 287.4 eV (ascribed to C=O in carbonyls), 288.7 eV (ascribed to O=C=O in carboxyls), and 290.0 eV (assigned to π-π* transitions) [21]. The obtained data indicate that the CF support was successfully oxidized during the catalyst preparation stage (see Section 3: Materials and Methods). On the other hand, the Zn 2p XPS spectrum shown in Figure 6B presents the characteristic doublet peaks of Zn 2p, corresponding to the Zn²⁺ oxidation state at 1022.2 eV for Zn 2p_{2/3} and at 1045.3 eV for Zn 2p_{1/2} [45,46].

2.2. Catalytic Results

The catalytic activities of the prepared CF_{ox}-supported samples were measured in the reaction of glycerol with urea performed under ambient pressure. For the sake of comparison, reactions without a catalyst (blank test) and in the presence of a homogeneous catalyst (ZnSO₄) were also performed.

To determine the influence of the support on urea glycerolysis, the CF_{ini_ox} sample was tested in the process as a catalyst on its own. Figure 7 shows the results obtained after 1 and 6 h of reaction performed over CF_{ini_ox} in comparison to the data achieved in the blank. As can be seen, under the conditions used, the reaction occurred without a catalyst; however, the glycerol conversion measured after 1 h for the blank test was quite

low, i.e., about 13%. Interestingly, X_{Gly} determined for the reaction over $\text{CF_ini}_{\text{ox}}$ was twice as small as for the blank (6.7% after 1 h). Importantly, the conversion of glycerol increased over time in both cases, reaching a higher value, i.e., of about 33% after 6 h, for the reaction applying $\text{CF_ini}_{\text{ox}}$. Finally, the glycerol carbonate yield (Y_{GC}) obtained in the process over $\text{CF_ini}_{\text{ox}}$ was about 30%, which was almost 10% higher than the value achieved for the blank. Interestingly, the use of $\text{CF_ini}_{\text{ox}}$ as a catalyst resulted in significant changes in the distribution of products, i.e., the selectivity to glycerol carbonate increased to about 97% after 1 h when using $\text{CF_ini}_{\text{ox}}$, and only traces of glycerol urethane (GU; the process intermediate) were detected in the reaction. On the other hand, in the case of the blank test, S_{GC} was equal to only ~66%. Instead, a fairly high selectivity to GU, of about 31%, was achieved in the first hour of the process. Some amounts of by-products, i.e., 5-(hydroxymethyl)oxazolidin-2-one and (2-oxo-1,3-dioxolan-4-yl)methyl carbamate, were also detected ($S_{\text{B-P}}$ of about 3%). S_{GU} achieved for the blank decreased significantly over time, and finally, at 6 h, this parameter was about 15%. At the same time, the selectivities to glycerol carbonate (S_{GC}) and by-products increased, albeit to a different extent. Finally, S_{GC} achieved at the 6th hour of the blank was only slightly higher than that obtained after the first hour of the reaction, and apparently, glycerol carbonate was mainly transformed into the by-products. In turn, in the presence of C_ini_{ox} , the process seems to be much more focused on the production of glycerol carbonate, as the selectivity to by-products was reduced compared to the blank.

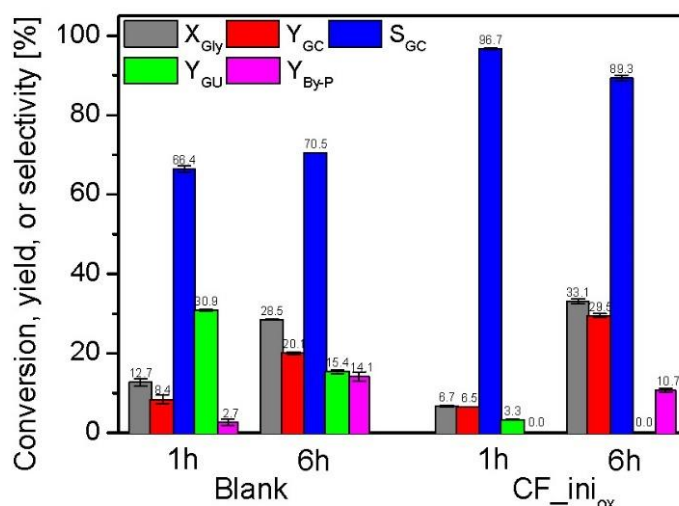


Figure 7. The results of urea glycerolysis performed without a catalyst (blank test) and in the presence of the $\text{CF_ini}_{\text{ox}}$ sample; temp. = 140 °C, Gly:U molar ratio = 1:1, Ar flowing through the reactor.

The differences between the results obtained for the blank and the $\text{CF_ini}_{\text{ox}}$ catalyst (Figure 7) most probably result from the differences in the mechanism of urea glycerolysis under non-catalytic and catalytic conditions. According to literature data [9], the crucial step of urea glycerolysis is urea splitting, which becomes the driving force for the blank process. On the other hand, the reaction performed in the presence of $\text{CF_ini}_{\text{ox}}$ most likely occurs through a different mechanism (which is much more complex than that of homogeneous/blank reaction) and it involves various stages, i.e., diffusion of the reactants to the catalyst surface, adsorption of reagents on the catalyst active sites, chemical reaction, and desorption and diffusion of the reaction products. Moreover, in this case, the catalytic process most probably occurs due to the abundance of different oxygen groups that are present on the surface of the $\text{CF_ini}_{\text{ox}}$ sample (see also Figure 6). It cannot be excluded that some of these groups combine with the reagents, forming quite stable bonds, and thus work as inhibition sites of the process (as the catalytic reaction is only possible when the

formation of unstable intermediates between the solid catalyst and the reagents takes place). As long as these types of groups are present on the catalyst surface, the catalytic reaction is inhibited, and the so-called induction period can be obtained. This might be a reason for the lower glycerol conversion observed for CF_ini_ox compared to the blank. Only after the “inhibition” sites have been consumed, and thus after the induction time, can other oxygen centers work unhindered, forming unstable intermediates with the reagents; therefore, the catalytic effect can become clearly visible after a longer time.

The catalytic performances of the prepared CF_ox-supported metal oxide catalysts in comparison to the blank and CF_ini_ox are shown in Figure 8. As can be seen in Figure 8A, the glycerol conversion obtained for most of the prepared catalysts after 1 h was in the range of 14–16%, which was only slightly higher than X_{Gly} achieved for the blank. The only exception was the Cr₂O₃/CF_ox sample, for which X_{Gly} measured after 1 h of reaction was only ~7%. The conversion of glycerol increased significantly over time for all of the samples, and finally, for the best-working catalyst, i.e., ZnO/CF_ox, it was 40% after 6 h. Nevertheless, the MgO/CF_ox catalyst also worked effectively, which was particularly noticeable at the beginning of the process. Considering the yield of glycerol carbonate presented in Figure 8B, it can be seen that using the CF_ox-supported systems (except for Cr₂O₃/CF_ox) resulted in a quite significant increase in Y_{GC} compared to the blank, and for the most active samples, i.e., ZnO/CF_ox and MgO/CF_ox, the yield of glycerol carbonate reached ~34% after 6 h of reaction. The material containing chromium oxide worked the worst in the reaction, presenting similar results to those obtained in the case of CF_ini_ox (other catalysts worked better than CF_ini_ox). This suggests that the activity of the Cr₂O₃/CF_ox material resulted only from the presence of the carbon support and that the Cr₂O₃ phase was practically not active in the reaction. However, this conclusion assumes that CF_ini_ox possesses the same properties as the CF_ox support in the Cr₂O₃/CF_ox system. In fact, the CF_ini_ox is a kind of model sample; therefore, the chemical nature of these two (the oxidation of CF with supported metals most probably occurs differently than the oxidation of the pure support, see also Section 3: Materials and Methods) and their catalytic effect in the reaction may be slightly different.

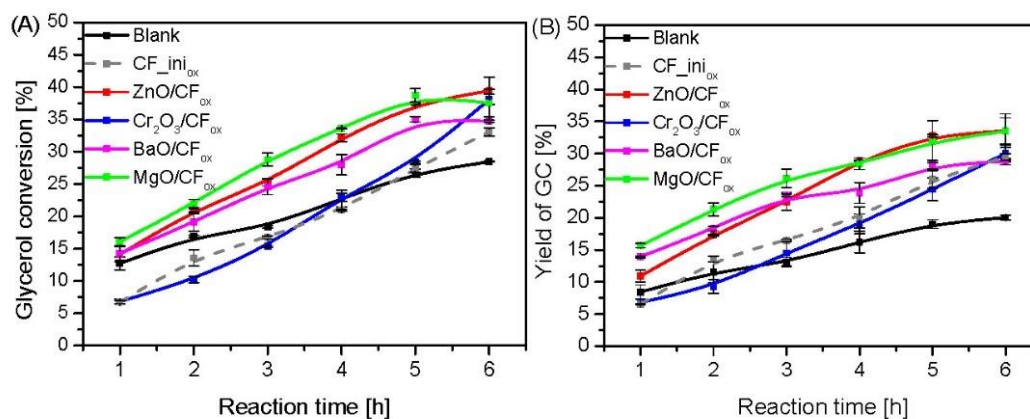


Figure 8. Catalytic performances of the prepared Me_xO_y/CF_{ox} systems in the process of urea glycerolysis versus time, expressed as glycerol conversion (A) and yield of GC (B), in comparison to the blank and the performance of the CF_ini_ox; temp. = 140 °C, Gly:U molar ratio = 1:1, Ar flowing through the reactor.

Interestingly, the distribution of individual reaction products differed significantly between the blank and the samples tested, as presented in Figure S1 in the Supplementary Materials. In the case of the blank test, the selectivity to GC through the whole process was significantly lower compared to those obtained using Me_xO_y/CF_{ox} catalysts. On the other hand, under these conditions, the selectivity to GU was the highest. With the

increasing conversion of glycerol over time (see also blank in Figure 8A), the selectivity to GU decreased. At the same time, the selectivity to glycerol carbonate was practically stable, and the by-products were formed. The use of $\text{Me}_x\text{O}_y/\text{CF}_{\text{ox}}$ catalysts changed the distribution of products significantly. When using $\text{ZnO}/\text{CF}_{\text{ox}}$, a fairly high selectivity to GU (an intermediate product) was observed in the initial hours of the process. GU was then gradually converted to glycerol carbonate, as well as some by-products. In the case of the other samples, the S_{GC} was initially very high. However, this parameter decreased slightly over time, as GC was probably further converted to by-products.

Importantly, when considering the catalytic performances of the $\text{Me}_x\text{O}_y/\text{CF}_{\text{ox}}$ systems, some differences in the samples' activities can be observed. According to literature reports, the process of urea glycerolysis requires the presence of both acidic and basic active sites. Furthermore, ensuring the appropriate ratio of acidic to basic centers is crucial for this reaction [16,47,48]. For example, Kondawar et al. [32] tested different supported Zn catalysts in urea glycerolysis and ascribed the promising performance of the most active sample to the appropriate balance of both acidic and basic sites in the catalytic system used. At the same time, the authors found that a decreased acidic-to-basic active site (A/B) ratio in the catalysts negatively affected the selectivity to glycerol carbonate, promoting the further reaction of GC towards by-products. Interestingly, Nguyen-Phu et al. [16] proved that urea glycerolysis with the use of solid catalysts can proceed by several different mechanisms. The authors reported that the reaction can occur both in a homogeneous or heterogeneous way or even according to both variants simultaneously (with a partial dissolution of the active phase) depending on the catalyst. Moreover, they proved that the process can occur through a direct reaction of urea with glycerol or by the formation of an intermediate metal isocyanate (Me NCO) complex. According to the authors, all these factors affected the reaction rate and catalytic performances of the tested samples. Therefore, it can be supposed that in our case, the differences in the catalytic activities of the CF_{ox} -supported systems were also related to the differences in the catalyst nature (e.g., acidic to basic site ratio) and to the differences (dissimilarities) in the reaction mechanism over various metal oxides used.

Figure 9 presents a comparison of the catalytic performances of $\text{ZnO}/\text{CF}_{\text{ox}}$ and a typical homogeneous zinc-based catalyst, i.e., ZnSO_4 . Surprisingly, the $\text{ZnO}/\text{CF}_{\text{ox}}$ sample converted glycerol much more efficiently than ZnSO_4 , reaching a 5% higher X_{Gly} after just 1 h of reaction (Figure 9A). The conversion of glycerol increased over time for both samples; however, $\text{ZnO}/\text{CF}_{\text{ox}}$ was significantly more active in the process, finally showing X_{Gly} of about 40% after 6 h. This suggests good dispersion of ZnO on the CF_{ox} support. On the other hand, considering the results of selectivity to GC (Figure 9B), it is clear that using $\text{ZnO}/\text{CF}_{\text{ox}}$ as a catalyst promoted the formation of a quite significant amount of intermediate and side products (see Figure S2). This was seen particularly clearly in the first hours of the process, when S_{GC} was in the range of 78 and 83%. S_{GC} increased slightly over time; however, it did not exceed 90% when using $\text{ZnO}/\text{CF}_{\text{ox}}$ as a catalyst. On the other hand, ZnSO_4 worked selectively to glycerol carbonate, and the S_{GC} parameter was almost 100% throughout the reaction. The highly selective performance of the homogeneous ZnSO_4 catalyst under the conditions used was probably due to the fact that every single catalytic entity could act as a single active site, which is a common advantage of homogeneous systems over heterogeneous ones [49]. Surprisingly, considering the results of GC yields presented in Figure 9C, it can be seen that using the $\text{ZnO}/\text{CF}_{\text{ox}}$ sample allowed us to obtain slightly higher Y_{GC} values than those achieved in the reaction with ZnSO_4 .

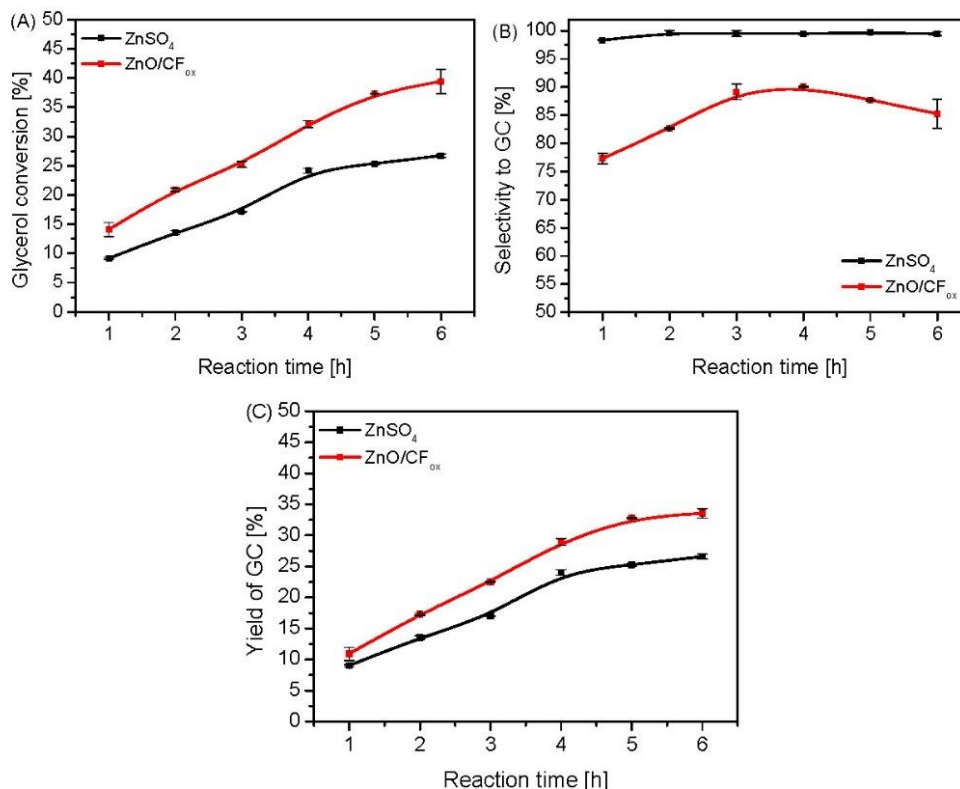


Figure 9. A comparison of the catalytic performances of the heterogeneous ZnO/CF_{ox} and homogeneous ZnSO₄ catalysts in urea glycerolysis expressed as glycerol conversion (A) selectivity to GC (B), and yield of GC (C); catalyst loading = 3 wt.% in both cases, temp. = 140 °C, Gly:U molar ratio = 1:1, Ar flowing through the reactor.

In order to investigate the effect of different reaction conditions (i.e., Gly:U molar ratio and a reaction temperature) on the urea glycerolysis, additional catalytic tests were carried out over ZnO/CF_{ox}. As can be seen in Figure 10, using a Gly:U molar ratio of 1:3 resulted in improved glycerol conversion compared to the value obtained in the reaction performed at an equimolar ratio of the reagents; however, this effect was observed only after 2.5 h of processing. Finally, the achieved X_{Gly} using a 1:3 Gly:U ratio was about 43% after 6 h. Importantly, there were substantial changes in the selectivity to GC when the reaction was performed at various glycerol-to-urea molar ratios, and the process was more selective when using a Gly:U ratio of 1:3, i.e., the use of urea excess resulted in a lower selectivity to GU, higher selectivity to GC, and a lower selectivity to by-products compared to the reaction using a Gly:U molar ratio of 1:1 (compare Figures 10B and S3). It can be assumed that this could be associated with shifting the reaction equilibrium towards the formation of glycerol carbonate due to the excess of urea. Similar results have also been reported by Mallesham et al. [6]. Consequently, the use of Gly:U molar ratio of 1:3 resulted in an almost 10% higher yield of GC after 6 h of processing compared to the reaction using a Gly:U molar ratio of 1:1, as observed in Figure 10C.

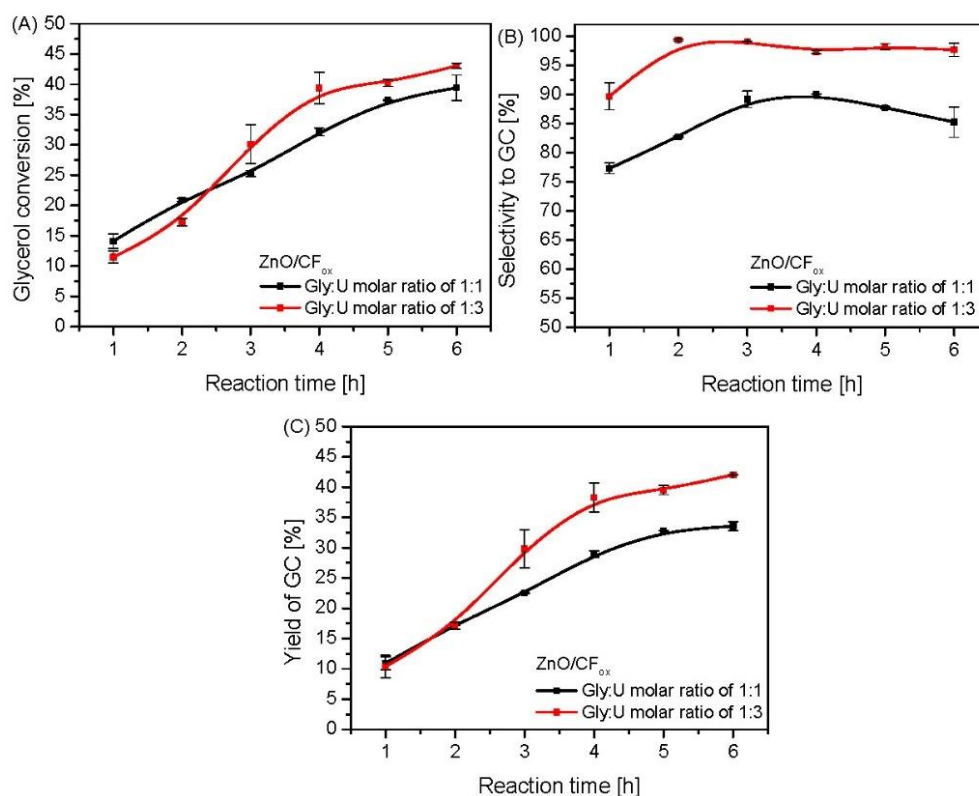


Figure 10. The influence of a Gly:U molar ratio on the process of urea glycerolysis (glycerol conversion (A), selectivity to GC (B), and yield of GC (C)) over the ZnO/CF_{ox} catalyst; temp. = 140 °C, Ar flowing through the reactor.

The data presented in Figure 11 show that temperature also had a significant impact on the reaction; specifically, using a temperature of 150 °C resulted in a significantly higher conversion of glycerol compared to a temperature of 140 °C, which was observed within 4 h of processing (Figure 11A). Interestingly, at this time, a slight decrease in the S_{GC} parameter over time was observed (in contrast to the reaction at 140 °C), indicating that the more drastic conditions (i.e., high temperature combined with excess urea in the reaction medium) promoted the occurrence of side reactions and further reaction of GC to by-products (see also Figure S4B). The same was observed by Mallesham et al. [6]. Surprisingly, after 4 h of reaction at 150 °C, X_{Gly} and S_{GC} decreased rapidly. This was probably due to the ineffective removal of ammonia from the reaction medium (Ar was flowing through the reactor, see also Figure 12), causing a reverse reaction, as presented in Figure 1. It is also worth mentioning that the higher the glycerol conversion to GC (as observed at 150 °C), the higher the concentration of NH₃ produced. This was probably the reason for the decrease in X_{Gly} , as well as the increase in selectivity to by-products at higher temperatures. The obtained profiles of the GC yield vs. time (Figure 11C) were similar to those of X_{Gly} vs. time.

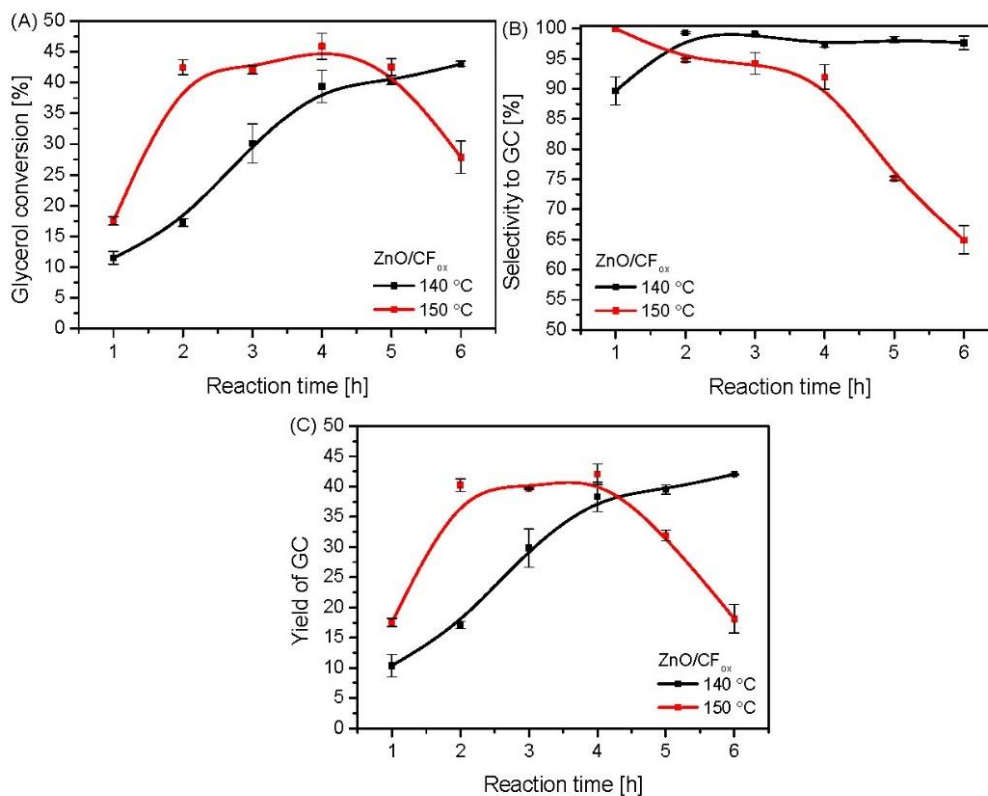


Figure 11. The influence of reaction temperature on the process of urea glycerolysis (glycerol conversion (A), selectivity to GC (B), and yield of GC (C)) over the ZnO/CF_{ox} catalyst; Gly:U molar ratio—1:3, Ar flowing through the reactor.

In order to effectively flush out the ammonia from the reaction system and thus minimize the undesirable reverse reactions that occurred during the process, an inert gas (Ar) was used and passed through the reactor (i.e., above the surface of the reaction mixture) or directly through the reaction mixture. The obtained results are collected in Figure 12. As can be seen in Figure 12A, the method of passing Ar through the system had a rather small impact on the glycerol conversion. Nevertheless, the value of X_{Gly} obtained in the process using the “through-mixture” mode was slightly increased compared to when using the “through-reactor” mode, especially at the beginning of the process. Interestingly, the method of passing Ar through the system significantly affected the selectivity to glycerol carbonate (Figure 12B) and resulted in S_{GC} increasing to 100%, unchanging over time, when using the “through-mixture” mode. This was most likely due to the efficient forced removal of ammonia from the reaction mixture, causing a shift in the chemical equilibrium towards glycerol carbonate and limiting the formation of by-products [4] (see also the results of selectivity to intermediate product and by-products provided in Figure S5). Similar conclusions were also drawn by Wang et al. [7], who in turn used high vacuum to obtain a satisfactory GC yield. Importantly, changing the method of ammonia removal from the reaction medium from the “through-reactor” to the “through-mixture” mode resulted in a significant increase in the yield of the most desired product, i.e., glycerol carbonate, as seen in Figure 12C.

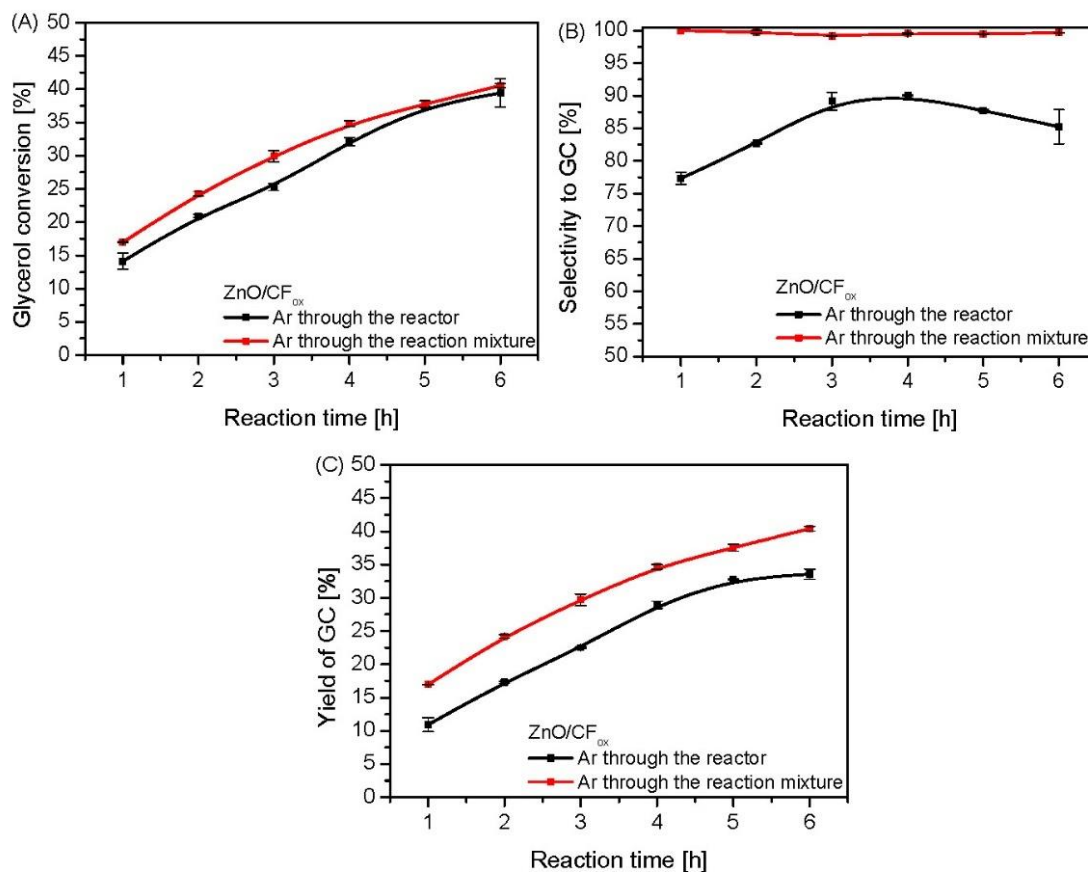


Figure 12. The results of urea glycerolysis (glycerol conversion (A), selectivity to GC (B), and yield of GC (C)) over ZnO/CF_{ox} performed in two variants of Ar flow; temp. = 140 °C, Gly:U molar ratio = 1:1.

Table 3 shows the results achieved in the presence of the best-working catalyst obtained in this study, i.e., ZnO/CF_{ox}, and other zinc-containing systems described in the literature.

As can be observed, the Zn-based catalysts reported in the literature gave similar or higher yields of GC compared to the sample used in our experiment. However, considering the selectivity to the most desirable product (i.e., glycerol carbonate; GC), it is obvious that our catalyst was one of the samples that worked most selectively to GC during the reaction. Although the Zn/MCM-41(im) and ZnCl₂ samples also showed almost complete selectivity to GC, these catalysts required aggressive conditions (i.e., higher temperature, the use of vacuum, or a large amount of catalyst) to work well in urea glycerolysis. In turn, our experiments were performed under relatively mild conditions, and this may be the reason for the rather moderate catalytic performance of the produced samples. Nevertheless, the obtained results are still quite attractive compared to those obtained in the presence of other zinc-containing systems, especially with regard to the limited production of by-products and a viable and affordable method of GC synthesis.

Table 3. A comparison of the catalytic performances of different Zn-based systems in urea glycerolysis.

Sample	Reaction Conditions	X _{Gly} [%]	Y _{GC} [%]	S _{GC} [%]	Reference
ZnO/CF _{ox}	140 °C; Gly:U molar ratio of 1:1; 6 h; Ar flow (20 mL/min); Catalyst loading of 3%wt. (with respect to glycerol mass)	40.5	40.4	99.7	This work
ZnO	130 °C; Gly:U molar ratio of 1:1; 3 h; reaction pressure of 3 kPa; Catalyst loading of 5.4%wt. (with respect to glycerol mass)	61.0	42.0	69.0	[18]
2.5 wt.%Au/ZnO	150 °C; Gly:U molar ratio of 1:1.5; 4 h; N ₂ flow; Catalyst loading of ~2%wt. (with respect to glycerol mass)	88.0	56.0	49.0	[29]
Zn ₂ CrO	140 °C; Gly:U molar ratio of 1:1; 3 h; reaction pressure of 3 kPa; Catalyst loading of ~5%wt. (with respect to glycerol mass)	76.0	57.0	74.0	[16]
Zn/MCM-41(im)	145 °C; Gly:U molar ratio of 1:1; 5 h; N ₂ flow; Catalyst loading of 5%wt. (with respect to glycerol mass)	75.0	73.0	98.0	[32]
ZnCl ₂	150 °C; Gly:U molar ratio of 1:1; 2 h; reaction pressure of 2.67 kPa; Catalyst loading of 2 mol% (with respect to glycerol mass)	80.4	80.2	99.7	[11]
Zn(OAc) ₂ ·2H ₂ O	150 °C; Gly:U molar ratio of 1:1; 2 h; reaction pressure of 2.67 kPa; Catalyst loading of 2 mol% (with respect to glycerol)	67.2	44.3	66.0	[11]
50%-Zn ₇ Al ₃ O _x /ARM	140 °C; Gly:U molar ratio of 1:1; 5 h; reaction pressure of 3 kPa; Catalyst loading of 5%wt. (with respect to glycerol)	69.0	58.1	84.2	[50]

3. Materials and Methods

3.1. Preparation of the Catalysts

Metal oxides supported on carbon fibers were produced and applied as catalysts for urea glycerolysis.

The synthesis of the initial carbon fibers (CF) was performed in a horizontal tube furnace by a catalytic chemical vapor deposition (CCVD) method using liquefied petroleum gas (LPG) as a carbon source and metallic nickel as a growth catalyst [51–53]. Briefly, 0.1 g of NiO was placed in a quartz boat and heated to 550 °C under argon flow (100 cm³/min; heating rate of 10 °/min). Upon reaching the desired temperature, the reduction of NiO to metallic Ni was performed by treating the sample under 20%H₂/Ar flow for 2 h. Subsequently, the oven temperature was increased to 600 °C, and LPG was passed through the reactor. The CCVD process was carried out for 4 h using a 50%LPG/50%H₂ gaseous mixture (total flow rate of 100 cm³/min) for carbon growth. To remove the residual metal catalyst, the obtained carbon sample was boiled with a 21% HCl solution under reflux conditions for 2 h. Afterward, it was filtered off and washed with hot distilled water until the pH of the filtrate was 7. Finally, the produced material was dried overnight at 110 °C and sieved to a particle size of ≤0.4 mm.

The obtained CF sample was used to support various metal oxides, i.e., Me_xO_y, including Zn, Ba, Cr, and Mg oxides. The deposition of the active phase on the CF was carried out by applying an incipient wetness impregnation technique and mixing the support with aqueous solutions of the respective metal nitrates (using the amounts suitable for obtaining 10 wt.% Me_xO_y loading). After a 24 h impregnation step at ambient temperature, the samples were dried overnight at 110 °C and sieved to a particle size of ≤0.4 mm. Afterward, they were thermally treated at 600 °C under Ar flow (30 cm³/min) for 1 h to decompose the nitrates. Finally, the samples were oxidized at 300 °C for 3 h under air/Ar and pure air flow (total flow rate of 20 cm³/min in both cases). The obtained materials were labeled according to the scheme Me_xO_y/CF_{ox}, where Me = Zn, Ba, Cr, or Mg. As in the process, in addition to metals, CF was also oxidized, the symbol CF_{ox} was used instead of CF in the above formula. In order to obtain a sample whose structure and properties would be similar to those of the CF_{ox} support, the initial CF sample was also oxidized (using the same reaction conditions as described above) and designated as CF_{ini_ox}.

3.2. Characterization of the Samples

The morphological features of the initial CF, CF_{ini,ox} support, and Me_xO_y/CF_{ox} catalysts were studied using a scanning electron microscope ZEISS EVO 40. The textural parameters of the samples were determined by nitrogen adsorption/desorption measurements performed at -196 °C and using a Quantachrome Autosorb IQ apparatus. The BET equation was used to calculate the apparent surface area (S_{BET}) of the samples, while the t-plot method was applied to determine the micropore volumes (V_{micro}) and the external surface areas (S_{ext}) of the materials. The total pore volumes (V_{tot}) of the samples were calculated from the amount of N₂ adsorbed at a relative pressure close to 1. Before the textural analysis, the samples were degassed under vacuum at 150 °C for 12 h. Thermogravimetric (TG) analysis was performed by applying a Setaram Setsys 1200 thermal analyzer working in an air flow and at a temperature range of 20–1000 °C (heating rate of 10 °C/min). X-ray diffraction (XRD) measurements were carried out using a Bruker AXS D8 Advance diffractometer equipped with a Johansson monochromator ($\lambda\text{Cu K}\alpha 1 = 1.5406 \text{ \AA}$) and a silicon strip detector LynxEye. X-ray photoelectron spectroscopy (XPS) studies were performed using a SPECS Phoibos 150 UHV-XPS spectrometer equipped with a Phoibos HSA3500 analyzer operating in a Fixed Analyzer Transmission (FAT) mode with a pass energy of 20 eV for core-level peaks. The acquired XPS spectra were processed with CasaXPS software (version 2.3.25PR1.0) using a Shirley-type background. The C 1s peak at 284.5 eV was applied as an internal standard and fitted with an asymmetric LF line shape. The other peaks in the C 1s and Zn 2p regions were constrained with a mixed Gaussian–Lorentzian (GL) function.

3.3. Catalytic Tests

The reaction of glycerol (Gly) with urea (U) was performed in a round-bottom flask equipped with a magnetic stirrer, thermocouple, condenser, and an inert gas (Ar) supply. The reagents, at a Gly:U molar ratio of 1:1 or 1:3, were placed in the reactor and homogenized. After heating the mixture to the desired temperature (140 or 150 °C), a catalyst (3 wt.% with respect to the glycerol mass) was added to the flask. The reaction was carried out under Ar flow, which was passed either through the reactor or directly through the reaction mixture. To monitor the progress of the process, samples of the reaction mixture were taken periodically and analyzed using a gas chromatograph (SRI 8610C) equipped with an MXT-5 capillary column, flame ionization detector (FID), and a split injector. Helium was used as a carrier gas, and the analyses were performed isothermally at 160 °C. The catalytic activities of the tested samples were expressed as conversion of glycerol (X_{Gly}), yield of glycerol carbonate (Y_{GC}), and selectivity to GC (S_{GC}). To determine the reproducibility of analytical data, the standard deviation values (SD) of these parameters were also calculated for each sample. Selectivities to glycerol urethane or by-products (S_{GU} and $S_{\text{B-Py}}$) were also calculated. The obtained data are presented in the Supplementary Materials. For the sake of comparison, reactions without a catalyst and in the presence of a homogeneous ZnSO₄ catalyst were also performed.

4. Conclusions

A series of metal oxides supported on modified carbon fibers were developed and used as catalysts for the conversion of glycerol to glycerol carbonate under ambient pressure. Among the prepared systems, ZnO/CF_{ox} and MgO/CF_{ox} gave the most promising catalytic results, which was probably due to the presence of well-balanced acid–base properties of these samples. The reaction temperature, molar ratio of the reagents, and the applied mode of the inert gas flow significantly affected the conversion of glycerol and/or selectivity to glycerol carbonate. Using an increased amount of urea (3 moles instead of 1 per 1 mole of glycerol) slightly improved the conversion of glycerol, whereas the selectivity to glycerol carbonate increased considerably (to almost 100%) under these conditions. Interestingly, the same effect was obtained when Ar was passed through the reaction mixture instead of passing Ar through the reactor (above the surface of the reaction mixture). On the

other hand, an increase in the reaction temperature resulted in an improvement in glycerol conversion; however, at the same time, this negatively affected the selectivity to glycerol carbonate. Under the best reaction conditions used, the high yield of glycerol carbonate of about 40%, together with ~100% selectivity to GC, was obtained over the ZnO/CF_{ox} catalyst.

Supplementary Materials: The following supporting information can be downloaded at: <https://www.mdpi.com/article/10.3390/molecules28186534/s1>, Figure S1. The results of selectivity to different products obtained in the blank test and in the reaction over CF_{ini,ox} sample and CF_{ox}-supported catalysts (GU – glycerol urethane; GC – glycerol carbonate); Figure S2. The results of selectivity to (A) glycerol urethane (GU) and (B) by-products obtained for the homogeneous and CF_{ox}-supported ZnO catalysts vs. time; Figure S3. The results of selectivity to (A) glycerol urethane (GU) and (B) by-products obtained over the CF_{ox}-supported ZnO catalyst using different glycerol to urea (Gly:U) molar ratios; Figure S4. The results of selectivity to (A) glycerol urethane (GU) and (B) by-products obtained over the CF_{ox}-supported ZnO catalyst at different temperatures; Figure S5. The results of selectivity to (A) glycerol urethane (GU) and (B) by-products obtained over the CF_{ox}-supported ZnO catalyst using different reaction set-ups.

Author Contributions: Conceptualization, K.P. and A.M.; Methodology, K.P.; Validation, K.P., A.M. and M.K.; Formal Analysis, K.K.; Investigation, K.K. and K.P.; Resources, M.K.; Data Curation, K.P. and A.M.; Writing—Original Draft Preparation, K.P. and A.M.; Writing—Review and Editing, K.P. and A.M.; Visualization, K.P., K.K. and A.M.; Supervision, M.K.; Funding Acquisition, M.K. All authors have read and agreed to the published version of the manuscript.

Funding: This research received no external funding.

Data Availability Statement: The data presented in this study are available on request from the corresponding authors.

Conflicts of Interest: The authors declare no conflict of interest.

Sample Availability: Not applicable.

References

1. Takkellapati, S.; Li, T.; Gonzalez, M.A. An overview of biorefinery derived platform chemicals from a cellulose and hemicellulose biorefinery. *Clean Technol. Environ.* **2018**, *20*, 1615–1630. [CrossRef]
2. Rokicki, G.; Rakoczy, P.; Parzuchowski, P.; Sobiecki, M. Hyperbranched aliphatic polyethers obtained from environmentally benign monomer: Glycerol carbonate. *Green Chem.* **2005**, *7*, 529–539. [CrossRef]
3. Sonnati, M.O.; Amigoni, S.; de Givenchy, E.P.T.; Darmanin, T.; Choulet, O.; Guittard, F. Glycerol carbonate as a versatile building block for tomorrow: Synthesis, reactivity, properties and applications. *Green Chem.* **2012**, *15*, 283–306. [CrossRef]
4. Zhang, H.; Liu, H.; Wang, A.; Xu, C.; Yang, S. Progress of catalytic valorization of bio-glycerol with urea into glycerol carbonate as a monomer for polymeric materials. *Adv. Polym. Technol.* **2020**, *2020*, 7207068. [CrossRef]
5. Narkhede, N.; Patel, A. Facile synthesis of glycerol carbonate via glycerolysis of urea catalysed by silicotungstates impregnated to MCM-41. *RSC Adv.* **2015**, *5*, 52801–52808. [CrossRef]
6. Malleshham, B.; Rangaswamy, A.; Rao, B.G.; Rao, T.V. Solvent-free production of glycerol carbonate from bioglycerol with urea over nanostructured promoted SnO₂ catalysts. *Catal. Lett.* **2020**, *150*, 3626–3641. [CrossRef]
7. Wang, L.; Ma, Y.; Wang, Y.; Liu, S.; Deng, Y. Efficient synthesis of glycerol carbonate from glycerol and urea with lanthanum oxide as a solid base catalyst. *Catal. Commun.* **2011**, *12*, 1458–1462. [CrossRef]
8. Rubio-Marcos, F.; Calvino-Casilda, V.; Bañares, M.A.; Fernandez, J.F. Novel hierarchical Co₃O₄/ZnO mixtures by dry nanodispersion and their catalytic application in the carbonylation of glycerol. *J. Catal.* **2010**, *275*, 288–293. [CrossRef]
9. Bartoli, M.; Zhu, C.; Chae, M.; Bressler, D. Value-added products from urea glycerolysis using a heterogeneous biosolids-based catalyst. *Catalysts* **2018**, *8*, 373. [CrossRef]
10. Wang, D.; Zhang, X.; Liu, C.; Cheng, T. Synthesis of glycerol carbonate from glycerol and urea over lanthanum compounds. *React. Kinet. Mech. Catal.* **2015**, *115*, 597–609. [CrossRef]
11. Park, J.-H.; Choi, J.S.; Woo, S.K.; Lee, S.D.; Cheong, M.; Kim, H.S.; Lee, H. Isolation and characterization of intermediate catalytic species in the Zn-catalyzed glycerolysis of urea. *Appl. Catal. A Gen.* **2012**, *433–434*, 35–40. [CrossRef]
12. Turney, T.W.; Patti, A.; Gates, W.; Shaheen, U.; Kulasegaram, S. Formation of glycerol carbonate from glycerol and urea catalysed by metal monoglycerolates. *Green Chem.* **2013**, *15*, 1925. [CrossRef]
13. Aresta, M.; Dibenedetto, A.; Nocito, F.; Ferragina, C. Valorization of bio-glycerol: New catalytic materials for the synthesis of glycerol carbonate via glycerolysis of urea. *J. Catal.* **2009**, *268*, 106–114. [CrossRef]

14. Chaves, D.M.; da Silva, M.J. A selective synthesis of glycerol carbonate from glycerol and urea over $\text{Sn}(\text{OH})_2$: A solid and recyclable in situ generated catalyst. *New J. Chem.* **2019**, *43*, 3698–3706. [CrossRef]
15. Fernandes, G.P.; Yadav, G.D. Selective glycerolysis of urea to glycerol carbonate using combustion synthesized magnesium oxide as catalyst. *Catal. Today* **2018**, *309*, 153–160. [CrossRef]
16. Nguyen-Phu, H.; Do, L.T.; Shin, E.W. Investigation of glycerolysis of urea over various ZnMeO (Me = Co, Cr, and Fe) mixed oxide catalysts. *Catal. Today* **2020**, *352*, 80–87. [CrossRef]
17. Charate, S.; Shinde, S.; Kondawar, S.; Desai, U.; Wadgaonkar, P.; Rode, C. Role of preparation parameters of Cu–Zn mixed oxide catalyst in solvent free glycerol carbonylation with urea. *J. Indian Chem. Soc.* **2021**, *98*, 100090. [CrossRef]
18. Fujita, S.; Yamanishi, Y.; Arai, M. Synthesis of glycerol carbonate from glycerol and urea using zinc-containing solid catalysts: A homogeneous reaction. *J. Catal.* **2013**, *297*, 137–141. [CrossRef]
19. Morawa Eblagon, K.; Arenillas, A.; Malaika, A.; Pereira, M.F.R.; Figueiredo, J.L. The influence of the surface chemistry of phosphorylated carbon xerogel catalysts on the production of HMF from fructose in water. *Fuel* **2023**, *334*, 126610. [CrossRef]
20. Malaika, A.; Ptaszyńska, K.; Kozłowski, M. Production of valuable chemicals from glycerol using carbon fiber catalysts derived from ethylene. *Sci. Rep.* **2021**, *11*, 20251. [CrossRef]
21. Malaika, A.; Ptaszyńska, K.; Morawa Eblagon, K.; Pereira, M.F.R.; Figueiredo, J.L.; Kozłowski, M. Solid acid carbon catalysts for sustainable production of biofuel enhancers via transesterification of glycerol with ethyl acetate. *Fuel* **2021**, *304*, 121381. [CrossRef]
22. Szymańska, M.; Malaika, A.; Rechnia, P.; Miklaszewska, A.; Kozłowski, M. Metal/activated carbon systems as catalysts of methane decomposition reaction. *Catal. Today* **2015**, *249*, 94–102. [CrossRef]
23. Gao, M.; Wang, L.; Yang, Y.; Sun, Y.; Zhao, X.; Wan, W. Metal and metal oxide supported on ordered mesoporous carbon as heterogeneous catalysts. *ACS Catal.* **2023**, *13*, 4060–4090. [CrossRef]
24. Min, K.; Kim, J.; Park, K.; Yoo, Y.J. Enzyme immobilization on carbon nanomaterials: Loading density investigation and zeta potential analysis. *J. Mol. Catal. B: Enzym.* **2022**, *83*, 87–93. [CrossRef]
25. Lam, E.; Luong, J.H.T. Carbon materials as catalyst supports and catalysts in the transformation of biomass to fuels and chemicals. *ACS Catal.* **2014**, *4*, 3393–3410. [CrossRef]
26. Buaki-Sogó, M.; Zubizarreta, L.; García-Pellicer, M.; Quijano-López, A. Sustainable carbon as efficient support for metal-based nanocatalyst: Applications in energy harvesting and storage. *Molecules* **2020**, *25*, 3123. [CrossRef]
27. Liang, Y.; Li, Y.; Wang, H.; Dai, H. Strongly coupled inorganic/nanocarbon hybrid materials for advanced electrocatalysis. *J. Am. Chem. Soc.* **2013**, *135*, 2013–2036. [CrossRef]
28. Kondawar, S.E.; Mane, R.B.; Vasishta, A.; More, S.B.; Dhengale, S.D.; Rode, C.V. Carbonylation of glycerol with urea to glycerol carbonate over supported Zn catalysts. *Appl. Petrochem. Res.* **2017**, *7*, 41–53. [CrossRef]
29. Hammond, C.; Lopez-Sanchez, J.A.; Hasbi Ab Rahim, M.; Dimitratos, N.; Jenkins, R.L.; Carley, A.F.; Hutchings, G.J. Synthesis of glycerol carbonate from glycerol and urea with gold-based catalysts. *Dalton Trans.* **2011**, *40*, 3927. [CrossRef]
30. Arsalani, N.; Bazazi, S.; Abuali, M.; Jodeyri, S. A new method for preparing ZnO/CNT nanocomposites with enhanced photocatalytic degradation of malachite green under visible light. *J. Photochem. Photobiol. A Chem.* **2020**, *389*, 112207. [CrossRef]
31. Malaika, A.; Ptaszyńska, K.; Kozłowski, M. Conversion of renewable feedstock to bio-carbons dedicated for the production of green fuel additives from glycerol. *Fuel* **2021**, *288*, 119609. [CrossRef]
32. Kondawar, S.E.; Potdar, A.S.; Rode, C.V. Solvent-free carbonylation of glycerol with urea using metal loaded MCM-41 catalysts. *RSC Adv.* **2015**, *5*, 16452–16460. [CrossRef]
33. Thommes, M.; Kaneko, K.; Neimark, A.V.; Olivier, J.P.; Rodriguez-Reinoso, F.; Rouquerol, J.; Sing, K.S.W. Physisorption of gases, with special reference to the evaluation of surface area and pore size distribution (IUPAC Technical Report). *Pure Appl. Chem.* **2015**, *87*, 1051–1069. [CrossRef]
34. Che, B.D.; Nguyen, B.Q.; Nguyen, L.T.T.; Nguyen, H.T.; Nguyen, V.Q.; Le, T.V.; Nguyen, N.H. The impact of different multi-walled carbon nanotubes on the X-band microwave absorption of their epoxy nanocomposites. *Chem. Cent. J.* **2015**, *9*, 10. [CrossRef] [PubMed]
35. Futaba, D.N.; Yamada, T.; Kobashi, K.; Yumura, M.; Hata, K. Macroscopic wall number analysis of single-walled, double-walled, and few-walled carbon nanotubes by X-ray diffraction. *J. Am. Chem. Soc.* **2011**, *133*, 5716–5719. [CrossRef]
36. Singh, D.K.; Iyer, P.K.; Giri, P.K. Diameter dependence of interwall separation and strain in multiwalled carbon nanotubes probed by X-ray diffraction and Raman scattering studies. *Diam. Relat. Mater.* **2010**, *19*, 1281–1288. [CrossRef]
37. Hoseini, L.; Bagheri Gh, A. Effect of the amount of BaO catalyst on the selective acetylation of benzyl alcohols and doxycycline degradation. *Chem. Afr.* **2019**, *2*, 377–382. [CrossRef]
38. Sone, B.T.; Manikandan, E.; Gurib-Fakim, A.; Maaza, M. Single-phase $\alpha\text{-Cr}_2\text{O}_3$ nanoparticles' green synthesis using Callistemon viminalis' red flower extract. *Green Chem. Lett. Rev.* **2016**, *9*, 85–90. [CrossRef]
39. Balakrishnan, G.; Velavan, R.; Batoo, K.M.; Raslan, E.H. Microstructure, optical and photocatalytic properties of MgO nanoparticles. *Results Phys.* **2020**, *16*, 103013. [CrossRef]
40. Malekkiani, M.; Magham, A.H.J.; Ravari, F.; Dadmehr, M. Facile fabrication of ternary MWCNTs/ZnO/Chitosan nanocomposite for enhanced photocatalytic degradation of methylene blue and antibacterial activity. *Sci. Rep.* **2022**, *12*, 5927. [CrossRef]
41. Ptaszyńska, K.; Malaika, A.; Kapska, M.; Kozłowski, M. SO_3H -functionalized carbon fibers for the catalytic transformation of glycerol to glycerol tert-butyl ethers. *Sci. Rep.* **2023**, *13*, 565. [CrossRef]

42. Liu, Y.; Ba, H.; Nguyen, D.-L.; Ersen, O.; Romero, T.; Zafeiratos, S.; Begin, D.; Janowska, I.; Pham-Huu, C. Synthesis of porous carbon nanotubes foam composites with a high accessible surface area and tunable porosity. *J. Mater. Chem. A* **2013**, *1*, 9508–9516. [[CrossRef](#)]
43. Figueiredo, J.L.; Pereira, M.F.R.; Freitas, M.M.A.; Órfão, J.J.M. Modification of the surface chemistry of activated carbons. *Carbon* **1999**, *37*, 1379–1389. [[CrossRef](#)]
44. Risoluti, R.; Gullifa, G.; Carcassi, E.; Masotti, A.; Materazzi, S. TGA/Chemometrics addressing innovative preparation strategies for functionalized carbon nanotubes. *J. Pharm. Anal.* **2020**, *10*, 351–355. [[CrossRef](#)]
45. Qu, G.; Fan, G.; Zhou, M.; Rong, X.; Li, T.; Zhang, R.; Sun, J.; Chen, D. Graphene-modified ZnO nanostructures for low-temperature NO₂ sensing. *ACS Omega* **2019**, *4*, 4221–4232. [[CrossRef](#)] [[PubMed](#)]
46. Claros, M.; Setka, M.; Jimenez, Y.P.; Vallejos, S. AACVD synthesis and characterization of iron and copper oxides modified ZnO structured films. *Nanomaterials* **2020**, *10*, 471. [[CrossRef](#)]
47. Kim, D.-W.; Park, K.-A.; Kim, M.-J.; Kang, D.H.; Yang, J.-G.; Park, G.-W. Synthesis of glycerol carbonate from urea and glycerol using polymer-supported metal containing ionic liquid catalysts. *Appl. Catal. A* **2014**, *473*, 31–40. [[CrossRef](#)]
48. Li, Y.; Liu, H.; Zheng, Z.; Fu, Z.; He, D.; Zhang, O. Synthesis of glycerol carbonate via alcoholysis of urea with glycerol: Current status and future prospects. *Ind. Eng. Chem. Res.* **2022**, *61*, 5698–5711. [[CrossRef](#)]
49. Fadhel, A.Z.; Pollet, P.; Liotta, C.L.; Eckert, C.A. Combining the benefits of homogeneous and heterogeneous catalysis with tunable solvents and nearcritical water. *Molecules* **2010**, *15*, 8400–8424. [[CrossRef](#)]
50. Nguyen-Phu, H.; Park, C.; Shin, E.W. Activated red mud-supported Zn/Al oxide catalysts for catalytic conversion of glycerol to glycerol carbonate: FTIR analysis. *Catal. Commun.* **2016**, *85*, 52–56. [[CrossRef](#)]
51. Malaika, A.; Możdżyńska, A.; Piwecki, D.; Kozłowski, M. Comparative studies of the CCVD-based synthesis of carbon nanofibers—The quantitative aspect. *Diam. Relat. Mater.* **2017**, *80*, 125–132. [[CrossRef](#)]
52. Dupuis, A.-C. The catalyst in the CCVD of carbon nanotubes—A review. *Prog. Mater. Sci.* **2005**, *50*, 929–961. [[CrossRef](#)]
53. Magrez, A.; Seo, J.W.; Smajda, R.; Mionić, M.; Forró, L. Catalytic CVD synthesis of carbon nanotubes: Towards high yield and low-temperature growth. *Materials* **2010**, *3*, 4871–4891. [[CrossRef](#)] [[PubMed](#)]

Disclaimer/Publisher's Note: The statements, opinions and data contained in all publications are solely those of the individual author(s) and contributor(s) and not of MDPI and/or the editor(s). MDPI and/or the editor(s) disclaim responsibility for any injury to people or property resulting from any ideas, methods, instructions or products referred to in the content.

SUPPLEMENTARY MATERIAL

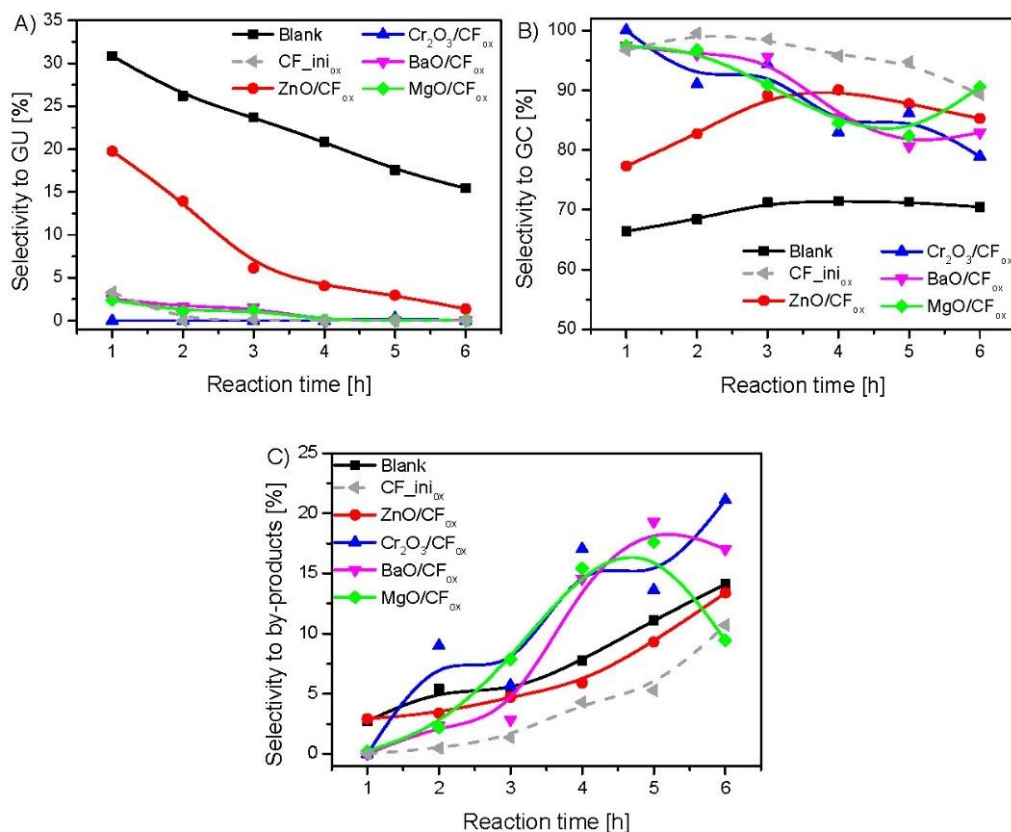


Figure S1. The results of selectivity to different products obtained in the blank test and in the reaction over $\text{CF}_{\text{ini}}_{\text{ox}}$ sample and CF_{ox} -supported catalysts (GU – glycerol urethane; GC – glycerol carbonate)

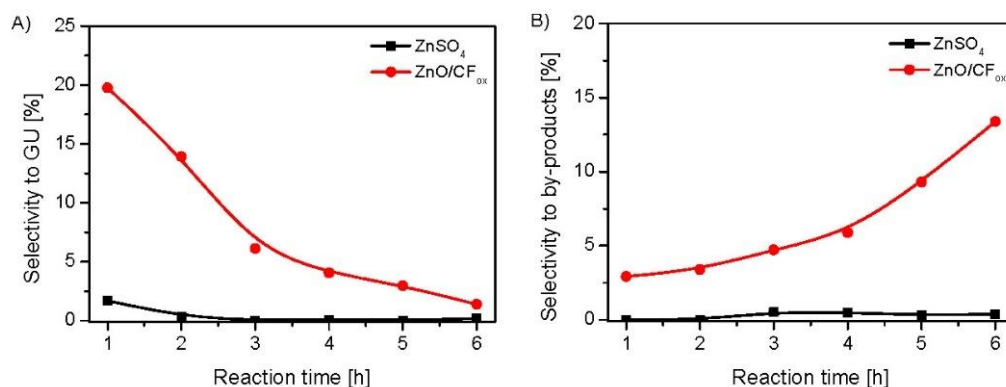


Figure S2. The results of selectivity to A) glycerol urethane (GU) and B) by-products obtained for the homogeneous and CF_{ox} -supported ZnO catalysts vs. time

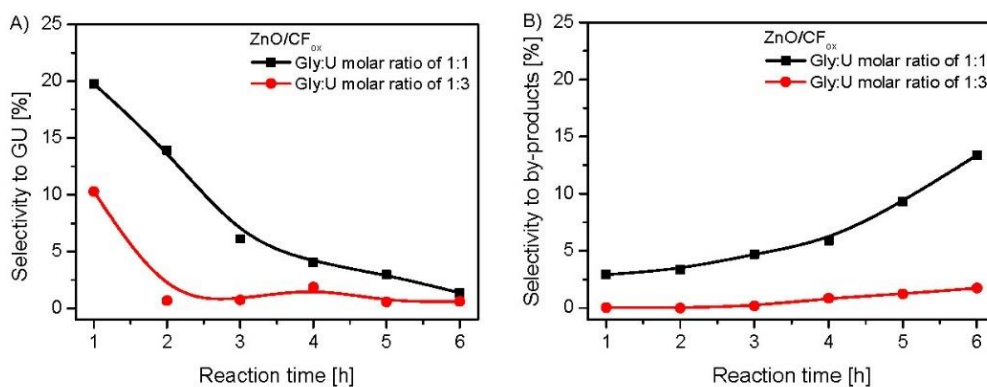


Figure S3. The results of selectivity to A) glycerol urethane (GU) and B) by-products obtained over the CF_{ox}-supported ZnO catalyst using different glycerol to urea (Gly:U) molar ratios

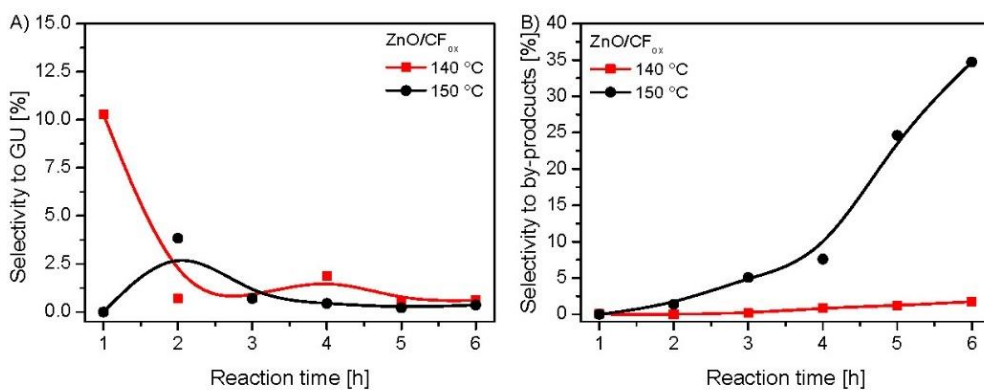


Figure S4. The results of selectivity to A) glycerol urethane (GU) and B) by-products obtained over the CF_{ox}-supported ZnO catalyst at different temperatures

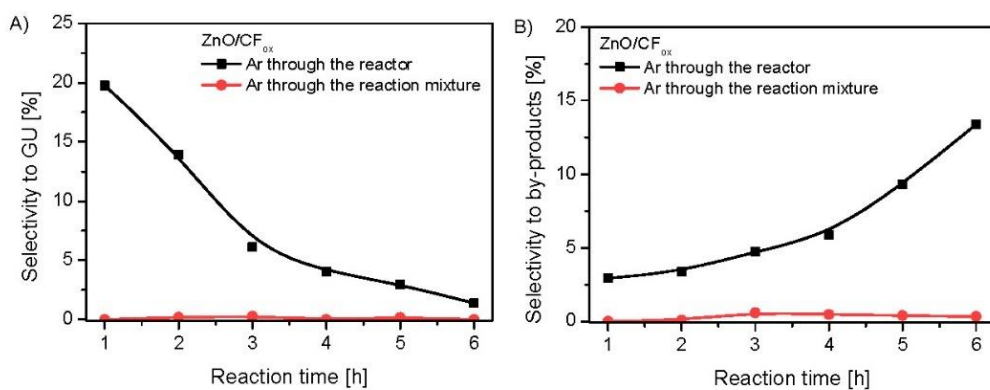


Figure S5. The results of selectivity to A) glycerol urethane (GU) and B) by-products obtained over the CF_{ox}-supported ZnO catalyst using different reaction set-ups

P4

Article

Promoting Effect of Ball Milling on the Functionalization and Catalytic Performance of Carbon Nanotubes in Glycerol Etherification

Karolina Ptaszyńska ^{1,*}, Anna Malaika ¹, Katarzyna Morawa Eblagon ^{2,3}, José Luís Figueiredo ^{2,3} and Mieczysław Kozłowski ^{1,*}

¹ Faculty of Chemistry, Adam Mickiewicz University in Poznań, Uniwersytetu Poznańskiego 8, 61-614 Poznań, Poland; amalaika@amu.edu.pl

² LSRE-I.CM—Laboratory of Separation and Reaction Engineering—Laboratory of Catalysis and Materials, Faculty of Engineering, University of Porto, Rua Dr. Roberto Frias, 4200-465 Porto, Portugal; keblagon@fe.up.pt (K.M.E.); jlfig@fe.up.pt (J.L.F.)

³ ALiCE—Associate Laboratory in Chemical Engineering, Faculty of Engineering, University of Porto, Rua Dr. Roberto Frias, 4200-465 Porto, Portugal

* Correspondence: karolina.ptaszynska@amu.edu.pl (K.P.); mkozlow@amu.edu.pl (M.K.)

Abstract: A facile and eco-friendly approach using in situ-generated 4-benzenediazonium sulfonate (BDS) was applied to prepare highly functionalized carbon nanotubes (CNTs). The effectiveness of this functionalization was additionally enhanced by a green and short-time ball milling process applied beforehand. The obtained BDS-modified CNTs presented significant activity in glycerol etherification, producing tert-butyl glycerol ethers, which are considered promising fuel additives. Excellent results of ~56% glycerol conversion and ~10% yield of higher-substituted tert-butyl glycerol ethers were obtained within just 1 h of reaction at 120 °C using a low catalyst loading of only 2.5 wt.%. Furthermore, the sulfonated CNTs were reusable over several reaction cycles, with only a minor decrease in activity. Additionally, the sample activity could be restored by a simple regeneration approach. Finally, a clear correlation was found between the content of -SO₃H groups on the surface of CNTs and the catalytic performances of these materials in glycerol etherification. Improved interaction between functionalized ball-milled CNTs and the reactants was also suggested to positively affect the activity of these catalysts in the tested process.

Keywords: carbon nanotubes; surface functionalization; ball milling; glycerol etherification; fuel additives



Citation: Ptaszyńska, K.; Malaika, A.; Morawa Eblagon, K.; Figueiredo, J.L.; Kozłowski, M. Promoting Effect of Ball Milling on the Functionalization and Catalytic Performance of Carbon Nanotubes in Glycerol Etherification. *Molecules* **2024**, *29*, 1623. <https://doi.org/10.3390/molecules29071623>

Received: 29 February 2024

Revised: 28 March 2024

Accepted: 30 March 2024

Published: 4 April 2024



Copyright: © 2024 by the authors. Licensee MDPI, Basel, Switzerland. This article is an open access article distributed under the terms and conditions of the Creative Commons Attribution (CC BY) license (<https://creativecommons.org/licenses/by/4.0/>).

1. Introduction

Due to their unusual properties, such as large surface area, low toxicity, high thermal and electrical conductivity, excellent mechanical strength, and the possibility of surface modifications, carbon nanotubes (CNTs) have gained significant attention in various branches of industry, being used as promising materials for flexible electronics, biomedical applications, adsorption processes, energy storage devices, water purification systems, or catalysis, among others [1–4]. Additionally, due to the continuous development of carbon nanotube synthesis methods and the possibility of their efficient production, the prices of these materials are constantly decreasing, making them more and more competitive with other materials used in industry [5].

Typically, CNTs in their raw form are scarcely used, and their functionalization is required to boost their applications. For example, Chen et al. [6] found raw multi-walled CNTs ineffective in adsorbing Hg(II) from water. At the same time, the sample performance was significantly enhanced by functionalization with the -COOH or -OH groups. Pantarotto et al. [7] showed that ammonium-functionalized CNTs form supramolecular complexes with plasmid DNA that can penetrate the cell membranes, working as advanced

delivery systems for therapeutics. In turn, Eblagon et al. [8] applied CNTs as supports for Au and obtained an efficient bifunctional catalyst for the direct conversion of cellobiose to gluconic acid, which outperformed Au supported on carbon xerogel or on ordered mesoporous carbon.

It should be taken into account that the functionalization of CNTs is challenging due to their rigid and inert structure [9,10]. For example, Wei et al. [11] introduced only 1.2% sulfur into the structure of multi-walled carbon nanotubes by sulfonation. Yu et al. [12] performed a two-step functionalization of CNTs by treating the sample with a mixture of 1:1 concentrated HNO₃ and HCl, followed by a reaction with H₂SO₄ at elevated temperatures up to 300 °C, and obtained a final acid density of only 0.67 mmol/g. In turn, Nowicki et al. [9] reported that the susceptibility of carbon nanotubes to oxidation with nitric acid was three times lower than that of activated carbon.

Cutting or crushing CNTs is an interesting method of changing their structural and morphological properties and, consequently, their chemical features. This approach breaks and opens the closed ends of CNTs, making the interior accessible for various atoms and molecules [13,14]. Furthermore, the mechanical pretreatment of CNTs can increase the number of exposed active graphene edges, thus activating the sample toward functionalization [15].

Several approaches for mechanical modification of CNT structure and morphology have been described in the literature [13,16]. Among them, the most useful option seems to be ball milling (BM), which proved to be a simple, reagent-free, effective, versatile, controllable, and reproducible method. Furthermore, BM can be applied under wet and dry conditions to a wide range of materials [16–19]. For example, Pierard et al. [18] showed that vibratory ball milling was effective in decreasing the single-walled carbon nanotube length, and adjusting the processing time enabled to vary the structural disorders and defects in the CNTs (showed by different intensity ratios between the D- and G-bands in Raman spectra). On the other hand, Soares et al. [19] found that the particle sizes and S_{BET} of CNTs could be controlled by changing the ball-milling vibration frequency. The obtained ball-milled samples showed an increased activity in the ozonation of oxalic acid due to changes in their textural properties. Gharegozloo et al. [20] found that a BM strategy can prepare effective Ni-CNT composite catalysts. In turn, Soares et al. [21] proposed a simple two-step mechanochemical method for functionalizing CNTs with heteroatoms, involving ball-milling of CNTs in the presence of adequate precursor and subsequent thermal treatment under an inert atmosphere. The ball milling allowed the creation of active sites for functionalization and homogenization of the mixture. In the following thermal step, the precursor was thermally decomposed, and the heteroatoms were attached to the previously created defects on the surface of CNTs. A ball milling strategy was also used to obtain CNT-polymer composites, enhancing the adhesion between CNTs and a polymer matrix and yielding samples with enhanced thermal, mechanical, or chemical properties [22].

Sulfonic groups (i.e., SO₃H)-functionalized carbons (so-called solid acids) are of special interest for acid-catalyzed reactions [23,24]. These catalysts are typically obtained via the sulfonation of samples with concentrated sulfuric acid, chlorosulfonic acid, or their mixtures [24–26]. However, to achieve a satisfactory SO₃H-functionalization degree of CNTs, harsh reaction conditions and/or aggressive reagents are generally required [27,28]. In the current work, a benign approach applying diazonium salt generated *in situ* was employed to produce green solid acids by anchoring Ph-SO₃H groups onto the surface of CNTs. Additionally, the effect of ball milling on the susceptibility of CNTs to sulfonation via arylation was studied for the first time. The obtained SO₃H-functionalized CNTs were applied as catalysts in glycerol etherification with TBA (tert-butyl alcohol) to produce tert-butyl glycerol ethers (TBGEs) via a green synthesis route. Active catalysts for this reaction are of great industrial interest because TBGEs are valuable oxygenated fuel additives that can limit particulate matter and NO_x emissions [29]. The relationship between the chemical nature of CNTs-SO₃H and their catalytic performances toward the formation of TBGEs was

established in this work. Recyclability tests were also carried out, and a simple method was proposed to recover the catalytic activity of the spent catalysts.

We believe the findings presented in the paper shed new light on the possible applications of CNTs as solid acid catalysts and lay the groundwork for developing other effective catalysts for the synthesis of sustainable fuel additives.

2. Results and Their Discussion

2.1. Characterization of the Samples

The results of elemental analysis and the amount of ash obtained for the tested nanotubes are presented in Figure 1. As observed, the raw carbon nanotubes, i.e., NC3100 and NC7000, differed quite significantly in their compositions. Elemental carbon was dominant for both materials; however, the NC7000 sample contained ~10% less C than NC3100. Instead, NC7000 indicated about 10% of ash, which was probably related to the presence of the metal catalysts used during the production process (i.e., catalytic chemical vapor deposition (CCVD)) that were not removed in the purification step [30]. On the contrary, NC3100 was free from inorganic residues (0% ash), suggesting thorough material purification after the CCVD. In both raw CNT samples, the oxygen and hydrogen contents were negligible.

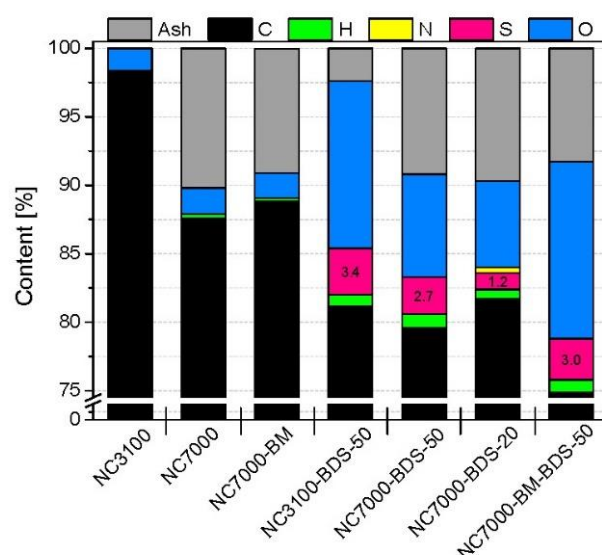


Figure 1. The results of elemental and ash analyses obtained for the raw, ball-milled, and modified carbon nanotubes.

As observed in Figure 1, the modifications of CNTs with diazonium salt introduced significant amounts of sulfur and oxygen to the structure of the raw materials. The content of S in the modified samples was between 1.2 and 3.4%, which is quite impressive considering the efficiency of sulfonation of CNTs reported in the literature. For example, Koskin et al. [31] used concentrated H_2SO_4 to treat CNTs at 200 °C and obtained only 0.15% sulfur content in the sample. The modification of CNTs with fuming sulfuric acid (oleum) was more effective as it introduced 0.89% of S to the material; however, this process also required a high temperature (175 °C). Furthermore, our previous studies showed that only about 0.5–0.6% of S could be introduced into CNTs when using concentrated H_2SO_4 at 180 °C [32]. Given the above, the S content results obtained here may suggest that modification with 4-benzenediazonium sulfonate is a particularly suitable option for the efficient functionalization of CNTs. Moreover, the method has additional advantages due to

mild reaction conditions applied during the treatment (see Experimental). The conclusions drawn here align with those of other authors [10].

Interestingly, NC3100 (i.e., high-purity CNTs) modified with BDS at 50 °C contained more sulfur than its technical grade counterpart, i.e., NC7000 (3.4 vs. 2.7% of S, respectively). Apparently, the metallic impurities present in NC7000 hampered the functionalization. It was also observed that the lower temperature used for the reaction with BDS, i.e., 20 °C, was not favorable for modification of CNTs (compare the S content in NC7000-BDS-20 and NC7000-BDS-50 in Figure 1), even though it was very efficient in functionalization of activated carbon, as shown in our previous work [33]. Interestingly, in the case of NC7000-BDS-20, a certain amount of nitrogen was also detected, indicating the presence of a small number of azo bonds formed in coupling reactions between diazonium cations and the surface of CNTs [24,33].

As stated above, CNTs are quite resistant to typical functionalizations. Thus, simple, reagents-free mechanical pretreatment of CNTs by BM was suggested to enhance their activity towards chemical modification. Indeed, comparing the results of S contents for NC7000-BDS-50 and NC7000-BM-BDS-50 in Figure 1, 11% higher S content was obtained for the latter sample, which clearly demonstrates that BM improved the susceptibility of NC7000 to functionalization, despite the short ball milling time applied (see Experimental). Importantly, the modifications of CNTs with diazonium sulfonate resulted not only in an increase in the S contents but also in the oxygen amounts (up to ~13%). This observation suggests that sulfur was introduced onto the sample surface as -SO₃H groups.

Table 1 presents the acidic properties of the tested CNTs. As can be observed, the raw and ball-milled samples showed only negligible total acidities (A_{tot}), probably related to a small number of acidic oxygen groups on the carbon surfaces (see also the oxygen content in Figure 1). A significant increase in the number of the -SO₃H group and A_{tot} was noted for all the modified samples, indicating that the functionalization was effective. Interestingly, in most cases, the values of A_{tot} and calculated contents of -SO₃H groups were not closely correlated. In the case of raw CNTs modified with BDS at 50 °C, the total acidity of the functionalized sample was lower than the calculated acidity induced by the -SO₃H groups. We also obtained similar results when modifying activated carbons or carbon fibers with BDS [24,33]. Such a phenomenon can occur when zwitterions (i.e., internal salts) are formed, resulting in the neutralization of -SO₃H sites [34]. The other possibility is the formation of a thick and tight layer of sulfonic species with restricted accessibility [35]. The possible surface structures formed during the modification of CNTs with BDS [36,37] are shown in Figure S1 in Supplementary Materials. The opposite effect (i.e., $A_{tot} >$ content of -SO₃H sites) was observed for the ball-milled NC7000 reacted with BDS at 50 °C (i.e., NC7000-BM-BDS-50 sample), indicating the presence of not only sulfonic groups on the sample surface but also small amounts of other types of acidic sites, most likely oxygen functionalities [24].

Table 1. The results of the total acidities determinations (A_{tot}) and content of -SO₃H groups obtained for the tested materials.

Parameter	NC3100	NC7000	NC7000-BM	NC3100-BDS-50	NC7000-BDS-20	NC7000-BDS-50	NC7000-BM-BDS-50
A_{tot} [mmolH ⁺ /g]	0.02	0.03	0.05	1.01	0.38	0.66	1.16
content of -SO ₃ H groups * [mmol/g]	0.00	0.00	0.00	1.05	0.37	0.83	0.94

* Calculated based on EA results.

Figure 2A, B depict the textural properties of the studied materials. As shown in Figure 2A, the raw carbon nanotubes, i.e., NC3100 and NC7000, differed significantly. Namely, the former presented a considerably higher S_{BET} than NC7000 (460 m²/g vs. 250 m²/g), which can be linked to the extensive post-synthesis washing of NC3100, resulting in the more accessible pores in this sample. A similar phenomenon was also observed elsewhere [38]. Interestingly, as shown by the data gathered in Figure 2B, for both raw CNTs, the S_{BET} parameters resulted mainly from the external surface areas (S_{ext}), i.e., meso-

and macropores, and the samples' porosity was probably related mostly to certain spaces between nanotubes [8,39].

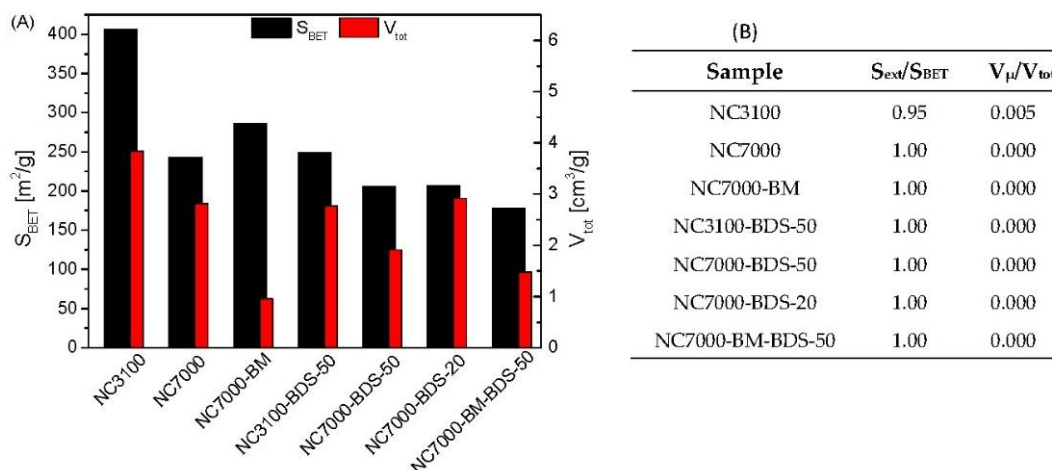


Figure 2. Results of the textural analysis performed for the raw and modified CNTs: (A) apparent surface areas of samples and total volume of pores; (B) contributions of external surface areas to the apparent surface areas and micropore volumes to the total volumes of pores.

Interestingly, ball milling increased the S_{BET} of NC7000, most likely due to agglomerates' fragmentation, shortening of the tubes, and caps opening during the mechanical treatment [19,39]. On the contrary, a drastic drop in the V_{tot} of NC7000 was observed after BM, which was probably the result of the CNTs colliding with the balls and the container walls, reducing the distance between the nanotubes in bundles [39]. A significant drop in all the textural parameters was observed in modified samples compared with the as-received CNTs, which suggested the successful introduction of the functional groups blocking the surfaces of the samples [34].

Figure 3 depicts high-resolution TEM images obtained for the raw and ball-milled CNTs. As observed in Figure 3A, research-grade NC3100 consisted of randomly organized and long nanotubes that showed small diameters with varied sizes. The presence of closed caps and open ends is visible in these micrographs. The images also suggest that the NC3100 sample was free of metallic impurities or amorphous carbon. Figure 3B, presenting the NC3100 material at higher magnification, revealed that a single carbon nanotube consisted of several perfectly arranged graphene sheets parallel to each other, thus representing the structure typical for multi-walled carbon nanotubes (MWCNTs). The morphology of a technical grade NC7000 (Figure 3C) was similar to that of the research-grade NC3100. The most important difference between these two types of CNTs was the presence of impurities (the CCVD catalyst mentioned before) trapped inside the NC7000 structure, observed as dark spots in Figure 3C. This finding also aligns with the increased ash in this sample (see Figure 1). Residues of the CCVD catalyst trapped in the CNT structure were also observed in TEM images presented elsewhere [40,41].

Similarly to NC3100, NC7000 also indicated a multi-walled CNT-type structure; however, the average number of walls seemed higher in the latter than in the former (Figure 3D). Figure 3E shows the TEM micrographs obtained for the ball-milled sample, i.e., NC7000-BM. Significant changes in the morphology are visible before and after the ball milling process (compare Figure 3C,E). Namely, carbon nanotubes were still visible after BM; however, they formed tight bundles, probably resulting from the collisions of tubes with balls during milling. This observation also agrees well with the decreased V_{tot} obtained for the ball-milled sample (shown in Figure 2A). Moreover, only small deformations of the arrangement of graphene layers of the tubes were observed after ball-milling (shown in

Figure 3F), which confirms the high mechanical stability of CNTs [42] and relatively mild BM conditions applied here (see Experimental).

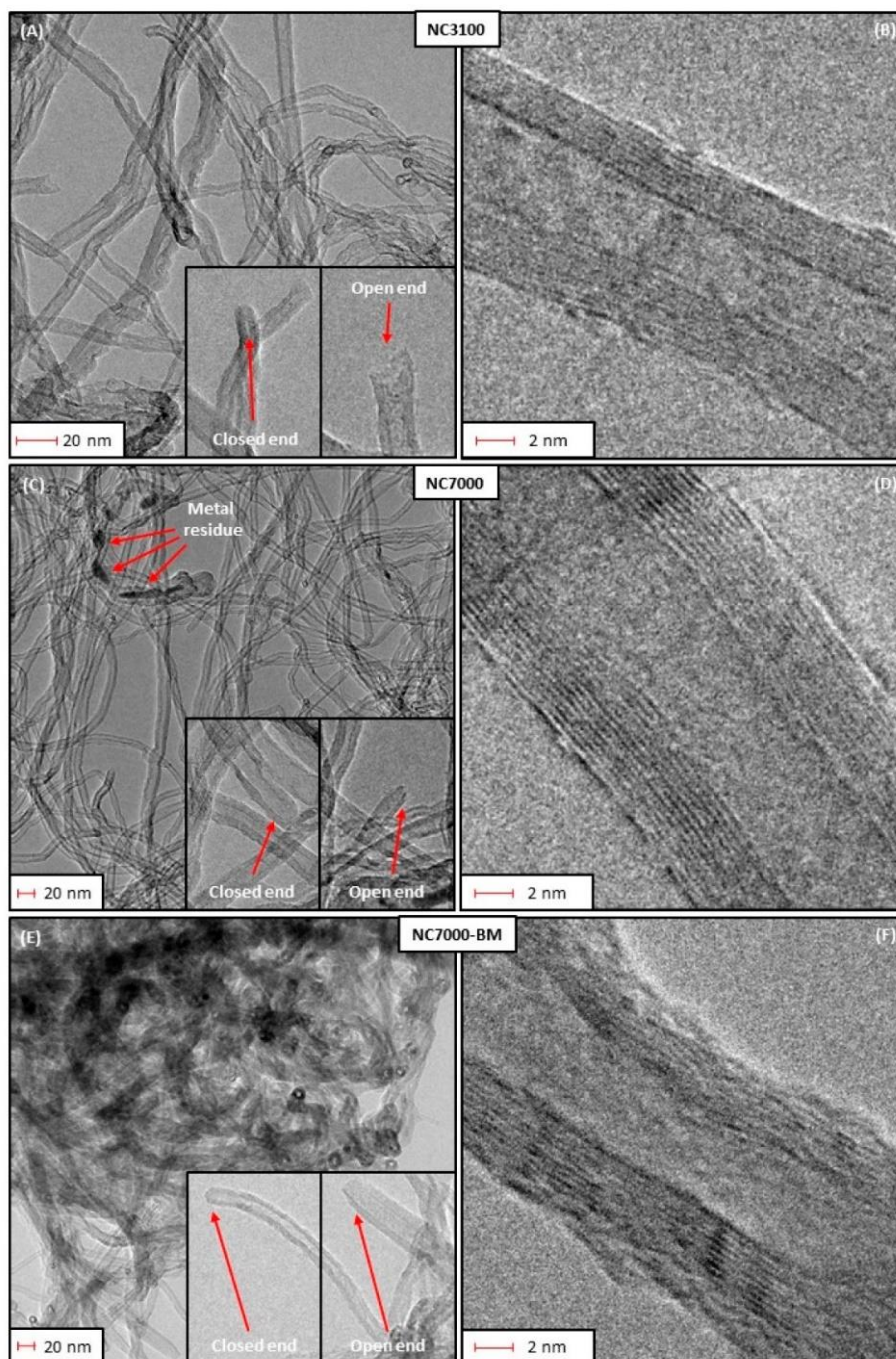


Figure 3. The high-resolution transmission electron microscopy (HRTEM) images of: (A–D) the as-received, (E,F) ball-milled CNTs.

SEM images of the raw and ball-milled CNTs are presented in Figure S2 in the Supplementary Materials. As observed, the raw sample showed a rather compact structure formed by long, tightly entangled fibers clumped into large agglomerates (Figure S2A). In turn, ball milling resulted in significant fragmentation of the CNT agglomerates, leading to more exposed particle edges (Figure S2B). This was probably the reason for the enhanced S_{BET} of NC7000-BM and a higher degree of its functionalization compared with NC7000 (compare results for NC7000-BM-BDS-50 and NC7000-BDS-50 in Figures 1 and 2 and Table 1).

Raman spectroscopy is a useful method to investigate the effect of ball milling on the structural integrity of CNTs, as demonstrated by Pierard et al. [18]. The Raman spectra obtained for the raw and ball-milled samples tested in this study are collected in Figure 4, together with the $I_{\text{D}}/I_{\text{G}}$ ratios for the selected samples. As can be seen in this figure, all of the samples showed intense signals at 1350 cm^{-1} , i.e., a D band typically assigned to disordered forms or structural defects, and at $\sim 1580\text{ cm}^{-1}$, i.e., a G band corresponding to in-plane vibrations of C sp^2 atoms and attributed to the ordered graphite structure [43,44]. Interestingly, research-grade NC3100 showed a lower degree of ordering and a higher number of defects than the NC7000 sample. Presumably, this could be related to the post-treatment purification process applied to NC3100 (to remove the CCVD catalyst), which led to the appearance of structural defects in this sample. Similar findings were reported by other authors [45,46]. As observed, the mechanical pretreatment of NC7000 did not result in significant changes in the structural ordering of the raw material, as the $I_{\text{D}}/I_{\text{G}}$ ratio obtained for NC7000-BM was only slightly higher than that observed for NC7000. This is in line with the TEM and SEM results, suggesting that ball milling resulted in the fragmentation of the agglomerates and did not affect the arrangement of the graphene layers; thus, the crystallinity of the CNTs was maintained. Li et al. [47] also did not notice an increase in $I_{\text{D}}/I_{\text{G}}$ achieved for ball-milled MWCNTs despite some structural deformations of the modified sample observed in the TEM images. In turn, Chebattina et al. [48] obtained an increased $I_{\text{D}}/I_{\text{G}}$ ratio for the mechanically treated CNTs only after an extended period of ball-milling (i.e., 20 h).

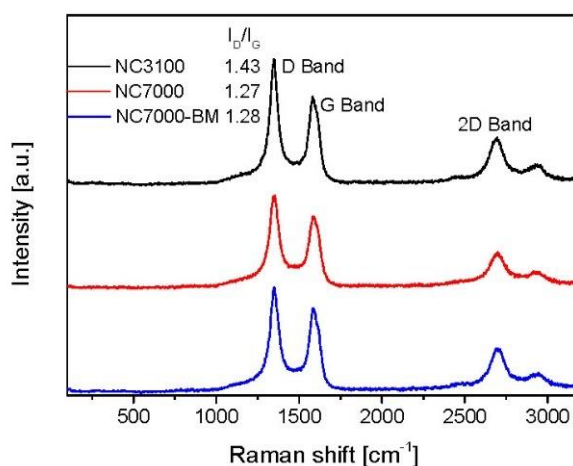


Figure 4. The Raman spectra obtained for the raw and ball-milled samples.

The TG analysis of raw CNTs was performed under airflow, and the DTG results are presented in Figure S3 in Supplementary Materials. As observed, the DTG patterns of both samples showed an intense peak with a minimum at $\sim 680\text{ }^{\circ}\text{C}$, typically observed in multi-walled CNTs [49]. Furthermore, the DTG profile of NC7000 had a poorly separated low-intensity peak at the temperature of $\sim 600\text{ }^{\circ}\text{C}$. It cannot be excluded that, in this case, the combustion of the sample was facilitated by the contaminants present in NC7000 (see also the ash amount in NC7000 in Figure 1). Kumar et al. [50] also observed that

oxidation of carbon in $\text{Co}_3\text{O}_4/\text{CNTs}$ nanocomposites occurred at lower temperatures than in the case of pristine CNTs.

TG analysis performed under an inert gas flow (nitrogen) can reflect the effectiveness of sample functionalization [24]. Figure 5 presents the TG results obtained for the raw and modified NC3100 and NC7000 samples (as DTG patterns). In the case of the pristine and ball-milled materials, no significant signals were observed, suggesting a very low number of surface functionalities in these samples. These results also align with data from EA (see Figure 1). As shown, the DTG profiles of the BDS-modified CNTs were significantly different from those of the parent materials, suggesting remarkable changes in the surface properties of CNTs after their functionalizations. In general, all the curves showed a peak with a minimum in the temperature range of 50–100 °C, typically attributed to moisture. Another signal at 180–260 °C was most likely related to the interlayered water evaporation [50]. However, the decomposition of $-\text{SO}_3\text{H}$ groups can also occur at similar temperatures [33]. In turn, the signals appearing at 300–350 °C and 500–550 °C can be associated with the gradual decomposition of the $-\text{PhSO}_3\text{H}$ functionalities, proceeding in two stages and related to de-sulfonation process and possibly to slight fragmentation of the benzene ring [51,52]. The peak with a minimum at 350 °C or a broad signal starting at 500 °C can also indicate the presence of oxygen species with different thermal stabilities, e.g., carboxylic anhydrides or phenolic groups [53].

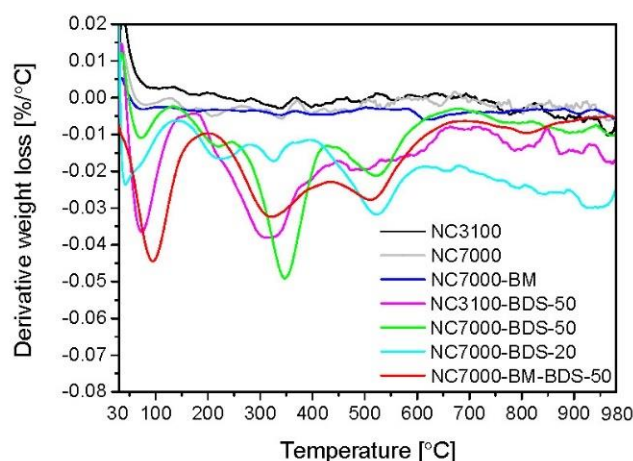


Figure 5. The DTG patterns of the raw and modified samples (N_2 atmosphere).

The XPS technique was applied to define the chemical composition of the samples' surfaces, and the results obtained for selected modified CNTs are presented in Tables 2 and 3 and Figure 6.

Table 2. The contents of carbon, sulfur, and oxygen determined for the selected samples.

Sample	C [wt.%]	O [wt.%]	S [wt.%]
NC7000-BDS-20	89.86	6.20	3.90
NC7000-BDS-50	87.02	8.40	4.60
NC7000-BM-BDS-50	81.88	11.30	6.80

The achieved results confirmed the presence of carbon, oxygen, and sulfur in the functionalized samples, and the relative concentrations of these elements on the samples' surfaces are presented in Table 2. All the samples contained quite a high amount of sulfur (3.9–6.8%). These quantities were higher than those obtained by EA, which suggests that S-containing moieties are more concentrated on the surface of these samples than

in the bulk. Interestingly, the functionalization of CNTs with BDS was strongly affected by the temperature of the treatment. The increase in the temperature from 20 to 50 °C resulted in a 0.7% increment in the S content. Moreover, the pretreatment of CNTs via ball-milling before the functionalization allowed the incorporation of 2.2% more sulfur into the material structure. Importantly, an increase in the S content in the modified CNTs was also accompanied by an increase in the amount of oxygen, which is also in line with the EA results (Figure 1), suggesting that S was introduced in the oxidized form onto the surface of CNTs.

Table 3. The relative contributions of various S- and O-species calculated from XPS S 2p and O 1s profiles.

Sample	S 2p		O 1s	
	S in SO ₃ H [at.%]	O in C=O, S=O [at.%]	O in C-O, S-O [at.%]	O in COOH [at.%]
NC7000-BDS-20	100.00 (3.90 wt.%)	69.70 (4.32 wt.%)	22.20 (1.38 wt.%)	4.30 (0.26 wt.%)
NC7000-BDS-50	100.00 (4.60 wt.%)	68.90 (5.78 wt.%)	24.60 (2.06 wt.%)	4.30 (0.36 wt.%)
NC7000- BM-BDS-50	100.00 (6.80 wt.%)	69.10 (7.80 wt.%)	23.70 (2.67 wt.%)	4.10 (0.46 wt.%)

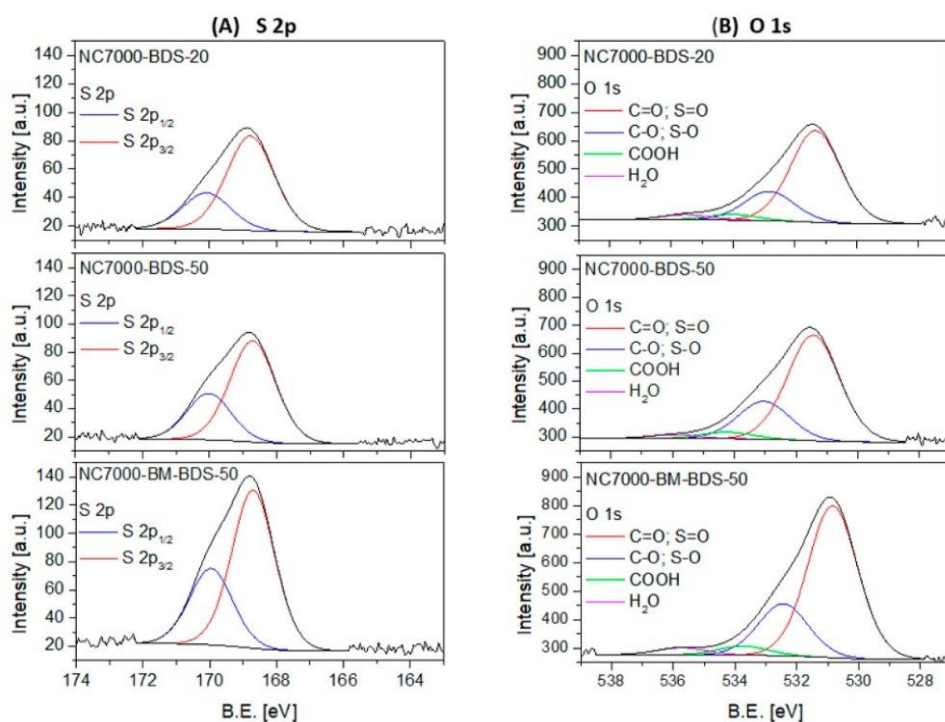


Figure 6. The high-resolution XPS S 2p (A) and O 1s (B) spectra of selected samples.

The chemical and electronic states of O and S were investigated by analyzing the high-resolution XPS O 1s and S 2p spectra.

Figure 6A presents the deconvoluted XPS S 2p spectra obtained for the modified samples. As observed, raw data was fitted with a doublet at B.E. ~168.7 eV and ~169.9 eV with an intensity ratio of 1:2 and a peak separation of 1.2 eV for all the samples, which was assigned to sulfur in -SO₃H moieties [54]. Importantly, no signals attributed to other S species were present in these materials, showing that the applied functionalization method selectively introduces S as sulfonic groups into the CNTs.

The deconvoluted high-resolution XPS O 1s spectra shown in Figure 6B revealed the presence of four signals belonging to different oxygen species. Two intense signals at B.E. of ~ 531 eV and ~ 532.6 eV were observed in each case, which can be ascribed to C=O and C-O bonds, respectively. The signals from sulfur in S=O and S-O can also be present in this region. Additional two small peaks were present in O 1s spectra at a BE ~ 534.2 eV and ~ 535.8 eV, which are typically attributed to -COOH groups and adsorbed H_2O , respectively [33,55,56].

The relative contributions of different sulfur or oxygen species detected in the BDS-modified CNTs are gathered in Table 3. The presented results show that the studied samples contained only oxidized forms of S in the form of -SO₃H functionalities. This observation is also in line with our previous findings [34]. Interestingly, similar relative contributions of individual O-species were observed for each sample, i.e., a dominant contribution of C=O and S=O species (68.1–69.7%), significant of C-O and S-O (22.2–24.6%), and negligible of COOH (<1%). There were, however, some differences in the concentrations of the abovementioned species expressed in wt.%, resulting from the effectiveness of functionalizations.

2.2. Catalytic Results

The catalytic performances of BDS-modified CNTs were investigated in the reaction of glycerol with tert-butyl alcohol (TBA). This process leads to mono-, di-, and tri-tert-butyl glycerol ethers (designated here MTBGEs, DTBGEs, and TTBGE, respectively); see Figure S4 in Supplementary Materials. For comparison, a blank test (reaction without a catalyst) and a reaction in the presence of a commercial catalyst, Amberlyst-15, were also performed. The obtained results are presented in Figure 7.

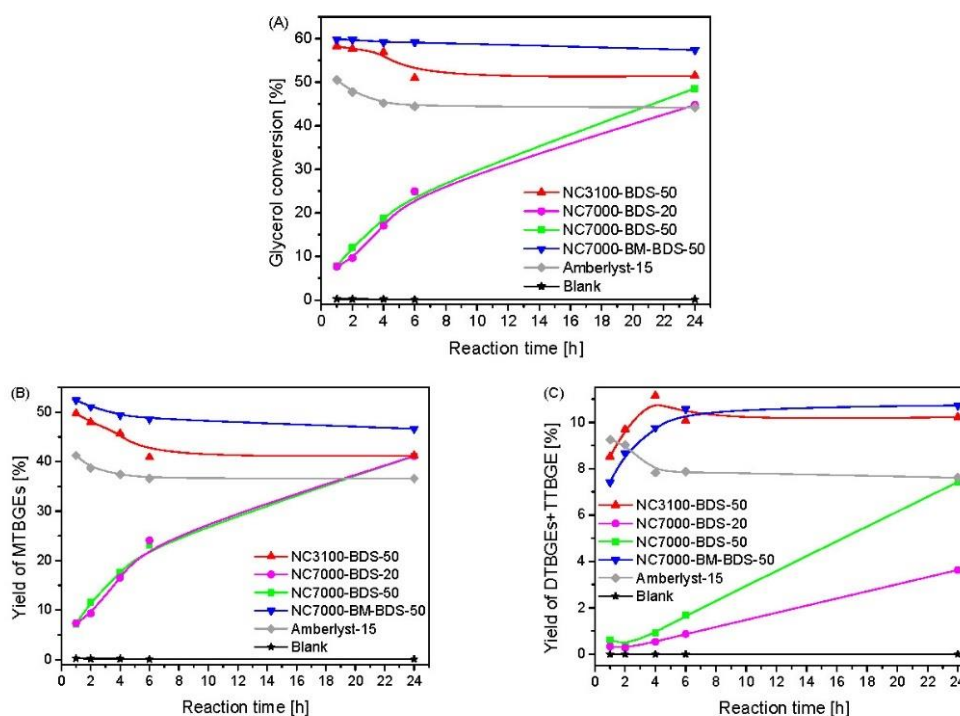


Figure 7. Results of the catalytic performance, i.e., glycerol conversion (A), yield of MTBGEs (B), and yield of DTBGEs+TTBGE (C), of the BDS-modified CNTs compared with the blank test and a reaction over Amberlyst-15 (temp. = 110 °C, G:TBA = 1:4, catalyst loading = 5 wt.%).

As presented, a reaction without a catalyst did not occur, as the final glycerol conversion (i.e., measured after 24 h) was negligible (~0.2%). The same was observed in the case of unmodified CNTs (results not shown for clarity) due to a lack of active sites for the etherification process, as confirmed by the characterization of the samples in Figure 1 and Table 1. A significant increase in glycerol conversion and the yield of TBGEs was observed with functionalized samples. Two different activity patterns were shown by the modified catalysts, as described below.

Glycerol conversions (X_G) obtained in glycerol etherification over the produced samples are gathered in Figure 7A. As seen from this figure, the lowest glycerol conversion was displayed by the samples based on technical grade NC7000 (i.e., NC7000-BDS-20 and NC7000-BDS-50), which initially obtained rather low X_G (~8% within 1 h of the process). However, a gradual increase in X_G was observed with time for both these catalysts, which finally presented X_G of 44% and 48% in the extended reaction time of 24 h. On the other hand, the remaining catalysts, i.e., BDS-modified research grade NC3100 (i.e., NC3100-BDS-50) and functionalized ball-milled NC7000 (i.e., NC7000-BM-BDS-50), were much more active in the reaction, showing a very high ~60% conversion of glycerol just within 1 h, which remained stable until the end of the testing time (due to reaching the reaction equilibrium). Only in the case of NC3100-BDS-50 was a slight decrease in X_G with reaction time observed, which was probably related to the subsequent de-etherification process [57]. A similar pattern of X_G versus time was also observed for Amberlyst-15. It should be noted that the reference catalyst showed worse catalytic performance in glycerol etherification than BDS-functionalized CNTs developed in the present work.

The excellent catalytic performances shown by NC3100-BDS-50 and NC7000-BM-BDS-50 were due to the effective functionalization, resulting in the high total acidities (A_{tot}) induced mostly by $-SO_3H$ moieties (see results in Tables 1–3 and Figure 6). The role of A_{tot} in the activity of samples is clear when analyzing the catalytic performance of NC7000-BDS-20 and NC7000-BDS-50, which showed the lowest A_{tot} among the prepared materials (see also the discussion about the results presented in Table 1). Furthermore, it should be underlined that the catalytic performance of the modified ball-milled CNTs (i.e., NC7000-BM-BDS-50) was better than that of the functionalized raw sample (i.e., NC7000-BDS-50), which can be attributed to the higher degree of functionalization of NC7000-BM (see also Figure 1 and Table 1). It is also suggested that the mechanical pretreatment of the sample, resulting in the fragmentation of CNT particles (see SEM images in Figure 1 SM), could improve the interaction between the catalyst and the reactants in the etherification of glycerol [13].

As shown in Figure 7B,C, mono-, di-, and tri-tert-butyl glycerol ethers were detected in the reaction mixture; however, their yields (Y) varied significantly between catalysts. In each case, mono tert-butyl glycerol ethers (MTBGEs) were the dominant products. Nevertheless, significant yields of higher substituted ethers (i.e., DTBGEs + TTBGE) were also formed. The lowest yields of products (i.e., MTBGEs + DTBGEs + TTBGE) were achieved over the NC7000-BDS-20 and NC7000-BDS-50 catalysts, especially in the first hours of the process. Interestingly, similar yields of MTBGEs were obtained over time using both of these catalysts, whereas the obtained $Y_{DTBGEs+TTBGE}$ varied between the samples (i.e., NC7000-BDS-50 gave higher $Y_{DTBGEs+TTBGE}$). The highest production of ethers was achieved over the NC3100-BDS-50 and NC7000-BM-BDS-50 catalysts, probably due to the significant surface acidities of these catalysts (see A_{tot} in Table 1). Concerning the Y_{MTBGEs} , the maximum value of over 50% was observed after 1 h. In the extended reaction time, Y_{MTBGEs} slightly decreased, which was accompanied by a simultaneous increase in the yield of higher-substituted ethers ($Y_{DTBGEs+TTBGE}$ up to ~11%). Thus, it can be concluded that the DTBGEs and TTBGE were obtained in consecutive reactions from MTBGEs intermediate products, which is consistent with the reaction mechanism proposed by other authors [29,58]. It is worth noting that after 6 h of the process, the yields of the products stabilized due to reaching the reaction equilibrium [57].

As shown above, the catalytic performances of CNTs tested in glycerol etherification were due to the chemical properties of their surfaces, affecting X_G and yields of ethers. The

relationship between the initial rates of glycerol consumption or yields of DTBGEs+TTBGE and the content of $-\text{SO}_3\text{H}$ groups present in CNTs is depicted in Figure 8. Due to the probability of zwitterions' formation and other effects limiting the availability of sulfonic groups (as mentioned before), for the samples showing $A_{\text{tot}} < \text{content of } -\text{SO}_3\text{H}$, the values of A_{tot} were considered to correspond to the amount of available active sites in the form of $-\text{SO}_3\text{H}$ species.

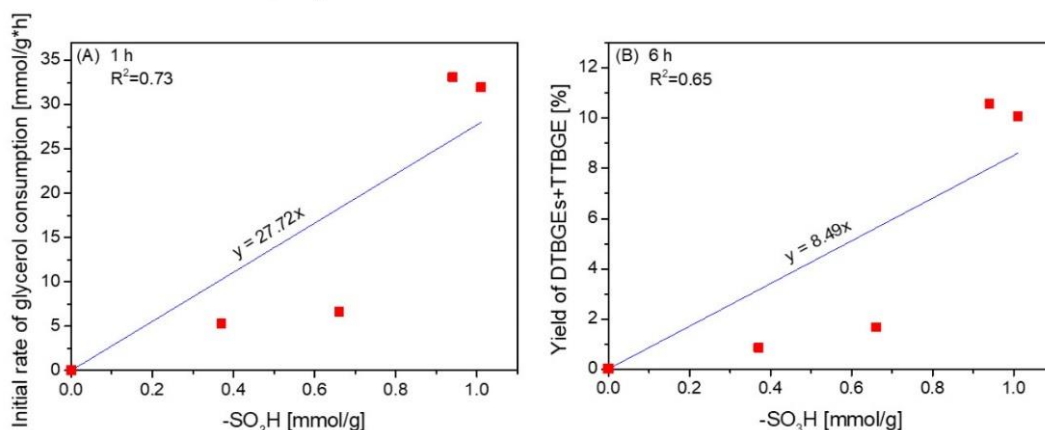


Figure 8. The dependence between the initial glycerol consumption rates (A) or yields of DTBGEs+TTBGE (B) and the content of $-\text{SO}_3\text{H}$ groups on the CNT surface.

As observed in Figure 8, there was a correlation between the initial rate of glycerol consumption and the concentration of $-\text{SO}_3\text{H}$ sites (Figure 8A), indicating a crucial role of strongly acidic sulfonic sites in the transformation of glycerol into glycerol ethers. The density of $-\text{SO}_3\text{H}$ groups also had an important influence on the formation of higher substituted glycerol ethers (Figure 8B); however, both dependencies were not straightforward. In our previous studies, we found a synergistic effect of sulfonic and O-containing functional groups in carbon fibers on the formation of tert-butyl glycerol ethers [24]. Apparently, in the case of CNTs, other physicochemical or structural features of the catalysts, e.g., limited or improved availability of active sites in the case of large raw CNT aggregates or ball-milled samples, respectively (see Figure S2), could play a significant role in the process, making the active sites on the catalyst's surface more or less accessible to the reagents [13].

For the best-performing catalyst, i.e., NC3100-BDS-50, the influence of selected reaction conditions (catalyst loading and reaction temperature) on the course of the process was studied. The obtained results are presented in Figures 9 and 10.

As shown in Figure 9, there were differences in the process efficiency when using various loadings of the catalyst (i.e., 5, 2.5, or 1 wt.%); however, the changes were not very significant, especially when 5 wt.% or 2.5 wt.% of catalyst were applied. The initial glycerol conversions observed for these two cases were comparable and very high and did not change significantly with time (only a slight de-etherification effect was observed after 4 h). Moreover, promising yields of ethers were achieved within just 1 h for both catalyst concentrations. Further lowering the catalyst loading to 1 wt.% strongly affected the initial rate of the DTBGEs and TTBGE formation. After 1 h, the glycerol conversion was still quite high (~45%); however, the yield of the most desired DTBGEs and TTBGE was negligible (~3%). These results improved with extended reaction time; however, the satisfactory results were only achieved after 4 h. Thus, these data suggest that lowering the CNT catalyst loading to 2.5 wt.% could make the process more economically viable. It should also be highlighted that the results obtained in the present work are superior to the ones presented in the literature, especially taking into consideration the minimum

catalysts loadings > 5 wt.% used by other laboratories to obtain satisfactory X_G and ether yields [57,59].

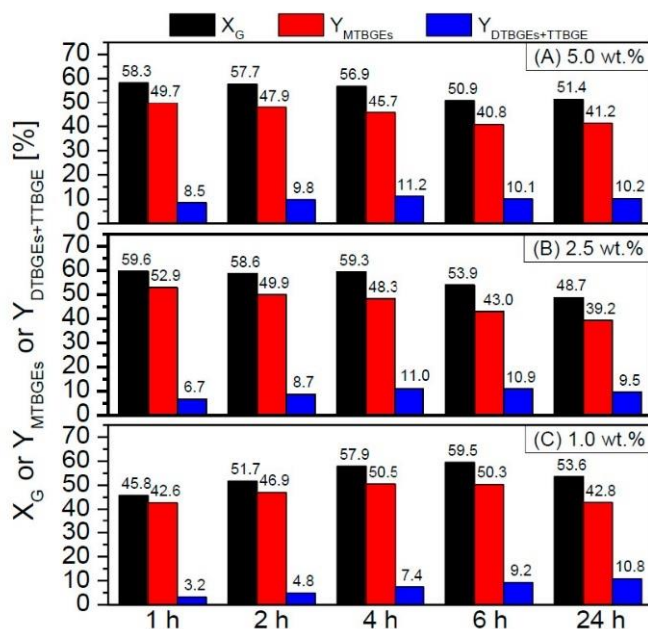


Figure 9. The effect of NC3100-BDS-50 catalyst loading, i.e., 5.0 wt.% (A), 2.5 wt.% (B), or 1.0 wt.% (C), on the glycerol etherification (temp. = 110 °C, G:TBA molar ratio = 1:4).

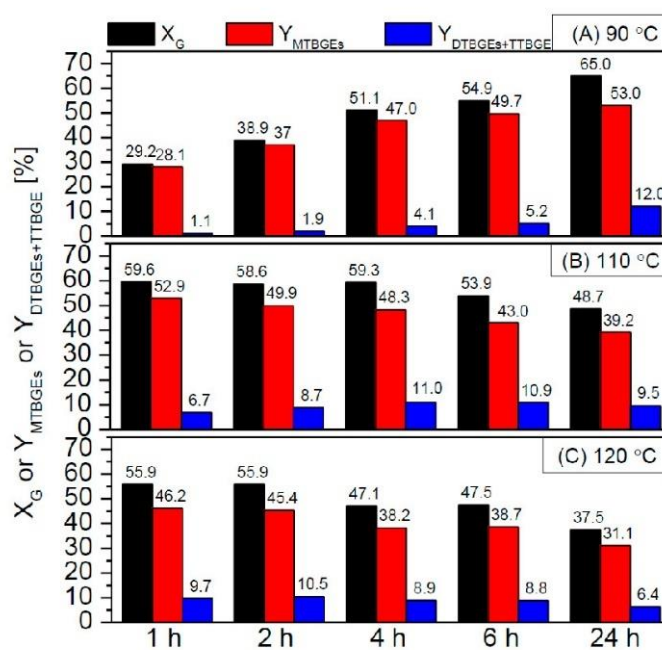


Figure 10. The effect of the reaction temperature, i.e., 90 °C (A), 110 °C (B), or 120 °C (C), on the activity of NC3100-BDS-50 in the glycerol etherification (catalyst loading = 2.5 wt.%, G:TBA molar ratio = 1:4).

Figure 10 compares the X_G and ethers' yields in the glycerol etherification performed at different temperatures, i.e., 90 °C, 110 °C, and 120 °C.

As can be observed, the temperature used significantly impacted the catalyst performance. At a temperature of 90 °C, the catalyst worked the least effectively, giving only a 30% conversion of glycerol within 1 h and virtually producing only MTBGEs. In this case, satisfactory yields of higher-substituted products (i.e., DTBGEs+TTBGE) were achieved only after 24 h of the reaction. On the other hand, higher temperatures positively affected the process, increasing the initial X_G parameters and facilitating the production of DTBGEs and TTBGE. This effect was particularly visible at 120 °C when the glycerol conversion as high as ~56% was obtained and the DTBGEs+TTBGE yield reached ~10% within 1 or 2 h. Interestingly, under the above conditions, the de-etherification effect was strongly favored at longer reaction times, resulting in a drastic drop in glycerol conversion and, consequently, yields of the reaction products. The promoting effect of high temperature on the hydrolysis of glycerol ethers was also reported by Klepáčová et al. [60] and Gonçalves et al. [57]. On the other hand, performing the reaction at 120 °C allowed us to achieve excellent catalytic results in a short time, thus enabling the reduction of TBGE production costs. Moreover, the achieved results were quite impressive compared with those presented by others. For example, Carvalho et al. [61] found that the sulfonated carbons prepared from rice husk could give only ~20% glycerol conversion within 1 h, while Miranda et al. [59] achieved a glycerol conversion of only 31–35% using sulfonated activated carbons, despite applying the extended reaction time (10 h) and quite a high catalyst loading (7.5 wt.%).

The reusability of heterogeneous catalysts is one of the most important advantages of these systems. Thus, selected modified CNT samples (i.e., the best working NC3100-BDS-50 and NC7000-BM-BDS-50 catalysts) were re-used in subsequent glycerol etherification reactions. The obtained results are depicted in Figures S5 and S6 in Supplementary Materials.

As shown in Figure S5, the NC7000-BM-BDS-50 sample showed comparable catalytic performance over three consecutive reaction cycles, with only a minor drop in glycerol conversions and yields of ethers in subsequent runs. However, after the third cycle, a significant decrease in the sample activity was observed. A regeneration process of the deactivated catalyst was performed according to our previously applied method (i.e., treating the sample with a 5% HCl solution for 20 h) [33]. Interestingly, the catalytic performance of the sample was partially restored, suggesting that the deterioration of the catalytic activity was probably related to a strong interaction between the surface active sites and reagents rather than the active site leaching [33,62]. The reusability of the NC3100-BDS-50 sample is depicted in Figure S6 in the Supplementary Materials. In this case, the catalyst was stable over four reaction cycles.

3. Materials and Methods

3.1. Materials

Research- and industrial-grade multi-walled carbon nanotubes (NC3100 and NC7000, respectively) were purchased from Nanocyl SA, Sambreville, Belgium. The products varied in their purity, i.e., NC3100 represented a high purity material with above 95% C content, whereas NC7000 contained $\geq 90\%$ of C. Sulfanilic acid (ACS, Reag. Ph. Eur.) was purchased from Merck, Germany, sodium nitrite (p.a.) and anhydrous glycerol (p.a., 99.5%) were obtained from Avantor Performance Materials, Poland, hydrochloric acid (35–38%, p.a.) was received from StanLab, Poland, whereas tert-butyl alcohol (p.a.) was purchased from Aktyń, Suchy Las, Poland.

3.2. Functionalization of the Samples

NC3100 and NC7000 were functionalized with 4-benzenediazonium sulfonate (BDS) generated in situ to anchor sulfonic groups to the CNT surface and induce the sample acidity. The applied procedure was as follows: 95 mL of distilled water, 1.5 g of CNTs, and 2.1 g of sulfanilic acid were mixed for 1.5 h using an ultrasonic bath. Afterward, 0.9 g of sodium nitrite and 15 mL of concentrated hydrochloric acid (added dropwise) were put

into the flask while mixing with a magnetic stirrer. The modification was performed at 20 °C or 50 °C for 20 h. The resulting samples were filtered and washed with hot distilled water, small portions of methanol, DMF, and acetone. Finally, the materials were dried at 110 °C overnight and sieved to a particle size of ≤ 0.4 mm.

A selected sample (i.e., NC7000) was also subjected to mechanical pretreatment before functionalization. This was performed using a Retsch MM200 ball mill equipped with zirconium oxide milling balls for 20 min with a vibrational frequency of 25 vibrations/s. The as-prepared material (denoted as NC7000-BM) was then modified with BDS according to the procedure described above.

The functionalized samples were labeled according to the scheme: sample type-type of modifying agent-temperature of modification. For example, NC7000-BM-BDS-50 means the ball-milled NC7000 sample was modified with 4-benzenediazonium sulfonate at 50 °C.

3.3. Characterization of the Samples

Quantitative C, H, N, and S elemental analysis (EA) of the samples was performed using a Flash 2000 analyzer. Ash was established as the residue after thermogravimetric (TG) analysis was performed in an air atmosphere. A potentiometric back titration method was used to determine the total acidity of the materials (i.e., the total number of Brønsted acid sites; A_{tot}). For this purpose, ~ 0.1 g of the sample was mixed with 50 mL of a 0.01 M NaOH solution for 20 h at ambient temperature. Afterward, the carbon was filtered, and 20 mL of the filtrate was titrated with 0.05 M HCl using a CerkoLab microtitrator. High-resolution transmission electron microscopy (HRTEM) using an FEI Tecnai G2 20 X-TWIN apparatus was applied to study the morphology of the samples. Selected CNT samples were also investigated with a ZEISS EVO 40 scanning electron microscope (SEM). The textural properties of the prepared materials were analyzed by performing N_2 adsorption/desorption measurements at -196 °C with Quantachrome Autosorb IQ equipment. The specific surface areas (S_{BET}) of samples were calculated using the BET equation, while the t-plot method was applied to establish the micropore volumes (V_{μ}) and external surface areas of carbons (S_{ext}). The total pore volumes (V_{tot}) of CNTs were measured from the amount of N_2 adsorbed at a relative pressure close to 1. Thermogravimetric (TG) analysis was performed using a Setaram Setsys 1200 thermal analyzer. The measurements were carried out in air or nitrogen flow and the temperature range of 20 °C–1000 °C (heating rate of 10 °C/min). X-ray photoelectron spectroscopy (XPS) studies were performed using a SPECS UHV multichamber analytical system. In turn, Raman spectra were obtained by applying a Renishaw InVia Reflex confocal Raman spectrometer equipped with an argon laser as an excitation source ($\lambda = 514$ nm, $P = 1$ mW).

3.4. Catalytic Measurements

The functionalized CNTs were tested as catalysts in the etherification of glycerol (G) with tert-butyl alcohol (TBA) under autogenous pressure. In each run, 10.2 g of glycerol and 42 mL of TBA (G:TBA molar ratio of 1:4) were transferred into a stainless-steel autoclave and stirred for complete homogenization. Afterward, catalyst (5, 2.5, or 1 wt.% based on the glycerol weight) was added to the mixture, and the reactor was sealed and flushed with Ar. The catalytic testing was performed at 90, 110, or 120 °C for 24 h. To monitor the progress of the reaction, aliquots of the reaction mixture were periodically taken out (after 1, 2, 4, 6, and 24 h), diluted with isopropanol, and analyzed using a SRI 8610C gas chromatograph equipped with a RESTEK MXT[®]—WAX capillary column (30 m \times 0.25 mm \times 0.25 μ m), a split injector, and FID detector. The catalytic activity of the samples was expressed as the conversion of glycerol (X_G) and yields of individual reaction products (i.e., mono-, di-, and tri-tertbutyl glycerol ethers; MTBGEs, DTBGEs, and TTBGE, respectively). Reusability tests were also performed on selected samples. For this purpose, the spent catalyst was recovered from the reaction mixture by filtration, washed with hot distilled water, then acetone, and dried. After sieving, the catalyst was re-used under standard reaction conditions. The catalyst regeneration was performed by mixing

the sample with a 5% HCl solution for 20 h, then washing it with hot distilled water and drying at 110 °C overnight. The reproducibility of all catalytic tests was very high, and the standard deviations calculated for glycerol conversions and ether yields were lower than 1.5%.

4. Conclusions

A facile method of obtaining highly active solid acid CNTs was proposed using 4-benzenediazonium sulfonate generated in situ. This strategy introduced significant amounts of $-SO_3H$ species onto the surface of CNTs, leading to a significant increase in the total acidity (A_{tot}) of these catalysts. It was demonstrated for the first time that the functionalization of chemically stable CNTs can be facilitated by a simple pretreatment of the sample using ball-milling, which fragmented the agglomerates and resulted in a generation of new “active” edges susceptible to functionalization. Moreover, the functionalization of CNTs with BDS was favored at higher temperatures, resulting in the introduction of higher quantities of sulfur into the materials’ structure. The proposed functionalization method selectively introduced sulfur in the form of sulfonic groups, known to be very active Brønsted acid sites.

The resulting sulfur-doped CNTs were tested in glycerol valorization to substituted ethers. All the prepared samples showed high activity in etherification due to their highly functionalized surface chemistry. The catalytic performances of the most active catalysts (i.e., NC3100-BDS-50 and NC7000-BM-BDS-50) exceed those of the commercial Amberlyst-15 catalyst. Under optimized reaction conditions, a remarkable ~56% glycerol conversion and ~10% yield of DTBGEs+TTBGE was obtained within just 1 h of the reaction. The catalyst acidity induced by the $-SO_3H$ groups was found to be a key factor for the efficient transformation of glycerol to glycerol ethers. Furthermore, the developed BDS-modified CNTs solid acid catalysts showed excellent recyclability, opening up new possibilities for the application of these materials in other acid-catalyzed industrial processes in the future.

Supplementary Materials: The following supporting information can be downloaded at: <https://www.mdpi.com/article/10.3390/molecules29071623/s1>; Figure S1. General scheme of CNTs modification with 4-benzenediazonium sulfonate, indicating some possible surface structures formed [36,37]; Figure S2: SEM images of (A) raw and (B) ball-milled NC7000 sample at different magnifications; Figure S3: The DTG patterns obtained for the raw NC7000 and NC3100 samples under an air gas flow; Figure S4: Reaction scheme of glycerol etherification with tert-butyl alcohol under acidic conditions; Figure S5: The results of the reusability tests performed for NC7000-BM-BDS-50 (temp. = 110 °C, catalyst loading = 5 wt.%, G:TBA molar ratio = 1:4); Figure S6: The results of the reusability tests performed the NC3100-BDS-50 (temp. = 110 °C, catalyst loading = 5 wt.%, G:TBA molar ratio = 1:4).

Author Contributions: Conceptualization, K.P., A.M. and K.M.E.; Methodology, K.P., A.M., K.M.E. and M.K.; Investigation, K.P. and K.M.E.; Data curation, K.P.; Formal analysis, K.P.; Writing—original draft preparation, K.P., A.M. and K.M.E.; Writing—review and editing, K.P., A.M., K.M.E., J.L.F. and M.K.; Supervision, M.K.; Visualization, K.P., A.M. and K.M.E.; Funding acquisition, K.P., K.M.E. and J.L.F. All authors have read and agreed to the published version of the manuscript.

Funding: KP would like to acknowledge the financial support received from ID-UB AMU (doctoral grant no. 017/02/SNŚ/0013). This work was supported by national funds through FCT/MCTES (PIDDAC): LSRE-LCM, UIDB/50020/2020 (DOI: 10.54499/UIDB/50020/2020), and UIDP/50020/2020 (DOI: 10.54499/UIDP/50020/2020); and ALiCE, LA/P/0045/2020 (DOI: 10.54499/LA/P/0045/2020). KME is grateful to FCT for the Junior Researcher grant (#2021.00535.CEECIND).

Institutional Review Board Statement: Not applicable.

Informed Consent Statement: Not applicable.

Data Availability Statement: The data presented in this study are available on request from the corresponding authors.

Conflicts of Interest: The authors declare no conflict of interest. The funders had no role in the design of the study, in the collection, analyses, or interpretation of data, in the writing of the manuscript, or in the decision to publish the results.

References

1. De Volder, M.F.L.; Tawfick, S.H.; Baughman, R.H.; Hart, A.J. Carbon nanotubes: Present and future commercial applications. *Science* **2013**, *339*, 535–539. [CrossRef]
2. Norizan, M.N.; Moklis, M.H.; Demon, S.Z.N.; Halim, N.A.; Samsuri, A.; Mohamad, I.S.; Knight, V.F.; Abdullah, N. Carbon nanotubes: Functionalisation and their application in chemical sensors. *RSC Adv.* **2020**, *10*, 43704–43732. [CrossRef] [PubMed]
3. Jain, N.; Kanu, N.J. The potential application of carbon nanotubes in water Treatment: A state-of-the-art-review. *Mater. Today Proc.* **2021**, *43*, 2998–3005. [CrossRef]
4. Wei, X.; Wang, J.; Ma, H.; Farha, F.I.; Bi, S.; Zhang, Q.; Xu, F. Super-strong CNT composite yarn with tight CNT packing via a compress-stretch process. *Nanoscale* **2022**, *14*, 9078–9085. [CrossRef] [PubMed]
5. Yun, K.; An, G.-H. Surface protection and nucleation enhancement of zinc anode with graphene and doped carbon nanotubes for high-performance energy storage. *Chem. Eng. J.* **2024**, *479*, 147303. [CrossRef]
6. Chen, P.H.; Hsu, C.-F.; Dah-wei Tsai, D.; Lu, Y.-M.; Huang, W.-J. Adsorption of mercury from water by modified multi-walled carbon nanotubes: Adsorption behavior and interference resistance by coexisting anions. *Environ. Technol.* **2014**, *35*, 1935–1944. [CrossRef] [PubMed]
7. Pantarotto, D.; Singh, R.; McCarthy, D.; Erhardt, M.; Briand, J.-P.; Prato, M.; Kostarelos, K.; Bianco, A. Functionalized Carbon Nanotubes for Plasmid DNA Gene Delivery. *Angew. Chem. Int. Ed.* **2004**, *43*, 5242–5246. [CrossRef] [PubMed]
8. Morawa Eblagon, K.; Pereira, M.F.R.; Figueiredo, J.L. One-pot oxidation of cellobiose to gluconic acid. Unprecedented high selectivity on bifunctional gold catalysts over mesoporous carbon by integrated texture and surface chemistry optimization. *Appl. Catal. B* **2016**, *184*, 381–396. [CrossRef]
9. Nowicki, P.; Szymanowski, W.; Pietrzak, R. Textural, surface, thermal and sorption properties of the functionalized activated carbons and carbon nanotubes. *Pol. J. Chem. Technol.* **2015**, *17*, 120–127. [CrossRef]
10. Konwar, L.J.; Mäki-Arvela, P.; Mikkola, J.-P. SO₃H-containing functional carbon materials: Synthesis, structure, and acid catalysis. *Chem. Rev.* **2019**, *119*, 11576–11630. [CrossRef]
11. Wei, Y.; Ling, X.; Zou, L.; Lai, D.; Lu, H.; Xu, Y. A facile approach towards preparation of sulfonated multi-walled carbon nanotubes and their dispersibility in various solvents. *Colloids Surf. A Physicochem. Eng. Asp.* **2015**, *482*, 507–513. [CrossRef]
12. Yu, H.; Jin, Y.; Li, Z.; Peng, F.; Wang, H. Synthesis and characterization of sulfonated single-walled carbon nanotubes and their performance as solid acid catalyst. *J. Solid State Chem.* **2008**, *181*, 432–438. [CrossRef]
13. Ahn, J.-H.; Shin, H.-S.; Kim, Y.-J.; Chung, H. Structural modification of carbon nanotubes by various ball milling. *J. Alloys Compd.* **2007**, *434–435*, 428–432. [CrossRef]
14. Rocha, R.P.; Soares, O.S.G.P.; Figueiredo, J.L.; Pereira, M.F.R. Tuning CNT properties for metal-free environmental catalytic applications. *C* **2016**, *2*, 17. [CrossRef]
15. Rubio, N.; Fabbro, C.; Herrero, M.A.; de la Hoz, A.; Meneghetti, M.; Fierro, J.L.G.; Prato, M.; Vázquez, E. Ball-milling modification of single-walled carbon nanotubes: Purification, cutting, and functionalization. *Nano Micro Small* **2011**, *7*, 665–674. [CrossRef] [PubMed]
16. Thambiliyagodage, C.; Wijesekera, R. Ball milling—A green and sustainable technique for the preparation of titanium based materials from ilmenite. *Curr. Res. Green Sustain. Chem.* **2022**, *5*, 100236. [CrossRef]
17. Liu, Z.Y.; Xu, S.J.; Xiao, B.L.; Xue, P.; Wang, W.G.; Ma, Z.Y. Effect of ball-milling time on mechanical properties of carbon nanotubes reinforced aluminum matrix composites. *Compos. Part A Appl. Sci. Manuf.* **2012**, *43*, 2161–2168. [CrossRef]
18. Pierard, N.; Fonseca, A.; Colomer, J.-F.; Bossuot, C.; Benoit, J.-M.; Van Tendeloo, G.; Pirard, J.-P.; Nagy, J.B. Ball milling effect on the structure of single-wall carbon nanotubes. *Carbon* **2004**, *42*, 1691–1697. [CrossRef]
19. Soares, O.S.G.P.; Gonçalves, A.G.; Delgado, J.J.; Órfão, J.J.M.; Pereira, M.F.R. Modification of carbon nanotubes by ball-milling to be used as ozonation catalysts. *Catal. Today* **2015**, *249*, 199–203. [CrossRef]
20. Gharegozloo, S.; Ataie, A.; Abdizadeh, H.; Mostafavi, E.; Parmian, M.J.; Khodadadi, A.A. High performance Ni-CNTs catalyst: Synthesis and characterization. *RSC Adv.* **2016**, *6*, 47072–47082. [CrossRef]
21. Soares, O.S.G.P.; Rocha, R.P.; Órfão, J.J.M.; Pereira, M.F.R.; Figueiredo, J.L. Mechanochemical approach for N-, S-, P-, and B-doping of carbon nanotubes: Methodology and catalytic performance in wet air oxidation. *C* **2019**, *5*, 30. [CrossRef]
22. Delogu, F.; Gorrasí, G.; Sorrentino, A. Fabrication of polymer nanocomposites via ball milling: Present status and future perspectives. *Prog. Mater. Sci.* **2017**, *86*, 75–126. [CrossRef]
23. Gong, R.; Ma, Z.; Wang, X.; Han, Y.; Guo, Y.; Sun, G.; Li, Y.; Zhou, J. Sulfonic-acid-functionalized carbon fiber from waste newspaper as a recyclable carbon based solid acid catalyst for the hydrolysis of cellulose. *RSC Adv.* **2019**, *9*, 28902. [CrossRef] [PubMed]
24. Ptaszynska, K.; Malaika, A.; Kapska, M.; Kozłowski, M. SO₃H-functionalized carbon fibers for the catalytic transformation of glycerol to glycerol tert-butyl ethers. *Sci. Rep.* **2023**, *13*, 565. [CrossRef] [PubMed]
25. Tamborini, L.H.; Militello, M.P.; Balach, J.; Moyano, J.M.; Barbero, C.A.; Acevedo, D.F. Application of sulfonated nanoporous carbons as acid catalysts for Fischer esterification reactions. *Arab. J. Chem.* **2019**, *12*, 3172–3182. [CrossRef]

26. Goswami, M.; Phukan, P. Enhanced adsorption of cationic dyes using sulfonic acid modified activated carbon. *J. Environ. Chem. Eng.* **2017**, *5*, 3508–3517. [CrossRef]
27. Oliveira, B.L.; Teixeira da Silva, V. Sulfonated carbon nanotubes as catalysts for the conversion of levulinic acid into ethyl levulinate. *Catal. Today* **2014**, *234*, 257–263. [CrossRef]
28. Janudin, N.; Abdullah, L.C.; Abdullah, N.; Md Yasin, F.; Saidi, N.M.; Kasim, N.A.M. Comparison and characterization of acid functionalization of multi walled carbon nanotubes using various methods. *Solid State Phenom.* **2017**, *264*, 83–86. [CrossRef]
29. Estevez, R.; Aguado-Deblas, L.; Luna, D.; Bautista, F.M. An Overview of the production of oxygenated fuel additives by glycerol etherification, either with isobutene or tert-butyl alcohol, over heterogeneous catalysts. *Energies* **2019**, *12*, 2364. [CrossRef]
30. Available online: https://www.tomo-e.co.jp/upload/cProductsJA/25QU033-cProductsJA_content-001.pdf (accessed on 28 February 2024).
31. Koskin, A.P.; Larichev, Y.V.; Mishakov, I.V.; Mel'gunov, M.S.; Vedyagin, A.A. Synthesis and characterization of carbon nanomaterials functionalized by direct treatment with sulfonating agents. *Microporous Mesoporous Mater.* **2020**, *299*, 110130. [CrossRef]
32. Ptaszyńska, K.; Morawa Eblagon, K.; Malaika, A.; Figueiredo, J.L.; Kozłowski, M. The role of mechano-chemical treatment of carbon nanotubes in promoting glycerol etherification. *submitted for publication. Catal. Sci. Technol.* **2024**.
33. Rechnia-Goraćy, P.; Malaika, A.; Kozłowski, M. Acidic activated carbons as catalysts of biodiesel formation. *Diam. Relat. Mater.* **2018**, *87*, 124–133. [CrossRef]
34. Rechnia, P.; Malaika, A.; Kozłowski, M. Synthesis of tert-amyl methyl ether (TAME) over modified activated carbon catalysts. *Fuel* **2015**, *154*, 338–345. [CrossRef]
35. Betelu, S.; Tijunelyte, I.; Boubekur-Lecaque, L.; Ignatiadis, I.; Ibrahim, J.; Gaboreau, S.; Berho, C.; Toury, T.; Guenin, E.; Lidgi-Guigui, N.; et al. Evidence of the grafting mechanisms of diazonium salts on gold nanostructures. *J. Phys. Chem. C* **2016**, *120*, 18158–18166. [CrossRef]
36. Sandomierski, M.; Voelkel, A. Diazonium modification of inorganic and organic fillers for the design of robust composites: A review. *J. Inorg. Organomet. Polym. Mater.* **2021**, *31*, 1–21. [CrossRef]
37. Toupin, M.; Belanger, D. Spontaneous functionalization of carbon black by reaction with 4-nitrophenyldiazonium cations. *Langmuir* **2008**, *24*, 1910–1917. [CrossRef] [PubMed]
38. Zolfaghari, Z.; Tavasoli, A.; Tabyar, S.; Pour, A.N. Enhancement of bimetallic Fe-Mn/CNTs nano catalyst activity and product selectivity using microemulsion technique. *J. Energy Chem.* **2014**, *23*, 57–65. [CrossRef]
39. Gomes, M.; Gomes, L.C.; Teixeira-Santos, R.; Pereira, M.F.R.; Soares, O.S.G.P.; Mergulhão, F.J. Optimizing CNT loading in antimicrobial composites for urinary tract application. *Appl. Sci.* **2021**, *11*, 4038. [CrossRef]
40. Guo, Z.; Zhong, S.; Cao, M.; Zhong, Z.; Xiao, Q.; Huang, J.; Chen, J. High-temperature-annealed multi-walled carbon nanotubes as high-performance conductive agents for LiNi_{0.5}Co_{0.2}Mn_{0.3}O₂ lithium-ion batteries. *Metals* **2023**, *13*, 36. [CrossRef]
41. White, C.M.; Banks, R.; Hamerton, I.; Watts, J.F. Characterisation of commercially CVD grown multi-walled carbonnanotubes for paint applications. *Prog. Org. Coat.* **2016**, *90*, 44–53. [CrossRef]
42. Salvetat, J.-P.; Bonard, J.-M.; Thomson, N.H.; Kulik, A.J.; Forró, L.; Benoit, W.; Zuppiroli, L. Mechanical properties of carbon nanotubes. *Appl. Phys. A* **1999**, *69*, 255–260. [CrossRef]
43. Rebelo, S.L.H.; Guedes, A.; Szeferczyk, M.E.; Pereira, A.M.; Araújo, J.P.; Freire, C. Progresses on the Raman spectra analysis of covalently functionalized multiwall carbon nanotubes: Unraveling disorder on graphitic materials. *Phys. Chem. Chem. Phys.* **2016**, *18*, 12784–12796. [CrossRef]
44. Wang, C.; Xu, J.; Yang, J.; Qian, Y.; Liu, H. In-situ polymerization and multifunctional properties of surface-modified multiwalled carbon nanotube-reinforced polyimide nanocomposites. *High Perform. Polym.* **2016**, *29*, 797–807. [CrossRef]
45. Liu, H.; Wang, J.; Wang, J.; Cui, S. Sulfonitric treatment of multiwalled carbon nanotubes and their dispersibility in water. *Materials* **2018**, *11*, 2442. [CrossRef] [PubMed]
46. Ge, Y.; Li, Z.; Xiao, D.; Xiong, P.; Ye, N. Sulfonated multi-walled carbon nanotubes for the removal of copper (II) from aqueous solutions. *J. Ind. Eng. Chem.* **2014**, *20*, 1765–1771. [CrossRef]
47. Li, F.; Lu, Y.; Liu, L.; Zhang, L.; Dai, J.; Ma, J. Relations between carbon nanotubes' length and their composites' mechanical and functional performance. *Polymer* **2013**, *54*, 2158–2165. [CrossRef]
48. Chebattina, K.R.R.; Srinivas, V.; Rao, N.M. Effect of size of multiwalled carbon nanotubes dispersed in gear oils for improvement of tribological properties. *Adv. Tribol.* **2018**, *2018*, 2328108. [CrossRef]
49. Abdel-Ghani, N.T.; El-Chaghaby, G.A.; Helal, F.S. Individual and competitive adsorption of phenol and nickel onto multiwalled carbon nanotubes. *J. Adv. Res.* **2015**, *6*, 405–415. [CrossRef] [PubMed]
50. Kumar, N.; Yu, Y.-C.; Lu, Y.H.; Tseng, T.Y. Fabrication of carbon nanotube/cobalt oxide nanocomposites via electrophoretic deposition for supercapacitor electrodes. *J. Mater. Sci.* **2016**, *51*, 2320–2329. [CrossRef]
51. Liu, X.-Y.; Huang, M.; Ma, H.-L.; Zhang, Z.-Q.; Gao, J.-M.; Zhu, Y.-L.; Han, X.-J.; Guo, X.-Y. Preparation of a carbon-based solid acid catalyst by sulfonating activated carbon in a chemical reduction process. *Molecules* **2010**, *15*, 7188–7196. [CrossRef]
52. Knyazheva, O.A.; Kokhanovskaya, O.A.; Vasilevich, A.V.; Trenikhin, M.V.; Bukhtiyarov, A.V.; Arbuzov, A.B.; Baklanova, O.N.; Lavrenov, A.V. Thermal stability of sulfonated carbon black. *Thermochim. Acta* **2023**, *728*, 179593. [CrossRef]
53. Figueiredo, J.L.; Pereira, M.F.R.; Freitas, M.M.A.; Órfão, J.J.M. Modification of the surface chemistry of activated carbons. *Carbon* **1999**, *37*, 1379–1389. [CrossRef]

54. Gan, L.; Zhu, J.; Lv, L. Cellulose hydrolysis catalyzed by highly acidic lignin-derived carbonaceous catalyst synthesized via hydrothermal carbonization. *Cellulose* **2017**, *24*, 5327–5339. [[CrossRef](#)]
55. Morawa Eblagon, K.; Malaika, A.; Ptaszyńska, K.; Pereira, M.F.R.; Kozłowski, M.; Figueiredo, J.L. Niobium oxide-phosphorylated carbon xerogel composites as solid acid catalysts for cascade conversion of glucose to 5-hydroxymethylfurfural (HMF) in pure water. *Catal. Today* **2023**, *418*, 114070. [[CrossRef](#)]
56. Yuan, S.; Tan, Z. Effect and mechanism of changes in physical structure and chemical composition of new biochar on Cu(II) adsorption in an aqueous solution. *Soil Ecol. Lett.* **2022**, *4*, 237–253. [[CrossRef](#)]
57. Gonçalves, M.; Souza, V.C.; Galhardo, T.S.; Mantovani, M.; Figueiredo, F.C.A.; Mandelli, D.; Carvalho, W.A. Glycerol conversion catalyzed by carbons prepared from agroindustrial wastes. *Ind. Eng. Chem. Res.* **2013**, *52*, 2832–2839. [[CrossRef](#)]
58. Estevez, R.; López, M.I.; Jiménez-Sanchidrián, C.; Luna, D.; Romero-Salguero, F.J.; Bautista, F.M. Etherification of glycerol with tert-butyl alcohol over sulfonated hybrid silicas. *Appl. Catal. A Gen.* **2016**, *526*, 155–163. [[CrossRef](#)]
59. Miranda, C.; Ramírez, A.; Sachse, A.; Pouilloux, Y.; Urresta, J.; Pinard, L. Sulfonated graphenes: Efficient solid acid catalyst for the glycerol valorization. *Appl. Catal. A Gen.* **2019**, *580*, 167–177. [[CrossRef](#)]
60. Klepáčová, K.; Mravec, D.; Hájeková, E.; Bajus, M. Etherification of glycerol. *Petrol. Coal.* **2003**, *45*, 54–57.
61. Carvalho, W.A.; Galhardo, T.S.; Simone, N.; Gonçalves, M.; Figueiredo, F.; Mandelli, D. Preparation of sulfonated carbons from rice husk and their application in catalytic conversion of glycerol. *ACS Sustain. Chem. Eng.* **2013**, *1*, 1381–1389.
62. Fraile, J.M.; García-Bordejé, E.; Roldán, L. Deactivation of sulfonated hydrothermal carbons in the presence of alcohols: Evidences for sulfonic esters formation. *J. Catal.* **2012**, *289*, 73–79. [[CrossRef](#)]

Disclaimer/Publisher’s Note: The statements, opinions and data contained in all publications are solely those of the individual author(s) and contributor(s) and not of MDPI and/or the editor(s). MDPI and/or the editor(s) disclaim responsibility for any injury to people or property resulting from any ideas, methods, instructions or products referred to in the content.

Supplementary Materials

Promoting Effect of Ball Milling on the Functionalization and Catalytic Performance of Carbon Nanotubes in Glycerol Etherification

Karolina Ptaszyńska^{1,*}, Anna Malaika¹, Katarzyna Morawa Eblagon^{2,3}, José Luís Figueiredo^{2,3} and Mieczysław Kozłowski^{1,*}

- ¹ Faculty of Chemistry, Adam Mickiewicz University in Poznań, Uniwersytetu Poznańskiego 8, 61-614 Poznań, Poland; amalaika@amu.edu.pl (A.M.)
² LSRE-LCM—Laboratory of Separation and Reaction Engineering—Laboratory of Catalysis and Materials, Faculty of Engineering, University of Porto, Rua Dr. Roberto Frias, 4200-465 Porto, Portugal; keblagon@fe.up.pt (K.M.E.); jlfig@fe.up.pt (J.L.F.)
³ ALiCE—Associate Laboratory in Chemical Engineering, Faculty of Engineering, University of Porto, Rua Dr. Roberto Frias, 4200-465 Porto, Portugal
* Correspondence: karolina.ptaszynska@amu.edu.pl (K.P.); mkozlow@amu.edu.pl (M.K.).

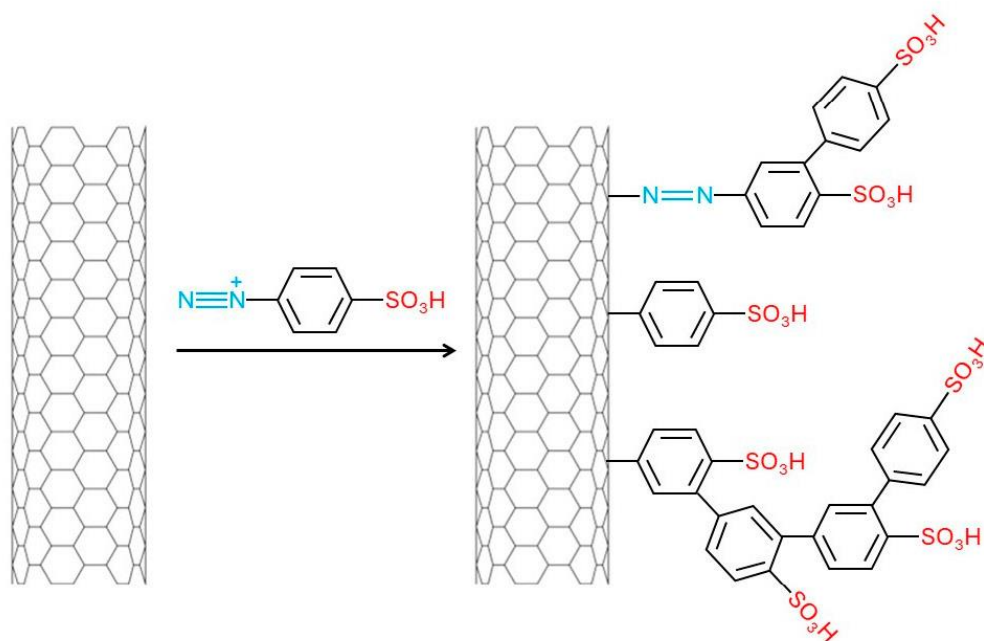


Figure S1. General scheme of CNTs modification with 4-benzenediazonium sulfonate, indicating some possible surface structures formed (based on [36,37]).

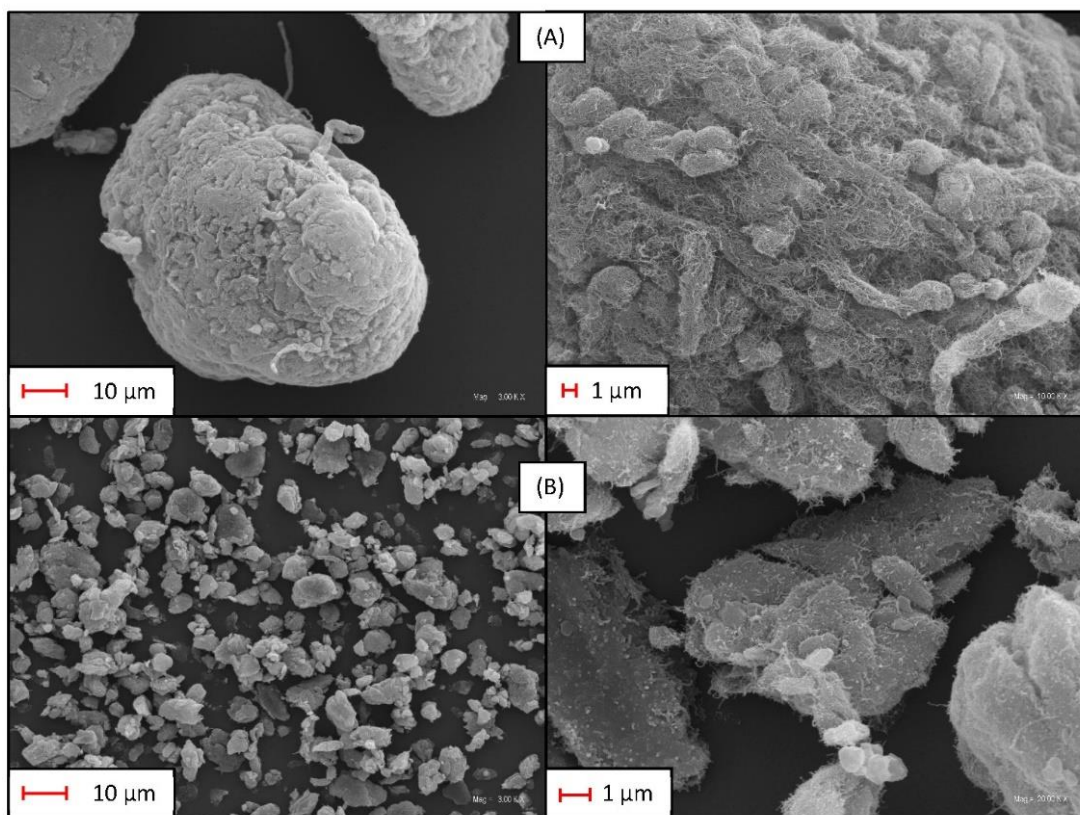


Figure S2. SEM images of (A) as-received and (B) ball-milled NC7000 samples at different magnifications.

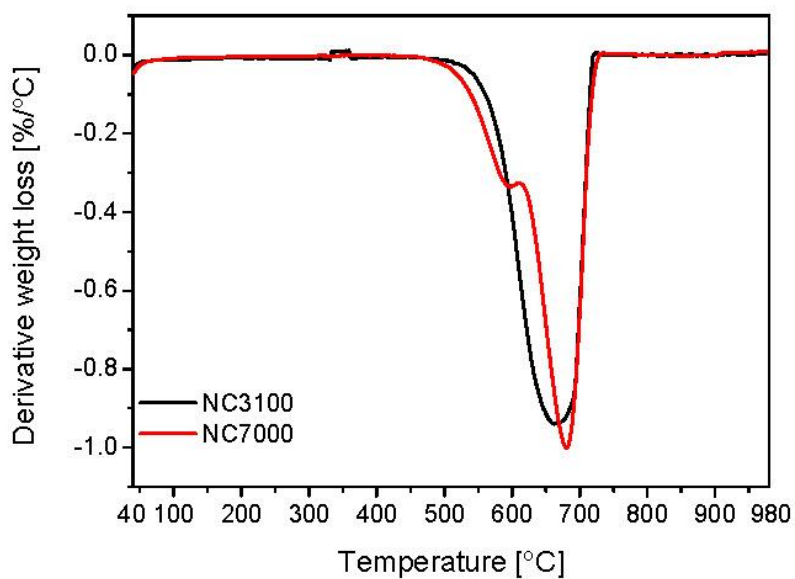


Figure S3. The DTG patterns obtained for the raw NC7000 and NC3100 samples under an air gas flow.

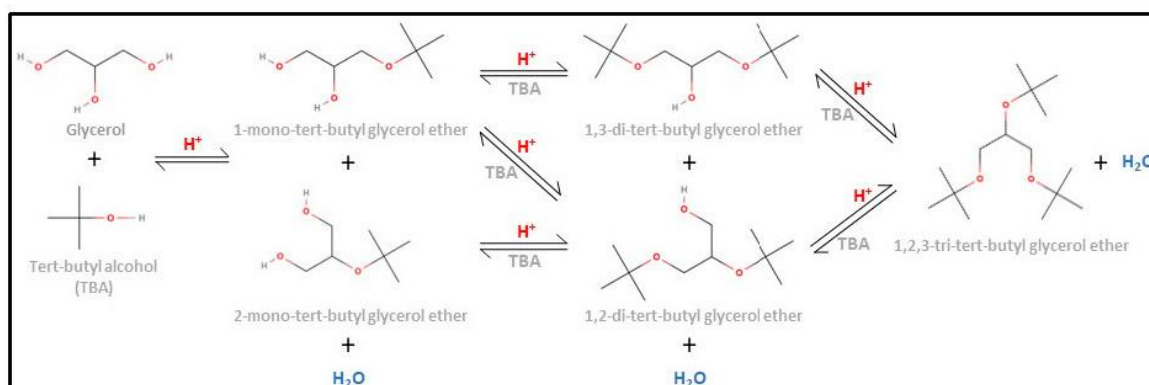


Figure S4. Reaction scheme of glycerol etherification with tert-butyl alcohol under acidic conditions.

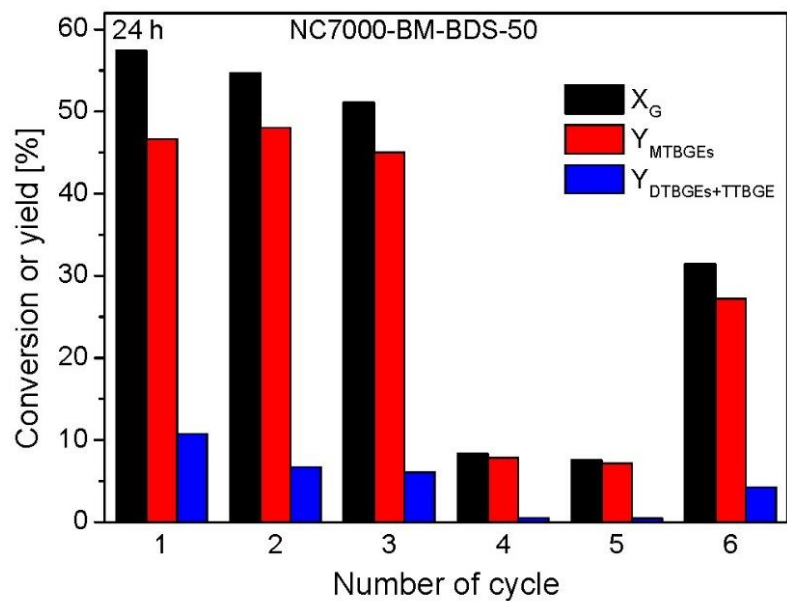


Figure S5. The results of the reusability tests performed for the NC7000-BM-BDS-50 (temp. = 110 °C, catalyst loading = 5 wt.%, G:TBA molar ratio = 1:4).

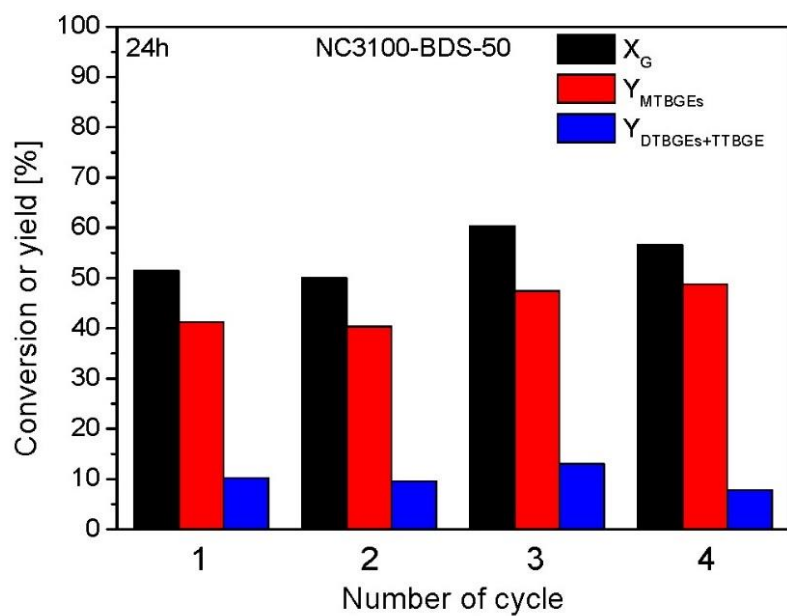


Figure S6. The results of the reusability tests performed for the NC3100-BDS-50 (temp. = 110 °C, catalyst loading = 5 wt.%, G:TBA molar ratio = 1:4).

P5

Cite this: *Catal. Sci. Technol.*, 2024,
14, 3184

The role of mechanochemical treatment of carbon nanotubes in promoting glycerol etherification

Karolina Ptaszyńska,^a Katarzyna Morawa Eblagon,^{a,b,c} Anna Malaika,^a
José Luís Figueiredo^{b,c} and Mieczysław Kozłowski^a

High-purity and technical-grade carbon nanotubes (CNTs) were functionalized and compared, for the first time applying various mechanochemical methods to endow their surfaces with strongly acidic features. The as-prepared samples were used as catalysts in glycerol etherification performed with *tert*-butyl alcohol at 110 °C under autogenous pressure, converting glycerol to glycerol *tert*-butyl ethers, *i.e.*, important fuel additives, in a green way. The best-performing catalyst was the CNT sample ball-milled with glucose and hydrothermally treated with fuming H₂SO₄, which showed a 52.4% glycerol conversion just after 6 h. The catalytic performance of the sample was ascribed to its improved functionalization when using glucose which worked as a “binding agent” for the active functional groups, facilitating the grafting of the –SO₃H sites on the CNT surface in a relatively short time and at a low temperature of modification. Furthermore, it was found that acidic oxygen functionalities, co-introduced with sulfonic groups during the modification, cooperated with –SO₃H sites and jointly worked to enhance the CNT activity in glycerol etherification. Finally, it was shown that adequately tailored technical-grade CNTs could act as promising and much cheaper solid acids than functionalized expensive high-purity CNTs typically used for industrial applications.

Received 14th February 2024,
Accepted 22nd April 2024

DOI: 10.1039/d4cy00203b

rsc.li/catalysis

1. Introduction

The co-production of huge amounts of glycerol (G) by the continuously developing biodiesel industry underlines the urge to develop suitable valorization methods for this side product.^{1,2} Furthermore, glycerol has tremendous potential to be transformed into valuable derivatives with a wide spectrum of practical applications.³

One of the most important glycerol derivatives are *tert*-butyl glycerol ethers (TBGEs), available in mono-, di- and tri-substituted forms (MTBGEs, DTBGEs, and TTBGE, respectively), of particular significance to the fuel sector. It was found that DTBGEs and TTBGE can be directly mixed with gasoline, diesel, or biodiesel and used as environmentally friendly fuel oxygenates or performance enhancers.^{4–6} MTBGEs were also confirmed to be useful as gasoline boosters; however, due to their poor miscibility with hydrocarbons, they often need to be converted into the

appropriate derivatives or mixed with higher-substituted *tert*-butyl glycerol ethers.^{5,7} It is also worth noting that TBGEs are considered sustainable substitutes for methyl *tert*-butyl ether (MTBE), which has been restricted in some countries for ecological and economic reasons.^{4,8}

Typically, *tert*-butyl glycerol ethers are obtained in the reaction between glycerol and *tert*-butyl alcohol (TBA) or isobutene (IB) using strong Brønsted acid catalysts, preferably heterogeneous ones.^{4,5} TBA as an etherifying agent is recommended as IB requires a costly approach, enabling mixing the gas with glycerol. In addition, IB can undergo troublesome oligomerization.⁶ Detailed comparison of the mechanisms of glycerol etherification with various solvents, including alcohols and olefins, and under solvent-free conditions can be found elsewhere.⁹ Moreover, an interesting summary of the different catalytic systems developed in recent years for glycerol etherification has been recently published.¹⁰

Strongly acidic ion exchange resins have been the most extensively studied catalysts for glycerol etherification.^{11–13} For example, Roze *et al.*¹¹ performed glycerol etherification with TBA at 83 °C using Amberlyst-15 and obtained a total yield of ethers of 21% within 2 h. Frusteri *et al.*¹² reported a high glycerol conversion of over 90% and a combined yield of DTBGEs and TTBGE of about 28% after 6 h of the reaction at 70 °C. In turn, Gonçalves *et al.*¹³ showed that using

^a Faculty of Chemistry, Adam Mickiewicz University in Poznań, Uniwersytetu
Poznańskiego 8, 61-614 Poznań, Poland. E-mail: karolina.ptaszynska@amu.edu.pl^b LSRE-LCM - Laboratory of Separation and Reaction Engineering - Laboratory of
Catalysis and Materials, Faculty of Engineering, University of Porto, Rua Dr.
Roberto Frias, 4200-465 Porto, Portugal. E-mail: keblagon@fe.up.pt^c ALiCE - Associate Laboratory in Chemical Engineering, Faculty of Engineering,
University of Porto, Rua Dr. Roberto Frias, 4200-465 Porto, Portugal

Amberlyst-15 at 120 °C for 4 h could result in only a 12% combined yield of DTBGEs + TTBGE. This reduced activity of the Amberlyst-15 catalyst under the used conditions was probably due to its low thermal stability (maximum operating temperature of 120 °C, according to the manufacturer's data).¹⁴ Importantly, the application of Amberlyst-15 in glycerol etherification is strongly restricted not only by its low thermal stability but also by high moisture sensitivity, as water is co-produced in this reaction.¹¹

On the other hand, appropriately functionalized carbon catalysts can be promising alternative solids, especially for glycerol etherification.^{15–17} For example, Gonçalves *et al.*¹⁶ showed that sulfonated black carbons from coffee ground wastes yielded 20% DTBGEs + TTBGE within 5 h of the reaction between glycerol and TBA. Furthermore, the catalyst exhibited high stability of active sites, which enabled its reuse. Galhardo *et al.*¹⁷ used sulfonated carbons from rice husk to convert glycerol with TBA and achieved a 53% glycerol conversion and selectivity to di- and tri-substituted products of 25% within 4 h. In turn, our previous studies showed that glucose-derived hydrothermal carbon could give a 54% conversion of glycerol and ~10% yield of DTBGEs + TTBGE within 1 h.¹⁸

Carbon nanotubes (CNTs) are one of the most important classes of carbon materials, showing such features as low toxicity, enhanced conductivity, ultimate tensile strength, thermal and chemical stability, and the possibility of functionalization. These unique properties make them perfect candidates for application in different branches, *e.g.*, in medicine, electronics, producing sports goods, energy storage, *etc.*^{19–21} Interestingly, particularly promising applications of CNTs relate to heterogeneous catalysis, where CNTs can be used as super-efficient catalysts or as support for active phases.^{22,23} It is noted that apart from our recently published pioneering work, focussing on carbon nanotubes functionalized with 4-benzene diazonium sulfonate (BDS),²⁴ there are no reports in the literature dealing with the application of sulfonated CNTs in the etherification of glycerol with *tert*-butyl alcohol (TBA). Our results showed that the BDS-functionalized CNTs were very active in glycerol etherification at 120 °C, reaching ~56% glycerol conversion and ~10% yield of higher-substituted ethers, using a low catalyst loading of only 2.5 wt%. These promising catalytic results were attributed to the high concentration of sulfonic groups present in the catalyst, and improved substrate access to the active sites due to fragmentation of CNT aggregates. In addition, sulfonated CNTs showed great performance in many other acid-catalyzed reactions. For example, Yee *et al.* reported outstanding catalytic results of sulfonated CNTs in etherification of TBA with ethanol, reaching 64% conversion and 68% selectivity to ethyl *tert*-butyl ether (ETBE). The results obtained were comparable to or even better than the ones reported using other heterogeneous catalysts. In addition, the authors reported excellent recyclability, of the sulfonated CNT catalysts.²⁵ On the other hand, Yu *et al.* applied sulfonated single-wall carbon nanotubes (SWCNTs)

in the esterification of acetic acid to ethyl acetate. They obtained twofold higher activity than sulfonated activated carbons.²⁶ In turn, Guan *et al.*²² obtained 97% biodiesel yield in the transesterification of trilaurin with ethanol using sulfonated CNTs. Importantly, the best catalysts showed comparable performance to that of a typically used and efficient homogeneous catalyst, *i.e.*, H₂SO₄. In contrast, Liu *et al.* showed that composite materials (CNT-P-SO₃H) obtained by covalent grafting of CNTs with sulfonic acid-functionalized polymers (P-SO₃H) presented outstanding catalytic activity in the production of fatty acid methyl ester.²⁷ Importantly, due to the constant development of the carbon nanotube market, manufacturing costs of CNTs have been declining over the years,²⁸ providing an opportunity for the practical use of such materials in industry.

Various modification approaches have been studied to endow CNTs with strongly acidic features required for acid-catalyzed reactions such as glycerol etherification among others. The covalent functionalization of CNTs *via* forming a strong linkage between the nanotube surface and a modifying molecule was found to be one of the most commonly applied strategies. This method typically uses concentrated sulfuric acid that reacts with CNTs at high temperatures to produce CNT-SO₃H with a significant density of sulfonic groups.^{29–31} However, despite these harsh reaction conditions, the degree of CNT functionalization obtained in this technique is typically much lower than that observed for other types of carbons treated with H₂SO₄. This is due to the rather inert and rigid structure of carbon nanotubes resistant to modifications.^{31,32} Diverse options have been tested to “activate” CNTs for functionalization. For example, Rocha *et al.*³³ demonstrated a convenient solvent-free approach for the pretreatment of CNTs *via* ball milling (BM) as the method enabling the shortening and opening of the CNT caps and thus making CNTs more prone to functionalization. The authors showed that using the BM approach for a CNT/melamine mixture before its heating resulted in the introduction of significantly higher amounts of N into the CNTs compared to the modification excluding the BM step. The easy BM method also allowed the introduction of large concentrations of heteroatoms such as N, S, B, or P into CNTs as found by Soares *et al.*³⁴ A very interesting method for CNT functionalization could also be a non-covalent approach involving the formation of CNT-polymer composites.³⁵ For example, Ji *et al.*³⁶ pyrolyzed glucose and taurine in the presence of CNTs to successfully deposit functional groups on the used nanotubes.

The current study investigates various methods of CNT functionalization with -SO₃H groups, for the first time considering the effect of different mechanochemical approaches on the physico-chemical features of the modified carbon nanotubes. The results shed new light on the facile possibilities of obtaining CNTs with an enhanced degree of functionalization. Furthermore, this work is important from a practical point of view, as it uses the obtained CNT samples for producing glycerol *tert*-butyl ethers, *i.e.*, important fuel

enhancers, *via* a green synthesis route. The influence of the surface chemistry of CNTs on their catalytic performances as solid acids in glycerol etherification was established. Finally, it was demonstrated that technical-grade CNTs could be a promising alternative to expensive high-purity carbon nanotubes in the tested reaction.

2. Experimental part

2.1. Preparation of the samples

Two types of commercial multi-walled CNTs differing in their purity, and thus their price, were used in this work, namely Nanocyl NC3100 (purity of over 95%, labeled here as CNT_{NC3100}) and Nanocyl NC7000 (purity of over 90%, labeled here as CNT_{NC7000}). These raw materials were used as purchased. Additionally, in order to “open” the sample structure, CNT_{NC7000} was subjected to mechanical treatment through ball-milling using a Retsch MM200 ball mill equipped with zirconium oxide milling balls ($t = 20$ min, frequency = 25 vibrations per s). The as-prepared material was labeled as CNT_{NC7000-BM}. The raw and ball-milled CNTs were further modified using different functionalization protocols. Details of these procedures can be found below.

2.1.1. Modification with concentrated sulfuric acid. Modification of the CNTs with concentrated sulfuric acid (H₂SO₄(conc.)) was performed in a three-neck round-bottom flask equipped with a magnetic stirrer and a condenser. In each case, 1 g of CNTs and 100 cm³ of concentrated H₂SO₄ were mixed and heated to 180 °C under an argon flow for 20 h. After the functionalization, the mixture was cooled, diluted with distilled water, and filtered. The obtained functionalized CNTs were then washed thoroughly with hot distilled water until a neutral pH of the filtrate was obtained. Finally, the material was dried at 110 °C overnight and sieved to a uniform particle size of ≤0.4 mm.

2.1.2. Functionalization with fuming sulfuric acid. 1 g of CNT_{NC7000-BM} was mixed under ultrasonic conditions with 20 cm³ of fuming H₂SO₄ (H₂SO₄(fum.)) for 0.5 h. The mixture was then transferred into a Teflon-lined autoclave and heated at 100 °C under self-generating pressure for 8 h. After finishing the process, the reactor was cooled to room temperature, and the mixture was diluted with distilled water. Subsequently, the material was recovered by filtration and washed thoroughly with hot distilled water, followed by ethanol. Finally, the sample was dried in a laboratory oven at 110 °C overnight and sieved to a particle size of ≤0.4 mm.

2.1.3. Glucose-aided functionalization with sulfuric acid. CNTs were modified with H₂SO₄ and glucose using different variants. In the first option, 1 g of CNT_{NC7000} was ball-milled with 4 g of glucose (Glu) using a Retsch MM200 ball mill ($t = 20$ min, frequency = 25 vibrations per s) to ensure complete homogenization. Next, the obtained sample was mixed with 20 cm³ of fuming sulfuric acid (H₂SO₄(fum.)) and heated in a Teflon-lined stainless steel autoclave at 180 °C under self-generated pressure for 12 h.

In the second method, 1.5 g of glucose was mixed in a glass vial with 5 cm³ of 5 M H₂SO₄ (H₂SO₄(5 M)) under ultrasonic conditions. When the mixture was homogenized, 0.5 g of ball-milled CNTs was slowly added. Finally, the vial was heated in an Anton Paar Monowave 200 microwave oven at 150 °C under self-generated pressure for 4 h.

In both functionalization approaches, the final mixtures were diluted with water, and the prepared samples were recovered by filtration and repeatedly washed with hot distilled water and ethanol. Afterward, the samples were dried at 110 °C overnight and sieved to a particle size of ≤0.4 mm.

All the functionalized CNTs were labeled according to the scheme: CNT type – modifying agent type – modification temperature – treatment time, e.g., CNT_{NC7000-BM}-Glu/H₂SO₄(fum.)-180-12h refers to ball-milled CNT_{NC7000} modified with fuming sulfuric acid in the presence of glucose at 180 °C for 12 h.

2.2. Characterization of the samples

Quantitative elemental analysis (EA) of the samples was performed using a Flash 2000 analyzer, and the ash content was determined by weighing the residue after combustion. Nitrogen adsorption/desorption measurements were performed at -196 °C with a Quantachrome Autosorb IQ apparatus and used to determine the textural properties of the samples. The specific surface areas (S_{BET}) of CNTs were calculated from the BET equation, whereas the micropore volumes (V_{p}) and the external surface areas (S_{ext}) were determined by the t -plot method. In turn, the total volumes of pores (V_{tot}) were measured from the amount of N₂ adsorbed at a relative pressure close to unity. The morphology of the samples was studied with a ZEISS EVO 40 scanning electron microscope. The total acidity of the materials was determined by means of a potentiometric back titration method with a CerkoLab microtitrator. Briefly, ~100 mg of the sample was mixed with 50 cm³ of a 0.01 M NaOH solution and shaken for 20 h at room temperature. Finally, the carbon was filtered out, and the filtrate (20 cm³) was titrated using a 0.05 M HCl solution. A blank test was also performed. Thermogravimetric (TG) analysis was carried out with a Setaram Setsys 1200 thermal analyzer under a nitrogen or air flow (heating rate of 10 °C min⁻¹). X-ray diffraction (XRD) measurements were performed using a Bruker AXS D8 Advance diffractometer. In turn, X-ray photoelectron spectroscopy (XPS) studies were done using a Specs UHV multichamber analytical system. All the spectra were calibrated by the C 1s peak centered at 284.5 eV, and CasaXPS (version 2.3.19PR1.0) was used for the spectra deconvolution.

2.3. Catalytic measurements

Glycerol etherification was performed in a stainless-steel autoclave equipped with a magnetic stirrer, a thermocouple, and a sampling system. In each case, 10.2 g of glycerol (G)

and 42 cm³ of *tert*-butyl alcohol (TBA; TBA:G molar ratio of 4:1) were introduced into the reactor and stirred to ensure complete homogenization. Afterward, 0.5 g of a catalyst (~5 wt% based on the glycerol weight) was added to the system. After sealing the autoclave, the reactor was flushed with argon several times and heated to 110 °C. During the process, aliquots of the reaction mixture were taken at various time intervals (*i.e.*, 1, 2, 4, 6, and 24 h) and analyzed using a gas chromatograph (SRI 8610C) equipped with a RESTEK MXT®—WAX capillary column (30 m × 0.25 mm × 0.25 μm), split injector, and a FID detector. The catalytic performances of the samples were expressed as conversions of glycerol (X_G), yields of products (*i.e.*, Y_{MTBGEs} , $Y_{DTBGEs+TTBGE}$), or selectivities to glycerol *tert*-butyl ethers (*i.e.*, S_{MTBGEs} , $S_{DTBGEs+TTBGE}$). Samples of the reaction mixture were diluted in isopropanol and analyzed using a gas chromatograph (SRI 8610C) equipped with a RESTEK MXT®—WAX capillary column (30 m × 0.25 mm × 0.25 μm) and a flame ionization detector (FID) working at a temperature of 210 °C, powered by hydrogen (25 cm³ min⁻¹) and air (270 cm³ min⁻¹). Helium was used as the carrier gas (1 cm³ min⁻¹), and the sample was injected using a split injector with a split ratio of 30, at $T = 230$ °C. The details of the GC analysis can be found in our previous work.³⁷

The stability of a selected CNT sample was tested in subsequent catalytic runs. For this purpose, carbon was recovered from the reaction mixture by filtration, washed with hot distilled water, and then with acetone. Afterward, it was dried at 110 °C overnight, sieved, and reused. A catalyst regeneration procedure was also applied. It was performed by mixing the spent catalyst with a 5% HCl solution at ambient temperature for 20 h, washing it with hot distilled water, and drying.

3. Results and discussion

3.1. Characterization of the samples

Table 1 presents the results of elemental analysis, total acidity measurements, and the determination of the $-SO_3H$ group contents obtained for the CNT-based samples. As can be seen, both types of raw carbon nanotubes, *i.e.*, CNT_{NC3100} and CNT_{NC7000}, consisted mainly of carbon; however, the

content of this element was different (~98% *vs.* 88%) depending on the CNTs purity. The amounts of heteroatoms, such as oxygen, were negligible, and the samples did not contain sulfur. On the other hand, the ash content observed for CNT_{NC7000} was quite high (about 10.2%). It was most probably related to the presence of a metal catalyst applied in the production process of CNTs, *i.e.*, the CCVD reaction (catalytic chemical vapor deposition, according to the producer's declaration).³⁸ No ash was detected for CNT_{NC3100}, suggesting thorough sample purification after the synthesis.³⁹ The obtained values of the ash contents obtained for CNT_{NC3100} and CNT_{NC7000} are in accordance with the manufacturer's data.^{38,39}

It was reported in the literature that ball-milling can introduce large amounts of oxygen functionalities to the surface of carbon xerogels.⁴⁰ However, in our case, the results from EA for the ball-milled carbon nanotubes (*i.e.*, CNT_{NC7000-BM} carbon) were comparable to those achieved for the untreated sample (*i.e.*, CNT_{NC7000}), suggesting that this mechanical treatment did not affect the elemental composition of CNTs. Importantly, the raw and ball-milled CNTs practically did not show acidic features (A_{tot} close to 0 mmol H⁺ per g).

The CNTs were modified to endow the samples with acidic properties. As shown in Table 1, the applied modifications enriched CNTs with heteroatoms, mainly sulfur, and oxygen; however, the effectiveness of the used methods varied significantly. The reaction of CNTs with concentrated or fuming sulfuric acid introduced about 0.5–0.8% S into the carbon structure. These values were not very high, considering the susceptibility of other types of carbons to sulfonation with H₂SO₄. For example, Rechnia *et al.*⁴¹ functionalized activated carbons prepared from sawdust with concentrated sulfuric acid and obtained a S content of 1.8–2.2%, while the use of fuming sulfuric acid resulted in the incorporation of 1.4–1.7% S into the carbon matrix. In turn, Malaika *et al.*⁴² introduced 4.3% sulfur into the structure of carbon spheres using concentrated H₂SO₄, while Zhou *et al.*⁴³ prepared an acidic carbon catalyst with a 6% sulfur content through partial carbonization of bamboo followed by subsequent sulfonation of the sample with concentrated H₂SO₄. Thus, the less effective functionalization of the raw

Table 1 The results of EA and the acidity measurements obtained for the raw and modified CNTs

Sample	Ash [wt%]	C [wt%]	H [wt%]	S [wt%]	O ^a [wt%]	$-SO_3H^b$ [mmol g ⁻¹]	Oxygen groups [mmol g ⁻¹]	A_{tot} [mmol H ⁺ per g]
CNT _{NC3100}	0.0	98.3	0.1	0.0	1.5	0.00	0.02	0.02
CNT _{NC7000}	10.2	87.6	0.3	0.0	1.9	0.00	0.03	0.03
CNT _{NC7000-BM}	9.1	88.8	0.29	0.0	1.8	0.00	0.05	0.05
CNT _{NC3100} -H ₂ SO ₄ (conc.)-180-20h	0.8	96.4	0.2	0.5	2.1	0.19	0.06	0.25
CNT _{NC7000} -H ₂ SO ₄ (conc.)-180-20h	3.9	93.0	0.2	0.5	2.4	0.19	0.04	0.23
CNT _{NC7000-BM} -H ₂ SO ₄ (conc.)-180-20h	0.0	94.9	0.3	0.6	4.2	0.22	0.08	0.30
CNT _{NC7000-BM} -H ₂ SO ₄ (fum.)-100-8h	0.0	97.0	0.3	0.8	1.9	0.31	0.11	0.42
CNT _{NC7000-BM} -Glu/H ₂ SO ₄ (fum.)-180-12h	0.7	73.0	1.0	1.2	24.1	0.66	1.95	2.61
CNT _{NC7000-BM} -Glu/H ₂ SO ₄ (5 M)-150-4h	2.7	78.4	2.1	1.6	15.2	0.22	1.66	1.88

^a Calculated by the difference. ^b Based on the sulfur content from XPS.

CNTs observed here confirms that the structure of carbon nanotubes is highly resistant to almost all modifications, including those using aggressive reagents.^{32,44} Interestingly, the S contents measured for the raw CNTs modified with concentrated H_2SO_4 were similar for both materials (independently of their purity) and, importantly, lower than that obtained for the ball-milled carbon nanotubes (by $\sim 17\%$). This may suggest that even the short-time mechanical treatment of CNTs (see Experimental part) can result in the formation of some active points in their structure (by CNT breaking or structure opening), *i.e.*, “extra” graphene edges exposed to reagents and susceptible to functionalization. Breaking and opening of the caps of carbon nanotubes during ball-milling was also observed by Li *et al.*⁴⁵ Importantly, the modification with concentrated H_2SO_4 also reduced the ash content in the $\text{CNT}_{\text{NC7000}}$, indicating the removal of impurities from the raw material and suggesting a partial purification of CNTs.

The same was also observed by Mortazavi *et al.*,⁴⁶ who concluded that sulfuric acid can remove a metal catalyst trapped inside the CNTs.

After the functionalization of CNTs with concentrated or fuming sulfuric acid, a slightly increased oxygen content was noted compared to the parent materials. This observation may confirm the formation of $-\text{SO}_3\text{H}$ groups in the modified samples and/or resulted from the CNT's oxidation.⁴¹ At the same time, some increase in the total acidities of the samples was noted; however, A_{tot} of CNTs modified with H_2SO_4 (concentrated or fuming) was not very high, *i.e.*, between 0.23 and 0.42 mmol H^+ per g. These values could be justified considering the poor functionalization of CNTs with sulfuric acid mentioned above. It should also be noted that for CNTs modified with H_2SO_4 (concentrated or fuming), the calculated content of $-\text{SO}_3\text{H}$ moieties was lower than A_{tot} , which can suggest introducing not only sulfonic groups into the carbon structure but also some oxygen functionalities. According to the data presented in Table 1, the oxidation effect of H_2SO_4 was particularly noticeable for the ball-milled CNTs modified with concentrated or fuming sulfuric acid, *i.e.*, $\text{CNT}_{\text{NC7000-BM-H}_2\text{SO}_4(\text{conc.})-180-20\text{h}}$ and $\text{CNT}_{\text{NC7000-BM-H}_2\text{SO}_4(\text{fum.})-100-8\text{h}}$, respectively, for which the oxygen groups accounted for $\sim 26-27\%$. The oxidation properties of H_2SO_4 have also been reported elsewhere for activated carbons, carbon xerogels, or carbon spheres treated with concentrated or fuming sulfuric acid.^{41,42}

In order to obtain CNT-carbon composites with acidic features, CNTs were also modified with sulfuric acid (fuming or a 5 M solution) in the presence of glucose (Glu). This process used glucose to form a layer of amorphous carbon, which could act as a “glue” allowing the easier attachment of functional groups to the surface of CNTs.³⁶ As can be observed in Table 1, the adopted approach produced materials with significantly higher contents of sulfur compared to the functionalization of CNTs with sulfuric acid only and no added glucose (*i.e.*, 1.2 and 1.6% *vs.* 0.5–0.8%, respectively). Interestingly, the CNTs modified with the aid of

glucose and 5 M sulfuric acid, *i.e.*, the $\text{CNT}_{\text{NC7000-BM-Glu/H}_2\text{SO}_4(5\text{ M})-150-4\text{h}}$ sample, showed a higher S content than the material obtained with glucose and fuming H_2SO_4 (*i.e.*, $\text{CNT}_{\text{NC7000-BM-Glu/H}_2\text{SO}_4(\text{fum.})-180-12\text{h}}$) despite the milder reaction conditions used in the first case (see Experimental part). The observed result was probably due to the promoting effect of microwave radiation applied to produce $\text{CNT}_{\text{NC7000-BM-Glu/H}_2\text{SO}_4(5\text{ M})-150-4\text{h}}$.⁴⁷ Interestingly, a high increase in the content of oxygen was observed in both cases (even up to 24%), which may suggest the carbonization of glucose to carbonaceous matter rich in oxygen functionalities under the conditions applied. Forming the oxygen-abundant biochar is typical for simple carbohydrates treated at high temperatures and was reported earlier.^{48,49} According to the literature, a complex set of chemical reactions occurs during the hydrothermal carbonization of glucose, leading primarily to glucose dehydration to 5-hydroxymethylfurfural. The anions formed react with each other *via* polymerization, resulting in condensed furan rings bridged by aliphatic regions. These reactions proceed until the polymerized intermediates achieve a critical concentration, producing the particles' nucleation and growth, forming a spherical-shaped structure with hydroxyl and carboxylic groups attached to their surface.^{50,51} On the other hand, if hydrothermal carbonization is carried out in the presence of CNTs, a thin layer of amorphous carbonaceous matter is formed, coating their surface, as was previously observed on the graphite felts.⁵² In our case, hydrothermal carbonization was carried out in the presence of H_2SO_4 . In this case, the 5-hydroxymethylfurfural obtained from glucose dehydration reacted with acid to ‘embed’ sulfonic acid groups into the carbonaceous material. The amorphous coating on CNT plays the role of so-called glue because it binds the sulfonic groups to the surface of CNT. Thus, significantly higher amounts of sulfur were observed in samples prepared in the presence of glucose (*i.e.*, $\text{CNT}_{\text{NC7000-BM-Glu/H}_2\text{SO}_4(5\text{ M})-150-4\text{h}}$ and $\text{CNT}_{\text{NC7000-BM-Glu/H}_2\text{SO}_4(\text{fum.})-180-12\text{h}}$). In accordance with these findings, higher contents of O were also observed in these samples, *i.e.*, 24.1% for the sample modified with glucose and $\text{H}_2\text{SO}_4(\text{fum.})$ and 15.2% for CNTs treated with glucose and 5 M sulfuric acid. The difference in O content between these samples was probably related to the differences in the oxidative power between fuming and diluted sulfuric acid. Both CNT-carbon composites were characterized by high total acidities (up to 2.61 mmol H^+ per g); however, the sample's acidic properties were mainly induced by the oxygen functionalities. The high A_{tot} values of carbohydrate-derived carbons, resulting from various oxygen groups, were also reported previously.^{48,49}

The results of the textural analysis of the CNT-based samples are collected in Table 2. As can be observed, there were significant differences in the textural parameters of both commercial raw CNTs (*i.e.*, $\text{CNT}_{\text{NC3100}}$ and $\text{CNT}_{\text{NC7000}}$). First, CNTs of higher purity (*i.e.*, $\text{CNT}_{\text{NC3100}}$) had a much larger (almost twice) apparent surface area (S_{BET}) compared to $\text{CNT}_{\text{NC7000}}$. Secondly, it exhibited almost 30% higher V_{tot} .

Table 2 The textural properties of the raw and modified CNTs

Sample	S_{BET} [$\text{m}^2 \text{g}^{-1}$]	S_{ext} [$\text{m}^2 \text{g}^{-1}$]	V_{tot} [$\text{cm}^3 \text{g}^{-1}$]	V_{μ} [$\text{cm}^3 \text{g}^{-1}$]
CNT _{NC3100}	406	384	3.84	0.02
CNT _{NC7000}	243	243	2.81	0.00
CNT _{NC7000-BM}	286	286	0.96	0.00
CNT _{NC3100} -H ₂ SO ₄ (conc.)-180-20h	353	353	2.68	0.00
CNT _{NC7000} -H ₂ SO ₄ (conc.)-180-20h	226	226	2.93	0.00
CNT _{NC7000-BM} -H ₂ SO ₄ (conc.)-180-20h	316	316	1.77	0.00
CNT _{NC7000-BM} -H ₂ SO ₄ (fum.)-100-8h	244	240	1.09	0.00
CNT _{NC7000-BM} -Glu/H ₂ SO ₄ (fum.)-180-12h	94	87	0.42	0.00
CNT _{NC7000-BM} -Glu/H ₂ SO ₄ (5 M)-150-4h	251	248	0.81	0.00

The deteriorated textural properties of CNT_{NC7000} were most likely partly due to the high amounts of metallic impurities clogging the sample pores (see also the ash content in CNT_{NC7000} in Table 1). A similar phenomenon was also reported elsewhere.⁵³ Importantly, the S_{BET} of both samples resulted only or almost only from the external surface areas, *i.e.*, meso- and macropores, as indicated by a high contribution of S_{ext} to S_{BET} . The contribution of V_{μ} to V_{tot} was practically 0 in both cases, and the porosity of samples was probably related to the free spaces of meso- and macropore sizes in the CNT bundles.^{54,55}

The ball milling of carbon nanotubes changed its textural properties, namely a slightly increased S_{BET} was noted for CNT_{NC7000-BM} compared to that of the parent material. The same effect was also observed by other authors who concluded that this was due to the CNT breaking and caps

opening.^{55,56} Interestingly, after the ball-milling process, the total volume of pores in CNT_{NC7000} significantly decreased, which was most probably related to the reduction of spaces between nanotubes and, thus, a more compact structure of CNT's after the mechanical treatment.⁵⁵

The modified CNTs showed decreased textural parameters compared to the starting samples, suggesting the efficient introduction of various functional groups during the used functionalizations. The smallest changes were observed for the CNTs modified with concentrated or fuming sulfuric acid, which agrees well with the moderate effectiveness of the functionalization of CNTs with these modifying agents (see also the results of EA in Table 1). The CNTs treated with glucose and H₂SO₄ (fuming or a 5 M solution) differed from those modified only with acid, showing a reduced S_{BET} and/or V_{tot} . This was especially well seen for the sample modified

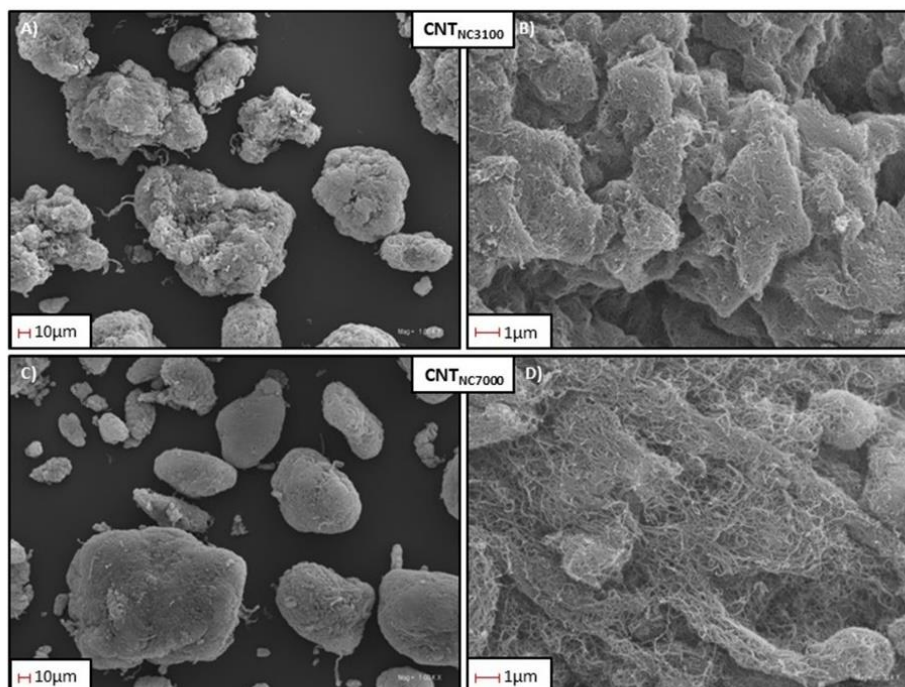


Fig. 1 SEM images of the commercial raw CNT samples: CNT_{NC3100} (A and B); CNT_{NC7000} (C and D).

with fuming sulfuric acid and glucose for a longer time and at a higher temperature, *i.e.*, CNT_{NC7000-BM}-Glu/H₂SO₄(fum.)-180-12h. The significant decrease in textural properties of this material was probably due to the formation of the thin carbonaceous layer from glucose on the outer surface of CNTs or in the free spaces in the CNT bundles, as described above.^{36,49}

SEM micrographs of the commercial raw CNTs are presented in Fig. 1. As can be seen in the lower magnification images (Fig. 1A and C), both types of samples formed agglomerates of carbon filaments, differing in shapes and sizes (even up to ~140 μm in the case of CNT_{NC7000}). The particles of CNT_{NC3100}, *i.e.*, CNTs of higher purity, had a rather irregular and rough surface, while the agglomerates of CNT_{NC7000} were more oval and smoother.

Details of the structure of raw CNTs can be observed in the higher-magnification micrographs presented in Fig. 1B and D. According to these images, the surface of CNT_{NC3100} particles was uneven and formed by tightly entangled filaments; however, many cavities and holes could also be observed. This was probably the reason for the enhanced textural properties of CNT_{NC3100} (of higher purity) compared to those of lower-purity CNT_{NC7000} (see also Table 2). On the other hand, CNT_{NC7000} showed a rather compact structure formed by long, tightly entangled fibers with a limited number of spaces and pores (Fig. 1D).

The morphological features of the ball-milled raw CNTs (*i.e.*, CNT_{NC7000-BM} carbon) and the samples functionalized with sulfuric acid with the aid of glucose are presented in Fig. 2. As can be seen in Fig. 2A and B, ball milling caused

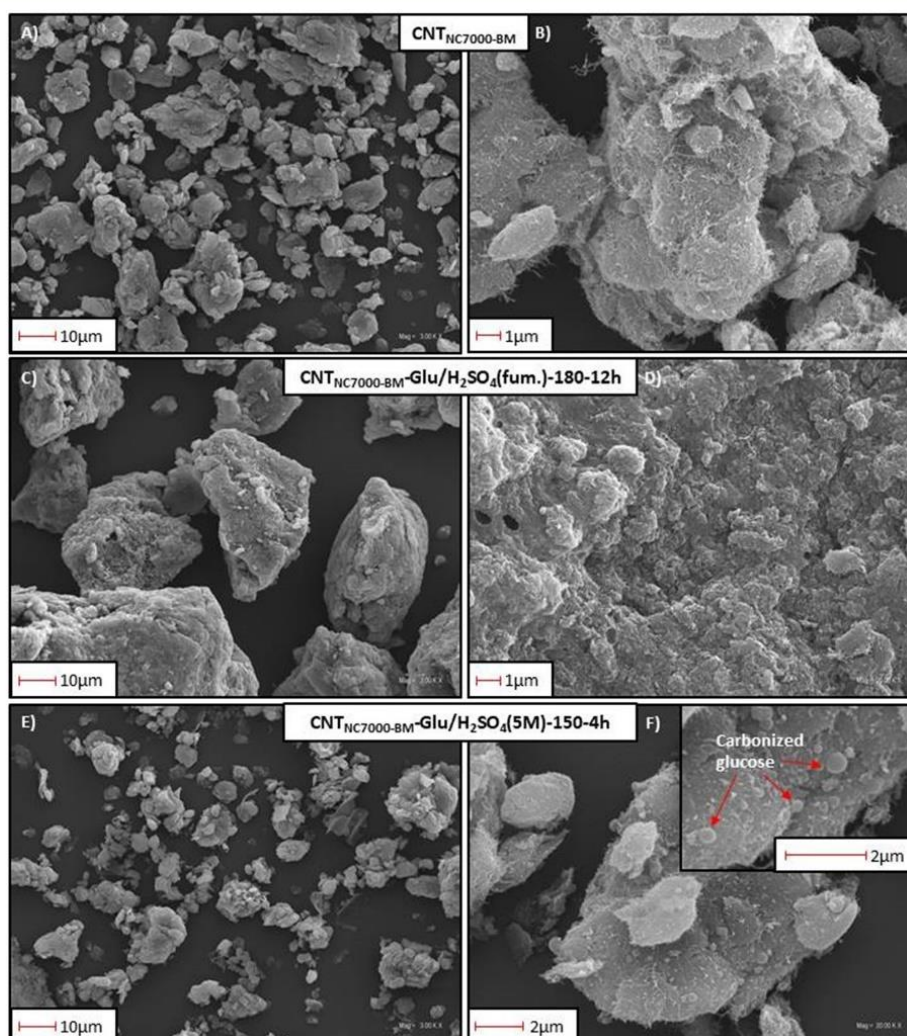


Fig. 2 SEM images of the ball-milled CNTs (A and B) and the samples obtained using CNTs, glucose, and H₂SO₄ under varied conditions (C-F).

considerable changes in the sample structure, namely a significant fragmentation of the CNT agglomerates took place, resulting in a decrease in the particle sizes. The surface of the agglomerates was still uneven, and sharp edges and some cavities between the individual fragments of particles were formed. Furthermore, a tangle of fibers could also be seen. The treatment of CNTs with glucose and fuming sulfuric acid at 180 °C resulted in large particles with a rough surface and rather poor porosity (Fig. 2C and D). The formation of the previously described carbonaceous layer (from hydrothermal carbonization of glucose) on the surface of CNT is visible when comparing SEM images of ball-milled CNTs before (see CNT_{NC7000}, Fig. 2B in the manuscript) and after hydrothermal treatment in the presence of glucose (see CNT_{NC7000-BM-Glu/H₂SO₄(fum.)-180-12h}, in Fig. 2D). From these images, the significant increase in the particle size after functionalization is evident, which aligns with the formation of a carbonaceous shell covering the filaments. This observation is further supported by the changes in textural parameters listed in Table 2.

Fig. 2E and F show the morphological properties of carbon nanotubes treated with glucose and 5 M H₂SO₄ using microwave irradiation (*i.e.*, the CNT_{NC7000-BM-Glu/H₂SO₄(5 M)-150-4h} sample). In this case, no significant differences between the morphological features of the modified and the initial CNT_{NC7000-BM} (Fig. 2A and B) were visible. However, at a higher magnification micrograph in Fig. 2F, single small spheres formed on the surface of particles could also be seen in the modified sample. These spheres were probably produced from glucose through hydrothermal treatment under the conditions used.^{42,48} A similar effect was also obtained by Morais *et al.*⁵⁰

Based on the textural analyses, EA and SEM results, it can be concluded that two types of mechanisms were employed in the present work to facilitate the functionalization of CNTs with sulfur. The first one was the creation of the new active graphene edges during ball-milling of CNTs, as evidenced by the breaking of large CNT aggregates (compare SEM

micrographs in Fig. 1C with 2A). In the second mechanism, the increase of sulfur content is associated with the functionalization of the carbonaceous layer formed during hydrothermal carbonization of glucose in the presence of CNTs. This newly formed carbon layer rich in -SO₃H groups acted as the so-called glue binding the functionalities to the otherwise highly resistant surface of CNTs.

Fig. 3 compares the XRD patterns of the raw and the ball-milled CNTs. As can be seen, both pristine CNTs showed two main diffraction peaks at 2θ of about 26° and 44°. The former one can be assigned to the C(002) reflection of the hexagonal structure of graphite,⁵⁷ and the latter is typically ascribed to the diffraction on the (100) and (101) planes related to the atomic structure of graphene sheets.^{58,59} The C(002) diffraction peak of CNT_{NC7000} showed a lower intensity than that of CNT_{NC3100}, which was most likely related to the presence of impurities in the CNT_{NC7000} structure (see also the ash content in Table 1).⁶⁰ As can be observed, the XRD patterns of the investigated CNTs also showed weak reflexes at 2θ of 54° and 78°, most likely belonging to the (004) and (110) planes of graphite-like materials.⁶¹ On the other hand, an additional low diffraction peak at 2θ of ~67° observed in the diffractograms of CNT_{NC7000} and CNT_{NC7000-BM} can be attributed to the crystalline impurities of the metal catalyst used for the CNTs production (see also the discussion on Table 1). Generally, the ball milling did not significantly affect the crystalline structure of the pristine CNTs, as the results obtained for CNT_{NC7000} and CNT_{NC7000-BM} were quite similar. Nevertheless, CNT_{NC7000-BM} showed a slightly lower C(002) diffraction peak intensity than the untreated sample. Furthermore, a new broad reflection peak of moderate intensity appeared at 2θ of 14°. This signal can be ascribed to the C(002) diffraction peak shifted towards lower 2θ angles, resulting from the increased spacing between the graphene layers.⁵⁷

The results of the TG analysis of the commercial raw CNTs differing in their purity performed under air flow are

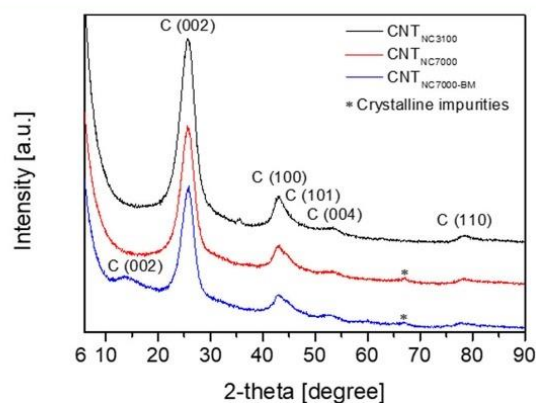


Fig. 3 The XRD results obtained for the raw and the ball-milled CNTs.

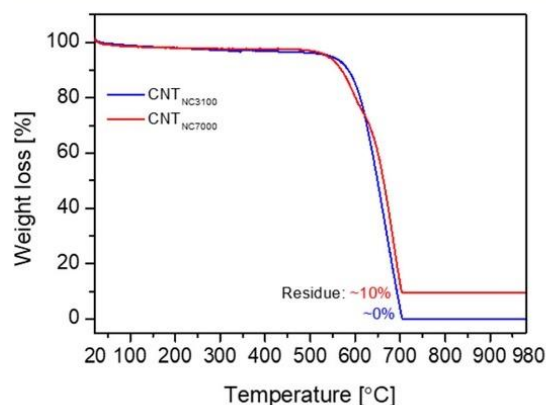


Fig. 4 The results of TG analysis performed for the raw CNTs under the flow of air.

presented in Fig. 4. As can be seen, in both cases, no significant weight losses were observed up to ~ 550 °C. Above this temperature, a rapid decrease in the sample mass due to the material combustion was observed. The residue after combustion was $\sim 0\%$ in the case of CNT_{NC3100} (the purified sample) and approximately 10% in the case of CNT_{NC7000} (the commercial sample without purification). These values agree well with the contents of ash given in Table 1 and the XRD results discussed above.

Thermogravimetric analysis under N₂ flow can be used to estimate the effectiveness of carbon functionalization, and the amount of released volatiles can be correlated with the presence of S and O moieties introduced during modifications.³⁷ The TG profiles of the CNTs analyzed under nitrogen flow are depicted in Fig. 5, whereas the DTG curves of these samples are shown in Fig. 6. As presented in Fig. 5, unmodified CNTs were thermally stable up to 980 °C, as only insignificant mass changes were observed for these materials (between $\sim 2\%$ and $\sim 4\%$ at the final temperature of the TG measurements). The chemically modified CNTs were characterized by higher weight losses than the initial samples, indicating an effective introduction of functional groups into the CNT structure. The observed effects varied depending on the functionalization used, *i.e.*, CNTs treated with glucose and acid (*i.e.*, CNT_{NC7000-BM-Glu/H₂SO₄(fum.)-180-12h} and CNT_{NC7000-BM-Glu/H₂SO₄(5M)-150-4h}) released the highest amounts of volatiles and lost finally as much as $\sim 41\%$ and $\sim 47\%$ of their initial mass, respectively. On the other hand, CNTs modified with concentrated or fuming sulfuric acid without glucose showed significantly lower weight losses, indicating the lower efficiency of this approach. The obtained results are in line with the data of EA (see Table 1), showing that the addition of glucose during the functionalization of CNTs with the acid significantly affects the surface chemistry of these samples, *e.g.*, by introducing large quantities of oxygen functionalities.⁴⁹

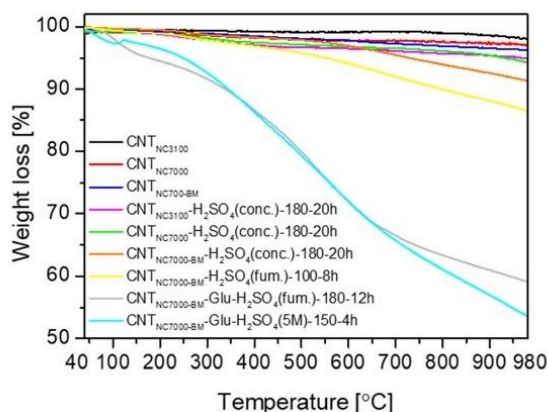


Fig. 5 The results of TG analysis of the prepared samples performed under a N₂ flow.

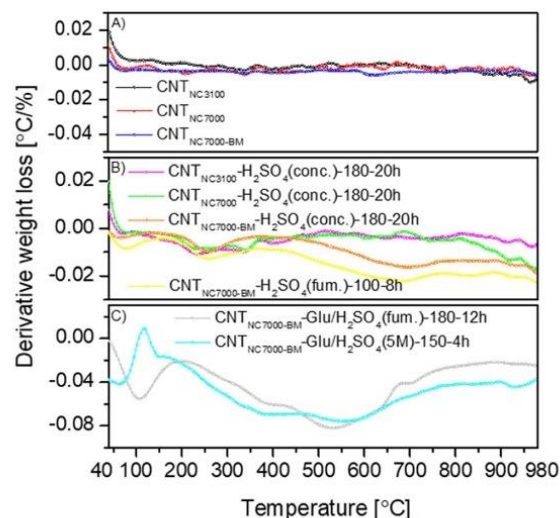


Fig. 6 The DTG patterns of the raw (A) and modified (B and C) CNTs.

The DTG patterns of the samples are presented in Fig. 6. The raw CNTs treated with concentrated H₂SO₄ showed relatively flat DTG profiles, resembling those of the unmodified samples (compare Fig. 6A and B), indicating that the nanotubes were modified to a very limited extent, which in turn agrees well with the results of EA in Table 1. The profiles of the sulfuric acid-modified ball-milled CNTs (*i.e.*, CNT_{NC7000-BM-H₂SO₄(conc.)-180-20h} and CNT_{NC7000-BM-H₂SO₄(fum.)-100-8h}) were slightly different from those of their unmodified counterparts and revealed higher weight losses at higher temperatures (Fig. 6B). In general, the DTG curves of the raw and ball-milled CNTs modified with concentrated or fuming sulfuric acid showed a small peak at about 250 °C, which can be ascribed to the presence of a small number of $-\text{SO}_3\text{H}$ groups.⁶² In turn, weak peaks with a minimum at 350 °C (observed for CNT_{NC3100-H₂SO₄(conc.)-180-20h} and CNT_{NC7000-H₂SO₄(conc.)-180-20h}) and a broad signal starting at 500 °C (observed for CNT_{NC7000-BM-H₂SO₄(conc.)-180-20h} and CNT_{NC7000-BM-H₂SO₄(fum.)-100-8h}) were probably related to the presence of small amounts of oxygen moieties, *e.g.*, carboxylic anhydrides or phenolic ones, respectively.⁶³ This hypothesis will be subsequently confirmed by XPS analysis.

The DTG patterns of the CNTs treated with glucose and acid were rather complex (Fig. 6C). Two intensive signals were observed: at about 100 °C, corresponding to the release of water, and a very broad peak starting at about 200 °C with the minima at about 375, 525, and 575 °C. This broad signal was probably partly related to the presence of oxygen groups of different thermal stability, which richly decorated the material surface (see also the O content in Table 1) and originated from the carbonized glucose (see Experimental part and the results of the SEM analysis). No signals typical for $-\text{SO}_3\text{H}$ groups were observed, probably because of the complexity of the obtained profiles and the peak overlap.

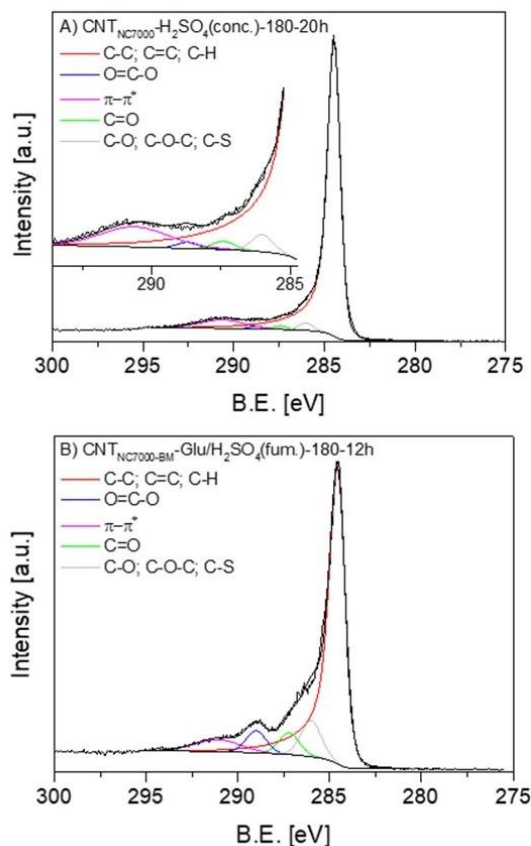


Fig. 7 High-resolution XPS C 1s spectra of selected samples.

X-ray photoelectron spectroscopy (XPS) was applied to define the surface chemistry of the samples. The results obtained for the prepared carbons are presented in Fig. 7 and 8 and Tables 3 and 4. The XPS results confirmed the

Table 3 The contents of carbon, sulfur, and oxygen measured for the selected CNTs by XPS

Sample	C [wt%]	S [wt%]	O [wt%]
CNT _{NC3100} -H ₂ SO ₄ (conc.)-180-20h	96.9	0.6	2.5
CNT _{NC7000} -H ₂ SO ₄ (conc.)-180-20h	96.4	0.6	3.0
CNT _{NC7000-BM} -H ₂ SO ₄ (conc.)-180-20h	95.2	0.7	4.1
CNT _{NC7000-BM} -H ₂ SO ₄ (fum.)-100-8h	93.2	1.0	5.8
CNT _{NC7000-BM} -Glu/H ₂ SO ₄ (fum.)-180-12h	79.5	2.5	18.0
CNT _{NC7000-BM} -Glu/H ₂ SO ₄ (5 M)-150-4h	79.1	1.7	19.2

presence of carbon, oxygen, and sulfur in the analyzed samples. According to the data in Table 3, the CNTs functionalized with the aid of glucose and H₂SO₄ (*i.e.*, CNT_{NC7000-BM}-Glu/H₂SO₄(5 M)-150-4h and CNT_{NC7000-BM}-Glu/H₂SO₄(fum.)-180-12h) showed higher amounts of S than the samples treated with only the acid. Moreover, the former treatment introduced significant amounts of oxygen, which also agrees well with the results of EA (see Table 1). Comparing the data from XPS and EA, it is seen that the sulfur contents measured by these methods were almost the same in most cases. The only exception was CNT_{NC7000-BM}-Glu/H₂SO₄(fum.)-180-12h, for which the S content measured by XPS was twice as high as that shown by EA (*i.e.*, 2.5% *vs.* 1.2%, respectively), suggesting that the amount of sulfur on the surface was higher than that in bulk. In other cases, S was homogeneously distributed in the functionalized materials.

Fig. 7 shows the high-resolution C 1s XPS spectra obtained for selected modified materials. As can be observed, five different carbon species were found in the samples, at BEs of ~284.5 eV, 286.0 eV, 287.4 eV, 288.7 eV, and 290.0 eV. These peaks can be ascribed to graphitic carbon (C-C/C=C), C-O/C-O-C/C-S groups, C=O in carbonyls, O-C=O in carboxyls, and π - π^* transitions, respectively.⁶⁴ Furthermore, the results showed that the distribution of different carbon species was distinct for various samples, *e.g.*, CNTs treated with glucose

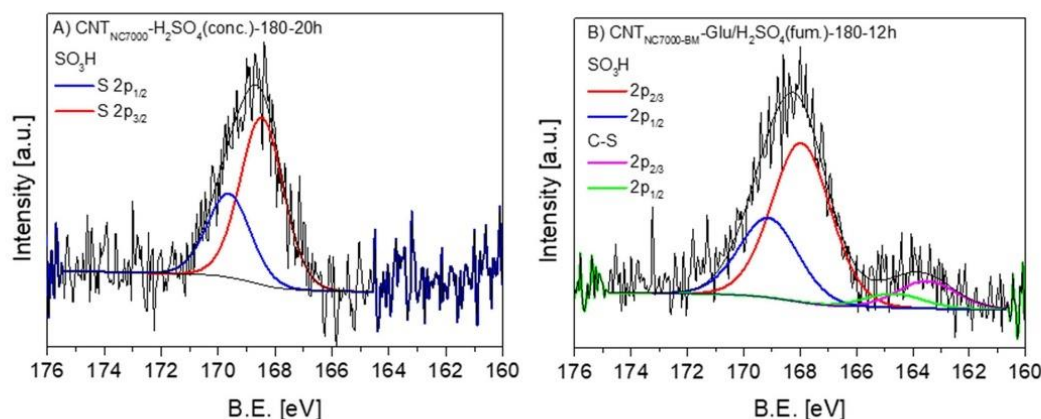


Fig. 8 High-resolution XPS S 2p spectra of selected samples.

Table 4 The relative contributions of various S and C species in S 2p and C 1s profiles (in wt% in brackets)

Sample	S 2p		C 1s			
	S in sulfonic groups	S in other S species	C in graphitic carbon	C in carboxyls	C in carbonyls	C in ethers, phenols, C-S species
CNT _{NC3100} -H ₂ SO ₄ (conc.)-180-20h	100.0 (0.6)	0.0 (0.0)	91.3 (88.5)	0.8 (0.8)	0.6 (0.6)	1.2 (1.1)
CNT _{NC7000} -H ₂ SO ₄ (conc.)-180-20h	100.0 (0.6)	0.0 (0.0)	89.7 (86.4)	0.7 (0.7)	0.9 (0.9)	1.8 (1.7)
CNT _{NC7000-BM} -H ₂ SO ₄ (conc.)-180-20h	100.0 (0.7)	0.0 (0.0)	89.4 (85.2)	1.3 (1.2)	0.6 (0.6)	2.8 (2.6)
CNT _{NC7000-BM} -H ₂ SO ₄ (fum.)-100-8h	100.0 (1.0)	0.0 (0.0)	87.2 (81.3)	0.9 (0.9)	1.2 (1.1)	4.5 (4.2)
CNT _{NC7000-BM} -Glu/H ₂ SO ₄ (fum.)-180-12h	85.7 (2.1)	14.3 (0.4)	71.8 (57.1)	5.8 (4.6)	5.4 (4.3)	9.0 (7.2)
CNT _{NC7000-BM} -Glu/H ₂ SO ₄ (5 M)-150-4h	40.4 (0.7)	59.6 (1.0)	76.8 (60.7)	4.5 (3.6)	1.3 (1.0)	15.8 (12.5)

and acid (Fig. 7B) contained an abundance of carboxylic and phenolic groups. In contrast, for the CNTs treated with only the acid (Fig. 7A), the content of these species was rather low.

Fig. 8 presents the high-resolution S 2p spectra obtained for selected samples (CNT_{NC7000}-H₂SO₄(conc.)-180-20h and CNT_{NC7000-BM}-Glu/H₂SO₄(fum.)-180-12h). A well-defined doublet at ~168 eV was observed in both cases, suggesting the presence of -SO₃H functionalities on the sample surface.⁶⁵ Interestingly, the spectrum of CNTs modified with fuming H₂SO₄ and glucose presented in Fig. 8B also showed an additional doublet at about ~164 eV, which suggests that sulfur was introduced to the material structure not only as sulfonic groups but also as other sulfur species, *e.g.*, thiophenes.⁶⁵ The same was also observed in the case of CNTs modified with 5 M H₂SO₄ and glucose, *i.e.*, CNT_{NC7000-BM}-Glu/H₂SO₄(5 M)-150-4h.

The relative contributions of different sulfur or carbon species present in the modified CNTs are gathered in Table 4. These results revealed that CNTs modified with sulfuric acid (raw and ball-milled) contained only -SO₃H functionalities. On the other hand, CNTs treated with glucose and acid also showed other types of S-containing groups. The contribution of C-S species was different for these materials; namely, the CNT_{NC7000-BM}-Glu/H₂SO₄(5 M)-150-4h sample showed about 60% of C-S type groups, whereas

CNT_{NC7000-BM}-Glu/H₂SO₄(fum.)-180-12h contained about 14% of these moieties. Moreover, CNTs modified with glucose and acid were characterized by a lower amount of graphitic carbon than H₂SO₄-modified CNTs, while a higher contribution of various oxygen species was observed in this case.

As shown in Table 4, the raw CNTs (both high purity and technical grade) modified with concentrated sulfuric acid were rather poor in oxygen functionalities, which was also in line with EA and TG analysis. In contrast, the ball-milled CNTs modified with H₂SO₄ (concentrated or fuming) had a fairly high contribution of C-O species as phenolic groups. On the other hand, CNTs treated with glucose and 5 M acid were characterized by a significant contribution of carboxylic and phenolic functionalities. At the same time, the modification with glucose and fuming sulfuric acid also introduced an appreciable amount of carbonyls.

3.2. Catalytic results

The obtained CNT-based samples were tested in glycerol etherification with TBA. For the sake of comparison, a reaction with a commercial acid catalyst (Amberlyst-15) and a blank test were also performed.

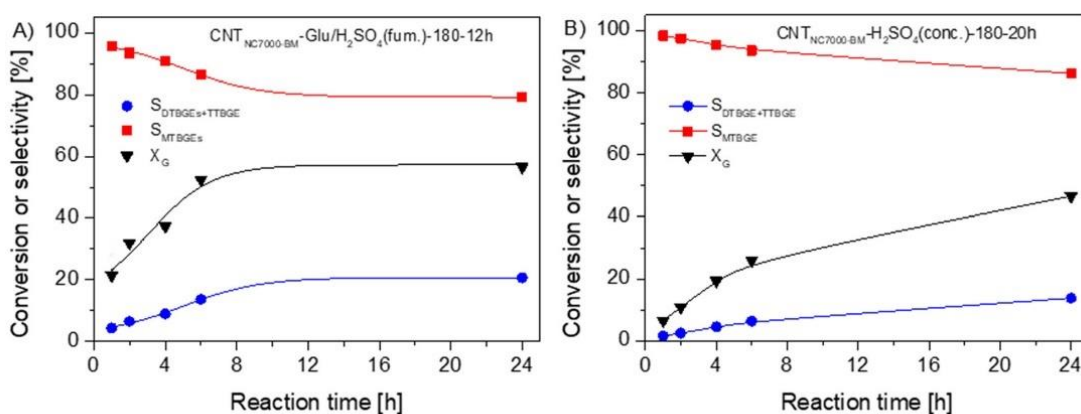


Fig. 9 The results of catalytic performances of (A) the CNT_{NC7000-BM}-Glu/H₂SO₄(fum.)-180-12h sample and (B) the CNT_{NC7000-BM}-H₂SO₄(conc.)-180-20h sample in glycerol etherification vs. time.

Fig. 9 shows the catalytic performances of two selected CNT samples *versus* the reaction time. As can be observed, the catalysts differed in their activities. The use of CNT_{NC7000-BM}-Glu/H₂SO₄(fum.)-180-12h in the process resulted in a quite significant initial conversion of glycerol (X_G), *i.e.*, about 21% after 1 h. X_G increased gradually over time, achieving ~52% within 6 h. The further rise in X_G was insignificant as the conversion of glycerol measured after 24 h was 57%. This effect was probably due to reaching the thermodynamic equilibrium.¹³ The other prepared catalysts worked quite similarly to CNT_{NC7000-BM}-H₂SO₄(conc.)-180-20h presented in Fig. 9B. These samples showed significantly lower initial conversions of glycerol compared to CNT_{NC7000-BM}-Glu/H₂SO₄(fum.)-180-12h. In this case, the thermodynamic equilibrium was not reached within the studied reaction time.

As shown in Fig. 9, the reaction over the functionalized CNTs produced all three types of substituted ethers, *i.e.*, mono-, di-, and tri-*tert*-butyl glycerol ethers; however, the amounts of TTBGE were negligible. MTBGEs were formed most efficiently during the whole process in both cases. Nevertheless, when comparing the results obtained for CNT_{NC7000-BM}-Glu/H₂SO₄(fum.)-180-12h and CNT_{NC7000-BM}-H₂SO₄(conc.)-180-20h, some differences are visible in the distribution of products over time. In the case of the CNT_{NC7000-BM}-Glu/H₂SO₄(fum.)-180-12h sample, the selectivity to MTBGEs measured after 1 h was ~95%. This parameter decreased quite considerably with time. Simultaneously, a gradual increase in the selectivity to higher-substituted glycerol ethers (*i.e.*, DTBGEs and TTBGE) was observed (Fig. 9A). The obtained results suggest that DTBGEs and TTBGE in the reaction over the applied catalysts are not formed directly from glycerol but are produced from MTBGEs. The conclusion above also aligns with the etherification mechanism presented in the literature.³⁷

Finally, after 24 h, S_{MTBGEs} achieved using CNT_{NC7000-BM}-Glu/H₂SO₄(fum.)-180-12h was ~80% and $S_{\text{DTBGEs+TTBGE}}$ was equal to about 20%. However, it should be underlined that in this case satisfactory catalytic results could be obtained just within 6 h. The very promising catalytic performances of the CNT_{NC7000-BM}-Glu/H₂SO₄(fum.)-180-12h were associated with the acidic features of the used material (see also Table 1), which will be discussed later. On the other hand, the use of CNT_{NC7000-BM}-H₂SO₄(conc.)-180-20h (Fig. 9B) favored mainly the formation of MTBGEs, and a significant extension of the reaction time was necessary to achieve satisfactory results of selectivity to higher glycerol ethers.

Fig. 10 shows a comparison of the results obtained in the glycerol etherification over the prepared CNTs and a commercial catalyst (Amberlyst-15) after 6 and 24 h. For the sake of comparison, the results of the blank test were also depicted. As can be seen, the reaction performed without a catalyst practically did not occur, as the glycerol conversion measured after 6 and 24 h was ~0%. A selected unmodified sample (CNT_{NC3100}, poor in surface functional groups, see Table 1) also presented negligible activity (not shown in the figure). On the other hand, the modified CNTs converted glycerol to glycerol ethers effectively; however, there were quite significant differences in the catalytic performances of the samples in terms of glycerol conversions and product distributions. Some catalysts worked less efficiently than others, giving moderate X_G values (<28%) and very low yields of DTBGEs and TTBGE after 6 h. Better results were noted after 24 h; however, they were still unsatisfactory. Those catalysts were the raw CNTs modified with concentrated sulfuric acid, *i.e.*, CNT_{NC3100}-H₂SO₄(conc.)-180-20h and CNT_{NC7000}-H₂SO₄(conc.)-180-20h, which presented a rather low degree of functionalization (see also the A_{tot} and -SO₃H contents of these samples in Table 1). The ball-milled CNTs treated with concentrated or fuming sulfuric acid worked

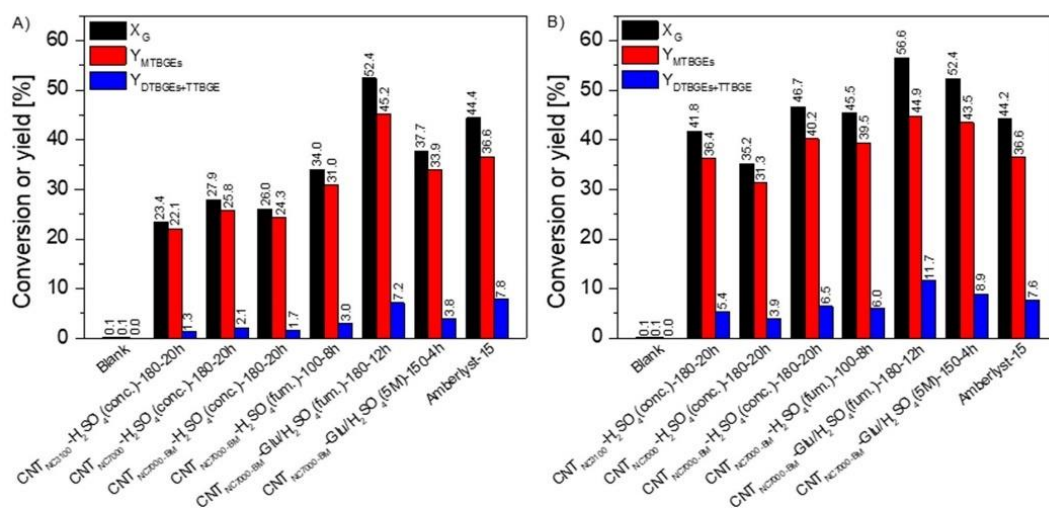


Fig. 10 The results of the catalytic performances of the modified CNTs in comparison to Amberlyst-15 and the blank after 6 h (A) and 24 h (B).

more efficiently, especially during a 24-h process. Y_{MTBGEs} obtained after that time was about 40%, and a combined yield of DTBGEs and TTBE achieved about 6%. As stated before, the ball-milled CNTs were more susceptible to functionalization than the pristine ones, showing a higher number of S- and O-containing surface groups and higher total acidities compared to the as-purchased samples (see also the results of EA in Table 1). This was probably a key factor determining the enhanced catalytic activity of these materials compared to the raw CNTs. The best catalytic results were obtained in the glycerol etherification over the CNTs treated with glucose and acid. These catalysts allowed achieving over 50% conversion of glycerol after 24 h; however, the results obtained after 6 h were also satisfactory, especially in the case of CNTs modified with glucose and fuming H_2SO_4 (*i.e.*, $\text{CNT}_{\text{NC7000-BM-Glu/H}_2\text{SO}_4(\text{fum.})-180-12\text{h}}$ sample). For this catalyst, X_{G} after 6 h reached over 52%, which was only ~5% lower than the value obtained after 24 h. Importantly, in this case, MTBGEs were more effectively converted to higher-substituted glycerol ethers than in the case of other catalysts, resulting in a combined yield of DTBGEs + TTBE of over 7% and almost 12% after 6 and 24 h, respectively. The CNTs treated with glucose and 5 M H_2SO_4 (*i.e.*, $\text{CNT}_{\text{NC7000-BM-Glu/H}_2\text{SO}_4(5\text{ M})-150-4\text{h}}$ carbon) worked slightly worse, but the final results of X_{G} , Y_{MTBGEs} and $Y_{\text{DTBGEs+TTBE}}$ were still satisfactory. Generally, both samples gave comparable or even slightly better results in the reaction than the commercial catalyst, Amberlyst-15. The high catalytic activities shown by the CNTs modified with glucose and sulfuric acid were probably related to the surface properties of these catalysts, *i.e.*, a high content of acidic surface groups, and thus their high total acidities (see also the results presented in Tables 1 and 4).

Some interesting conclusions can be drawn by comparing the catalytic performances of the modified CNTs presented

in Fig. 10 with the XPS data in Table 4. First, the activities of the modified CNTs (high-purity and technical grade), *i.e.*, $\text{CNT}_{\text{NC3100-H}_2\text{SO}_4(\text{conc.})-180-20\text{h}}$ and $\text{CNT}_{\text{NC7000-H}_2\text{SO}_4(\text{conc.})-180-20\text{h}}$, were related to the presence of sulfonic groups, as the samples contained only $-\text{SO}_3\text{H}$ functionalities and only small amounts of acidic oxygen moieties were detected (see the data for an exemplary sample in Table 4). Secondly, it was found that the ball-milled CNTs modified with 5 M sulfuric acid in the presence of glucose (*i.e.*, $\text{CNT}_{\text{NC7000-BM-Glu/H}_2\text{SO}_4(5\text{ M})-150-4\text{h}}$) showed a very high contribution of sulfur in the form of non-sulfonic moieties (Table 4). Nevertheless, the calculated content of sulfonic functionalities was still significant, about 0.7%, and was comparable to the value shown by $\text{CNT}_{\text{NC7000-BM-H}_2\text{SO}_4(\text{conc.})-180-20\text{h}}$. Importantly, despite the comparable values of $-\text{SO}_3\text{H}$ groups, these samples differed significantly in their activities, *i.e.*, $\text{CNT}_{\text{NC7000-BM-Glu/H}_2\text{SO}_4(5\text{ M})-150-4\text{h}}$ worked considerably more effectively. Interestingly, this catalyst worked even better than $\text{CNT}_{\text{NC7000-BM-H}_2\text{SO}_4(\text{fum.})-100-8\text{h}}$, presenting an even higher content of sulfonic groups. Thus, it seems that the catalytic activity of the CNT-based samples in glycerol etherification was not only induced by $-\text{SO}_3\text{H}$ functionalities, but apparently, other factors also played a vital role in this process. As $\text{CNT}_{\text{NC7000-BM-Glu/H}_2\text{SO}_4(5\text{ M})-150-4\text{h}}$ contained an abundance of various oxygen groups (see also the discussion on TG and the results in Table 4), it might be suggested that these functionalities were important for the process, enhancing the catalyst activity, *e.g.*, by facilitating adsorption of the reagents on the sample surface. This synergistic effect of $-\text{SO}_3\text{H}$ - and O-containing groups was also suggested elsewhere when using carbon catalysts in glycerol etherification or glycerol esterification.^{37,48,66}

As stated above, the catalytic performances of the modified CNTs in glycerol etherification were correlated to

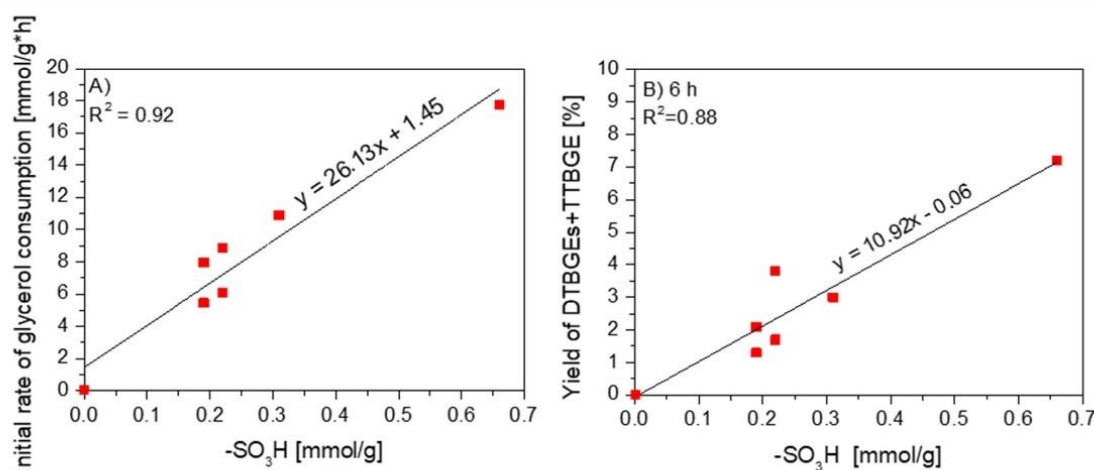


Fig. 11 Initial rate of glycerol consumption (A) or yield of DTBGEs + TTBE obtained in the glycerol etherification after 24 h (B) vs. the amount of $-\text{SO}_3\text{H}$ moieties in the samples.

their surface chemistry, mainly to the content of strongly acidic sulfonic groups. Fig. 11 presents the dependence of the catalytic activity of the samples (expressed as the initial reaction rates of glycerol consumption or yield of DTBGEs + TTBGE) on the concentration of $-\text{SO}_3\text{H}$ groups (calculated based on the XPS analysis). As can be observed in Fig. 11A, a clear correlation was obtained between the rate of glycerol consumption (measured after 1 h) and the concentration of surface sulfonic functionalities, indicating that the presence of these moieties was of key importance for the transformation of glycerol in the studied process. The calculated TOF value (expressed as the amount of glycerol consumed per active site and per unit time; h^{-1}) was equal to about 26.13 h^{-1} . The formation of higher glycerol ethers was also affected by the presence of $-\text{SO}_3\text{H}$ groups, as can be observed in Fig. 11B, and generally, the higher the concentration of $-\text{SO}_3\text{H}$ functionalities, the higher the yields of DTBGEs + TTBGE obtained. Nevertheless, this correlation is not directly proportional, indicating that not only sulfonic groups were critical for the reaction. It is suggested here that surface oxygen functionalities may play an important role in the tested process. The XPS analysis showed the presence of oxygen in the functionalized samples in the form of carboxylic, phenolic, ether, and carbonyl functionalities (see Table 4). Of these functionalities, only carboxylic and phenolic groups display acidic character and could act as active sites for the etherification reaction. It was previously shown that carbons rich in acidic oxygen functionalities displayed only limited activity in etherification due to the relatively low acid strength of $-\text{COOH}$ and $-\text{OH}$ moieties.^{18,66} Nevertheless, carbon catalysts containing $-\text{SO}_3\text{H}$ and $-\text{COOH}$ / $-\text{OH}$ functionalities showed enhanced catalytic performance in etherification compared to their counterparts having lower concentrations of acidic oxygen groups.⁶⁷ The reaction is mostly catalyzed by sulfonic groups, but oxygen functionalities could act as additional active sites. However, it is believed that the main role of $-\text{COOH}$ and $-\text{OH}$ functionalities is to increase the hydrophilicity of the catalyst's surface, which could favor the adsorption of

glycerol and *tert*-butyl alcohol and promote the consecutive reaction of MTBGEs to DTBGEs and TTBGE. This conclusion aligns with the reports by Miranda *et al.*, who observed higher selectivity to poly-substituted ethers obtained by sulfonated graphene catalysts containing higher concentrations of $-\text{COOH}$ and $-\text{OH}$ functionalities in proximity to SO_3H active sites.⁶⁶ The positive effect of the oxygen functionalities was reported by us in the acetylation of glycerol.⁴⁸ Moreover, Yang *et al.* reported synergistic effects between $-\text{COOH}$ and $-\text{SO}_3\text{H}$ in the alcoholysis of furfuryl alcohol and *n*-butanol.⁶⁸

The stability of samples in subsequent runs is important when considering the industrial applications of the catalyst. Thus, Fig. 12 presents the catalytic performance of a selected sample, *i.e.*, $\text{CNT}_{\text{NC7000-BM-Glu/H}_2\text{SO}_4(\text{fum.})-180-12\text{h}}$, in subsequent glycerol etherification reactions.

As can be seen from the presented results, a significant decrease in the catalytic performance of the tested sample was observed in a second reaction run, as the glycerol conversion decreased by almost 40%, and only trace amounts of the higher-substituted ethers were formed. The obtained results, however, were still better than those achieved in the blank. Interestingly, the treatment of the used catalyst with 5% hydrochloric acid resulted in the restoration of the sample activity, and the catalytic results after the sample regeneration were comparable to those obtained in the presence of a fresh catalyst. These observations suggested that CNT's deactivation was caused by blocking the catalyst's active sites by adsorbed reactants and/or reaction products rather than the active site leaching.^{69–71} To verify this speculation, we characterized the spent catalyst after regeneration. The EA demonstrated the presence of 0.92% sulfur, which compared to 1.2% present in the fresh catalyst (see sample $\text{CNT}_{\text{NC7000-BM-Glu/H}_2\text{SO}_4(\text{fum.})-180-12\text{h}}$ in Table 3), confirmed that most of the active sites were stable under the reaction conditions. These results aligned with a slight drop in A_{tot} from 2.61 mmol H^+ per g to 2.35 mmol H^+ per g after regeneration. Thus, it was confirmed that the primary deactivation mechanism of $\text{CNT}_{\text{NC7000-BM-Glu/H}_2\text{SO}_4(\text{fum.})-180-12\text{h}}$ was the blocking of the active sites by the reactants.

Table 5 compares the catalytic results achieved in glycerol etherification using $\text{CNT}_{\text{NC7000-BM-Glu/H}_2\text{SO}_4(\text{fum.})-180-12\text{h}}$ to those obtained by other laboratories using various catalysts and reaction conditions. As can be observed, catalytic materials described in the literature converted glycerol with low to significant efficiency (X_G of about 12% to 80%), giving in most cases a mixture of mono-, di- and tri-*tert*-butyl glycerol ethers. The contribution of the most valuable higher-substituted ethers (*i.e.*, DTBGEs and TTBGE) was between 0% and 27% depending on the catalyst and reaction conditions. Nevertheless, in some cases, despite satisfactory results obtained, by-products (such as isobutylene or diisobutylene) were detected in the reaction mixture or more aggressive conditions had to be used. Furthermore, some catalysts (*e.g.*, sulfonated reduced graphene oxide (GO)

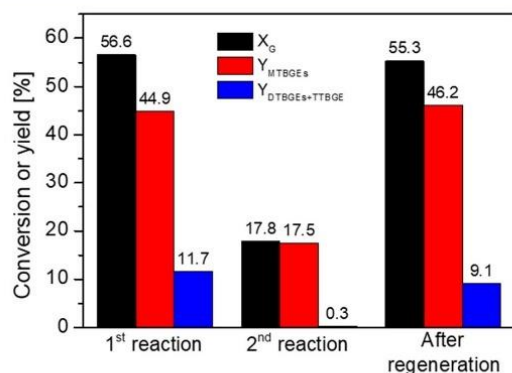


Fig. 12 The results of the reuse tests performed for $\text{CNT}_{\text{NC7000-BM-Glu/H}_2\text{SO}_4(\text{fum.})-180-12\text{h}}$ ($t = 24 \text{ h}$).

Table 5 A comparison of catalytic performances of various carbon-based catalysts in the reaction of glycerol with *tert*-butyl alcohol, using an autoclave reactor and a G : TBA molar ratio of 1 : 4

Catalyst	Temperature (°C)	Catalyst loading (wt%)	Time (h)	X_G (%)	S_{MTBGEs} (Y_{MTBGEs}) (%)	$S_{DTBGEs+TTBGE}$ ($Y_{DTBGEs+TTBGE}$) (%)	Reference
Sulfonated carbon prepared from rice husk TC-L	120	5	4	53.0	—	25.0 (13.2)	17
Sulfonated carbon prepared from rice husk TC-V	120	5	10	12.0	100.0 (12.0)	0.0 (0.0)	17
Sulfonated carbon prepared from sugar cane bagasse SCC-S	120	5	4	80.9	—	21.3 (17.2)	13
Sulfonated carbon fibers prepared from ethylene CF_{et} -H ₂ SO ₄	110	5	6	31.2	91.9 (28.7)	8.1 (2.5)	37
Sulfonated activated carbon (AC)-S	90	7.5	10	35.0	80.0 (28.0)	20.0 (7.0)	66
Sulfonated reduced activated carbon (AC) _{RH} -S	90	7.5	10	31.0	86.0 (26.7)	14.0 (4.3)	66
Sulfonated graphene oxide (GO)-S	90	7.5	10	50.0	78.0 (39.0)	22.0 (11.0)	66
Sulfonated reduced graphene oxide (GO) _{RA} -S	90	7.5	10	77.0	73.0 (56.2)	27.0 (20.8)	66
H-beta zeolite ^a	160	10	4	55.0	98 (53.9)	2.0 (1.1)	72
H-Y zeolite	95	5	6	59.0	72.0 (42.5)	28.0 (16.5)	73
Sulfonic acid functionalized mesoporous polymer MP-SO ₃ H-8	95	5	6	82.0	66.0 (54.1)	34.0 (27.8)	73
CNT _{NC7000-BM} -Glu/H ₂ SO ₄ (fum.)-180-12h	110	5	6	52.4	86.3 (45.2)	13.7 (7.2)	This work
Amberlyst 15	110	5	6	44.4	83.4 (36.6)	17.6 (7.8)	This work

^a G : TBA = 1 : 9.

R_A-S) were obtained using a time-consuming and complex preparation method. In view of the above, our catalyst gave quite satisfactory catalytic results, showing high glycerol conversion (of 52.4%) and about 86% and 14% selectivity to MTBGEs and DTBGEs + TTBGE, respectively, within a relatively short time and under mild reaction conditions. Furthermore, our catalyst was prepared using a facile method and can be reused without significant activity loss in subsequent runs. Interestingly, the results achieved here significantly exceed those obtained in our previous work using the same conditions for sulfonated carbon fibers.³⁷

4. Conclusions

Commercially available CNTs of different purity were modified with sulfuric acid (concentrated, fuming, or 5 M solution) with or without the aid of glucose, applying different modification protocols, and tested in glycerol etherification with *tert*-butyl alcohol. The functionalized samples were active in the reaction, transforming glycerol to *tert*-butyl glycerol ethers; however, the catalytic performances of the CNTs varied considerably depending on the functionalization method and thus the sample functionalization degree. The ball-milled CNTs treated with glucose and fuming sulfuric acid (CNT_{NC7000-BM}-Glu/H₂SO₄(fum.)-180-12h) worked the most effectively in the reaction, giving a 57% glycerol conversion and significant yields of higher-substituted ethers (*i.e.*, DTBGEs and TTBGE) of ~12% after 24 h; however, satisfactory catalytic results could also be obtained with this sample just within 6 h. Furthermore, the used CNT catalyst was even more active than the commercial ion-exchange resin Amberlyst-15. It was also found that CNT_{NC7000-BM}-Glu/H₂SO₄(fum.)-180-12h can

be used in subsequent reaction cycles without a significant decrease in its activity after proper regeneration. The characterization of the regenerated catalyst confirmed the high stability of sulfonic groups introduced to CNTs with the aid of glucose. At the same time, it seems that commercially available CNTs of lower purity, and thus of lower prices, when adequately modified, can be used as efficient catalysts for various acid-type reactions. Finally, it was concluded that the catalytic activity of the CNT-based samples in glycerol etherification strictly depended on the presence of -SO₃H functionalities decorating the catalysts. Nevertheless, the oxygen-containing moieties were also shown to improve the performances of the samples, probably by adsorbing reactants and making the active sites more accessible to the reagents.

Author contributions

Karolina Ptaszyńska: conceptualization, data curation, formal analysis, founding acquisition, investigation, methodology, visualization, writing – original draft, review and editing. Katarzyna Morawa Eblagon: conceptualization, investigation, methodology, writing – original draft, review and editing. Anna Malaika: conceptualization, methodology, writing – original draft, review and editing. José Luís Figueiredo: formal analysis, funding acquisition, writing – review and editing. Mieczysław Kozłowski: methodology, supervision, writing – review and editing.

Conflicts of interest

There are no conflicts to declare.

Acknowledgements

This work was supported by national funds through FCT/MCTES (PIDDAC): LSRE-LCM, UIDB/50020/2020 (DOI: <https://doi.org/10.54499/UIDB/50020/2020>), UIDP/50020/2020 (DOI: <https://doi.org/10.54499/UIDP/50020/2020>), and ALiCE, LA/P/0045/2020 (DOI: <https://doi.org/10.54499/LA/P/0045/2020>). KP would like to acknowledge the financial support from ID-UB AMU (doctoral grant no. 017/02/SNS/0013). KME is grateful to the FCT for the Junior Researcher grant (no. 2021.00535.CEECIND).

References

- IEA, *Renewables 2020*, IEA, Paris, <https://www.iea.org/reports/renewables-2020/transport-biofuels>, 2020.
- M. R. Monteiro, C. L. Kugelmeier, R. S. Pinheiro, M. O. Batalha and A. da Silva César, *Renewable Sustainable Energy Rev.*, 2018, **88**, 109–122.
- F. Chang, Q. Zhou, S. Pan and Y. He, *Biomass, Biofuels, Biochem.*, 2020, **15**, 395–405.
- W. Zhao, B. Yang, Ch. Yi, Z. Lei and J. Xu, *Ind. Eng. Chem. Res.*, 2010, **49**, 12399–12404.
- Ö. D. Bozkurt, F. Yılmaz, N. Bağlar, S. Çelebi and A. Uzun, *Fuel*, 2019, **255**, 115767.
- A. L. Olson, M. Tunér and S. Verhelst, *Heliyon*, 2023, **9**, e13041.
- P. M. Veiga, C. O. Veloso, A. G. Dias and C. A. Henriques, *J. Braz. Chem. Soc.*, 2018, **29**, 1328–1335.
- Ö. D. Bozkurt, F. M. Tunç, N. Bağlar, S. Çelebi, İ. D. Günbas and A. Uzun, *Fuel Process. Technol.*, 2015, **138**, 780–804.
- P. Palanychamy, S. Lim, Y. H. Yap and L. K. Leong, *Catalysts*, 2022, **12**, 1487.
- A. Bhargava, S. Shelke, M. Dilkash, N. S. Chaubal-Durve, P. D. Patil, S. S. Nadar, D. Marghade and M. S. Tiwari, *Rev. Chem. Eng.*, 2023, **39**, 1187–1226.
- M. Roze, V. Kampars, K. Teivena, R. Kampare and E. Liepins, *Mater. Sci. Appl. Chem.*, 2013, **28**, 67–72.
- F. Frusteri, F. Arena, G. Bonura, C. Cannilla, L. Spadaro and O. Di Blasi, *Appl. Catal., A*, 2009, **367**, 77–83.
- M. Gonçalves, V. C. Souza, T. S. Galhardo, M. Mantovani, F. C. A. Figueiredo, D. Mandelli and W. A. Carvalho, *Ind. Eng. Chem. Res.*, 2013, **52**, 2832–2839.
- https://www.sigmaaldrich.com/GB/en/product/sial/216380?gclid=EAIaIQobChMIlcEkjNk7_gIVGACiAx0ZrwMGEEAAYASAAEgJTF_D_BwE&gclid=aw.ds.
- L. Frusteri, C. Cannilla, G. Bonura, A. L. Chuvilin, S. Perathoner, G. Centi and F. Frusteri, *Catal. Today*, 2016, **277**, 68–77.
- M. Gonçalves, F. C. Soler, N. Isoda, W. A. Carvalho, D. Mandelli and J. Sepúlveda, *J. Taiwan Inst. Chem. Eng.*, 2015, **60**, 294–301.
- T. S. Galhardo, N. Simone, M. Gonçalves, F. C. A. Figueiredo, D. Mandelli and W. A. Carvalho, *ACS Sustainable Chem. Eng.*, 2013, **1**, 1381–1389.
- A. Malaika, K. Ptaszynska, M. Kapska and M. Kozłowski, *Fuel*, 2024, **358**, 130147.
- M. L. Terranova, V. Sessa and M. Rossi, *Chem. Vap. Deposition*, 2006, **12**, 315–325.
- J.-P. Salvétat, J.-M. Bonard, N. H. Thomson, A. J. Kulik, L. Forró, W. Benoit and L. Zuppiroli, *Appl. Phys. A: Mater. Sci. Process.*, 1999, **69**, 255–260.
- M. F. L. De Volder, S. H. Tawfick, R. H. Baughman and A. J. Hart, *Science*, 2013, **339**, 535–539.
- Q. Guan, Y. Li, Y. Chen, Y. Shi, J. Gu, B. Li, R. Miao, Q. Chen and P. Ning, *RSC Adv.*, 2017, **7**, 7250–7258.
- X. Ji, Y. Chen, X. Wang and W. Liu, *Kinet. Catal.*, 2011, **52**, 555–558.
- K. Ptaszynska, A. Malaika, K. Morawa Eblagon, J. L. Figueiredo and M. Kozłowski, *Molecules*, 2024, **29**, 1623.
- K. F. Yee, E.-P. Ng, A. R. Mohamed, F. Adam and S. H. Tan, *Chem. Eng. Commun.*, 2016, **203**, 1385–1394.
- H. Yu, Y. Jin, Z. Li, F. Peng and H. Wang, *J. Solid State Chem.*, 2008, **181**, 432–438.
- H. Liu, J. Chen, L. Chen, Y. Xu, X. Guo and D. Fang, *ACS Sustainable Chem. Eng.*, 2016, **4**, 3140–3150.
- <https://www.maximizemarketresearch.com/market-report/global-carbon-nanotubes-cnt-market/2662/>.
- Y. Ge, Z. Li, D. Xiao, P. Xiong and N. Ye, *J. Ind. Eng. Chem.*, 2014, **20**, 1765–1771.
- B. L. Oliveira and V. Teixeira da Silva, *Catal. Today*, 2014, **234**, 257–263.
- P. Nowicki, W. Szymanowski and R. Pietrzak, *Pol. J. Chem. Technol.*, 2015, **17**, 120–127.
- L. J. Konwar, P. Mäki-Arvela and J.-P. Mikkola, *Chem. Rev.*, 2019, **119**, 11576–11630.
- R. P. Rocha, O. S. G. P. Soares, J. L. Figueiredo and M. F. R. Pereira, *C*, 2016, **2**, 17.
- O. S. G. P. Soares, R. P. Rocha, J. J. M. Órfão, M. F. R. Pereira and J. L. Figueiredo, *C*, 2019, **5**, 30.
- R. Dubey, D. Dutta, A. Sarkar and P. Chattopadhyay, *Nanoscale Adv.*, 2021, **3**, 5722–5744.
- H. Ji, J. Fu and T. Wang, *Catalysts*, 2018, **8**, 517.
- K. Ptaszynska, A. Malaika, M. Kapska and M. Kozłowski, *Sci. Rep.*, 2023, **13**, 565.
- https://www.tomo-e.co.jp/upload/eProductsJA/25QU033-eProductsJA_content-001.pdf.
- <https://www.nanocyl.com/product/nc3100/>.
- K. Morawa Eblagon, N. Rey-Raap, J. L. Figueiredo and M. F. R. Pereira, *Appl. Surf. Sci.*, 2021, **548**, 149242.
- P. Rechnia, A. Malaika and M. Kozłowski, *Fuel*, 2015, **154**, 338–345.
- A. Malaika and M. Kozłowski, *Fuel Process. Technol.*, 2019, **184**, 19–26.
- Y. Zhou, S. Niu and J. Li, *Energy Convers. Manage.*, 2016, **114**, 188–196.
- N. G. Karsli, S. Yesil and A. Aytac, *Composites, Part B*, 2014, **63**, 154–160.
- F. Li, Y. Lu, L. Liu, L. Zhang, J. Dai and J. Ma, *Polymer*, 2013, **54**, 2158–2165.
- S. Z. Mortazavi, A. J. Novinrooz, A. Reyhani and S. Mirershadi, *Cent. Eur. J. Phys.*, 2010, **8**, 940–946.

- 47 N. Kong, J. Park, X. Yang, O. Ramström and M. Yan, *ACS Appl. Bio Mater.*, 2019, **2**, 284–291.
- 48 A. Malaika, M. Heinrich, J. Gościańska and M. Kozłowski, *Fuel*, 2020, **280**, 118523.
- 49 A. Malaika, K. Ptaszynska and M. Kozłowski, *Fuel*, 2021, **288**, 119609.
- 50 R. G. Morais, N. Rey-Raap, R. S. Costa, C. Pereira, A. Guedes, J. L. Figueiredo and M. F. R. Pereira, *J. Compos. Sci.*, 2020, **4**, 20.
- 51 M. Sevilla and A. B. Fuertes, *Chem. – Eur. J.*, 2009, **15**, 4195–4203.
- 52 L. Roldán, I. Santos, S. Armenise, J. M. Fraile and E. García-Bordejé, *Carbon*, 2012, **50**, 1363–1372.
- 53 Z. Zolfaghari, A. Tavasoli, S. Tabyar and A. N. Pour, *J. Energy Chem.*, 2014, **23**, 57–65.
- 54 K. Morawa Eblagon, M. F. R. Pereira and J. L. Figueiredo, *Appl. Catal., B.*, 2016, **184**, 381–396.
- 55 M. Gomes, L. C. Gomes, R. Teixeira-Santos, M. F. R. Pereira, O. S. G. P. Soares and F. J. Mergulhão, *Appl. Sci.*, 2021, **11**, 4038.
- 56 O. S. G. P. Soares, A. G. Gonçalves, J. J. Delgado, J. J. M. Órfão and M. F. R. Pereira, *Catal. Today*, 2015, **249**, 199–203.
- 57 B. D. Che, B. Q. Nguyen, L. T. T. Nguyen, H. T. Nguyen, V. Q. Nguyen, T. V. Le and N. H. Nguyen, *Chem. Cent. J.*, 2015, **9**, 10.
- 58 D. N. Futaba, T. Yamada, K. Kobashi, M. Yumura and K. Hata, *J. Am. Chem. Soc.*, 2011, **133**, 5716–5719.
- 59 D. K. Singh, P. K. Iyer and P. K. Giri, *Diamond Relat. Mater.*, 2010, **19**, 1281–1288.
- 60 A. M. Abbas, F. H. Abdulrazzak, I. M. Radhi, A. I. AbdulLatif, T. A. Himdan and F. H. Hussein, *J. Phys.: Conf. Ser.*, 2020, **1660**, 012022.
- 61 A. N. Popova, *Coke Chem.*, 2017, **60**, 361–365.
- 62 J. Gościańska and A. Malaika, *Catal. Today*, 2020, **357**, 84–93.
- 63 J. L. Figueiredo, M. F. R. Pereira, M. M. A. Freitas and J. J. M. Órfão, *Carbon*, 1999, **37**, 1379–1389.
- 64 A. Malaika, K. Ptaszynska, K. Morawa Eblagon, M. F. R. Pereira, J. L. Figueiredo and M. Kozłowski, *Fuel*, 2021, **304**, 121381.
- 65 M. Kozłowski, *Fuel*, 2004, **83**, 259–265.
- 66 C. Miranda, A. Ramírez, A. Sachse, Y. Pouilloux, J. Urresta and L. Pinard, *Appl. Catal., A*, 2019, **580**, 167–177.
- 67 L. J. Cote, J. Kim, V. C. Tung, J. Luo, F. Kim and J. Huang, *Pure Appl. Chem.*, 2011, **83**, 95–110.
- 68 J. Yang, H. Zhang, Z. Ao and S. Zhang, *Catal. Commun.*, 2019, **123**, 109–113.
- 69 P. Manjunathan, M. Kumar, S. R. Churipard, S. Sivasankaran, G. V. Shanbhag and S. P. Maradur, *RSC Adv.*, 2016, **6**, 82654–82660.
- 70 J. M. Fraile, E. García-Bordejé and L. Roldán, *J. Catal.*, 2012, **289**, 73–79.
- 71 P. Rechnia-Gorący, A. Malaika and M. Kozłowski, *Diamond Relat. Mater.*, 2018, **87**, 124–133.
- 72 N. Viswanadham, S. Debnath, S. K. Saxena and H. Ala'a, *RSC Adv.*, 2016, **6**, 41364–41368.
- 73 H. Liu, J. Chen, L. Chen, Y. Xu, X. Guo and D. Fang, *ACS Sustainable Chem. Eng.*, 2016, **4**, 3140–3150.

**OŚWIADCZENIA
AUTORÓW O UDZIALE
W POWSTANIU
PUBLIKACJI**



Mgr Karolina Ptaszyńska

Poznań, 18.09.2024

Uniwersytet im. Adam Mickiewicza w Poznaniu

Wydział Chemii

Zakład Technologii Chemicznej

ul. Uniwersytetu Poznańskiego 8, 61-614 Poznań

OŚWIADCZENIE DOKTORANTKI

W związku z przedłożoną rozprawą doktorską oświadczam, że w opublikowanych artykułach naukowych wymienionych poniżej:

P1) A. Malaika, **K. Ptaszyńska**, J. Gaidukevič, M. Kozłowski, *The impact of surface groups of functionalized graphene on glycerol acetylation*, Fuel, 2022, 313(73), 122987

mój udział obejmował: przegląd literatury, analizę właściwości fizykochemicznych materiałów na bazie termicznie zredukowanego tlenku grafenu, zbadanie aktywności katalitycznej tych próbek w procesie estryfikacji glicerolu za pomocą kwasu octowego, uczestnictwo w omówieniu otrzymanych wyników oraz graficznej prezentacji danych;

P2) **K. Ptaszyńska**, A. Malaika, M. Kapska, M. Kozłowski, *SO₃H-functionalized carbon fibers for the catalytic transformation of glycerol to glycerol tert-butyl ethers*, Scientific Reports, 2023, 13(1), 565

mój udział obejmował pozyskanie finansowania badań (minigrant doktorancki), przegląd literatury, uczestnictwo w opracowaniu koncepcji badań, walidację, analizę właściwości fizykochemicznych testowanych materiałów węglowych, określenie wpływu tych parametrów na aktywność katalityczną próbek w procesie eteryfikacji glicerolu za pomocą alkoholu tert-butyłowego, omówienie otrzymanych wyników, graficzną prezentację danych, opracowanie manuskryptu i materiałów uzupełniających, współudział w przygotowaniu odpowiedzi na recenzje oraz wprowadzeniu korekt do manuskryptu zgodnie z uwagami otrzymanymi od recenzentów;

P3) **K. Ptaszyńska**, A. Malaika, K. Kozigrodzka, M. Kozłowski, *A Green Approach to Obtaining Glycerol Carbonate by Urea Glycerolysis Using Carbon-Supported Metal Oxide Catalysts*, Molecules, 2023, 28(18), 6534

mój udział obejmował przegląd literatury, uczestnictwo w opracowaniu koncepcji badań i metodologii, walidację, analizę właściwości fizykochemicznych testowanych materiałów węglowych, określenie wpływu tych parametrów na aktywność katalityczną próbek w procesie glicerolizy mocznika, omówienie otrzymanych wyników, graficzną prezentację danych, opracowanie manuskryptu i materiałów uzupełniających, współudział w przygotowaniu odpowiedzi na recenzje oraz wprowadzeniu korekt do manuskryptu zgodnie z uwagami otrzymanymi od recenzentów. Jestem również wskazana w pracy jako autor korespondencyjny;



Collegium Chemicum, ul. Uniwersytetu Poznańskiego 8, 61-614 Poznań
NIP 777 00 06 350, REGON 000001293

www.chemia.amu.edu.pl



- P4) K. Ptaszyńska, A. Malaika, K. Morawa Eblagon J. L. Figueiredo, M. Kozłowski, *Promoting Effect of Ball Milling on the Functionalization and Catalytic Performance of Carbon Nanotubes in Glycerol Etherification*, *Molecules*, 2024, 29(7), 1623

mój udział obejmował pozyskanie finansowania badań (minigrant doktorancki), przegląd literatury, uczestnictwo w opracowaniu koncepcji badań i metodologii, walidację, preparatykę katalizatorów węglowych, analizę właściwości fizykochemicznych testowanych w ramach prac próbek węglowych, zbadanie aktywności katalitycznej otrzymanych materiałów w procesie eteryfikacji glicerolu za pomocą alkoholu tert-butyłowego, określenie wpływu właściwości fizykochemicznych próbek na aktywność katalityczną w badanym procesie, omówienie otrzymanych wyników, graficzną prezentację danych, opracowanie manuskryptu i materiałów uzupełniających, współudział w przygotowaniu odpowiedzi na recenzje oraz wprowadzeniu korekt do manuskryptu zgodnie z uwagami otrzymanymi od recenzentów. Jestem również wskazana w pracy jako autor korespondencyjny;

- P5) K. Ptaszyńska, K. Morawa Eblagon, A. Malaika, J. L. Figueiredo, M. Kozłowski, *The role of mechano-chemical treatment of carbon nanotubes in promoting glycerol etherification*, *Catalysis Science & Technology*, 2024, 14(11), 3184-3200

mój udział obejmował pozyskanie finansowania badań (minigrant doktorancki), przegląd literatury, uczestnictwo w opracowaniu koncepcji badań i metodologii, walidację, preparatykę katalizatorów węglowych, analizę właściwości fizykochemicznych testowanych w ramach prac próbek węglowych, zbadanie aktywności katalitycznej otrzymanych materiałów w procesie eteryfikacji glicerolu za pomocą alkoholu tert-butyłowego, określenie wpływu właściwości fizykochemicznych próbek na aktywność katalityczną w badanym procesie, omówienie otrzymanych wyników, graficzną prezentację danych, opracowanie manuskryptu, współudział w przygotowaniu odpowiedzi na recenzje oraz wprowadzeniu korekt do manuskryptu zgodnie z uwagami otrzymanymi od recenzentów. Jestem również wskazana w pracy jako autor korespondencyjny.

Kierownik
Zakładu Technologii Chemicznej

prof. dr hab. Mieczysław Kozłowski

Podpis promotora

Karolina Ptaszyńska

Podpis doktorantki



UCZELNIA
BADAWCZA



HR EXCELLENCE IN RESEARCH



EPICUR
EUBAN UNIVERSITY

Collegium Chemicum, ul. Uniwersytetu Poznańskiego 8, 61-614 Poznań
NIP 777 00 06 350, REGON 000001293

www.chemia.amu.edu.pl



Dr Anna Malaika

Poznań 16.09.2024 r.

Zakład Technologii Chemicznej

Wydział Chemii UAM

ul. Uniwersytetu Poznańskiego 8

61-614 Poznań

tel. 61-829-1718

OŚWIADCZENIE PROMOTORA POMOCNICZEGO O WKŁADZIE W PUBLIKACJE NAUKOWE DOKTORANTA

W związku z przedłożoną przez Panią mgr Karolinę Ptaszyńską rozprawą doktorską oświadczam, że w publikacjach P1-P5 moja rola jako współautora prac uwzględniała udziały określone poniżej:

P1) A. Malaika, K. Ptaszyńska, J. Gaidukevič, M. Kozłowski, *The impact of surface groups of functionalized graphene on glycerol acetylation*, Fuel, 2022, 313(73), 122987.

Opracowanie koncepcji badań i metodologii, sprawowanie opieki merytorycznej i technicznej nad doktorantką (K.P.) wykonującą testy katalityczne, udział w walidacji, analizie i dyskusji wyników, wizualizacji otrzymanych rezultatów, przygotowaniu manuskryptu i materiałów uzupełniających, a także prowadzenie dyskusji z recenzentami (autor korespondencyjny), tj. przygotowanie odpowiedzi na recenzje oraz wprowadzenie korekty do manuskryptu zgodnie z uwagami otrzymanymi od recenzentów.

P2) K. Ptaszyńska, A. Malaika, M. Kapska, M. Kozłowski, *SO₃H-functionalized carbon fibers for the catalytic transformation of glycerol to glycerol tert-butyl ethers*, Scientific Reports, 2023, 13(1), 565.

Opracowanie koncepcji badań i metodologii, walidacja, udział w przygotowaniu ostatecznej wersji manuskryptu oraz odpowiedzi na recenzję, korespondencja z edytorem i recenzentami (autor korespondencyjny).

P3) K. Ptaszyńska, A. Malaika, K. Kozigrodzka, M. Kozłowski, *A green approach to obtaining glycerol carbonate by urea glycerolysis using carbon-supported metal oxide catalysts*, Molecules, 2023, 28(18), 6534.

Opracowanie koncepcji badań, walidacja, udział w wizualizacji otrzymanych wyników, przygotowaniu ostatecznej wersji manuskryptu i odpowiedzi na recenzje.



Collegium Chemicum, ul. Uniwersytetu Poznańskiego 8, 61-614 Poznań
NIP 777 00 06 350, REGON 000001293

www.chemia.amu.edu.pl



P4) K. Ptaszyńska, **A. Malaika**, K. Morawa Eblagon J. L. Figueiredo, M. Kozłowski, *Promoting effect of ball milling on the functionalization and catalytic performance of carbon nanotubes in glycerol etherification*, *Molecules*, 2024, 29(7), 1623.

Opracowanie koncepcji badań i metodologii, udział w wizualizacji rezultatów, przygotowaniu ostatecznej wersji manuskryptu i odpowiedzi na recenzje.

P5) K. Ptaszyńska, K. Morawa Eblagon, **A. Malaika**, J. L. Figueiredo, M. Kozłowski, *The role of mechanochemical treatment of carbon nanotubes in promoting glycerol etherification*, *Catalysis Science & Technology*, 2024, 14(11), 3184-3200.

Opracowanie koncepcji badań i metodologii, udział w wizualizacji otrzymanych wyników, przygotowaniu ostatecznej wersji manuskryptu i odpowiedzi na recenzje.

Z poważaniem,

Anna Malaika



Collegium Chemicum, ul. Uniwersytetu Poznańskiego 8, 61-614 Poznań
NIP 777 00 06 350, REGON 000001293

www.chemia.amu.edu.pl



Prof. dr hab. Mieczysław Kozłowski
Zakład Technologii Chemicznej
Wydział Chemii UAM
ul. Uniwersytetu Poznańskiego 8
61-614 Poznań
tel. 61-829-1664

Poznań 17.09.2024 r.

OŚWIADCZENIE PROMOTORA

W związku z przedłożoną przez Panią mgr Karolinę Ptaszyńską rozprawą doktorską oświadczam, że w publikacjach wymienionych poniżej:

P1) A. Malaika, K. Ptaszyńska, J. Gaidukevič, **M. Kozłowski**, *The impact of surface groups of functionalized graphene on glycerol acetylation*, Fuel, 2022, 313(73), 122987

P2) K. Ptaszyńska, A. Malaika, M. Kapska, **M. Kozłowski**, *SO₃H-functionalized carbon fibers for the catalytic transformation of glycerol to glycerol tert-butyl ethers*, Scientific Reports, 2023, 13(1), 565

mój udział obejmował (w przypadku obu prac - P1 i P2) pozyskanie finansowania badań, nadzór merytoryczny oraz współudział w przygotowaniu ostatecznej wersji manuskryptu;

P3) K. Ptaszyńska, A. Malaika, K. Kozigrodzka, **M. Kozłowski**, *A Green Approach to Obtaining Glycerol Carbonate by Urea Glycerolysis Using Carbon-Supported Metal Oxide Catalysts*, Molecules, 2023, 28(18), 6534

mój udział obejmował pozyskanie finansowania badań, walidację, nadzór merytoryczny, współudział w przygotowaniu ostatecznej wersji manuskryptu oraz korespondencję z edytorem i recenzentami;

P4) K. Ptaszyńska, A. Malaika, K. Morawa Eblagon J. L. Figueiredo, **M. Kozłowski**, *Promoting Effect of Ball Milling on the Functionalization and Catalytic Performance of Carbon Nanotubes in Glycerol Etherification*, Molecules, 2024, 29(7), 1623

mój udział obejmował opracowanie metodologii, nadzór merytoryczny, współudział w przygotowaniu ostatecznej wersji manuskryptu oraz korespondencję z edytorem i recenzentami;

P5) K. Ptaszyńska, K. Morawa Eblagon, A. Malaika, J. L. Figueiredo, **M. Kozłowski**, *The role of mechanochemical treatment of carbon nanotubes in promoting glycerol etherification*, Catalysis Science & Technology, 2024, 14(11), 3184-3200

mój udział obejmował opracowanie metodologii, nadzór merytoryczny oraz współudział w przygotowaniu ostatecznej wersji manuskryptu.

Z poważaniem,

Kierownik
Zakładu Technologii Chemicznej


Prof. dr hab. Mieczysław Kozłowski

Collegium Chemicum, ul. Uniwersytetu Poznańskiego 8, 61-614 Poznań
NIP 777 00 06 350, REGON 000001293
tel.: +48 61 829 16 64, e-mail: mkozlow@amu.edu.pl

www.chemia.amu.edu.pl





13 September 2024

Dr Katarzyna Morawa Eblagon
University of Porto, Faculty of Engineering
Laboratory of Separation and Reaction Engineering-Laboratory of Catalysis and Materials (LSRE-LCM)
Associate Laboratory in Chemical Engineering (AliCE)
Rua Dr. Roberto Frias, 4200-465 Porto, Portugal

DECLARATION OF CO-AUTHORSHIP

To Whom it may concern,

In reference to the doctoral dissertation submitted by MSc. Karolina Ptasińska, I would like to confirm that in the publications listed below:

P4) K. Ptasińska, A. Malaika, **K. Morawa Eblagon**, J. L. Figueiredo, M. Kozłowski, *Promoting effect of ball milling on the functionalization and catalytic performance of carbon nanotubes in glycerol etherification*, *Molecules*, 2024, 29(7), 1623

my contribution included conceptualization, methodology, providing commercial carbon nanotubes (Nanocyl NC3100 and Nanocyl NC7000), preparation of ball-milled carbon nanotubes (CNT_{NC7000-BM}), visualization, critical revision of the initial draft, and finalization of the manuscript;

P5) K. Ptasińska, **K. Morawa Eblagon**, A. Malaika, J. L. Figueiredo, M. Kozłowski, *The role of mechano-chemical treatment of carbon nanotubes in promoting glycerol etherification*, *Catalysis Science & Technology*, 2024, 14(11), 3184-3200

my contribution included conceptualization, methodology, providing commercial carbon nanotubes (Nanocyl NC3100 and Nanocyl NC7000), preparation of ball-milled carbon nanotubes (CNT_{NC7000-BM}) and functionalized carbon materials (CNT_{NC7000-BM}-H₂SO₄(fum.)-100-8h, CNT_{NC7000-BM}-Glu/H₂SO₄(fum.)-180-12h, CNT_{NC7000-BM}-Glu/H₂SO₄(5M)-150-4h), conducting textural analyses, critical revision of the initial draft, finalization of the manuscript and submission, pre-publication revision of the manuscript and article proof, and acquisition of the financial support.

Sincerely,
Dr Katarzyna Morawa Eblagon

Assinado por: **Katarzyna Anna Morawa Eblagon**
Num. de identificação: 32674820
Data: 2024.09.13 11:42:06+01'00'

Porto, 16th September 2024

DECLARATION OF CO-AUTHORSHIP

In reference to the doctoral dissertation submitted by MSc. Karolina Ptasińska, I would like to confirm that in the publications listed below:

- P4)** K. Ptasińska, A. Malaika, K. Morawa Eblagon, **J. L. Figueiredo**, M. Kozłowski, *Promoting effect of ball milling on the functionalization and catalytic performance of carbon nanotubes in glycerol etherification*, *Molecules*, 2024, 29(7), 1623
- P5)** K. Ptasińska, K. Morawa Eblagon, A. Malaika, **J. L. Figueiredo**, M. Kozłowski, *The role of mechano-chemical treatment of carbon nanotubes in promoting glycerol etherification*, *Catalysis Science & Technology*, 2024, 14(11), 3184-3200

my contribution included formal analysis, financial support and writing (review and editing).



(José Luís Figueiredo)
Professor Emeritus

Phone: +(351) 22-508 1663

Email: jlfig@fe.up.pt

Assoc. prof. dr. Justina Gaidukevič
Vilnius University
Faculty of Chemistry and Geosciences
Naugarduko 24, LT-03225, Vilnius, Lithuania

Vilnius, 16-09-2024

DECLARATION OF CO-AUTHORSHIP

In reference to the doctoral dissertation submitted by MSc. Karolina Ptasińska, I would like to confirm that in the publication listed below:

P1) A. Malaika, K. Ptasińska, **J. Gaidukevič**, M. Kozłowski, *The impact of surface groups of functionalized graphene on glycerol acetylation*, *Fuel*, 2022, 313(73), 122987

my contribution included preparation of functionalized carbon materials, physicochemical analysis, validation, formal analysis, taking part in writing and revision of the manuscript.

Yours Sincerely,
Dr. Justina Gaidukevič





UNIwersYTET IM. ADAMA MICKIEWICZA W POZNANIU

Wydział Chemii

Mgr Magdalena Kapska

Poznań, 16.09.2024

Uniwersytet im. Adam Mickiewicza w Poznaniu

Wydział Chemii

Zakład Technologii Chemicznej

ul. Uniwersytetu Poznańskiego 8, 61-614 Poznań

OŚWIADCZENIE O WSPÓLAUTORSTWIE

W związku z przedłożoną przez Panią mgr Karolinę Ptaszyńską rozprawą doktorską oświadczam, że w publikacji wymienionej poniżej:

P2) K. Ptaszyńska, A. Malaika, **M. Kapska**, M. Kozłowski, *SO₃H-functionalized carbon fibers for the catalytic transformation of glycerol to glycerol tert-butyl ethers*, Scientific Reports, 2023, 13(1), 565

mój udział polegał na preparatyce funkcjonalizowanych katalizatorów węglowych, analizie wybranych właściwości fizykochemicznych otrzymanych próbek, zbadaniu aktywności katalitycznej próbek w procesie eteryfikacji glicerolu za pomocą alkoholu tert-butyłowego oraz analizie formalnej.

Z poważaniem



Collegium Chemicum, ul. Uniwersytetu Poznańskiego 8, 61-614 Poznań
NIP 777 00 06 350, REGON 000001293

www.chemia.amu.edu.pl



Poznań, 19 09 2024 r.

Mgr Klaudia Kozigrodzka
Uniwersytet im. Adam Mickiewicza w Poznaniu
Wydział Chemii
Zakład Technologii Chemicznej
ul. Uniwersytetu Poznańskiego 8, 61-614 Poznań

OŚWIADCZENIE O WSPÓLAUTORSTWIE

W związku z przedłożoną przez Panią mgr Karolinę Ptaszyńską rozprawą doktorską oświadczam, że w publikacji wymienionej poniżej:

P3) K. Ptaszyńska, A. Malaika, K. Kozigrodzka, M. Kozłowski, *A Green Approach to Obtaining Glycerol Carbonate by Urea Glycerolysis Using Carbon-Supported Metal Oxide Catalysts*, *Molecules*, 2023, 28(18), 6534

mój udział polegał na preparatyce modyfikowanych katalizatorów węglowych (tlenki wybranych metali osadzone na włóknach węglowych), analizie wybranych właściwości fizykochemicznych otrzymanych próbek, zbadaniu aktywności katalitycznej próbek w procesie glicerolizy mocznika oraz analizie formalnej.

Z poważaniem

Klaudia Trąbkowska
(Kozigrodzka)



Collegium Chemicum, ul. Uniwersytetu Poznańskiego 8, 61-614 Poznań
NIP 777 00 06 350, REGON 000001293

www.chemia.amu.edu.pl